SELF-EXCITATION AND CONSTANT FLUX OPERATION OF INDUCTION GENERATORS IN STAND-ALONE APPLICATIONS

YONG WEI LIAO

A thesis submitted in partial fulfilment of the requirements of Liverpool John Moores University for the degree of Doctor of Philosophy

November 1998

ABSTRACT

This thesis deals with applications of variable speed induction generators in stand-alone power systems. The plant consists of an induction generator, a reactive power compensator and a control system. Four different reactive power compensation schemes for a stand-alone induction generator, namely parallel capacitor bank, voltage source inverter with scalar control of frequency, a current controlled PWM voltage source inverter (VSI) with direct stator flux oriented control, and a current controlled PWM voltage source inverter with direct rotor flux oriented control, have been investigated.

Dynamics of self-excitation process of an induction generator, using fixed capacitor bank, have been investigated both experimentally and by simulation for a single-cage and a double-cage induction machine. Detailed experimental investigations of the induction generator self-excitation process with star and delta connected capacitor bank, under variable speed conditions, and evaluation of load voltage variation compensation using additional series capacitor bank, have been conducted and the results are presented.

Simulation of variable speed operation of the induction generator with scalar control of a PWM voltage source inverter has been performed. Two novel vector control strategies for the PWM VSI based reactive power compensator, a direct stator flux oriented control scheme and a direct rotor flux oriented control scheme, with a goal of achieving constant flux operation of the generator under varying speed and load conditions, have been developed and verified by simulation. A novel saturation adaptive rotor flux estimator is developed for the case of rotor flux oriented control scheme.

Rotor flux oriented control scheme offers the most favourable behaviour. The proposed vector controlled variable speed induction generators can be used to supply both autonomous a.c. power systems and autonomous d.c. power systems.

ACKNOWLEDGEMENTS

I would like to express my sincere gratitude to my Director of studies, Dr. Emil Levi, for his professional guidance and support throughout the course of this project. I would also like to acknowledge my second supervisor, Professor Roger Morgan, for his assistance.

I would like to thank my colleagues Dr. Matija Sokola, Mr. Mingyu Wang and Mr. Zulkifilie Ibrahim for their useful comments and discussions.

Finally, I would like to thank my parents and my wife for their support and encouragement throughout the years.

CONTENTS

LIST OF PRINCIPAL SYMBOLS

C	capacitance of parallel capacitor
C_s	capacitance of series capacitor
H	hystersis band
J	rotor inertia coefficient
K	gain
L	dynamic inductance
L_{mr}	mutual leakage inductance between the two rotor winding
L_m	steady state magnetising inductance
L_{ddm}, L_{qqm}	dynamic inductances along d- and q-axes
m	modulation index
P	number of pole pairs
p.u.	per unit
R_c	common end-ring resistance between the two cages
R_s, R_r	stator and rotor resistance
S	switching function for inverter leg
T_e, T_L	electrical torque and load torque
T_r	rotor time constant
v, i	instantaneous voltage and current
Λ	generalised inductance
ψ	generalised flux
ϕ	angular position
ω, ω_a	angular electrical velocity of rotor and arbitrary reference frame
ω_{sl}	slip angular frequency
μ	angle between the d axis of common reference frame and the magnetising current and flux space vectors
ψ_m	magnetising flux

$\underline{v}, \underline{i}, \underline{\Psi}$	voltage, current and flux vectors
$\varepsilon_s, \varepsilon_r, \phi_s, \phi_r$	instantaneous angular positions of the stator current, rotor current, stator flux and rotor flux space vectors, respectively, with respect to the stationary stator phase 'a' magnetic axis

Superscripts

*	reference value
e	estimated value
s	space vector in stationary reference frame

Subscripts

σ	leakage inductance
α, β	α, β stationary axes
a, b, c	three-phase quantities
c	variables associated with series capacitor
d, q	direct and quadrature axes components
l	electrical load on generator terminals
m	variables associated with magnetising flux
N	neutral
n	rated value
r	rotor variable or parameter
r1	variable or parameter associated with the first rotor winding
r2	variable or parameter associated with the second rotor winding
s	stator variable or parameter

LIST OF FIGURES AND TABLES

Chapter 1

INTRODUCTION

1.1 Electricity generation from alternative energy sources

Emphasis on environmental problems throughout the world has led to enormous increase in activities correlated with electric energy generation from so-called alternative energy sources [Hammons (1993)]. Alternative energy sources are thought to be one of the solutions to the environmental problems and are expected to make a major contribution to the overall electric energy production in the next millennium. Alternative energy sources produce electricity without polluting the environment, thus reducing emission of huge amounts of harmful gases such as carbon dioxide (CO_2), nitrogen oxides (NO_x) and sulphur oxides (SO_x) that are responsible for the greenhouse effect and acid rain.

Among alternative energy sources such as wind, hydro, wave, tidal, solar, biomass and geothermal, wind energy could contribute significantly and economically due to its free, clean and renewable character and its extremely large potential. Wind is considered not just as an environment-friendly energy source, but as the least-costly choice of energy source as well. Wind as a potential source is obviously much higher than the world's hydro energy potential. It is sensible to expect that wind energy will become a significant component of total energy supplies in the near future, given the advanced state of wind turbine technology and availability of wind in the world.

Wind turbine technology has by now matured enough for widespread and large-scale applications after 20 years of intensive development. Wind power is already a commercial technology since equipment is readily available from manufacturers worldwide. Large-scale wind power projects in both North America and Europe have been undertaken during the last decade. More than 16000 wind turbines are currently

installed in California with a total generating capacity approaching 1700 MW [Gipe (1997)] which is more than the capacity generated from the nuclear power plants. Denmark and Netherlands are committed to generating about 10% of their power requirements by wind power. The world wind generating capacity has reached 6000 MW in 1996 (Figure 1.1) and is expected to exceed 10000 MW by the end of the century [Gipe (1997)]. The production of wind-generated electricity has risen from nearly zero in the early 1980s to more than 10 Terawatt-hours (TWh) per year in 1996 and generation will reach 20 TWh by the year 2000 (Figure 1.2).

Today, the United States dominates the world for wind energy production, about 3 TWh of wind-generated electricity being now produced annually in America, but the lead is quickly evaporating as wind power plants are going on-line in different sites around the world. Wind turbines with a generating capacity in excess of 1400 MW have been installed in 1996 by manufacturers world-wide (Figure 1.3) [Gipe (1997)]. Germany and India account for three-quarters of new capacity. Germany has the most expanding market for wind energy in the world and the installed capacity in Germany was expected exceed the installed capacity in the United States by the end of 1997 [Gipe (1997)].

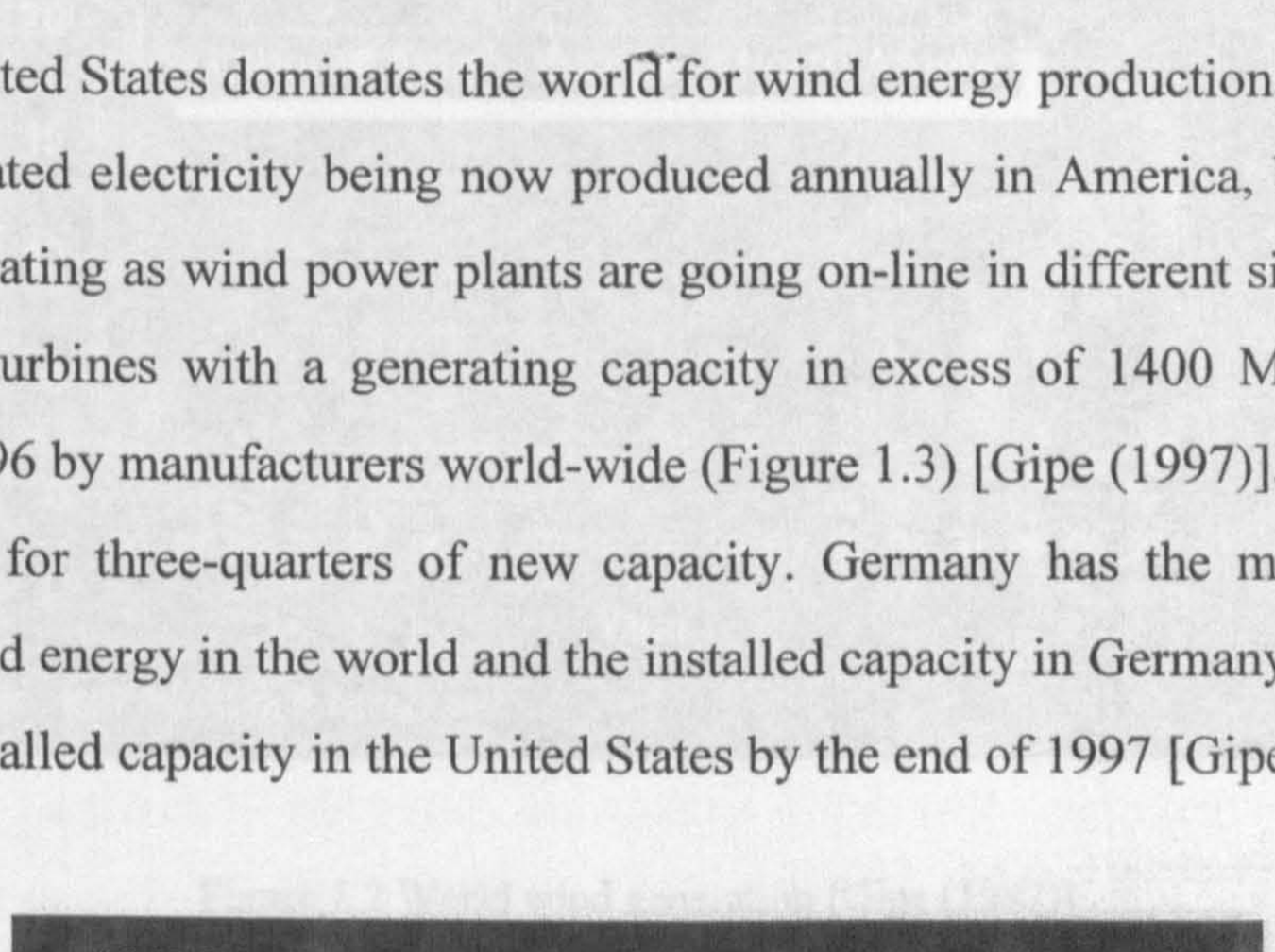

Figure 1.1 World wind generation capacity [Gipe (1997)]

The ongoing and projected wind generations for some developing countries are impressive [Jayadev (1995)]. India has planned to produce nearly 1200 MW of wind

power at the end of this century. Another country with ambitious plans is China, which announced that it had set a goal of having available 1 GW of wind power by the year 2000. Estimate of wind resource that can be utilised in China is about 253 GW. China manufactures each year 30,000 small wind turbines. These small turbines provide electrical need in the rural areas of the country.

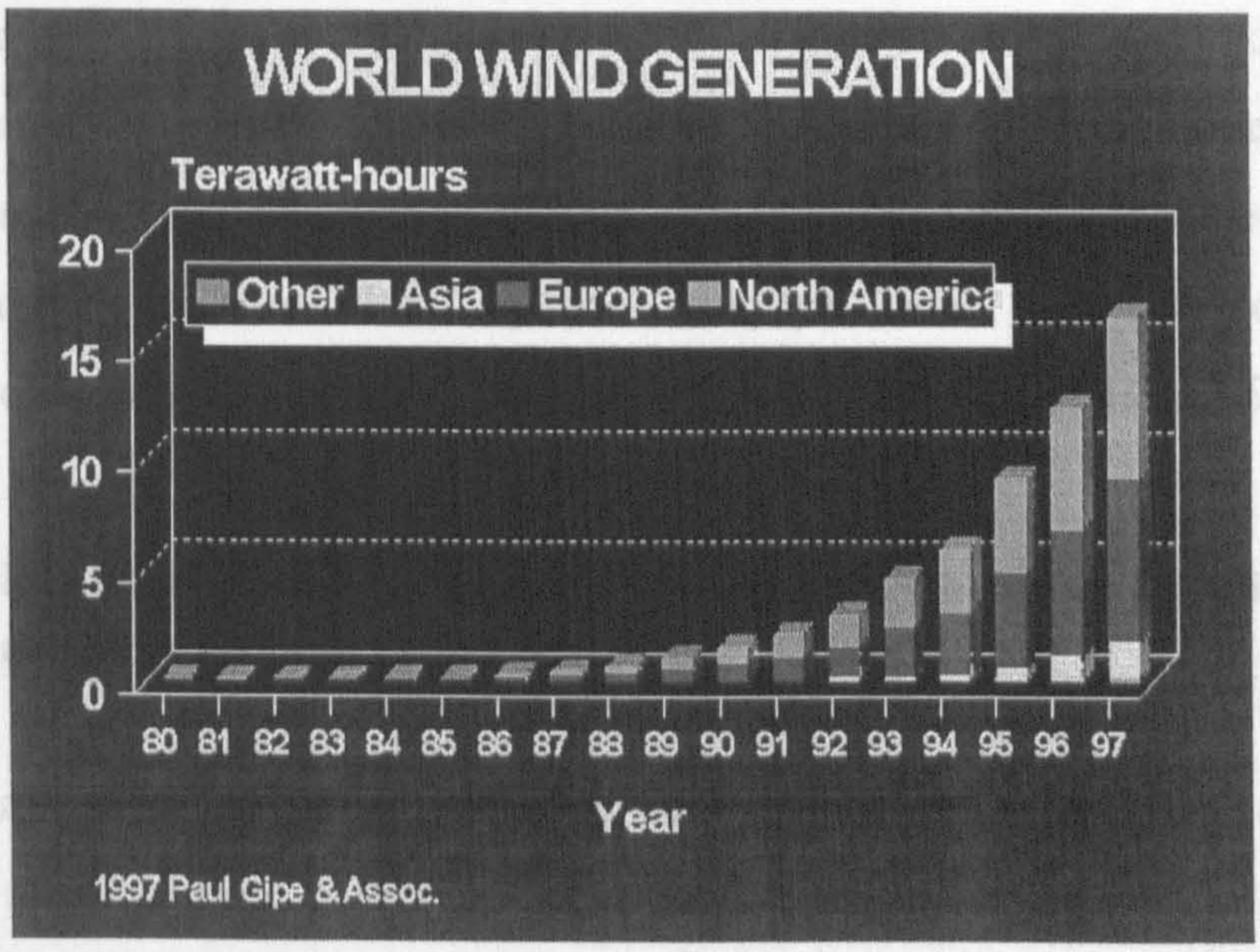

Figure 1.2 World wind generation [Gipe (1997)]

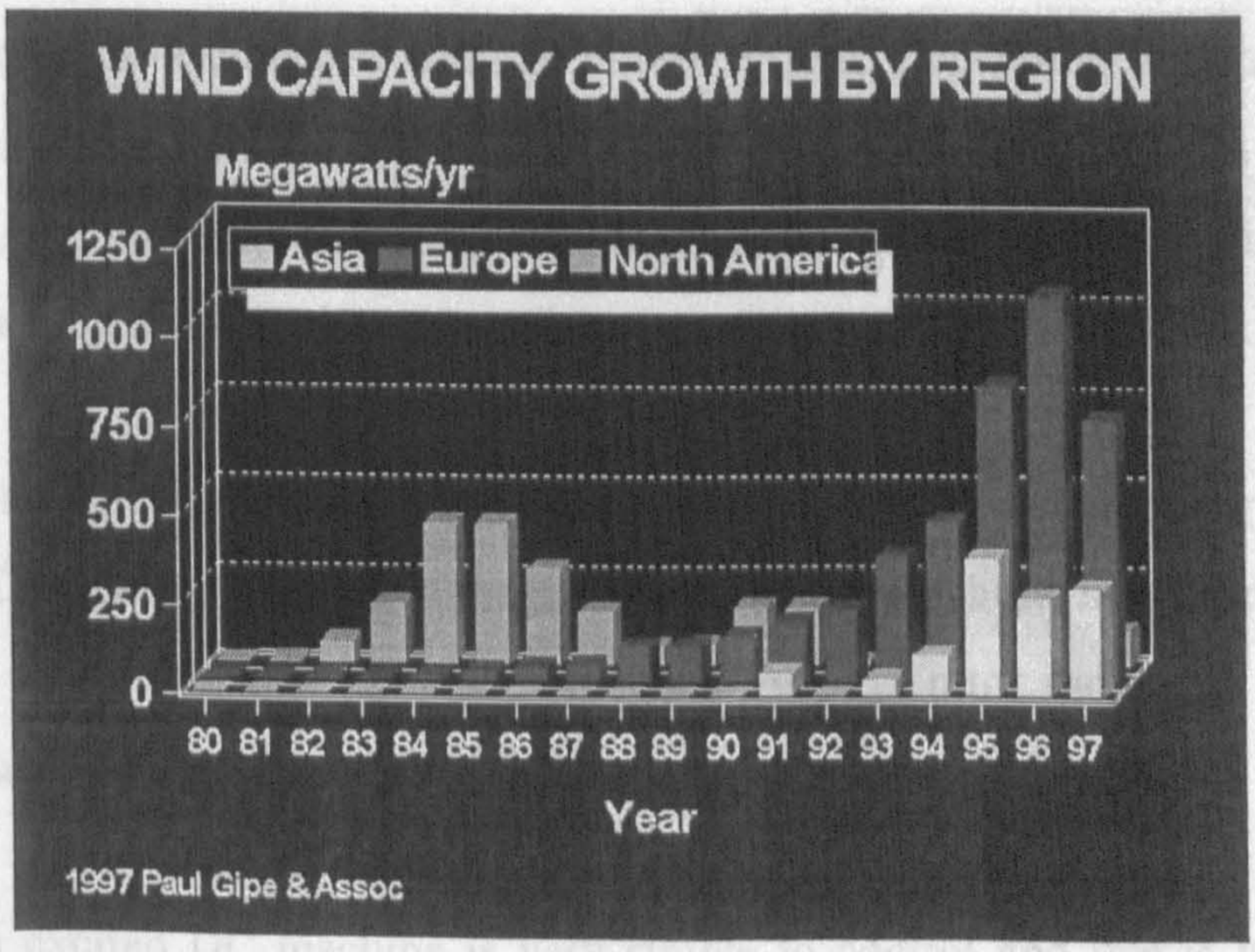

Figure 1.3 Wind capacity growth by region [Gipe (1997)]

Wind energy is one of the most promising sources of alternative energy as far as the UK is concerned, due to general availability of the wind and due to possibilities of realising electro-mechanical conversion with high efficiency [Halliday (1993)]. The UK has the largest wind resource in Europe. The overall accessible wind resource on land is greater than the UK's current electricity consumption [Blocklehurst (1996)] and the wind resource offshore is much lager than onshore due to the large areas with high wind speeds. There are now nearly 700 wind turbines installed on numerous wind energy sites with a total capacity of about 287 MW. Britain's newest and Europe's largest wind farm has just opened in 1997 at Carno in Powys, Wales. It is designed to generate up to 33 MW, which will produce 15% of the country's total electricity consumption, contributing over 40% to electricity generation by the wind [CADDET (1997)].

1.2 Application of induction generators for stand-alone and embedded electricity generation

In general, a wind electricity generation scheme can be operated as a part of an autonomous power system or it can be connected to the national grid. The first solution appears to be particularly attractive for remote areas with relatively low density of population where a large grid construction or expansion is too costly to build, while the second approach is more attractive for developed countries with high density of population and well-established national power system. Depending on whether a wind electricity generation scheme operates on autonomous power system or as a part of the national grid, the problems that are encountered differ considerably, especially when an induction machine is used as electric generator.

Many electric machines have been considered for use in wind energy generation including DC machine, permanent magnet synchronous machine, synchronous machine with wound rotor, switched reluctance machine, wound rotor induction machine and cage induction machine [Catto (1996)].

A separately excited DC machine is very simple to control and this is its main good feature. However, it has a more complex construction and hence is more expensive in

comparison with induction machines. The presence of commutator and brushes that require regular maintenance is considered as a serious drawback because the wind turbines are often located in remote regions and will be off-shore in the future, where the air is salty.

Synchronous generators with excitation winding are generally used in high power applications above 1 MW because of their high efficiency. Their operation does not require presence of the utility grid and they do not need external reactive power source for magnetisation. Synchronous generators with excitation winding require more maintenance and are much more expensive than the induction generators.

Permanent magnet (PM) synchronous machine is attractive because of high efficiency, smooth torque production and high power factor, but PM machines are more expensive than induction machines. PM machines are not widely used at power levels greater than 20 kW due to the requirement for costly magnet material. Direct-drive variable speed wind energy systems (that eliminate the use of gearbox), based on a specially designed permanent magnet machine, are being developed [Spooner and Williamson (1996), Spooner et al (1996)].

Wound rotor induction machines allow the control of rotor current and hence the slip. They are therefore used in variable speed operation of large wind turbines [Pena et al (1996)]. The machine can be controlled by means of a power electronic converter placed in the rotor circuit. The required power rating of the converter is therefore smaller than when the converter is at the stator side. However, wound rotor induction machine has the high maintenance cost problem due to brushes and the slip rings and there is also the increased probability of rotor faults. When compared to a cage induction machine, the price and size of such machine for the same power rating is much higher because of the wound rotor winding and slip rings.

The switched reluctance machine has the following benefits: simple and reliable construction, control simplicity, higher efficiency compared to induction machine and theoretically it could be built to run at any speed. Switched reluctance machines in the

power range greater than 100 kW have not been built yet. Use of switched reluctance machines as generators in wind energy systems is still in early stage of development. It appears that switched reluctance machines are a promising alternative for high efficiency variable speed operation in the future[Abouzeid (1998)].

Squirrel-cage induction machines are simple, of low cost, robust, rugged and require virtually no maintenance. Induction machines as generators for low cost, reliable and efficient electric power generation from alternative energy sources are nowadays the most popular choice among many types of electric machines [Catto (1996), Ermis et al (1992), Singh (1995)].

The most important parameter that influences the feasibility of wind electricity generation is the amount of wind energy available at potential sites. The cubic relation between instantaneous wind speed and available energy means that if the wind speed doubles then the energy of the wind increases by a factor of eight. However the total energy output of a power plant strongly depends on wind electricity generation system design. Two options are in general possible, variable shaft speed and constant shaft speed operation of the generator.

Grid connected wind generation system in which a generator is directly connected to the utility grid forces the generator to run at a constant frequency and therefore at nearly constant speed. The generator will commonly be either an induction machine or a synchronous machine. The induction machines are much cheaper than the synchronous machines. The advantage of constant speed wind energy system is the simplicity and reliability. Up to now, the majority of wind turbines in operation run at constant speed in synchronism with the utility grid.

When the induction generator is externally excited by the power grid, the induction machine takes its excitation in terms of lagging magnetising current from the power grid to produce its rotating magnetic field necessary for generation. The induction machine starts generating when running above its synchronous speed, which is dictated by the frequency of the power grid and the number of poles in stator winding of the induction

machine. The generator generates active electrical power and supplies it to the power grid, while taking reactive power from the grid. The voltage and frequency at the terminal output are the same as the frequency and voltage of the power grid.

Unlike induction generators connected to the power utility grid, the major difficulty associated with an induction generator used in autonomous power systems as a stand-alone unit is that the induction machine does not have the inherent ability to produce the reactive power required for its excitation and by the load. Therefore, the reactive power required by the induction machine must externally be provided by a reactive power generator of some sort connected to the machine stator terminals.

A variable speed, squirrel-cage induction generator based wind energy conversion scheme has numerous advantages when compared with a constant speed conversion scheme [Ermis et al (1992)]. The most important advantage is better wind energy capture, yielding approximately 10% higher energy output for the same wind conditions. Another obvious advantage is that induction generator itself is cheaper than other types of generators. Other advantages are reduction of mechanical stresses and acoustic noise at low wind speeds. However, due to inherent lack of reactive power source within a squirrel-cage induction machine, an external reactive power source is always required.

The emphasis in this research is placed on utilisation of cage induction generator based variable speed wind electricity generation in autonomous power system. When the generator operates on autonomous power system, it is possible to utilise as reactive power source either a capacitor bank or a static VAr compensator. In either case, self-excitation of the machine has to occur first, followed by, if possible, constant flux operation regardless of the operating speed, driving torque and loading conditions. As self-excitation process and subsequent constant flux operation are entirely dependent on the shape of the magnetising curve of the machine, it is absolutely necessary to account for main flux saturation [Vas (1992)] in any analysis which encompasses variable speed operation of self-excited induction generator.

1.3 Static reactive power compensators

Static reactive power VAr compensator as a source of reactive power for the induction generator is the second important component of the system under consideration. There are four types of static VAr compensators that are commonly used [Gyugyi (1979)]:

1. Thyristor-controlled reactor (TCR).
2. Thyristor-switched capacitor (TSC).
3. Current source inverter (CSI).
4. Voltage source inverter (VSI).

Additionally, a bank of fixed capacitors connected in parallel or series with stator winding may be used under certain conditions. Shunt capacitors increase the power factor of an inductive load and can be used as reactive power source for an isolated induction generator. Series capacitors are used to compensate for the series inductance in the power system. The series capacitors reduce the system reactance and hence compensate for the voltage variation. However, the use of series capacitors can cause instability problems, that can be overcome by careful system design [Saad-Saoud et al (1995)].

Thyristor based static VAr compensators such as thyristor controlled reactor and thyristor switched capacitor provide fast, repetitive, in some cases continuous control of the effective fundamental frequency susceptance presented to the power system by a set of inductors and capacitors. The circuit topologies are based on the naturally commutated thyristors.

In thyristor-controlled reactor (TCR) scheme, a reactor and an anti-parallel connection of two thyristors are incorporated in each phase branch (Figure 1.4). The split arrangement of the reactor in each phase provides extra protection to the thyristor controller in the event of a reactor fault. The power is changed by controlling the current through the reactor by means of a valve with anti-parallel connected thyristors which

conduct on each half-cycle of the supply frequency. The duration of conduction interval is controlled by delaying in each half-cycle the firing angle of the thyristor valve in relation to the natural current zero. The current can be changed from zero to maximum lagging within one half-cycle. The TCR has a characteristic of continuously varied current, without steps, between zero and a maximum value corresponding to full conduction. The current is essentially reactive, lagging the voltage by ideally 90 degrees, so that reactive power can only be absorbed. Full conduction is obtained with a gating angle of 90 degrees. The effect of increasing the gating angle, from 90 degrees to 180 degrees (the firing angle range corresponding to the voltage peak and voltage zero crossing), is to reduce the fundamental harmonic component of current which is equivalent to an increase in the inductance of the reactor, reducing its reactive power as well as its current. Increasing the gating angle leads to a decrease of the power losses both in the thyristor controller and the reactor, but the TCR generates harmonic current as the current waveform becomes less sinusoidal. A TCR is used together with a fixed capacitor when reactive power generation is required. The fixed capacitor must be of higher rating than the inductor in order to provide variable leading VArs. Reactive power can then be changed within one half-cycle from maximum leading to maximum lagging or vice versa [Miller (1982)].

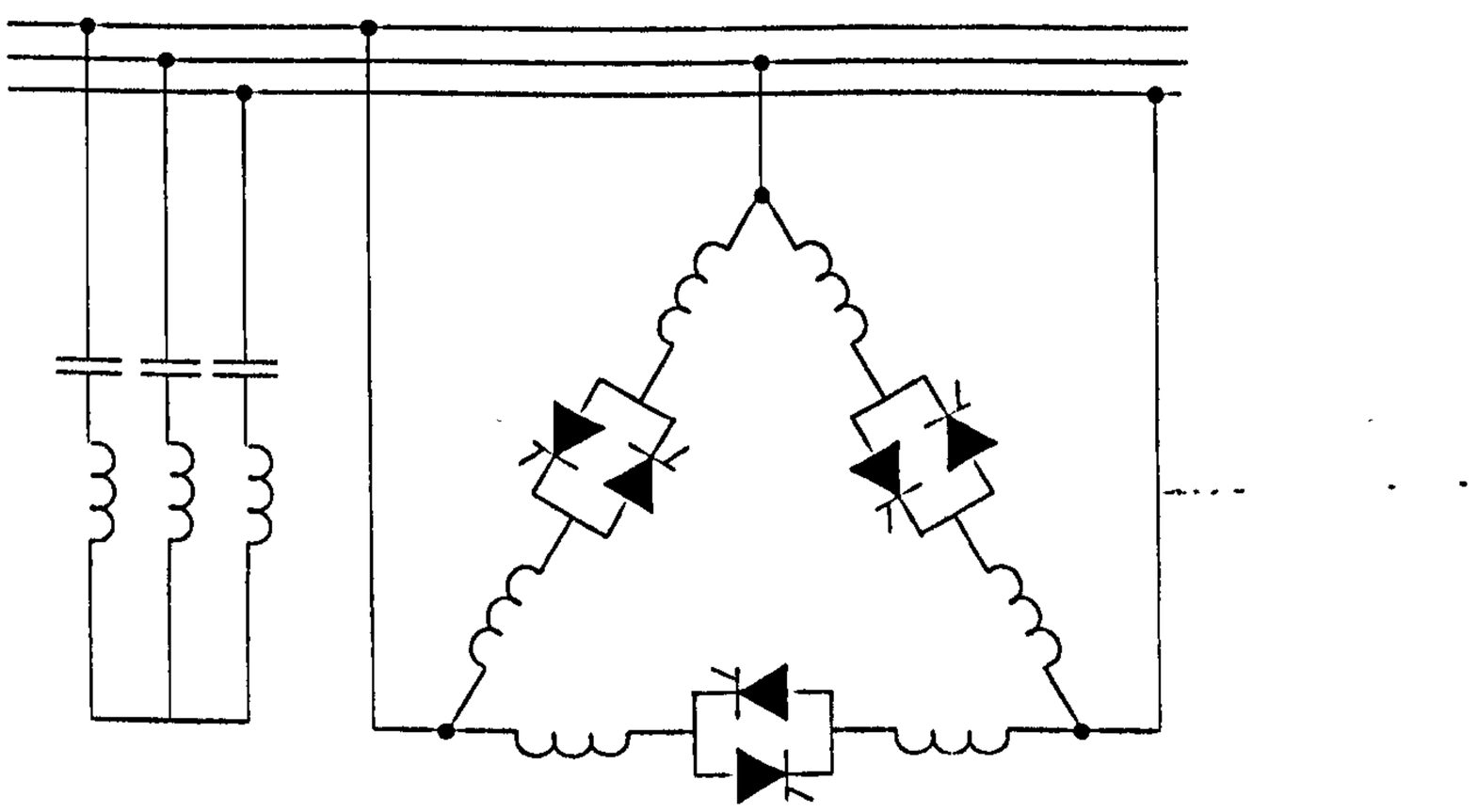

Figure 1.4 Three-phase thyristor-controlled reactor (TCR) compensator

In thyristor switched capacitor (TSC) scheme (Figure 1.5), a shunt capacitor bank is divided into a suitable number of branches depending on the maximum allowable step

change of reactive current. A small current limiting inductor (not shown in the figure) is used in series with each capacitor bank to limit the current. The controllable leading VAr for an a.c. system is provided by switching in or out appropriately dimensioned capacitor banks by means of the thyristor valves. Switching occurs when the a.c. voltage is equal to the pre-charge voltage across the capacitor bank, thus providing almost transient-free switching due to natural zero crossings of the capacitor current at the instants of switching. It takes at least one cycle for switching in a non-conducting capacitor bank and at least one half-cycle for switching out a conducting capacitor. There are no harmonics generated. The disadvantage of TSC scheme is that the VAr compensation is not continuous [Miller (1982)], each capacitor bank requires a separate thyristor switch and it is not economical for high-voltage application unless a step-down transformer is used.

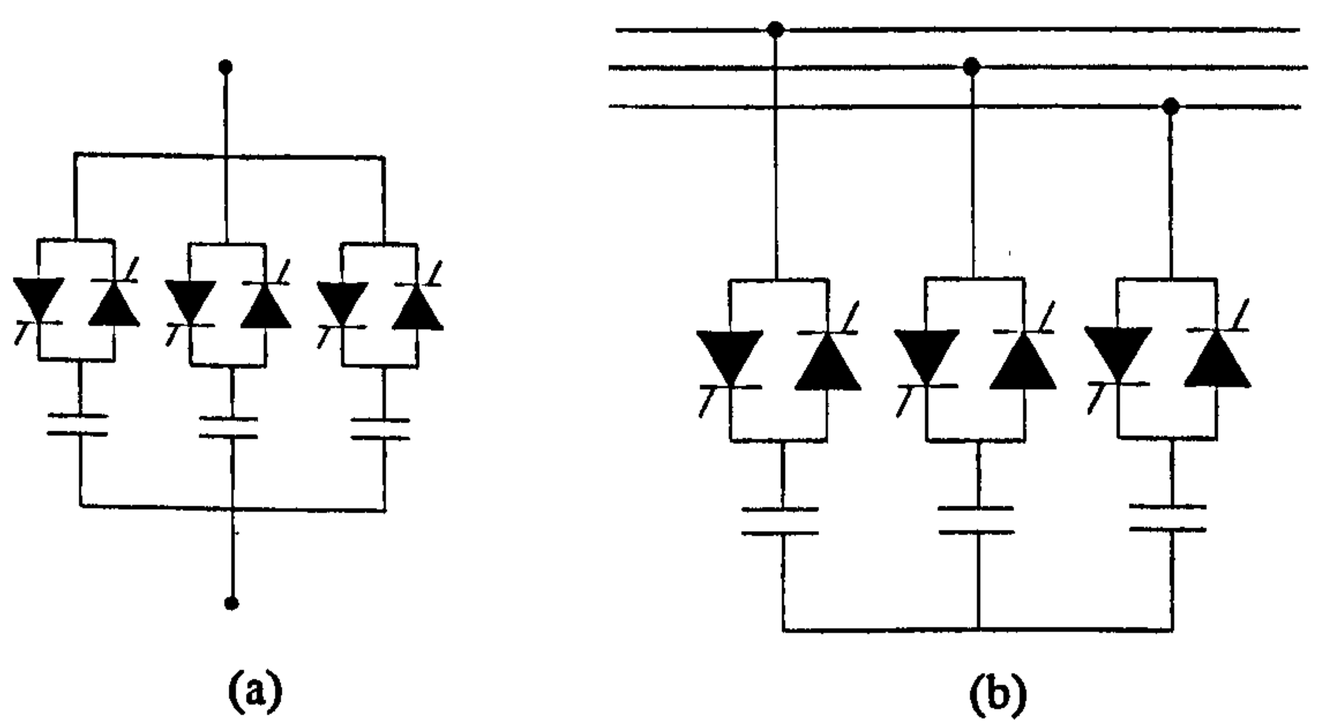

Figure 1.5 Single-phase three-stage (a) and three-phase single-stage (b) thyristor-switched capacitor (TSC) compensator

With a combined TSC/TCR compensator (Figure 1.6), continuous variable reactive power is obtained throughout the complete control range as well as the full control of both the inductive and the capacitive parts of the compensator. The maximum reactive power that can be absorbed is equal to inductor reactive power rating while the maximum leading power that can be supplied corresponds to the sum of all the capacitor ratings. This combination significantly reduces the inductor rating as the total capacitance is subdivided into small units. This is an advantageous feature permitting optimum performance during large voltage disturbances in the power system as all the capacitors can be switched out of the system. However, the combined device is more

expensive than a single device although the reactor rating is reduced.

The thyristor controlled compensators consist of energy storage components such as inductors and capacitors which enable production or consumption of reactive power. They cannot provide instantaneous VAr control because of their inherent time delays [Gyugyi (1979)].

Reactive power compensators, described so far, are predominantly used at transmission and distribution voltage levels within power systems. Their limited speed of response makes them inappropriate for use in variable speed induction generator based autonomous power systems. It is for this reason that the three topologies introduced in the preceding text, will not be considered in any greater depth in the remainder of the thesis.

Current source type inverter (CSI) and voltage source type inverter (VSI) based static VAr compensators (SVCs) function as controllable a.c. current and voltage sources. The force commutated CSI can provide both leading and lagging VArs since it is capable of operating over the firing angle range 0-360° and the magnitude of the a.c. line current can be controlled by adjustment of the firing delay angle. However the response time of this type of SVC is slow since current through an inductor cannot be changed instantaneously. Additionally, it introduces considerable amount of harmonic currents into the system as the current reflected in the mains is the worst case quasi square-wave [Gyugyi (1979)].

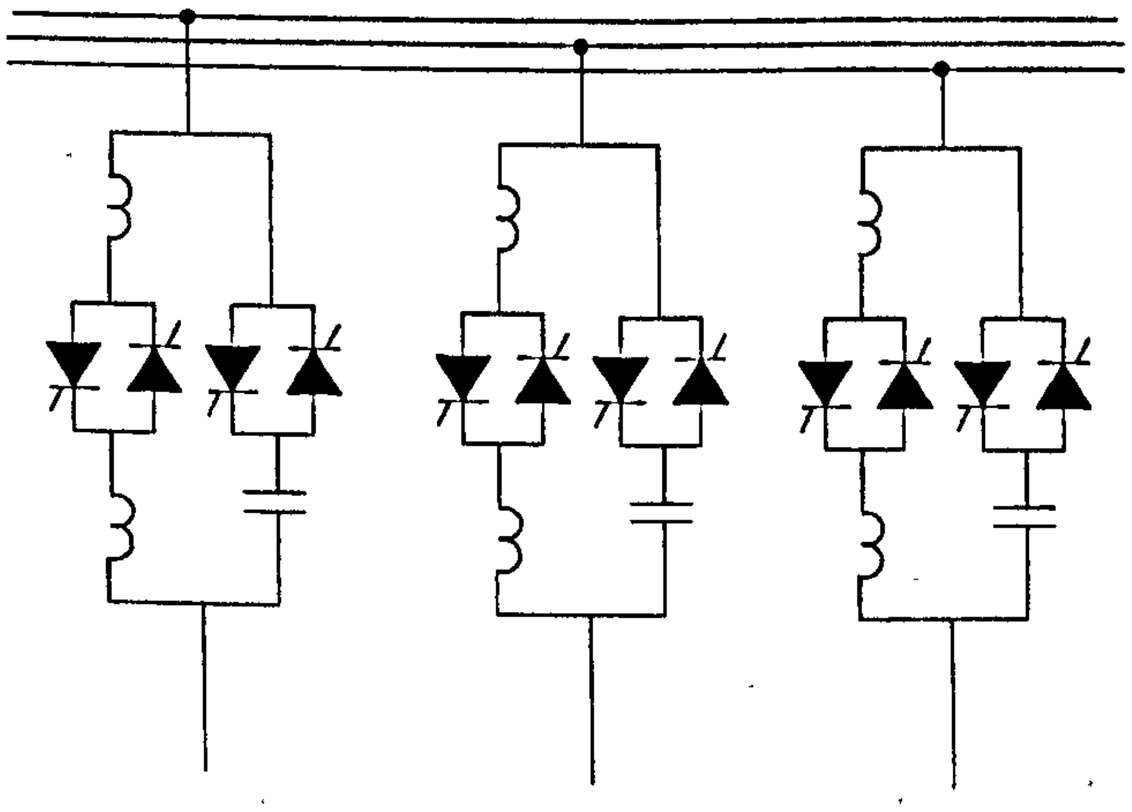

Figure 1.6 Three-phase combined TSC/TCR compensator

When a voltage source inverter is used, the reactive power can be controlled from full leading to full lagging by controlling the amplitude of the output voltage and it can provide continuously variable leading and lagging VArs without using large energy storage components. The fundamental harmonic of the inverter output voltage is controlled to be in phase with the system voltage, so that only reactive currents flow through the inductance between the network and the inverter. When inverter voltage is higher than the network voltage, reactive current is delivered to the network. When the inverter voltage is smaller than the network voltage, reactive current is drawn from the network. The rating of the d.c. side capacitor is typically 20% of the rating of conventional SVCs [Craig and Davidson (1995)]. This gives a substantial reduction in size which is particularly important at higher ratings.

VSI, operated in pulse width modulation (PWM) mode with high switching frequency, enables very fast control of the converter so that it reacts to the demand change practically instantaneously. High frequency PWM scheme of SVCs eliminates the harmonics generated by the compensator itself as the inverter is interfaced with the power system through interconnecting inductors or interconnecting transformers so that the current harmonics that are injected into the system are of high frequencies and very small amplitude. The PWM VSI based SVC compensator appears to be the most attractive option [Gardner (1996)] and is therefore reactive power source predominately dealt with in the thesis.

1.4 Aims of the Research

1.4.1 Research objectives

The PhD project deals with so-called variable speed wind energy generating system, aimed at supplying an autonomous power system. The major components of such a system are an induction generator, a static reactive power compensator and an associated control circuitry. As optimal variable speed operation of an induction generator results only if flux is kept at constant value, the role of control is to achieve such an operation under varying operating conditions. As flux is to be kept at constant

value during both transient and steady-state operation, application of advanced static reactive power compensators and advanced control techniques is mandatory. The main objectives of the project can be summarised as follows:

- Investigation of induction generator self-excitation with reactive power being provided by capacitor bank and by static VAr compensator of VSI type
- Investigation of load voltage variation compensation for stand-alone induction generator using an additional auxiliary series capacitor bank, apart from the main parallel capacitor bank
- detailed experimental investigation of the induction generator self-excitation and load voltage variation compensation, using fixed capacitor banks, with emphasis on variable speed operation
- Investigation of scalar control of a PWM voltage source inverter based reactive power compensation
- Investigation of current control strategies for static VAr compensator of current controlled PWM voltage source inverter type
- Investigation of stator flux oriented control in conjunction with control of the induction generator and static VAr compensator
- Investigation of rotor flux oriented control in conjunction with control of the induction generator and static VAr compensator

1.4.2 Originality of the research

Application of variable speed induction generators in wind energy generation systems is a rather new research topic, which has attracted significant attention of the research community worldwide only recently. One specific aspect, investigated in this thesis, is application of such generating plants in as stand-alone units in autonomous power systems. Original research results, arrived at during the course of the project, constitute major portions of Chapters 4, 5, 6, 7 and 8. The original contributions of the thesis can be summarised as follows:

1. Investigation of the self-excitation process, using fixed capacitor bank, in doubled-cage induction machines by means of reduced-order single-cage induction machine model.
2. An experimental investigation of the self-excitation process, using fixed capacitor bank, under variable speed operating conditions, and experimental evaluation of load variation compensation using additional series capacitor bank.
3. Development of the an original implementation of the voltage source inverter model in MATLAB/SIMULINK environment.
4. Detailed simulation analysis of performance of an induction generator with voltage source inverter type of reactive power compensator with scalar method of inverter control, with the emphasis placed on variable speed operation.
5. Development and verification by simulation of a novel stator flux oriented control scheme for an induction generator with reactive compensator of current-controlled voltage source type.
6. Development and verification by simulation of a novel rotor flux oriented control scheme for an induction generator with reactive compensator of current-controlled voltage source type.
7. Development of a novel, saturated adaptive, rotor flux estimator.

1.5 Organisation of the thesis

The thesis is divided into nine chapters. The first Chapter highlights the importance of alternative energy due to increasing concern for environmental damage caused by the uncontrolled emission of greenhouse effect related gases from conventional power stations, explains why an induction machine is the most popular generator for reliable, efficient and low-cost electric power generation from alternative energy sources, and introduces the concept and need for static reactive power compensation in the autonomous power system in which the induction generator is a stand-alone unit.

A thorough literature review of schemes for reactive power compensation of induction generators has been undertaken and is summarised in Chapter 2. Compensation schemes using a capacitor bank, current source inverters and voltage source inverters are

described with emphasis on a PWM voltage source inverter based reactive power compensator. Aspect of embedded systems are reported as well although the research project concentrates on the induction generators applied in autonomous power systems.

Chapter 3 explains the need for utilisation of saturated induction machine models and further details mathematical modelling techniques for saturated single-cage and double-cage induction machines. A simplified single-cage representation of saturated double-cage induction machines is developed and described.

Self-excitation of induction generator by means of a capacitor bank has been analysed both experimentally and by simulation for a single-cage and for a double-cage induction machine and results of no-load self-excitation and loading transients for both single-cage and double-cage induction machines are given in Chapter 4. Load voltage variation compensation for stand-alone induction generator using an additional auxiliary series capacitor bank, apart from the main parallel capacitor bank, has also been investigated. Chapter 4 concludes with results of the experimental study of induction generator operation with capacitor based reactive power compensation.

Chapter 5 deals with modelling and simulation of static reactive power compensator based on a PWM voltage source inverter. Detailed model implementation using SIMULINK package is presented. Simulation results related to operation of a single-phase and a three-phase PWM voltage source inverter for different operating conditions are shown.

Chapter 6 focuses on the scalar control scheme with a PWM VSI reactive power compensator for the stand-alone induction generator system. Simulation results are given and the disadvantages of this control scheme are addressed.

Various vector control techniques aimed at providing constant flux operation of induction generator are examined next. Chapter 7 deals with stator flux oriented control of a PWM VSI reactive power compensator for a stand-alone induction generator. The design of stator flux and d.c. link voltage control loops is outlined. The design of current

controller and the stator flux estimator is presented. Simulation results showing dynamic performance of the system operating in base speed region and in the field weakening region are given.

Chapter 8 describes the control a PWM VSI reactive power compensator in a reference frame aligned with rotor flux space vector for a stand-alone induction generator. A rotor flux control strategy based on the direct field orientation approach is developed. Development of a novel, saturation adaptive rotor flux estimator is presented. Simulation results of self-excitation, load application and speed variation both in base speed region and in field weakening region are given, for two specific loading situations: load placed at a.c. side of the inverter and load placed at d.c. side of the inverter.

The thesis concludes with chapter 9, which contains conclusions that have been drawn from this study and recommendations for future work.

Chapter 2

REVIEW OF SCHEMES FOR REACTIVE POWER COMPENSATION OF INDUCTION GENERATORS

2.1 Three-phase parallel capacitor bank

The phenomenon of self-excitation in induction machines has been known for many years. When induction generators are used to supply electricity to autonomous power systems, self-excitation of the induction generators must be provided and maintained throughout the operation. Self-excitation of induction generator can occur when the machine is driven at certain speed and an external reactive power source is provided by a capacitor bank or a static VAr compensator. Self-excitation is most frequently achieved by the use of a capacitor bank connected in parallel to the induction generator stator terminals [Elder et al (1983)]. In this case, self-excitation depends on the value of capacitance, speed of rotation and the load. As self-excitation is dependent on the operating point at the magnetising curve of the machine, non-linearity of the magnetising circuit has to be accounted for in any analysis.

The analyses of self-excitation of induction generator using a capacitor bank have been extensively covered in literature. The per-phase equivalent circuit of an induction machine has been used for study of steady-state performance of self-excited induction generators with a capacitor bank. Murthy et al (1982), Malik and Al-Bahrani (1990) have adopted the loop-impedance method. They have derived polynomials from loop equations of equivalent circuit of the induction machine. Two non-linear simultaneous equations in terms of per unit frequency and magnetising reactance are obtained by equating the real and imaginary parts of the complex loop impedance to zero. The obtained non-linear equations are arranged for unknown variables such as magnetising reactance and frequency, while the rest of the machine parameters and operating regime are considered to be constant. Newton Raphson numeric method is used for solving

these equations. The steady-state performance of the self-excited induction generator is computed for the given value of the capacitance, load and speed. Unlike the above methods which need the separation of real and imaginary components of the complex impedance and need different models for different types of loads and capacitor connection configurations at the machine terminals, a method, based on the impedance of equivalent circuit considering the core loss of the induction machine, has been reported by [Singh and Jain (1995)] where the evaluation of steady-state performance of self-excited induction generator is formulated as multivariable unconstrained non-linear optimisation problem. The optimisation problem is solved employing numeric technique, Rosenbrock' methods of rotating coordinates, to calculate performance of self-excited induction generators in steady-state operating conditions. Quazene and McPherson (1983) and Chan (1993) have proposed the nodal admittance method. In the method proposed by [Quazene and McPherson (1983)], the admittances connected across the air gap nodes are considered. A polynomial in terms of per unit frequency is obtained by equating the sum of real parts to zero, while the magnetising reactance can be determined by equating the sum of imaginary parts to zero using the value of per unit frequency. Based on the nodal admittance method applied to the equivalent circuit model, Chan (1996) develops a simple iterative method to determine the per unit frequency of self-excitation, where only simple algebraic manipulations are involved and the complete equivalent circuit is solved. A circle diagram approach based on the induction machine equivalent circuit has been used by Muljadi et al (1993) to illustrate the operation of an isolated induction generator. The changes of the operating condition of self-excited induction generator can be visualised from the admittance diagram as the parameters, such as capacitance and load resistance, are changed.

There is a minimum and maximum capacitance requirement to sustain self-excitation for a specific rotor speed and load. Numerous numerical methods based on steady-state equivalent circuit models have been proposed to find the minimum capacitance for self-excitation of induction generator by solving non-linear simultaneous equations. Malik and Mazi (1987) have proposed an indirect method that requires initial guess in a trial-and-error procedure to find the minimum capacitor value required for self-excitation. Al Jabri and Alolah (1990), Chan (1993), Chakraborty and Bhadra (1996) have presented a

direct method to compute minimum capacitance for self-excitation. Malik and Al-Bahrani (1990) and Chan (1993) have tried to find the maximum value of capacitance as well. Wang and Lee (1997a) proposed a new method based on eigenvalues and eigenvalue sensitivity analyses, instead of solving a non-linear polynomial, to determine both minimum and maximum capacitor values for induction generator self-excitation. While most of the analyses are based on per-phase equivalent circuit model, a method for predicting the minimum values of capacitance, necessary to initiate self-excitation, using the d-q axis model has been proposed by Grantham et al (1989) and Teissier et al (1992).

The per-phase equivalent circuit approach, valid for a steady-state condition, can not be used for studying transient behaviour of a self-excited induction generator. Transient analysis of stand-alone self-excited induction generators has received considerable attention for many years. Small signal saturated machine models [Melkebeek (1983a)] have been used, where the effect of saturation is taken into account by computing the saturated magnetising inductance and dynamic inductance. In the corresponding large signal mode, machine currents are again selected as state-space variables and differential equations are solved considering the ratios of magnetising flux to magnetising current and derivative of magnetising flux with respect to magnetising current as instantaneous and incremental values of the magnetising inductance [Levi and Rauski (1993), Vas (1992)]. In other case, flux linkages in the machine are selected as state-space variables in the analysis of transient performance of self-excited induction generators [Sakkoury et al (1993)].

2.2 Voltage source inverter

The static VAr compensators mentioned in Chapter one, namely, TCR, TSC and combined TCR and TSC, function as variable inductance and variable capacitance. In contrast to this, voltage source inverters and current source inverters can be used as static VAr compensators that function as controllable a.c. voltage source or controllable a.c. current source. The power switches in the compensator operate as force commutated devices and the instant of turn-on/turn-off of the semiconductor devices can be

controlled. The power electronic circuits implemented in the compensator are capable of operating as both a rectifier and as an inverter.

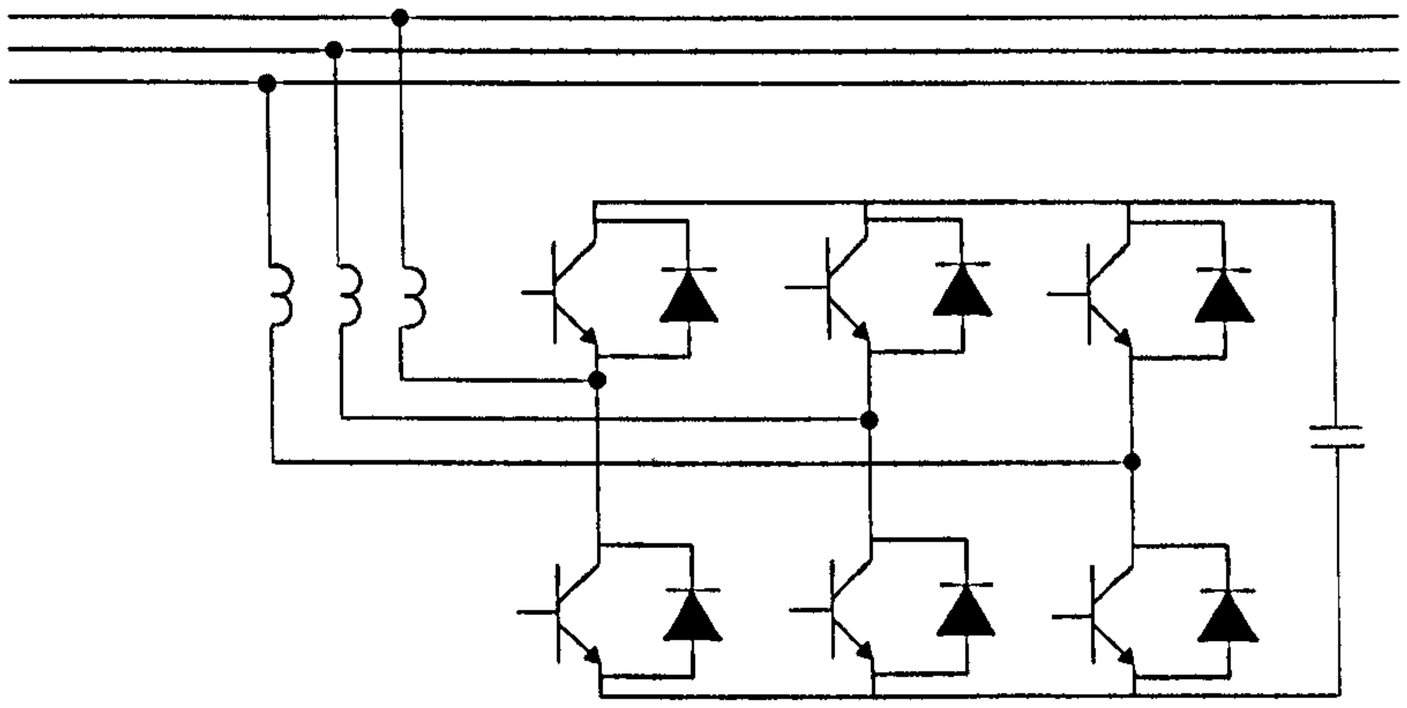

Figure 2.1 Three-phase voltage source inverter based static VAr compensator

A three-phase voltage source inverter (VSI), connected to the power utility grid, is shown in Figure 2.1. A diode is connected in parallel with each power switch and the capacitor on the d.c. side can be replaced with a battery. The inverter output is connected to the grid through a set of three-phase inductors or through an interfacing transformer. The voltage source inverter operates in 180 degrees conduction mode (six-step mode) so that at any instant time three switches are on. The inverter output voltages are kept in phase with the grid voltage for purely reactive power flow. The reactive power can be controlled from full leading to full lagging by controlling the amplitude of the inverter output voltages. Reactive power will flow from the inverter to the grid if fundamental harmonic of the inverter output voltage is greater than the system voltage; reactive power will flow from grid to the inverter if fundamental harmonic of the inverter output voltage is smaller than the system voltage. The current will be either leading or lagging and the magnitude of the current depends on the voltage difference between the grid and the system, and values of inductors inserted between the grid and the inverter. If the inverter output voltages are kept in phase with the grid voltages, the inverter absorbs no real power from the grid. Therefore a d.c. source, like a battery, would have to be used to cover the inverter losses. However a capacitor can supersede the battery and each inverter output voltage can be made to lag slightly the corresponding grid voltage. Then a real component of current flows from the grid to the inverter and the internal losses in the inverter will be covered by the a.c. system instead

of d.c. source. In this case, there is active power flow from grid to the d.c. side of the inverter, while reactive power can flow in either of the two directions.

In order to improve the harmonic content of the inverter output voltages (harmonics of the order 5,7,11,13 and so on are present when inverter is operated in six-step mode), a number of inverters, connected in parallel at the d.c. side, are used. All the inverters operate in six-step mode and the output voltages of the inverters are shifted one with respect to the other. Six voltage source inverters can be used [Sumi et al (1981)] and the resulting output waveform obtained at the output is a 36-pulse waveform instead of a six-pulse waveform which results with a single inverter. A 48-pulse multiple inverter system based on GTO devices has been reported in [Mori et al (1993)]. The multiple inverter configuration is usually applied in high power applications of reactive power compensators.

The modern approach to static reactive power compensator design is the use of pulse width modulation (PWM) technique for control of inverter output voltage and frequency. VSI SVCs operated in PWM mode provide the possibility to generate compensating current with response times much faster than the fundamental power frequency cycle [Van Wyk et al (1986)]. The application of PWM controlled voltage source inverter reduces harmonic content of the currents injected into the power system. Harmonic content of the PWM voltage waveform depends on the switching frequency of the inverter. Higher frequency PWM leads to generation of harmonics in the inverter output voltages of higher frequency. At high switching frequencies, the current harmonics injected into the network are greatly attenuated by the interfacing reactors. Only current harmonics of high frequency and small amplitude are injected into the network. However, increasing the inverter switching frequency will increase the inverter switching losses as well.

A well-known method of PWM is the sinusoidal PWM where three-phase sinusoidal reference voltages are compared with a triangular carrier wave of fixed frequency and fixed amplitude. The inverter voltage outputs contain the frequency and fundamental component equal to the reference sinusoidal signal. By varying the modulation ratio

(i.e., varying the amplitude of the reference sine wave), amplitude of the fundamental output voltage is varied, hence the reactive power flow can be controlled. In order to provide reactive power flow from the inverter to the mains, it is necessary that the value of d.c. voltage at the inverter d.c. side is sufficiently high so that the fundamental harmonic at the inverter output can be made greater than the power system voltage.

It is possible to build VSI type compensators without energy storage components if reactive power compensation is implemented on the basis of instantaneous reactive power rather than the fundamental reactive power compensation in steady-state. An instantaneous reactive power compensator based on current controlled PWM VSI was reported by [Akagi et al (1984)]. Instantaneous reactive power compensation is provided using hysteresis current control technique where the current references are calculated without time delay by using the instantaneous voltages and currents on the load side. The system requires very small value of capacitors while still providing full reactive power compensation in both transients and steady-states. Three-phase inverter is not suitable for unbalanced loads although it can handle some degrees of unbalance in the three-phase system. In the case of three-phase unbalanced loads, three single-phase PWM VSIs building a three-phase unit should be used, with each single-phase inverter providing independent reactive power control for each phase.

2.3 Current source inverter

A three-phase current source inverter (CSI) is given in Figure 2.2 where the commutation circuit is not shown. The CSI without commutation circuit operates as thyristor bridge rectifier and is capable of supplying only lagging VAr [Gyugyi and Taylor (1979)]. The CSI with the commutating diodes and capacitors is capable of providing both leading and lagging VAr. The d.c. side consists of an inductor in which the resistance of the choke is not shown. If the inductance of the choke is high enough then the current at the d.c. side is almost constant. For lagging VAr operation, the line currents lag the mains voltage by an angle equal to the firing delay angle. If pure inductor is assumed at the d.c. side, the average voltage at the d.c. side must be kept at zero at all time, then the firing angle must be equal to 90 degrees for lagging VAr

operation. In practice, the firing angle is less than 90 degrees so that enough d.c. voltage is provided to cover the losses in the choke resistance and in semiconductors. For leading VAr operation, the inverter input currents lead the mains voltage by 90 degrees. In practice, the firing angle is advanced, with respect to the earliest point of natural commutation, slightly less than 90 degrees in order to establish and maintain the d.c. current in the inductor. The magnitude of the d.c. current and the amplitude of the a.c. current can be controlled by adjusting the firing delay angle. CSI can provide both leading and lagging line currents since the forced commutated converter can operate over the firing angle range from 0 to 360 degrees.

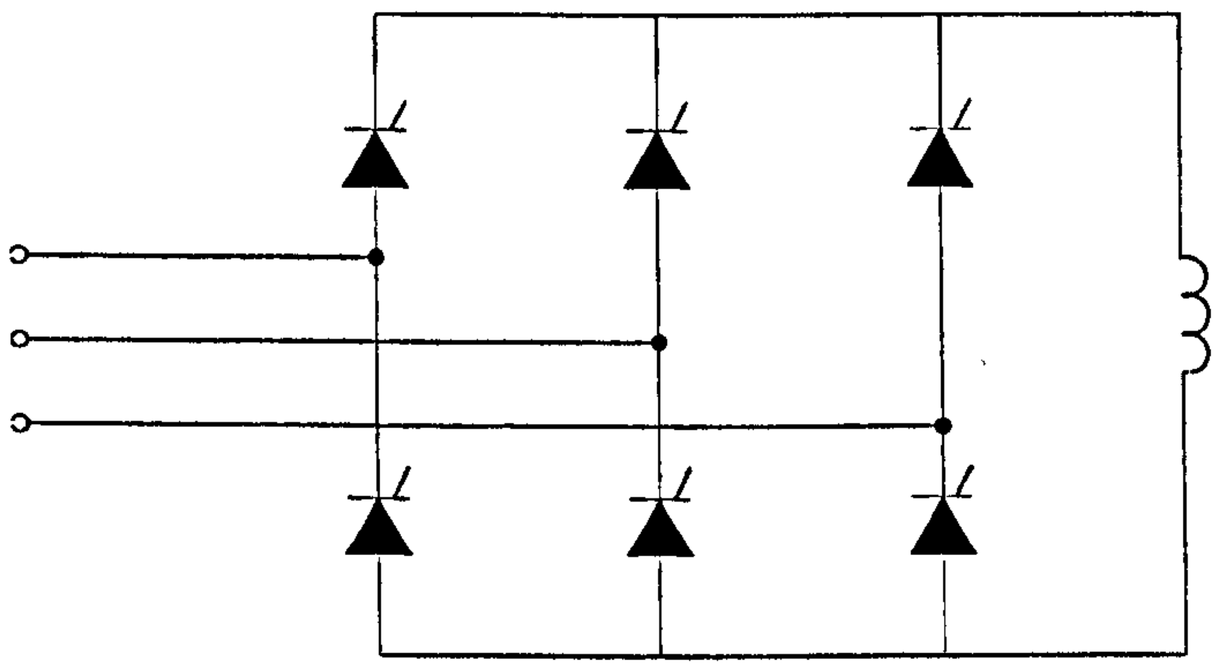

Figure 2.2 Three-phase current source inverter

In practice, it is unnecessary to have a high value of inductance. If a smaller value of inductance is chosen then the fundamental component of the line current will be smaller resulting in smaller corresponding reactive power. In a study on optimising the value of the choke inductance [Alexandrovitz et al (1984)], it is indicated that the choke inductance appears to be necessary to assure operation of the compensator over a wide range rather than for compensation capability. The choke inductance can be greatly reduced in a three-phase circuit as energy storage components are not required for reactive power compensation. Dynamic performance of CSI type static VAr compensator is similar to the fastest TCR compensators. It is indicated in [Walker (1986)] that static VAr compensator based on CSI is slightly faster in response than TCR in lagging mode and slightly slower in leading mode of operation. This is the shortcoming of current source inverter and is due to the fact that current flowing through the inductor can not be changed instantaneously. The harmonic currents of order 5th and

7th can be very high when the inverter operates in six-step mode. Two inverters can be connected in a 12-pulse configuration to reduce the harmonics [Walker (1986)].

2.4 Compensation schemes for stand-alone applications

An induction machine used as an autonomous generator requires a reactive power supply to magnetise the machine. The reactive power is supplied by either a capacitor bank or a static converter connected to the machine terminals. The solution using a capacitor bank is the most common, the simplest and gives satisfactory results under certain conditions. Such a solution is acceptable if generator speed is reasonably constant, so that a single capacitor bank can be used. When self-excited induction generators with a bank of capacitors connected to the machine terminals run at variable speed, the value of capacitance required for self-excitation is almost inversely proportional to the square of the prime mover speed [Salama and Homles (1996)]. So large values of capacitance are required at low speeds. Furthermore capacitance has to be varied as function of speed. Capacitor bank is therefore not suitable for variable speed operation of wind generation systems. An adjustable VAr generator connected to the stator terminals is necessary. A TCR reactive power compensator can be used [Uctug and Demirekler (1988)]. But the control of reactive power is tedious and is not continuous.

Novotny et al (1977), Melkebeek and Novotny (1983) presented a detailed study of self-excited induction generator operation using either current source inverter or voltage source inverter, both operated in six-step mode. Comparison of different converters and steady-state analysis has been carried out to study the conditions under which the voltage can be sustained and the effects of parameters like stator and rotor resistances, slip, nonlinearity of magnetising curve and load resistance on the output voltage have been investigated. A system consisting of a d.c. capacitor connected to the induction generator through a PWM voltage source inverter was proposed by Bhadra et al (1996) and Leplat et al (1996), where the d.c. load was connected across the capacitor. The dynamic analysis indicated that it is possible to maintain constant d.c. voltage over a wide range of prime mover speeds and loads by controlling inverter frequency and the

modulation index without the need for change of capacitor value. However, the system is very sensitive to rotor speed and load variation as it is an open loop system. A single-phase induction generator excited by a battery-fed PWM voltage source inverter and by a current controlled voltage source inverter have been reported by Ojo and Gonoh (1996) and by Mucko and Gientkowski (1994), respectively. Margato and Santana (1996) present a study of an induction generator excited by a current source inverter. Their conclusion is that good performance is only achieved by current or voltage closed-loop control.

Kragset and Nilssen (1994) proposed a simple control method for excitation of induction generators with PWM converter where only the d.c. link capacitor voltage is measured and used as input for the control. The system configuration is the same as in Bhadra et al (1996) and Leplat et al (1996), except that closed-loop power control is used. The active and reactive power flow in the induction generator are controlled by varying the stator voltage frequency. It is noted that a large value of capacitance must be used in the PWM converter.

Vector control techniques have recently been applied to the control of PWM voltage source inverter in conjunction with stand-alone induction generators. Both stator flux oriented [Silva and Lyra (1993), (1995), Lyra et al (1995)] and rotor flux oriented control [Jacobina et al (1996), Colliez et al (1997)] are applied with flux space position calculation using either indirect method or a variety of direct schemes. The PWM voltage source inverter is operated with either current control in stationery reference frame [Silva and Lyra (1993), (1995), Lyra et al (1995)] or in rotational reference frame [Jacobina et al (1996), Colliez et al (1997)]. Methods of obtaining instantaneous flux space vector spatial position include stator flux position calculation from measured stator voltages and currents [Silva and Lyra (1993), (1995)], rotor flux position estimation using indirect feed-forward approach [Jacobina et al (1996)] and rotor flux position calculation from measured stator currents and rotor speed. Vector controlled induction generator operated in variable speed mode can be used to supply an autonomous power system consisting of either a.c. load [Lyra et al (1995), Miranda et al (1997)] or d.c. load [Silva and Lyra (1993), (1995)].

2.5 Compensation schemes for embedded generation

When the induction generator is used for embedded generation, the voltage and frequency at the stator terminals are the same as the voltage and frequency of the utility grid to which the generator is connected, provided that interfacing of generator to the grid is direct. The reactive power required by the induction generator for excitation is supplied by the utility grid and the generator returns real power to the utility. The induction generator output frequency depends on the rotor speed. For the constant frequency of 50 Hz dictated by the utility, the induction machine must be operated in a very restricted speed range.

Variable speed operation of induction generators is preferred in order to capture maximum energy over a wide range of speed. In applications such as wind energy conversion systems, the wind turbine drives the induction generator which generates three-phase voltage at a frequency dependent on wind speed. The induction generator must be interfaced with the utility grid by means of power electronics, i.e., a.c.-d.c.-a.c. conversion or a.c.-a.c. conversion [Simoes and Bose (1997)]. In the a.c.-d.c.-a.c. conversion system, the variable frequency a.c. voltages are at first rectified into d.c. voltage. Next, the second converter, a d.c.-a.c. converter is used to provide a.c. voltages at utility frequency. The rectifier can be either controlled or uncontrolled. In the case of an uncontrolled rectifier, a d.c. chopper may be used to maintain the d.c. link voltage at constant value, while the reactive power is furnished by adding a capacitor bank at the machine terminals.

Uncontrolled rectifiers or line-commutated converters are not appropriate for use as line-side converters due to the fact that their power factor decreases when the firing angle increases. Furthermore the 5th and the 7th harmonic of the line currents are relatively high as they are six-pulse phase controlled converters. To tackle the problem, a force-commutated line-side converter, based on advanced power transistors like IGBTs to achieve fast switching and minimum harmonic distortion, should be used. By controlling the line-side converter, the voltage and the frequency at the inverter output terminals can be kept constant regardless of the rotor speed and the load. The PWM

voltage source inverter appears to be the most attractive due to its excellent dynamic performance and the possibility of power factor control. The high performance of PWM inverter is possible only if the d.c. voltage at the inverter input terminals is kept constant.

Jones and Smith (1993) have proposed an embedded generation system where a wind turbine driven induction generator is interfaced to the utility grid using two back-to-back vector controlled PWM voltage source converters. The generator side converter is vector controlled. The advantage of utilisation of vector control technique is that it allows the separate control of active and reactive power. The PWM converter is controlled in such a way that the active power is consumed in order to maintain a constant d.c. link voltage, while the reactive power necessary for magnetisation is supplied to the induction generator. The network side converter operates as a sinusoidal rectifier and is controlled using pulse width modulation technique. The control scheme is intended to achieve unity power factor supply to the network as the network side converter can produce leading and lagging VArs by adjusting the reactive power reference. The implementation of such system on a wind turbine has later been reported by Jones and Gilmore (1995). The use of vector controlled cage induction generator has the advantages of wide speed range, good overloading capacity and fast torque response. The additional good feature is very low harmonic content of the current being injected into the network compared with the case using a six pulse phase controlled converter. In a similar study reported by Hayakawa et al (1993), an even better quality of three-phase a.c. voltage or a.c. current (5th harmonic current = 0.4925% of the amplitude of the fundamental current) has been achieved, by using current control technique for both the generator side converter and the line-side converter. Additionally, the d.c. link voltage is controlled to an almost constant value against the rotating speed from stop to rated point, with the aid of energy storage battery combined with solar-photovoltaic system and fuel cell systems.

2.6 Other possibilities

Solutions for reactive power compensation, reviewed in Section 2.1 to Section 2.5,

apply to the case when induction generator is of cage-type. If the induction machine is of wound-rotor type, then some other solutions exist as well. In particular, so called doubly-fed induction generators (DFIG) can be used [Pena et al (1996)]. The advantage of such a system is the reduction in power rating of the rotor side converter (a fraction of generator power rating, which depends on the operating speed range of the generator), but the increased cost and maintenance requirements for the slip ring system of wound rotor induction machines may outweigh the reduction in rating and cost of the power converters. Two configurations for embedded systems using Static Kramer and Static Scherbius schemes are reported. In the Kramer scheme, a diode rectifier and a line-commutated converter are used between the rotor and the stator of the DFIG and the operation of the generator is restricted to subsynchronous speeds. Two back-to-back converters connected between the rotor and the stator of the generator are used in the Scherbius scheme where the operation of the generator can be extended to supersynchronous speed. The Scherbius scheme can be implemented using two back-to-back vector controlled PWM voltage source converters in order to reduce the harmonics generated into the utility grid and to control the system power factor [Pena et al (1996)].

Another method of variable speed constant frequency operation, applicable in conjunction with doubly-fed induction generator, is the use of a direct matrix converter to avoid two-stage power conversion (a.c.-d.c.-a.c.) and costly energy storage components in the d.c. link [Zhang et al (1997), Zuckerberger et al (1994), (1996)]. Matrix converters are still in the development stage and the problems associated with requirement for a switch with bi-directional current flow are likely to prevent their wider application in near future.

As this thesis is primarily concerned with squirrel-cage induction generators, schemes specifically developed for DFIG are not considered further on.

2.7 Load types in stand-alone applications

The common application of stand-alone systems is to provide electrical supply in remote areas. Self-excited induction generators using capacitor bank connected at the

machine terminals are particularly useful in the situations where frequency regulation is not a requirement, such as lighting, resistive heating and water pumping for irrigation or drinking. In these cases the generator supplies a.c. loads. These systems are reliable, simple to operate and have low capital cost and minimal maintenance.

The common stand-alone application in the developing countries has been water pumping, especially on remote farms. An economic solution to the energy storage problem is the utilisation of variable speed operation of induction generator directly applied to water pumping [Shaltout (1995), Miranda et al (1997)]. The system consists of a wind-driven induction generator directly feeding an induction motor without any power electronic converters. The generator is driven by a wind turbine and the motor is driving a water pump.

Another possible application of the stand-alone system is a plant comprising a self-excitation induction generator that charges a storage battery by means of an a.c.-d.c. converter. The feeding of remote loads is provided in parallel with the battery charging. The energy of the battery is delivered to the users when the generator does not produce sufficient energy. Two conversion topologies, using a thyristor bridge [Gerlando et al (1994)], and using a diode bridge and chopper [Dezza et al (1995, 1997)], have been studied. It is shown that the solution using a controlled thyristor bridge allows a wider speed range and a higher battery recharging energy, while the solution using a diode bridge and chopper provides better control of the static conversion system.

Self-excited induction generators can be used as a d.c. power supply source to feed remote d.c. loads. Margato and Santana (1996) present a d.c. power supply source comprising an induction generator, a current source inverter and a diode bridge. The current source inverter supplies the reactive power needed for the induction generator, while the diode bridge supplies the active power to the load.

Summarising, a stand-alone system can be used to supply a variety of d.c. and a.c. loads. The type of the load has significant impact on the choice of the reactive power compensator.

Chapter 3

MODELLING OF SATURATED INDUCTION MACHINES

3.1 Introduction

Induction machines are becoming preferred choice for alternative energy generating systems, due to numerous advantages that their application offers when compared to a synchronous machine. Simulation analysis of such a system requires that main flux saturation is included in the induction machine model. Indeed, the classical induction machine model, which assumes that magnetising flux varies linearly with the magnetising current, will lead to unsatisfactory results of modelling and simulation of induction machines under a number of steady-state and transient conditions. For example, dynamic analysis of self-excitation requires application of a model of an induction machine that accounts for main flux saturation. It is important to incorporate the effects of main flux saturation in modelling of stand-alone application of self-excited induction generators [Melkebeek (1983b)] and other applications like inverter-fed induction motor drives and vector-controlled induction machines. Self-excitation study of a stand-alone induction generator where reactive power is provided by a capacitor bank connected to the machine terminals can not be modelled and simulated without incorporating the main flux saturation. A small signal saturated induction machine model with currents selected as state-space variable was derived in [Melkebeek (1983a)]. This model was then used to investigate the dynamic behaviour of a voltage-fed induction motor and of a self-excited induction generator. The main flux saturation effects are much more important when the induction machine is fed from a current source than when it is fed from a voltage source. The main flux saturation effect, in this case, influences the system behaviour significantly and should be accounted for. On the other hand, the effect of main flux saturation can be neglected if the induction machine is fed from the mains or from a voltage source inverter, provided that the voltage to frequency ratio is kept constant and that the value of the magnetising inductance in the

linear model corresponds to the steady-state saturated value of the magnetising inductance at the operating point of the magnetising curve. Cross-saturation effect can cause degraded performance in vector controlled induction machine systems as well if main flux saturation effect is not taken into account. Compensation of the main flux saturation effect in vector controlled induction machines has been developed in [Levi et al (1990), Levi and Vuckovic (1993)]. Main flux saturation plays an important role in the analysis of electrical braking of induction motors using capacitor. It is shown in [Vas et al (1997)] that unsaturated induction machine model leads to incorrect simulation results in the study of capacitor braking of double-cage induction motors. A detailed study on operating regimes where saturated induction machine models are required has been carried out by [Levi (1994a)].

Modelling of main flux saturation of induction machines has for all these reasons received considerable attention since the early 1980's. Space vector theory was utilised for derivation of transient models of saturated induction machines and two models were made available. The first model utilises d-q axis winding currents as state-space variables [Brown et al (1983), Vas (1992), Levi and Rauski (1993), Levi (1994a)] while the other model uses the d-q axis winding flux linkages as state-space variables [He and Lipo (1984), Uctug and Demirekler (1988), Sakkoury et al (1993), Papadopouslos et al (1996)]. Both models yield identical results under steady-state and transient conditions [Osama et al (1993), Vas and Li (1993)]. The flux state-space model is simpler but it conceals the explicit effect of cross-saturation (dynamic inductance is not required). System matrix of the flux model is a unity matrix, which is advantageous. However, flux linkages are usually of no interest and additional algebraic equations have to be used for calculation of currents. Saturated induction machine model with winding currents as state-space variables contains variables that are of interest as state-space variables, so that additional algebraic equations are not needed. However, system matrix is full, with all the elements being saturation dependent, so that matrix inversion is required at every computation step. Apart from the pure winding current state-space model and the pure winding flux state-space model, one mixed current-flux model where magnetising flux and rotor current space vectors are selected as state-space variables can be found in [Kerkman (1985)]. Another mixed current-flux model where

stator current and rotor flux state-space vectors are selected as state-space variables is developed in [Krzeminski (1988)]. A full set of mixed current-flux state-space saturation models has been derived only recently by [Levi and Krzeminski (1996)], where one of the state-space variables is stator, rotor or magnetising current space vector while the other one is one of the flux linkage space vectors (magnetising, stator or rotor). Unlike the flux state-space model with stator and rotor flux linkages as state-space variables, each model contains the explicit terms that describe the cross-saturation effect.

Recently introduced principle of 'generalised flux' and 'generalised inductance' [Levi (1995a)] has enabled derivation of a whole range of new saturated single-cage induction machine models, for arbitrary selection of state-space variables, so that there are at present numerous models that describe saturated single-cage induction machine (14 models) and saturated double-cage induction machine (48 models). All the models yield identical simulation results. This was proved by performing simulation and experimental investigation of induction generator self-excitation, for a single-cage machine [Levi (1995a)] and for a double-cage machine [Levi (1996), (1997)]. Based on the concept of 'generalised flux' and 'generalised inductance', it is possible to derive a saturated induction machine model with any chosen set of state-space variables. The generalised flux space vector is the product of the generalised inductance and the magnetising current space vector. Main flux saturation can be modelled in terms of the magnetising current and generalised flux space vectors regardless of the selection of state-space variables. A number of saturated single-cage induction machine models with mixed current-flux set of state-space variables are presented in the following section.

3.2 Single-cage saturated induction machine models

Basic constant parameter mathematical model of a single-cage induction machine, in an arbitrary reference frame rotating at ω_a, can be described in terms of space vectors with the simple complex model [Vas (1992), Krause et al (1995)]. Stator and rotor voltage equations are expressed as

$$\underline{v}_s = R_s \underline{i}_s + \frac{d\underline{\psi}_s}{dt} + j\omega_a \underline{\psi}_s \tag{3.2-1}$$

$$0 = R_r \underline{i}_r + \frac{d\underline{\psi}_r}{dt} + j(\omega_a - \omega)\underline{\psi}_r \tag{3.2-2}$$

Stator and rotor flux linkages are defined as

$$\underline{\psi}_s = L_s \underline{i}_s + L_m \underline{i}_r \qquad \underline{\psi}_r = L_r \underline{i}_r + L_m \underline{i}_s \tag{3.2-3}$$

The electromagnetic torque is defined as

$$T_e = (\frac{3}{2}) P \underline{\psi}_s \times \underline{i}_s \tag{3.2-4}$$

The mechanical motion equation is given by

$$T_e - T_L = (\frac{J}{P}) \frac{d\omega}{dt} \tag{3.2-5}$$

It is assumed that stator and rotor flux linkages can be subdivided into main flux and leakage flux and that main flux saturation and leakage flux saturation can be treated separately. Therefore, stator and rotor flux linkages can be given as:

$$\underline{\psi}_s = L_{\sigma s} \underline{i}_s + \underline{\psi}_m \qquad \underline{\psi}_r = L_{\sigma r} \underline{i}_r + \underline{\psi}_m \tag{3.2-6}$$

$$\underline{\psi}_m = L_m \underline{i}_m \qquad \underline{i}_m = \underline{i}_s + \underline{i}_r \tag{3.2-7}$$

As main flux saturation is much more important than the leakage flux saturation in operating regimes encompassed by this project, saturation of leakage flux paths is neglected. Leakage inductances (denoted with index σ) in the above equations are taken as constants, as only main flux saturation is considered. The magnetising curve, which shows relationship between magnetising flux linkage space vector modulus and magnetising current space vector modulus, is assumed to be known. The non-linear

function of the magnetising curve is obtained by a standard no-load test on an induction machine. The mathematical model of a single-cage induction machine given with (3.2-1) - (3.2-7) is obtained using the standard assumptions of the generalised theory of electrical machines [Vas (1992), Krause et al (1995)].

The single-cage induction machine model given in terms of space vectors can be further resolved into orthogonal d-q axis model. Equations (3.2-1) - (3.2-4) can be expanded as follows:

$$v_{ds} = R_s i_{ds} + \frac{d\psi_{ds}}{dt} - \omega_a \psi_{qs} \tag{3.2-1a}$$

$$v_{qs} = R_s i_{qs} + \frac{d\psi_{qs}}{dt} + \omega_a \psi_{ds} \tag{3.2-1b}$$

$$0 = R_r i_{dr} + \frac{d\psi_{dr}}{dt} - (\omega_a - \omega)\psi_{qr} \tag{3.2-2a}$$

$$0 = R_r i_{qr} + \frac{d\psi_{qr}}{dt} + (\omega_a - \omega)\psi_{dr} \tag{3.2-2b}$$

$$\begin{aligned} \psi_{ds} &= L_s i_{ds} + L_m i_{dr} \\ \psi_{qs} &= L_s i_{qs} + L_m i_{qr} \\ \psi_{dr} &= L_r i_{dr} + L_m i_{ds} \\ \psi_{qr} &= L_r i_{qr} + L_m i_{qs} \end{aligned} \tag{3.2-3a}$$

$$T_e = \frac{3}{2} P L_m (i_{dr} i_{qs} - i_{qr} i_{ds}) \tag{3.2-4a}$$

$$T_e - T_L = \left(\frac{J}{P}\right) \frac{d\omega}{dt} \tag{3.2-5}$$

The d-q axis model of a single-cage induction machine is the fifth order system of differential equations. Electro-magnetic sub-system is described with the fourth order system of differential equations.

Transformation of three-phase variables to the arbitrary reference frame is given by:

$$\begin{bmatrix} x_{ds} \\ x_{qs} \\ x_{os} \end{bmatrix} = [k_s] \begin{bmatrix} x_{as} \\ x_{bs} \\ x_{cs} \end{bmatrix} \tag{3.2-8}$$

where x stands for voltage, current or flux linkage and transformation matrix is

$$[k_s] = \frac{2}{3} \begin{bmatrix} \cos\theta & \cos(\theta - \frac{2\pi}{3}) & \cos(\theta - \frac{4\pi}{3}) \\ -\sin\theta & -\sin(\theta - \frac{2\pi}{3}) & -\sin(\theta - \frac{4\pi}{3}) \\ \frac{1}{2} & \frac{1}{2} & \frac{1}{2} \end{bmatrix} \tag{3.2-9}$$

$$[k_s]^{-1} = \begin{bmatrix} \cos\theta & -\sin\theta & 1 \\ \cos(\theta - \frac{2\pi}{3}) & -\sin(\theta - \frac{2\pi}{3}) & 1 \\ \cos(\theta - \frac{4\pi}{3}) & -\sin(\theta - \frac{4\pi}{3}) & 1 \end{bmatrix} \tag{3.2-10}$$

and $\theta = \int \omega_a dt$. As zero sequence components cannot exist in the cases that are of interest in this project, equations for zero sequence components are omitted. Derivation of saturated single-cage induction machine models in the state-space form, from the basic model given with (3.2-1) - (3.2-7) is illustrated next on the basis of [Levi (1995a), Levi and Krzeminski (1996)]. The set of state-space variables can be chosen from the overall six possible space vector state-space variables shown in (3.2-11). Two space vectors are to be selected from the available set for each model, namely $\underline{x}_1, \underline{x}_2$.

$$[x] = \begin{bmatrix} \underline{i}_s & \underline{i}_r & \underline{i}_m & \underline{\psi}_s & \underline{\psi}_r & \underline{\psi}_m \end{bmatrix}^t \tag{3.2-11}$$

The available set of state-space variables can be expressed in terms of the selected pair of state-space variables as

$$\begin{bmatrix} \underline{i}_s \\ \underline{i}_r \\ \underline{i}_m \\ \underline{\psi}_s \\ \underline{\psi}_r \\ \underline{\psi}_m \end{bmatrix} = \begin{bmatrix} c_{11} c_{12} \\ c_{21} c_{22} \\ c_{31} c_{32} \\ c_{41} c_{42} \\ c_{51} c_{52} \\ c_{61} c_{62} \end{bmatrix} \begin{bmatrix} \underline{x}_1 \\ \underline{x}_2 \end{bmatrix} \tag{3.2-12}$$

Coefficients $c_{11}..c_{62}$ follow from (3.2-1) - (3.2-7) for any selected pair of state-space variables. Fourteen models are available as any two space vectors (except one pair)can be selected from six possible state-space variables (The magnetising flux and magnetising current space vectors can not be selected together as a pair). Saturated single-cage induction machine models are classified and derived according to whether $d(1/\Lambda)/dt$ or $d\Lambda/dt$ is required, where Λ is the so-called generalised inductance which is dependent on the saturation level. Eight models ($\underline{i}_s,\underline{\psi}_s$; $\underline{i}_s,\underline{\psi}_m$; $\underline{i}_s,\underline{\psi}_r$; $\underline{i}_r,\underline{\psi}_s$; $\underline{i}_r,\underline{\psi}_m$; $\underline{i}_r,\underline{\psi}_r$; $\underline{\psi}_s,\underline{\psi}_m$; $\underline{\psi}_r,\underline{\psi}_m$) are classified as $1/\Lambda$ model group where $d(1/\Lambda)/dt$ is required. Five models ($\underline{i}_s,\underline{i}_r$; $\underline{i}_s,\underline{i}_m$; $\underline{i}_r,\underline{i}_m$; $\underline{i}_m,\underline{\psi}_s$; $\underline{i}_m,\underline{\psi}_r$) are classified as Λ model group, where $d\Lambda/dt$ is needed. Only one model ($\underline{\psi}_s,\underline{\psi}_r$), where neither $d(1/\Lambda)/dt$ nor $d\Lambda/dt$ is required, does not belong to these two groups.

Generalised flux linkage space vector is expressed as

$$\underline{\Psi} = a\underline{x}_1 + b\underline{x}_2 \tag{3.2-13}$$

Coefficients a and b have to be saturation independent for all the $1/\Lambda$ models. As the generalised flux linkage space vector must be aligned with magnetising current and magnetising flux space vectors, it can be represented as

$$\underline{\Psi} = \Lambda \underline{i}_m \tag{3.2-14}$$

Derivation procedure for $1/\Lambda$ models is presented as follows. From (3.2-12), time derivatives of the stator and rotor flux linkage space vectors in terms of derivatives of

the selected state-space variables are given as

$$\frac{d\underline{\psi}_s}{dt} = c_{41}\frac{d\underline{x}_1}{dt} + c_{42}\frac{d\underline{x}_2}{dt} + \underline{x}_1\frac{dc_{41}}{dt} + \underline{x}_2\frac{dc_{42}}{dt}$$
$$\frac{d\underline{\psi}_r}{dt} = c_{51}\frac{d\underline{x}_1}{dt} + c_{52}\frac{d\underline{x}_2}{dt} + \underline{x}_1\frac{dc_{51}}{dt} + \underline{x}_2\frac{dc_{52}}{dt} \qquad (3.2\text{-}15)$$

Time derivative of any of the coefficients c_{ij} can be expressed as

$$\frac{dc_{ij}}{dt} = \frac{dc_{ij}}{d(1/\Lambda)}\frac{d(1/\Lambda)}{dt} \qquad (3.2\text{-}16)$$

where

$$\frac{d(1/\Lambda)}{dt} = \frac{d(1/\Lambda)}{d\Psi}\frac{1}{\Psi}\left(\Psi_d\frac{d\Psi_d}{dt} + \Psi_q\frac{d\Psi_q}{dt}\right) \qquad (3.2\text{-}17)$$

$$\frac{d(1/\Lambda)}{d\Psi} = \left(\frac{1}{\Lambda'} - \frac{1}{\Lambda}\right)\frac{1}{\Psi} \quad . \qquad (3.2\text{-}18)$$

Therefore, $d(1/\Lambda)/dt$ can be given in the final form as

$$\frac{d(1/\Lambda)}{dt} = \left(\frac{1}{\Lambda'} - \frac{1}{\Lambda}\right)\frac{1}{\Psi^2}\left(\Psi_d\frac{d\Psi_d}{dt} + \Psi_q\frac{d\Psi_q}{dt}\right) \qquad (3.2\text{-}19)$$

where $\frac{1}{\Lambda'} = \frac{di_m}{d\Psi}$ and $\frac{1}{\Lambda} = \frac{i_m}{\Psi}$.

Substituting (3.2-16) and (3.2-19) into (3.2.15), the d-q axis components of time derivatives of flux linkages are obtained in the following form:

$$\frac{d\psi_{dx}}{dt} = \alpha\frac{dx_{1d}}{dt} + \beta\frac{dx_{2d}}{dt} + \gamma\left(\frac{1}{\Lambda'} - \frac{1}{\Lambda}\right)\left(\frac{\Psi_d^2}{\Psi^2}\frac{d\Psi_d}{dt} + \frac{\Psi_q\Psi_d}{\Psi^2}\frac{d\Psi_q}{dt}\right) \qquad (3.2\text{-}20)$$

$$\frac{d\psi_{qx}}{dt} = \alpha \frac{dx_{1q}}{dt} + \beta \frac{dx_{2q}}{dt} + \gamma \left(\frac{1}{\Lambda'} - \frac{1}{\Lambda} \right) \left(\frac{\Psi_q^2}{\Psi^2} \frac{d\Psi_q}{dt} + \frac{\Psi_q \Psi_d}{\Psi^2} \frac{d\Psi_d}{dt} \right) \tag{3.2-21}$$

since

$$\begin{aligned} x_{1d} \frac{dc_{i1}}{d(1/\Lambda)} + x_{2d} \frac{dc_{i2}}{d(1/\Lambda)} &= \gamma \Psi_d \\ x_{1q} \frac{dc_{i1}}{d(1/\Lambda)} + x_{2q} \frac{dc_{i2}}{d(1/\Lambda)} &= \gamma \Psi_q \end{aligned} \tag{3.2-22}$$

where $i = 4$ or 5, and α and β equal the corresponding c values in equation (3.2-15).

Values of x and γ are chosen from Table 3.1 for a particular pair of state-space variables. Generalised flux space vector for all the eight models is selected from Table 3.2.

Table 3.1 Value of x and γ for different $1/\Lambda$ models

Model	x	γ
$\underline{i}_s, \underline{\psi}_r$	s	$-L_{\sigma r}$
$\underline{i}_s, \underline{\psi}_m$; $\underline{i}_s, \underline{\psi}_s$; $\underline{\psi}_s, \underline{\psi}_m$	r	$L_{\sigma r}$
$\underline{i}_r, \underline{\psi}_s$	r	$-L_{\sigma s}$
$\underline{i}_r, \underline{\psi}_m$; $\underline{i}_r, \underline{\psi}_r$; $\underline{\psi}_r, \underline{\psi}_m$	s	$L_{\sigma s}$

Table 3.2 Selection of generalised flux space vector

Model	$\underline{\Psi}$	Λ
$\underline{i}_s, \underline{\psi}_s$	$\underline{\psi}_s - L_{\sigma s} \underline{i}_s$	L_m
$\underline{i}_s, \underline{\psi}_m$	$\underline{\psi}_m$	L_m
$\underline{i}_s, \underline{\psi}_r$	$\underline{\psi}_r + L_{\sigma r} \underline{i}_s$	$L_{\sigma r} + L_m$
$\underline{i}_r, \underline{\psi}_s$	$\underline{\psi}_s + L_{\sigma s} \underline{i}_r$	$L_{\sigma r} + L_m$
$\underline{i}_r, \underline{\psi}_m$	$\underline{\psi}_m$	L_m
$\underline{i}_r, \underline{\psi}_r$	$\underline{\psi}_r - L_{\sigma r} \underline{i}_r$	L_m
$\underline{\psi}_s, \underline{\psi}_m$	$\underline{\psi}_m$	L_m
$\underline{\psi}_r, \underline{\psi}_m$	$\underline{\psi}_m$	L_m

Derivation procedure for Λ model is similar to the previous one. Generalised flux space vector is equal to the magnetising flux space vector in all the five models. Equation (3.2-15) remains the same while time derivatives of the coefficients c_{ij} and time

derivative of Λ now become

$$\frac{dc_{ij}}{dt}=\frac{dc_{ij}}{d\Lambda}\frac{d\Lambda}{dt} \qquad \frac{d\Lambda}{di_m}=(\Lambda'-\Lambda)\frac{1}{i_m} \tag{3.2-23}$$

$$\frac{d\Lambda}{dt}=(\Lambda'-\Lambda)\frac{1}{i_m^2}\left(i_{dm}\frac{di_{dm}}{dt}+i_{qm}\frac{di_{qm}}{dt}\right) \tag{3.2-24}$$

where $\Lambda'=\frac{d\Psi}{di_m}=\frac{d\psi_m}{di_m}=L$ equals dynamic inductance and $\Lambda=\frac{\Psi}{i_m}=\frac{\psi_m}{i_m}=L_m$ equals steady-state saturated magnetising inductance.

Substituting (3.2-23) and (3.2-24) into (3.2.15), the d-q axis components of time derivatives of stator flux linkages are then given in the following form:

$$\frac{d\psi_{ds}}{dt}=c_{41}\frac{dx_{1d}}{dt}+c_{42}\frac{dx_{2d}}{dt}+(\Lambda'-\Lambda)\left(\frac{i_{dm}^2}{i_m^2}\frac{di_{dm}}{dt}+\frac{i_{qm}i_{dm}}{i_m^2}\frac{di_{qm}}{dt}\right) \tag{3.2-25}$$

$$\frac{d\psi_{qs}}{dt}=c_{41}\frac{dx_{1q}}{dt}+c_{42}\frac{dx_{2q}}{dt}+(\Lambda'-\Lambda)\left(\frac{i_{qm}^2}{i_m^2}\frac{di_{qm}}{dt}+\frac{i_{qm}i_{dm}}{i_m^2}\frac{di_{dm}}{dt}\right) \tag{3.2-26}$$

since

$$\begin{aligned}\frac{x_{1d}dc_{41}}{d\Lambda}+\frac{x_{2d}dc_{42}}{d\Lambda}&=i_{dm}\\ \frac{x_{1q}dc_{41}}{d\Lambda}+\frac{x_{2q}dc_{42}}{d\Lambda}&=i_{qm}\end{aligned} \tag{3.2-27}$$

Utilising this procedure, three models (two $1/\Lambda$ models and one Λ model) are derived and presented in the following section. These models are used for simulations and control system design in subsequent chapters. Pure winding current model ($\underline{i}_s, \underline{i}_r$) is used in Chapter 4, mixed current-flux $\underline{i}_s, \underline{\psi}_s$ model is used in Chapter 7 and mixed current-flux $\underline{i}_s, \underline{\psi}_r$ model is used in Chapter 6 and 8.

3.2.1 Model with $\underline{i}_s, \underline{\psi}_s$ as state-space variables

The d-q model of a saturated single-cage induction machine with $\underline{i}_s, \underline{\psi}_s$ as state-space variables is expressed in the following form:

$$\left[v_{dq}\right] = [A]\frac{d\left[x_{dq}\right]}{dt} + [B]\left[x_{dq}\right]$$

$$\left[v_{dq}\right] = \begin{bmatrix} v_{ds} & v_{qs} & 0 & 0 \end{bmatrix}'$$

$$\left[x_{dq}\right] = \begin{bmatrix} i_{ds} & i_{qs} & \psi_{ds} & \psi_{qs} \end{bmatrix}'$$

$$[A] = \begin{bmatrix} 0 & 0 & 1 & 0 \\ 0 & 0 & 0 & 1 \\ L_{\sigma s} + L_{\sigma r} + \frac{L_{\sigma s}L_{\sigma r}}{L_{dd}} & \frac{L_{\sigma s}L_{\sigma r}}{L_{dq}} & -1 - \frac{L_{\sigma r}}{L_{dd}} & -\frac{L_{\sigma r}}{L_{dq}} \\ \frac{L_{\sigma s}L_{\sigma r}}{L_{dq}} & L_{\sigma s} + L_{\sigma r} + \frac{L_{\sigma s}L_{\sigma r}}{L_{qq}} & -\frac{L_{\sigma r}}{L_{dq}} & -1 - \frac{L_{\sigma r}}{L_{qq}} \end{bmatrix}$$

$$[B] = \begin{bmatrix} R_s & 0 & 0 & -\omega_a \\ 0 & R_s & \omega_a & 0 \\ R_r\frac{L_{\sigma s} + L_m}{L_m} & -(\omega_a - \omega)(L_\sigma + \frac{L_{\sigma s}L_{\sigma r}}{L_m}) & -\frac{R_r}{L_m} & (\omega_a - \omega)\frac{L_{\sigma r} + L_m}{L_m} \\ (\omega_a - \omega)(L_\sigma + \frac{L_{\sigma s}L_{\sigma r}}{L_m}) & R_r\frac{L_{\sigma s} + L_m}{L_m} & -(\omega_a - \omega)\frac{L_{\sigma r} + L_m}{L_m} & -\frac{R_r}{L_m} \end{bmatrix} \quad (3.2\text{-}28)$$

Saturation dependent coefficients are given by:

$$\left(\frac{1}{L_{dd}}\right) = \left(\frac{1}{\Lambda'}\right)\cos^2\mu + \left(\frac{1}{\Lambda}\right)\sin^2\mu$$

$$\left(\frac{1}{L_{qq}}\right) = \left(\frac{1}{\Lambda}\right)\cos^2\mu + \left(\frac{1}{\Lambda'}\right)\sin^2\mu \quad (3.2\text{-}29)$$

$$\left(\frac{1}{L_{dq}}\right) = \left(\frac{1}{\Lambda'} - \frac{1}{\Lambda}\right)\cos\mu\sin\mu$$

where

$$\cos\mu = \frac{\Psi_d}{\Psi} \qquad \sin\mu = \frac{\Psi_q}{\Psi} \quad (3.2\text{-}30)$$

and

$$\Psi_d = \psi_{ds} - L_{\sigma s} i_{ds} \equiv \psi_{dm} \quad \Psi_q = \psi_{qs} - L_{\sigma s} i_{qs} \equiv \psi_{qm} \tag{3.2-31}$$

$$\Lambda = \frac{\psi_m}{i_m} = L_m \qquad \Lambda' = \frac{d\psi_m}{di_m} = L \ . \tag{3.2-32}$$

3.2.2 Model with $\underline{i}_s, \underline{\psi}_r$ as state-space variables

The d-q model of a saturated single-cage induction machine with $\underline{i}_s, \underline{\psi}_r$ as state-space variables is expressed in the following form:

$$\left[v_{dq}\right] = [A]\frac{d\left[x_{dq}\right]}{dt} + [B]\left[x_{dq}\right]$$

$$\left[v_{dq}\right] = \left[v_{ds} \quad v_{qs} \quad 0 \quad 0\right]^t$$

$$\left[x_{dq}\right] = \left[i_{ds} \quad i_{qs} \quad \psi_{dr} \quad \psi_{qr}\right]^t$$

$$[A] = \begin{bmatrix} L_{\sigma s} + L_{\sigma r} - \frac{L_{\sigma r}^2}{L_{dd}} & -\frac{L_{\sigma r}^2}{L_{dq}} & 1 - \frac{L_{\sigma r}}{L_{dd}} & -\frac{L_{\sigma r}}{L_{dq}} \\ -\frac{L_{\sigma r}^2}{L_{dq}} & L_{\sigma s} + L_{\sigma r} - \frac{L_{\sigma r}^2}{L_{qq}} & -\frac{L_{\sigma r}}{L_{dq}} & 1 - \frac{L_{\sigma r}}{L_{qq}} \\ 0 & 0 & 1 & 0 \\ 0 & 0 & 0 & 1 \end{bmatrix}$$

$$[B] = \begin{bmatrix} R_s & -\omega_a\left(L_\sigma - \frac{L_{\sigma r}^2}{L_{\sigma r} + L_m}\right) & 0 & -\omega_a \frac{L_m}{L_{\sigma r} + L_m} \\ \omega_a\left(L_\sigma - \frac{L_{\sigma r}^2}{L_{\sigma r} + L_m}\right) & R_s & \omega_a \frac{L_m}{L_{\sigma r} + L_m} & 0 \\ -R_r \frac{L_m}{L_{\sigma r} + L_m} & 0 & \frac{R_r}{L_{\sigma r} + L_m} & -(\omega_a - \omega) \\ 0 & -R_r \frac{L_m}{L_{\sigma r} + L_m} & (\omega_a - \omega) & \frac{R_r}{L_{\sigma r} + L_m} \end{bmatrix}$$

(3.2-33)

where

$$\Psi_d = \psi_{dr} + L_{\sigma r} i_{ds} \equiv \left(L_{\sigma r} + L_m\right) i_{dm}$$
$$\Psi_q = \psi_{qr} + L_{\sigma r} i_{qs} \equiv \left(L_{\sigma r} + L_m\right) i_{qm} \tag{3.2-34}$$

$$\Lambda = \frac{\Psi}{i_m} = L_{\sigma r} + L_m \qquad \Lambda' = \frac{d\Psi}{di_m} = L_{\sigma r} + L \ . \tag{3.2-35}$$

3.2.3 Model with $\underline{i}_s, \underline{i}_r$ as state-space variables

The d-q model of a saturated single-cage induction machine with $\underline{i}_s, \underline{i}_r$ as state-space variables is expressed in the following way:

$$\left[v_{dq}\right] = [A]\frac{d\left[x_{dq}\right]}{dt} + [B]\left[x_{dq}\right]$$

$$\left[v_{dq}\right] = \begin{bmatrix} v_{ds} & v_{qs} & 0 & 0 \end{bmatrix}'$$

$$\left[x_{dq}\right] = \begin{bmatrix} i_{ds} & i_{qs} & i_{dr} & i_{qr} \end{bmatrix}'$$

$$[A] = \begin{bmatrix} L_{\sigma s} + L_{ddm} & L_{dq} & L_{ddm} & L_{dq} \\ L_{dq} & L_{\sigma s} + L_{qqm} & L_{dq} & L_{qqm} \\ L_{ddm} & L_{dq} & L_{\sigma r} + L_{ddm} & L_{dq} \\ L_{dq} & L_{qqm} & L_{dq} & L_{\sigma r} + L_{qqm} \end{bmatrix}$$

$$[B] = \begin{bmatrix} R_s & -\omega_a(L_{\sigma s} + L_m) & 0 & -\omega_a L_m \\ \omega_a(L_{\sigma s} + L_m) & R_s & \omega_a L_m & 0 \\ 0 & -(\omega_a - \omega)L_m & R_r & -(\omega_a - \omega)(L_{\sigma r} + L_m) \\ (\omega_a - \omega)L_m & 0 & (\omega_a - \omega)(L_{\sigma r} + L_m) & R_r \end{bmatrix} \tag{3.2-36}$$

Saturation dependent inductances are defined as:

$$\begin{aligned} L_{ddm} &= \Lambda' \cos^2 \mu + \Lambda \sin^2 \mu \\ L_{qqm} &= \Lambda \cos^2 \mu + \Lambda' \sin^2 \mu \\ L_{dq} &= (\Lambda' - \Lambda) \cos \mu \sin \mu \end{aligned} \tag{3.2-37}$$

and

$$\Lambda = \frac{\psi_m}{i_m} = L_m \qquad \Lambda' = \frac{d\psi_m}{di_m} = L$$

$$\cos \mu = \frac{i_{dm}}{i_m} \qquad \sin \mu = \frac{i_{qm}}{i_m} \ . \tag{3.2-38}$$

3.3 Double-cage saturated induction machine models

Many double-cage and deep-bar induction machines are nowadays used in industry. Deep-bar induction machines are utilised more frequently than double-cage induction machines in high power applications. However, from the modelling point of view both deep-bar and double-cage induction machines can be represented with the same mathematical model, in which rotor is equivalented with two (or more) rotor windings. Modelling of main flux saturation in double-cage and deep-bar induction machine models was rarely found in literature until recently. The current state-space model where stator current and rotor current of both windings are selected as state-space variables can be found in [Vas (1992), Vas and Li (1992), (1993), Levi and Rauski (1993), Smith et al (1996)]. The flux state-space model where stator flux and both rotor flux linkages are selected as state-space variables has been developed by [Vas (1992), Vas and Li (1992), (1993)] . The flux state-space model is simpler than the current state-space model, but is not widely used as additional algebraic equations are needed in order to calculate d-q axis stator currents.

The model of the double-cage induction machine that is most frequently used when main flux saturation has to be considered in transient analysis is again the current state-space model. Applications of current state-space model of a saturated double-cage or deep-bar induction machine are in analysis of start-up transients [Vas (1992), Vas and Li (1992), (1993)], start-up transients with wye-delta starter [Thorsen and Dalva (1992)] and vector control of induction machines [Healey et al (1995), Williamson and Healey (1996)]. A detailed study of self-excitation in double-cage and deep-bar induction generators [Levi and Rauski (1993)], based on current state-space model of a saturated induction machine with two rotor windings, has shown that very good agreement of experimental and simulation results may be achieved by means of this model. Capacitor breaking of a double-cage induction machine is studied in [Vas et al (1997)]. However, the inductance matrix in the current state-space model is full and it contains 36 elements that are all saturation dependent. Simulation with such model is therefore time consuming as such a complex matrix must be inverted at each computation time step.

The principle of 'generalised flux' and 'generalised inductance', introduced in [Levi (1995a)], has enabled derivation of a whole range of new saturated single-cage induction machine models, for arbitrary selection of state-space variables. The method has been extended to modelling of double-cage and deep-bar induction machines in [Levi (1996), (1997)]. It is possible, using this method, to derive a model of a saturated double-cage (or deep-bar) induction machine for any set of state-space variables selected from the available eight space vectors, so that forty-eight transient models that describe a saturated induction machine with two equivalent rotor windings are available.

The constant parameter mathematical model of double-cage induction machine, in an arbitrary reference frame rotating at ω_a, can be described in terms of space vectors with the following equations [Vas (1992)]. Stator and rotor voltage equations are expressed as

$$\underline{v}_s = R_s \underline{i}_s + \frac{d\underline{\psi}_s}{dt} + j\omega_a \underline{\psi}_s \tag{3.3-1}$$

$$0 = R_{r1} \underline{i}_{r1} + \frac{d\underline{\psi}_{r1}}{dt} + j(\omega_a - \omega)\underline{\psi}_{r1} + R_c\left(\underline{i}_{r1} + \underline{i}_{r2}\right) \tag{3.3-2}$$

$$0 = R_{r2} \underline{i}_{r2} + \frac{d\underline{\psi}_{r2}}{dt} + j(\omega_a - \omega)\underline{\psi}_{r2} + R_c\left(\underline{i}_{r1} + \underline{i}_{r2}\right) \tag{3.3-3}$$

Stator and rotor flux linkages are defined as

$$\begin{aligned} \underline{\psi}_s &= L_s \underline{i}_s + L_m(\underline{i}_{r1} + \underline{i}_{r2}) \\ \underline{\psi}_{r1} &= L_{r1} \underline{i}_{r1} + L_m \underline{i}_s + L_{12} \underline{i}_{r2} \\ \underline{\psi}_{r2} &= L_{r2} \underline{i}_{r2} + L_m \underline{i}_s + L_{12} \underline{i}_{r1} \end{aligned} \tag{3.3-4}$$

where $L_{12} = L_m + L_{mr}$, and symbols L_{mr} and R_c stand for mutual leakage inductance between the two rotor windings and common end-ring resistance between the two cages in a double-cage induction machine, respectively.

The electromagnetic torque is defined as

$$T_e = (\frac{3}{2}) P \underline{\psi}_s \times \underline{i}_s \tag{3.3-5}$$

The equation of mechanical motion is given with

$$T_e - T_L = (\frac{J}{P}) \frac{d\omega}{dt} \tag{3.3-6}$$

Stator flux linkage, rotor flux linkages and magnetising flux linkage can be given as

$$\begin{aligned} \underline{\psi}_s &= L_{\sigma s} \underline{i}_s + \underline{\psi}_m \\ \underline{\psi}_{r1} &= L_{\sigma r1} \underline{i}_{r1} + L_{mr}\left(\underline{i}_{r1} + \underline{i}_{r2}\right) + \underline{\psi}_m \\ \underline{\psi}_{r2} &= L_{\sigma r2} \underline{i}_{r2} + L_{mr}\left(\underline{i}_{r1} + \underline{i}_{r2}\right) + \underline{\psi}_m \end{aligned} \tag{3.3-7}$$

$$\underline{\psi}_m = L_m \underline{i}_m \qquad \underline{i}_m = \underline{i}_s + \underline{i}_{r1} + \underline{i}_{r2} \tag{3.3-8}$$

It is assumed that the non-linear magnetising curve of the machine is known. The magnetising curve, which shows relationship between magnetising flux linkage space vector modulus and magnetising current space vector modulus, is obtained by a standard no-load test on an induction machine. Leakage inductances (denoted with index σ) are again taken as constants, as leakage flux saturation is neglected and only main flux saturation is considered. The main assumptions are the same as those used for derivation of the state-space equations of single-cage induction machines.

The double-cage induction machine model can be given in terms of orthogonal d-q axis variables. Equations (3.3-1) - (3.3-5) are expanded as follows:

$$v_{ds} = R_s i_{ds} + \frac{d\psi_{ds}}{dt} - \omega_a \psi_{qs} \tag{3.3-1a}$$

$$v_{qs} = R_s i_{qs} + \frac{d\psi_{qs}}{dt} + \omega_a \psi_{ds} \tag{3.3-1b}$$

$$0 = R_{r1} i_{dr1} + \frac{d\psi_{dr1}}{dt} - (\omega_a - \omega)\psi_{qr1} + R_c\left(i_{dr1} + i_{dr2}\right) \tag{3.3-2a}$$

$$0 = R_{r1} i_{qr1} + \frac{d\psi_{qr1}}{dt} + (\omega_a - \omega)\psi_{dr1} + R_c\left(i_{qr1} + i_{qr2}\right) \tag{3.3-2b}$$

$$0 = R_{r2} i_{dr2} + \frac{d\psi_{dr2}}{dt} - (\omega_a - \omega)\psi_{qr2} + R_c\left(i_{dr1} + i_{dr2}\right) \tag{3.3-3a}$$

$$0 = R_{r2} i_{qr2} + \frac{d\psi_{qr2}}{dt} + (\omega_a - \omega)\psi_{dr2} + R_c\left(i_{qr1} + i_{qr2}\right) \tag{3.3-3b}$$

$$\psi_{ds} = L_s i_{ds} + L_m (i_{dr1} + i_{dr2}) \tag{3.3-4a}$$

$$\psi_{qs} = L_s i_{qs} + L_m (i_{qr1} + i_{qr2}) \tag{3.3-4b}$$

$$\psi_{dr1} = L_{r1} i_{dr1} + L_m i_{ds} + L_{12} i_{dr2} \tag{3.3-4c}$$

$$\psi_{qr1} = L_{r1} i_{qr1} + L_m i_{ds} + L_{12} i_{qr2} \tag{3.3-4d}$$

$$\psi_{dr2} = L_{r2} i_{dr2} + L_m i_{qs} + L_{12} i_{dr1} \tag{3.3-4e}$$

$$\psi_{qr2} = L_{r2} i_{qr2} + L_m i_{qs} + L_{12} i_{qr1} \tag{3.3-4f}$$

$$T_e = \frac{3}{2} P L_m [(i_{dr1} + i_{dr2}) i_{qs} - (i_{qr1} + i_{qr2}) i_{ds}] \tag{3.3-5a}$$

The rotor is now described with four differential equations in the d-q reference frame as the machine rotor circuit is modelled with two windings. The electro-magnetic sub-system of a double-cage induction machine is represented with the sixth order system of differential equations. Complete dynamic behaviour of a double-cage induction machine is thus modelled with the 7th order differential equation system.

Derivation of a saturated double-cage induction machine model is illustrated next on the basis of [Levi (1996), (1997)]. The set of state-space variables can be chosen from the overall eight possible state-space variables shown below:

$$[x] = \left[\underline{i}_s \quad \underline{i}_{r1} \quad \underline{i}_{r2} \quad \underline{i}_m \quad \underline{\psi}_s \quad \underline{\psi}_{r1} \quad \underline{\psi}_{r2} \quad \underline{\psi}_m\right]^t \tag{3.3-9}$$

Three space vectors, namely, $\underline{x}_1, \underline{x}_2, \underline{x}_3$, are to be selected from the above equation. Generalised flux space vector is given in terms of selected state-space variables $\underline{x}_1, \underline{x}_2, \underline{x}_3$ as

$$\underline{\Psi} = a\underline{x}_1 + b\underline{x}_2 + c\underline{x}_3 \qquad (3.3\text{-}10)$$

and it has to be aligned with magnetising current and magnetising flux space vectors, so that

$$\underline{\Psi} = \Lambda \underline{i}_m \qquad (3.3\text{-}11)$$

Total number of combinations is fifty-six models, as three variables are selected as state-space variables out of the eight space vectors. However, only forty-eight model are available for representation of a saturated double-cage or deep-bar induction machine, since eight models ($\underline{i}_s, \underline{i}_m, \underline{\psi}_s$, $\underline{i}_s, \underline{\psi}_m, \underline{\psi}_s$, and $\underline{i}_m, \underline{\psi}_m$ with any of the remaining six space vectors) can not be derived. Fifteen models are classified as Λ model group where $d\Lambda/dt$ is required while thirty-two models are classified as $1/\Lambda$ model group where $d(1/\Lambda)/dt$ is required. The third group (neither $d\Lambda/dt$ or $d(1/\Lambda)/dt$ is required) consists of a single model where stator flux linkage and flux linkages of both rotor windings are selected as state-space variables. In what follows only one model, namely $\underline{i}_s, \underline{i}_{r1}, \underline{i}_{r2}$ model, is derived. This model is used in Chapter 4.

3.3.1 Model with $\underline{i}_s, \underline{i}_{r1}, \underline{i}_{r2}$ as state-space variables

The self-inductances of the stator winding and rotor windings and the mutual inductance between two rotor windings are defined as

$$L_{r1} = L_m + L_{\sigma r1} + L_{mr} \qquad L_{r2} = L_m + L_{\sigma r2} + L_{mr} \qquad (3.3\text{-}12)$$

$$L_s = L_m + L_{\sigma s} \qquad L_{12} = L_m + L_{mr} \qquad (3.3\text{-}13)$$

The d-q axis components of the stator flux linkage, rotor flux linkages and main flux linkage can be rewritten as

$$\psi_{ds} = L_{\sigma s} i_{ds} + \psi_{dm} \qquad (3.3\text{-}14a)$$

$$\psi_{qs} = L_{\sigma s} i_s + \psi_{qm} \tag{3.3-14b}$$

$$\psi_{dr1} = L_{\sigma r1} i_{dr1} + L_{mr}\left(i_{dr1} + i_{dr2}\right) + \psi_{dm} \tag{3.3-14c}$$

$$\psi_{qr1} = L_{\sigma r1} i_{qr1} + L_{mr}\left(i_{qr1} + i_{qr2}\right) + \psi_{qm} \tag{3.3-14d}$$

$$\psi_{dr2} = L_{\sigma r2} i_{dr2} + L_{mr}\left(i_{dr1} + i_{dr2}\right) + \psi_{dm} \tag{3.3-14e}$$

$$\psi_{qr2} = L_{\sigma r2} i_{qr2} + L_{mr}\left(i_{qr1} + i_{qr2}\right) + \psi_{qm} \tag{3.3-14f}$$

$$\psi_{dm} = L_m i_{dm} \qquad i_{dm} = i_{ds} + i_{dr1} + i_{dr2} \tag{3.3-15a}$$

$$\psi_{qm} = L_m i_{qm} \qquad \mathrm{i}_{qm} = i_{qs} + i_{qr1} + i_{qr2} \tag{3.3-15b}$$

$$\psi_m = (\psi_{dm}{}^2 + \psi_{qm}{}^2)^{1/2} \qquad i_m = (i_{dm}{}^2 + i_{qm}{}^2)^{1/2} \tag{3.3-16}$$

Time derivatives of all the winding flux linkages are further eliminated from (3.3-1a) - (3.3-3b) by means of (3.3-14a) - (3.3-14f). Time derivatives of the d-q axis main flux components are determined as follows:

$$\frac{d\psi_{qm}}{dt} = \frac{d}{dt}(\psi_m \frac{i_{qm}}{i_m}) = \frac{d\psi_m}{di_m}\frac{di_m}{dt}\frac{i_{qm}}{i_m} + \psi_m \frac{d}{dt}(\frac{i_{qm}}{i_m}) \tag{3.3-17}$$

$$\frac{d\psi_{qm}}{dt} = L\frac{di_m}{dt}\frac{i_{qm}}{i_m} + \frac{\psi_m}{i_m{}^2}(i_m \frac{di_{qm}}{dt} - i_{qm}\frac{di_m}{dt}) \tag{3.3-18}$$

$$\frac{di_m}{dt} = \frac{d}{dt}(i_{dm}{}^2 + i_{qm}{}^2)^{1/2} = \frac{\partial_m}{\partial_{qm}}\frac{di_{qm}}{dt} + \frac{\partial_m}{\partial_{dm}}\frac{di_{dm}}{dt} \tag{3.3-19}$$

$$\frac{\partial_m}{\partial_{qm}} = \frac{i_{qm}}{i_m} \qquad \frac{\partial_m}{\partial_{dm}} = \frac{i_{dm}}{i_m} \tag{3.3-20}$$

$$\frac{d\psi_{qm}}{dt} = L(\frac{di_{qm}}{dt}\frac{i_{qm}}{i_m} + \frac{di_{dm}}{dt}\frac{i_{dm}}{i_m})\frac{i_{qm}}{i_m} + \frac{L_m}{i_m}[i_m \frac{di_{qm}}{dt} - i_{qm}(\frac{di_{qm}}{dt}\frac{i_{qm}}{i_m} + \frac{di_{dm}}{dt}\frac{i_{dm}}{i_m})] \tag{3.3-21}$$

$$\begin{aligned}\frac{d\psi_{qm}}{dt} = {} & L\sin^2\mu\frac{di_{qm}}{dt} + L\cos\mu\sin\mu\frac{di_{dm}}{dt} + L_m(\cos^2\mu + \sin^2\mu)\frac{di_{qm}}{dt} \\ & - L_m\sin^2\mu\frac{di_{qm}}{dt} + L_m\cos\mu\sin\mu\frac{di_{dm}}{dt})\end{aligned} \tag{3.3-22}$$

Therefore

$$\frac{d\psi_{qm}}{dt} = L_{qqm}\frac{di_{qm}}{dt} + L_{dqm}\frac{di_{dm}}{dt} \tag{3.3-23}$$

Similarly,

$$\frac{d\psi_{dm}}{dt} = L_{ddm}\frac{di_{dm}}{dt} + L_{qdm}\frac{di_{qm}}{dt} \tag{3.3-24}$$

Saturation dependent inductances are defined as:

$$\begin{aligned} L_{ddm} &= \Lambda'\cos^2\mu + \Lambda\sin^2\mu \\ L_{qqm} &= \Lambda\cos^2\mu + \Lambda'\sin^2\mu \\ L_{dqm} &= L_{qdm} = L_{dq} = (\Lambda'-\Lambda)\cos\mu\sin\mu \end{aligned} \tag{3.3-25}$$

where

$$\Lambda = \frac{\psi_m}{i_m} = L_m \qquad \Lambda' = \frac{d\psi_m}{di_m} = L$$

$$\cos\mu = \frac{i_{dm}}{i_m} \qquad \sin\mu = \frac{i_{qm}}{i_m} \tag{3.3-26}$$

and

$$L_m = \frac{\psi_m}{i_m} \quad \text{where} \quad L_m = L_m(i_m)$$

$$L = \frac{d\psi_m}{di_m} \quad \text{where} \quad L = L(i_m). \tag{3.3-27}$$

The time derivatives of the main flux components are obtained as

$$\frac{d\psi_{qm}}{dt} = L_{qqm}\frac{di_{qm}}{dt} + L_{dqm}\frac{di_{dm}}{dt} = L_{qqm}\left(\frac{di_{qs}}{dt} + \frac{di_{qr1}}{dt} + \frac{di_{qr2}}{dt}\right) + L_{dqm}\left(\frac{di_{ds}}{dt} + \frac{di_{dr1}}{dt} + \frac{di_{dr2}}{dt}\right)$$

(3.3-28)

$$\frac{d\psi_{dm}}{dt} = L_{ddm}\frac{di_{dm}}{dt} + L_{qdm}\frac{di_{qm}}{dt} = L_{ddm}\left(\frac{di_{ds}}{dt} + \frac{di_{dr1}}{dt} + \frac{di_{dr2}}{dt}\right) + L_{qdm}\left(\frac{di_{qs}}{dt} + \frac{di_{qr1}}{dt} + \frac{di_{qr2}}{dt}\right)$$

(3.3-29)

where $L_{dqm} = L_{qdm} = L_{dq}$ due to the cylindrical symmetry of the induction machine.

The final d-q model of a saturated double-cage induction machine with $\underline{i}_s, \underline{i}_{r1}, \underline{i}_{r2}$ as state-space variables is expressed in the following form:

$$\left[v_{dq}\right] = [A]\frac{d\left[x_{dq}\right]}{dt} + [B]\left[x_{dq}\right] \tag{3.3-30}$$

$$\left[v_{dq}\right] = \left[v_{ds} \quad v_{qs} \quad 0 \quad 0\right]^t \tag{3.3-31}$$

$$\left[x_{dq}\right] = \left[i_{ds} \quad i_{qs} \quad i_{dr1} \quad i_{qr1} \quad i_{dr2} \quad i_{qr2}\right]^t \tag{3.3-32}$$

The matrices [A] and [B] are given with

$$A] = \begin{bmatrix} L_{ss}+L_{dldm} & L_{dq} & L_{dldm} & L_{dq} & L_{dldm} & L_{dq} \\ L_{dq} & L_{ss}+L_{qqm} & L_{dq} & L_{qqm} & L_{dq} & L_{qqm} \\ L_{dldm} & L_{dq} & L_{sr1}+L_{mr}+L_{dldm} & L_{dq} & L_{mr}+L_{dldm} & L_{dq} \\ L_{dq} & L_{qqm} & L_{dq} & L_{sr1}+L_{mr}+L_{qqm} & L_{dq} & L_{mr}+L_{qq} \\ L_{dldm} & L_{dq} & L_{mr}+L_{dl} & L_{dq} & L_{sr2}+L_{mr}+L_{dldm} & L_{dq} \\ L_{dq} & L_{qqm} & L_{dq} & L_{mr}+L_{qqm} & L_{dq} & L_{sr2}+L_{mr}+L_{qqm} \end{bmatrix} \tag{3.3-33}$$

$$B] = \begin{bmatrix} R_s & -\omega_a L_s & 0 & -\omega_a L_m & 0 & -\omega_a L_m \\ \omega_a L_s & R_s & -\omega_a L_m & 0 & \omega_a L_m & 0 \\ 0 & -\omega_{sl} L_m & R_{r1}+R_c & -\omega_{sl}(L_m+L_{sr1}+L_{mr}) & R_c & -\omega_{sl}(L_m+L_{mr}) \\ \omega_{sl} L_m & 0 & \omega_{sl}(L_m+L_{sr1}+L_{mr}) & R_{r1}+R_c & \omega_{sl}(L_m+L_{mr}) & R_c \\ 0 & -\omega_{sl} L_m & R_c & -\omega_{sl}(L_m+L_{mr}) & R_{r2}+R_c & -\omega_{sl}(L_m+L_{sr2}+L_{mr}) \\ \omega_{sl} L_m & 0 & \omega_{sl}(L_m+L_{mr}) & R_c & \omega_{sl}(L_m+L_{sr2}+L_{mr}) & R_{r2}+R_c \end{bmatrix} \tag{3.3-34}$$

where $\omega_{sl} = \omega_a - \omega$.

3.4 Single-cage representation of saturated double-cage induction machines

A model of a saturated double-cage induction machine, regardless of the selection of state-space variables, requires sixth order system of differential equations for

description of the electro-magnetic sub-system. A saturated double-cage induction machine model for self-excitation study is therefore a ninth order system (or an eighth order system if constant speed operation is considered). On the other hand, electro-magnetic sub-system of a saturated single-cage induction machine is represented with a fourth order system of differential equations. It therefore appears advantageous to represent a double-cage machine with a single-cage machine model. Such an approach will be undertaken in Chapter 4, Section 4.5. The purpose is to examine the consequences of simplified deep-bar and double-cage induction machine representation on accuracy of simulation results regarding self-excitation process under no-load conditions. A double-cage induction machine will be represented with a single-cage machine model and impact of such a reduced order representation will be studied for self-excitation process by comparing the results with those obtained by means of the full sixth order induction machine model and by experiments.

The major problem in accurate single-cage representation of a machine with two rotor circuits is determination of appropriate rotor parameter values. Calculation of parameters for the model with two rotor windings can be done rather accurately if design data are known and this is how the parameters of the machine, used in studies whose results are reported in Section 4.5, were determined [Rauski and Levi (1992)]. On the other hand, standard tests on an induction machine (no-load and locked rotor tests) will yield rotor parameters for single-cage representation at rotor frequency equal to rated (50 Hz). However, an induction generator will always operate with rather low rotor frequency, of the order of up to 5 Hz. A study of impact of rotor parameter variations on steady-state operation of a deep-bar induction generator [Sutanto and Grantham (1993)] concludes that calculation of minimum capacitance required for self-excitation can be done using 50 Hz values of rotor parameters without any loss in accuracy. However, the same study [Sutanto and Granham (1993)] shows that rotor parameter variations should be accounted for in the calculations of the final steady-state when the machine is loaded. It appears that a similar study for transients is not available at present and that it is for the first time undertaken in this project.

The potential benefit of using single-cage representation, provided that it leads to

reasonably accurate results, is that utilisation of a simpler model means faster simulations.

3.5 Summary

This chapter reviews mathematical modelling of saturated single-cage and double-cage induction machines. The need for utilisation of saturated induction machine models is explained and details of mathematical modelling techniques for saturated single-cage and double-cage induction machines are given. Pure winding current model ($\underline{i}_s, \underline{i}_r$), and mixed current-flux $\underline{i}_s, \underline{\psi}_s$ and $\underline{i}_s, \underline{\psi}_r$ models for single-cage induction machine are derived, as well as is pure winding current $\underline{i}_s, \underline{i}_{r1}, \underline{i}_{r2}$ model for double-cage induction machine. A simplified single-cage representation of saturated double-cage induction machines is discussed and potential benefit of such simplified representation is also described.

Chapter 4

MODELLING, SIMULATION AND EXPERIMENTAL INVESTIGATION OF AN INDUCTION GENERATOR WITH PARALLEL CAPACITOR BANK

4.1 Introduction

Self-excitation phenomenon in three-phase induction machines, although known for more than half a century [Wagner (1939), Basset and Potter (1935)], is still a subject of considerable attention primarily due to application of self-excited induction generators (SEIG) in isolated power systems. Source of reactive power, that is required for self-excitation and subsequent generating operation, can be any of the numerous types of static reactive power compensators [Elders et al (1984)]. The cheapest and the most frequently analysed solution, discussed in this chapter as well, is the one based on a three-phase capacitor bank.

Physical background of the self-excitation process has been described in considerable depth in [Elder et al (1983)]. The initiation of the excitation in the machine that runs at certain speed can be viewed as the response of the resonant circuit which comprises the machine and the capacitor bank connected to its terminals. As steady-state operation takes place in the point of intersection of the capacitor voltage line and the no-load voltage characteristic (essentially, magnetising curve) of the machine, it is an imperative in any analysis of the self-excitation that main flux saturation is taken into account. The available literature regarding self-excitation process and operation of self-excited induction generators can be classified into two major groups. The first group deals with various aspects of steady-state operation and encompasses calculation of minimum capacitance required for self-excitation with and without load [Al Jabri and Alolah (1990), Saloma and Holmes (1996)], determination of generator operating characteristics at various speeds [Saloma and Holmes (1996)], techniques and numerical procedures for steady-state analysis of SEIG operation [Murthy et al (1982), Rajakaruna

and Bonert (1993), Malik and Haque (1986)], impact of generator parameters on operating characteristics [Shridhar et al (1993)], parallel operation of SEIGs [Al-Bahrani and Malik (1993)] and improvement in voltage regulation by means of long-shunt [Bim et al (1989)] and short-shunt [Shridhar et al (1995b)] connection.

The second group discusses dynamic models and transient simulation of self-excited induction generators under various no-load and loading conditions. Successful simulation of any of the transients associated with SEIG operation requires that an appropriate dynamic saturated machine model is used. Such a model, with winding d-q axis currents selected as state-space variables, was proposed for the first time in [Smith and Sriharan (1968)]. This model has subsequently been further refined [Hallenius et al (1991), Levi and Rauski (1993)] and is nowadays the most frequently applied model in SEIG simulation [Levi (1994a), Wang and Su (1998), Shridhar et al (1995a), Wang and Lee (1998)], although model with winding d-q axis flux linkages as state-space variables [Ojo (1995)], as well as all the other models with differing selection of the state-space variable set [Levi (1995a)], are equally applicable.

This chapter presents at first modelling and simulation of both single-cage and double-cage induction generators with parallel capacitor bank. No-load self-excitation, loaded operation of single-cage induction generator and compensation of load voltage variation by means of an additional series capacitor bank are simulated. Applicability of single-cage machine models for self-excitation analyses in double-cage induction generators is investigated. This chapter also reports on results of an extensive experimental investigation of a SEIG operation. Operation with capacitors connected in star and delta under no-load conditions, connection of a purely resistive load, and connection of a resistive load with short-shunt compensation are elaborated.

4.2 Self-excitation process

The self-excitation can be achieved by connecting a capacitor bank in parallel to the running induction machine stator terminals, allowing the induction machine to operate as a stand-alone generator. Self-excitation is a process of voltage build-up when the

machine is driven at certain speed by an external prime mover like a wind turbine, provided an appropriate capacitor bank is connected across the machine terminal. The initiation of the machine excitation can be viewed as the response of a resonant circuit which comprises the machine and the capacitor bank. The self-excitation takes place due to remanent voltage that exists at machine terminals when shaft is rotated by the turbine. Once the machine is excited, the magnitude of steady-state voltage generated will be determined by value of capacitance, rotor speed and the non-linear magnetising curve of the machine. The point of intersection between the magnetising curve and the capacitor characteristic determines a point of stable self-excitation and defines the no-load terminal voltage and exciting current in final steady-state.

In order to provide high reliability of self-excitation process, the capacitance of the capacitor bank has to be selected carefully as there is cut-off speed below which self-excitation is impossible. Therefore, there is a minimum value of capacitance required to initiate and maintain self-excitation. But the value of capacitance chosen must be greater than the minimum self-excitation capacitance in order to achieve steady-state operation. The capacitance should not be too high in order to avoid large overvoltages when the machine is excited. It is recommended that in all situations the terminal capacitors are connected when the final machine speed is reached and load should be disconnected until the machine is fully excited.

Self-excitation process, although a transient phenomena, is most easily explained by means of the induction machine's per-phase steady-state equivalent circuit. The equivalent circuit is easily derived from the general dynamic model (3.2-1) - (3.2-7) under the assumption of steady-state operation with sinusoidal supply. Taking speed of the arbitrary reference frame as equal to the supply angular frequency ω_e (synchronously rotating reference frame), and substituting (3.2-6) and (3.2-7) into (3.2-1) and (3.2-2), one obtains

$$\begin{aligned} \underline{v}_s &= R_s \underline{i}_s + j\omega_e \left[L_{\sigma s} \underline{i}_s + L_m (\underline{i}_s + \underline{i}_r) \right] \\ 0 &= R_r \underline{i}_r + j(\omega_e - \omega) \left[L_{\sigma r} \underline{i}_r + L_m (\underline{i}_s + \underline{i}_r) \right] \end{aligned} \qquad (4.2\text{-}1)$$

where the condition $d/dt = 0$, imposed by selection of the synchronously rotating reference frame, has been accounted for. Stator voltage space vector becomes $\underline{v}_s = \sqrt{2}V$, where V is the rms value of the machine's phase to neutral voltages. If per-unit slip is introduced in standard way as $s = (\omega_e - \omega)/\omega_e$, equation (4.2-1) can be re-written in terms of reactances X at angular frequency equal to ω_e:

$$\begin{aligned} \underline{v}_s &= R_s \underline{i}_s + jX_{os}\underline{i}_s + jX_m(\underline{i}_s + \underline{i}_r) \\ 0 &= (\frac{R_r}{s})\underline{i}_r + jX_{or}\underline{i}_r + jX_m(\underline{i}_s + \underline{i}_r) \end{aligned} \qquad (4.2\text{-}2)$$

Equations (4.2-2) describe the well-known steady-state equivalent circuit of an induction motor. As the equivalent steady-state circuit is normally given on the per-phase basis in terms of phasors, space vectors need only to be substituted with appropriate phasors. The equivalent steady-state circuit is illustrated in Figure 4.2.1 (capital underlined symbols stand for phasors).

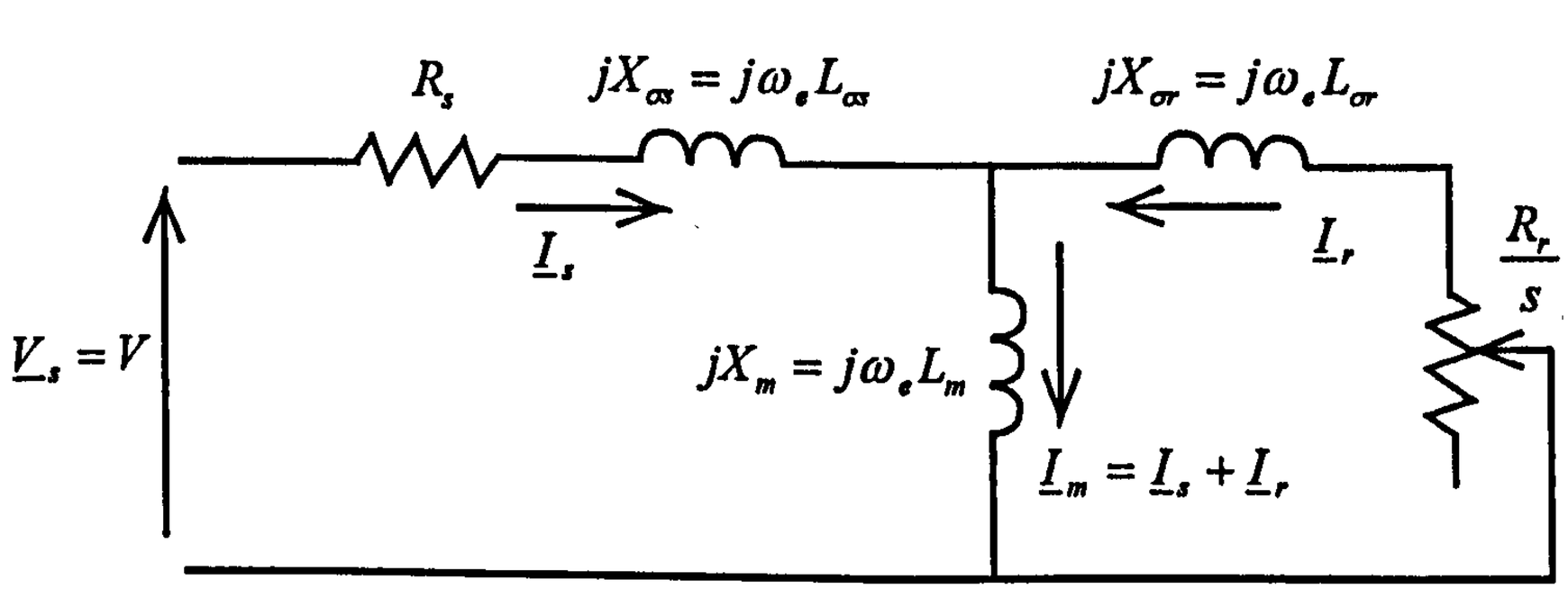

Figure 4.2.1 Steady-state per-phase equivalent circuit of an induction motor under sinusoidal supply conditions

When operation of an isolated induction generator is considered and the reactive power source is a capacitor bank, stator voltage is a dependent variable rather than an independent variable. Let us suppose that a capacitor bank, of C capacitance per phase, is connected to the stator terminals and that the generator runs at certain constant speed ω under no-load conditions. Let the capacitive reactance at rated stator frequency be X_c and let all the machine reactances, defined in Figure 4.2.1, be those that apply to the rated stator frequency. If the ratio of stator operating frequency to rated stator frequency

is denoted as ν and the ratio of the rotor angular speed to rated stator angular frequency is denoted as Ω (note that Ω is a constant for any given operating speed), then one can write instead of (4.2-2) the following equations that describe the generator under no-load conditions:

$$\begin{aligned} j\underline{I}_s \frac{X_c}{\nu} &= R_s \underline{I}_s + j\nu\left[X_{\sigma s}\underline{I}_s + X_m(\underline{I}_s + \underline{I}_r)\right] \\ 0 &= R_r \underline{I}_r + j\nu\left[X_{\sigma r}\underline{I}_r + X_m(\underline{I}_s + \underline{I}_r)\right](1 - \frac{\Omega}{\nu}) \end{aligned} \tag{4.2-3}$$

Division of the both equations with the relative stator frequency ν yields:

$$\begin{aligned} j\underline{I}_s \frac{X_c}{\nu^2} &= \frac{R_s}{\nu}\underline{I}_s + j\left[X_{\sigma s}\underline{I}_s + X_m(\underline{I}_s + \underline{I}_r)\right] \\ 0 &= (\frac{R_r}{\nu - \Omega})\underline{I}_r + j\left[X_{\sigma r}\underline{I}_r + X_m(\underline{I}_s + \underline{I}_r)\right] \end{aligned} \tag{4.2-4}$$

Equivalent circuit, constructed on the basis of (4.2-4) is shown in Figure 4.2.2. As the operation takes place under no-load conditions, then rotor branch of the circuit can be omitted from further consideration (Figure 4.2.3). Hence it follows that self-excitation under no-load conditions is governed by the response of the resonant circuit composed of stator resistance, stator leakage inductance, magnetising inductance and the external capacitance.

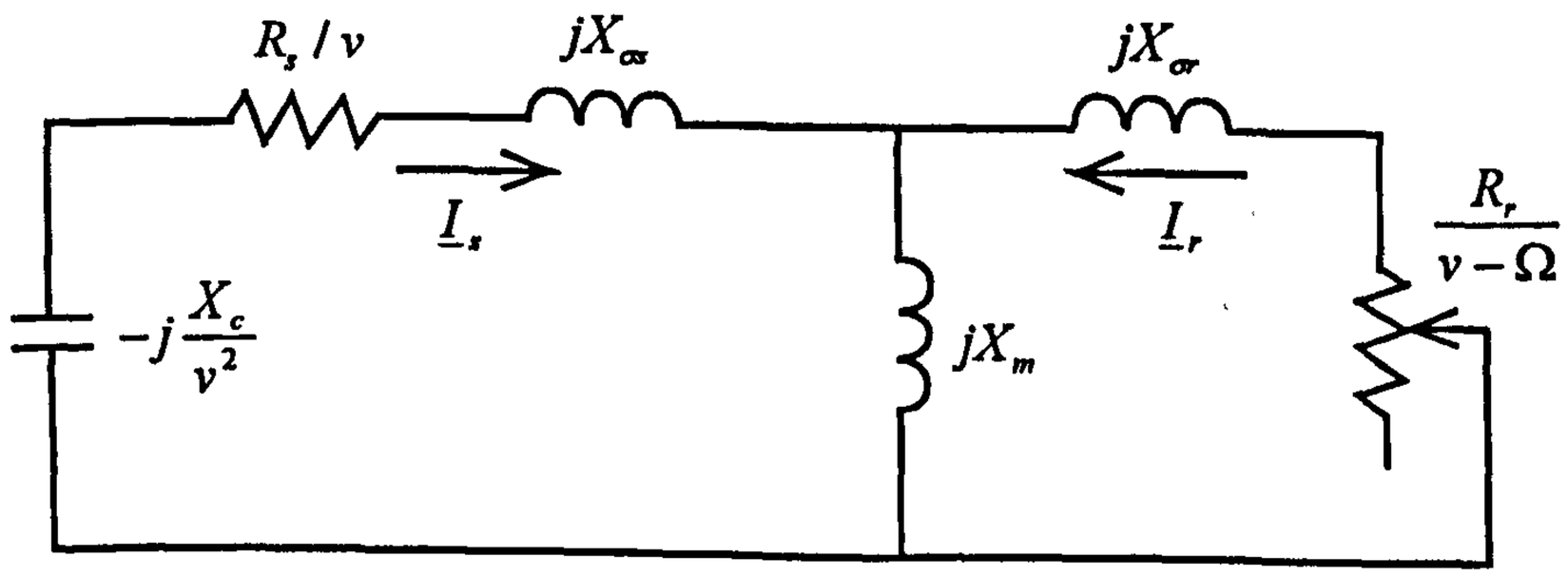

Figure 4.2.2 Complete per-phase equivalent circuit of a capacitor excited induction generator for no-load operation

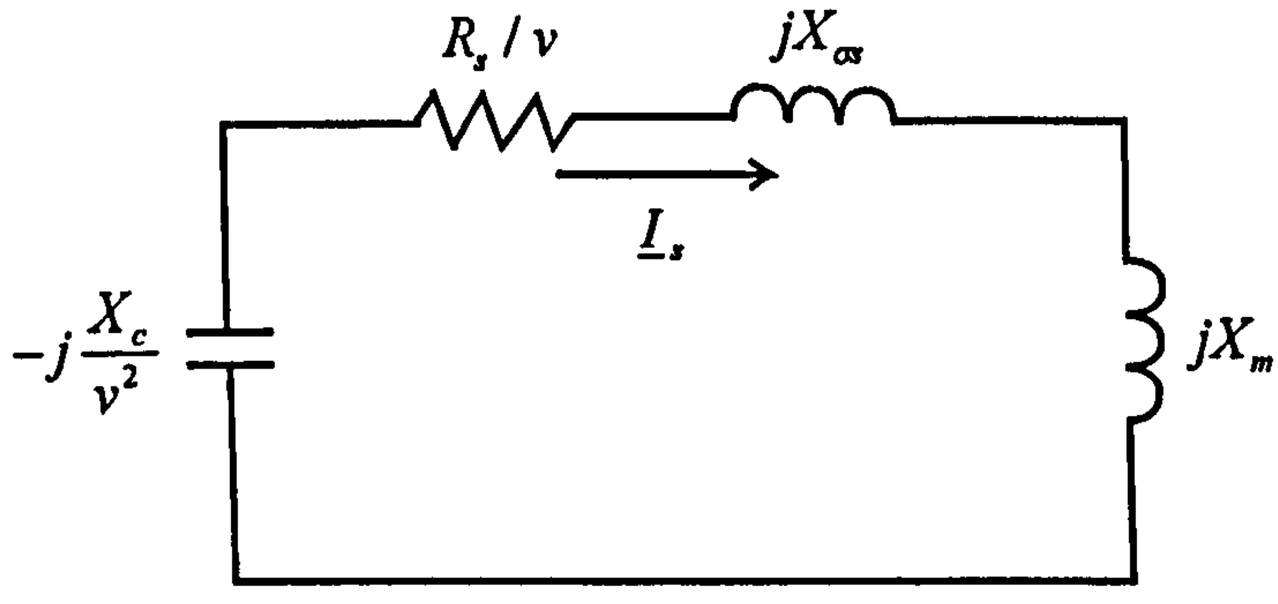

Figure 4.2.3 Per-phase equivalent circuit of a capacitor excited induction generator for ideal no-load operation (stator frequency equals electrical frequency of rotation)

As there are no voltage sources in the Figure 4.2.3, self-excitation process can only be initiated if a remanent voltage exists in the machine running at certain speed. This remanent voltage, which is the consequence of the remanent flux, will cause the initiation of the current flow in the circuit once when the capacitors are connected.

Magnetising reactance in Figure 4.2.3 is a non-linear element whose value is the function of the current through it. Figure 4.2.4 illustrates no-load generator voltage and capacitor voltage for the rated constant speed of operation, as functions of the magnetising current (that equals stator current under no-load conditions). Once when the self-excitation process is initiated due to the existence of the remanent voltage, the generator no-load voltage and the capacitor voltage will increase until the point of intersection of the two voltage curves is reached. Steady-state operation will take place in the point of intersection. Figure 4.2.4 immediately suggests the procedure for calculation of the required capacitor value. No-load voltage curve of the induction machine is determined from the no-load motoring test and the point in which the voltage is rated corresponds to the rated magnetising current. In order to find the required capacitor value it is only necessary to equate generator rated no-load voltage with the capacitor voltage, at rated stator frequency. Hence the value

$$C = \frac{I_{mn}}{V_n}\frac{1}{\omega_e} \tag{4.2-5}$$

is the capacitor value that will yield operation with rated voltage at machine terminals under no-load conditions at rated synchronous speed of rotation.

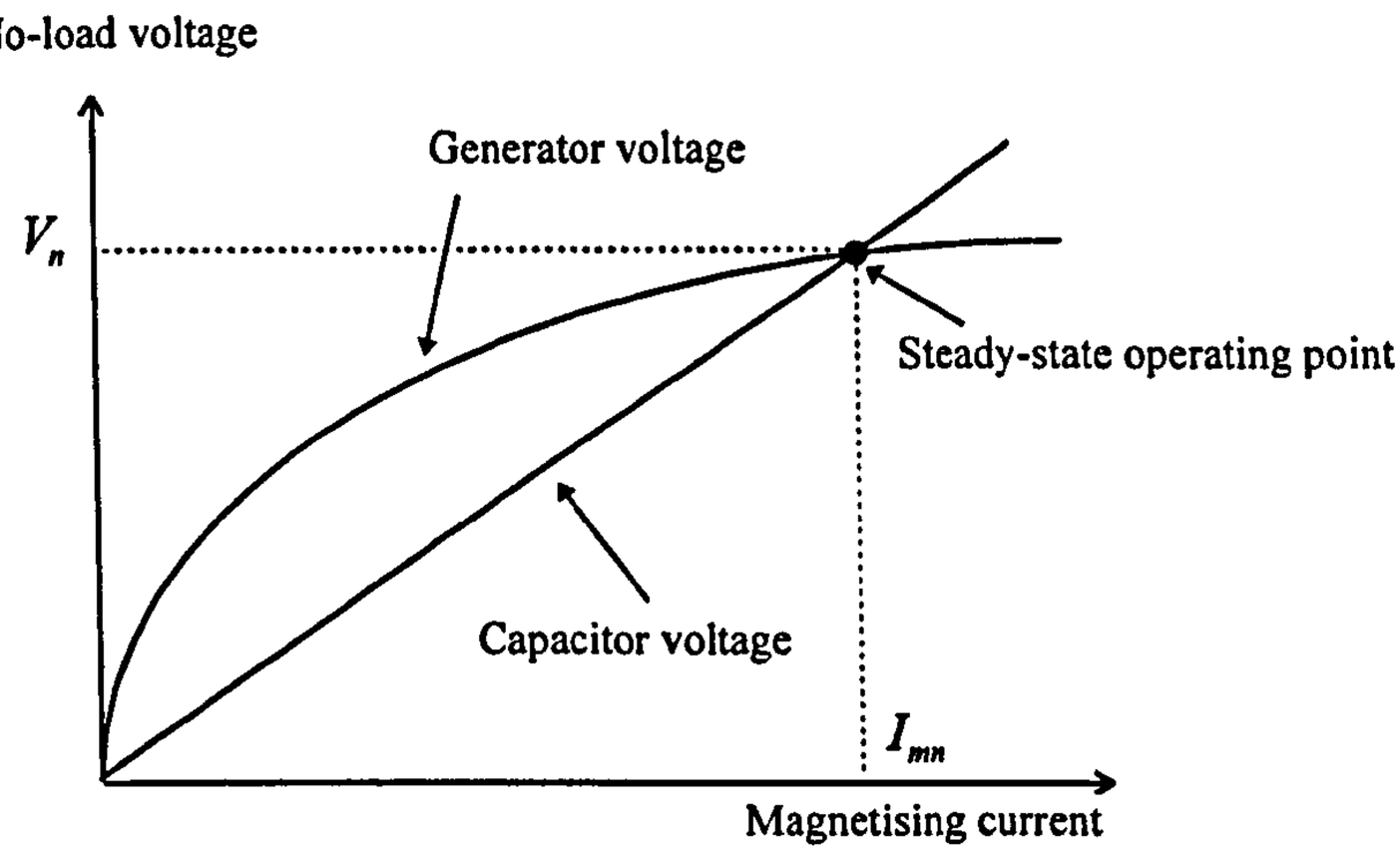

Figure 4.2.4 Induction generator's no-load voltage and capacitor voltage at rated synchronous speed of rotation

The pre-condition for the successful self-excitation is that the point of intersection of the generator no-load voltage curve and capacitor voltage line does exist. If the capacitor value is too small, no intersection will exist and self-excitation cannot take place.

4.3 Dynamic model of a single-cage induction generator and three-phase capacitor bank for no-load self-excitation analysis

The d-q axis single-cage induction machine models have been derived in Chapter 3. A complete saturated single-cage induction machine model is used here for simulation of self-excitation process with a three-phase capacitor bank. As already pointed out, any of the saturated machine models may be used, as choice of state-space variables does not affect results of simulation. If winding currents are selected as state-space variables, the saturated single-cage induction machine model in matrix form is given in arbitrary reference frame with equations (3.2-36) - (3.2-38). The electromagnetic torque is defined by (3.2-4a) and mechanical motion equation is given with (3.2-5).

Steady-state magnetising flux and magnetising current are given by

$$\psi_m = (\psi_{dm}^2 + \psi_{qm}^2)^{1/2} \qquad i_m = (i_{dm}^2 + i_{qm}^2)^{1/2} \tag{4.3-1}$$

where

$$\psi_{dm} = L_m i_{dm} \qquad i_{dm} = i_{ds} + i_{dr} \tag{4.3-2a}$$

$$\psi_{qm} = L_m i_{qm} \qquad i_{qm} = i_{qs} + i_{qr} \tag{4.3-2b}$$

The complete model of single-cage induction machine that accounts for main flux saturation is described by equations (3.2-4a), (3.2-5), (3.2-36) - (3.2-38) and (4.3-1) - (4.3-2). The reactive power required for self-excitation is provided by a three-phase capacitor bank which is connected in parallel to the machine stator terminals. Connection of capacitor bank adds two differential equations to the model. Therefore the additional differential equations that describe the capacitor bank are given with

$$\frac{dv_{ds}}{dt} = \omega_a v_{qs} - \frac{i_{ds}}{C} \tag{4.3-3a}$$

$$\frac{dv_{qs}}{dt} = -\omega_a v_{ds} - \frac{i_{qs}}{C} \tag{4.3-3b}$$

It is assumed in the simulation that induction generator operates at constant synchronous 50 Hz speed. Therefore, the mechanical motion equation (3.2-5) is omitted.

4.4 Load model for analysis of loaded operation

The model described so far is suitable for analysis of no-load self-excitation. In reality, a three-phase load will be switched in when self-excitation is completed and steady-state is achieved. Figure 4.4.1 illustrates a self-excited induction generator with three-phase capacitor bank, where a three-phase load will be connected in series with the induction generator stator terminals upon completion of self-excitation process.

When there is no load connected, the magnitude of capacitor current equals the induction generator current. Therefore

$$C\frac{dv_{ds}}{dt} = \omega_a C v_{qs} - i_{ds} \tag{4.4-1a}$$

$$C\frac{dv_{qs}}{dt} = -\omega_a C v_{ds} - i_{qs} \qquad (4.4\text{-}1b)$$

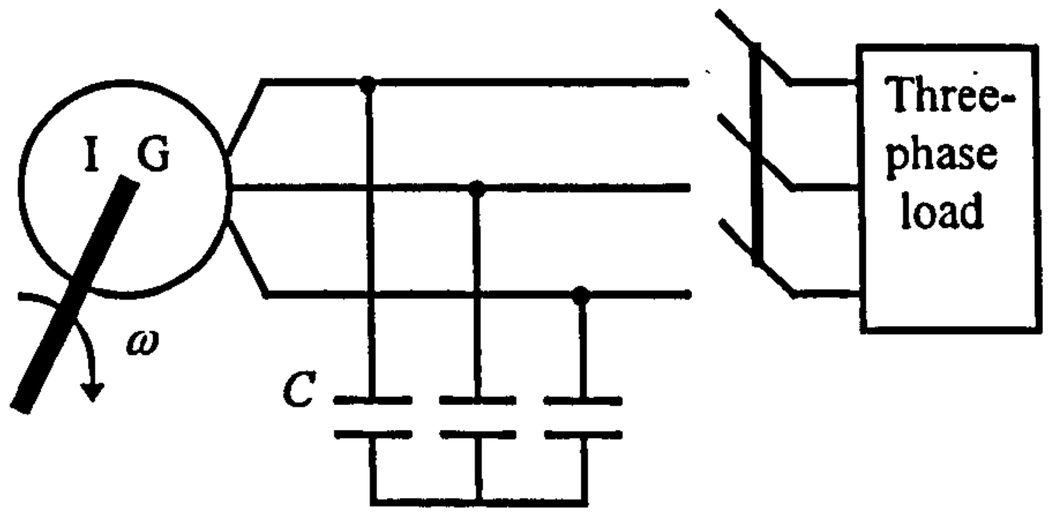

Figure 4.4.1 Self-excitation scheme comprising three-phase capacitor bank

It is assumed that a three-phase resistive load with equal resistances will be switched in after steady-state has been reached. Then the load currents in direct and quadrature axes are

$$i_{dl} = \frac{v_{ds}}{R} \qquad i_{ql} = \frac{v_{qs}}{R} \qquad (4.4\text{-}2)$$

Thus the magnitude of capacitor current equals the sum of load current and the induction generator current, i.e.,

$$C\frac{dv_{ds}}{dt} = \omega_a C v_{qs} - i_{ds} - i_{dl} \qquad (4.4\text{-}3a)$$

$$C\frac{dv_{qs}}{dt} = -\omega_a C v_{ds} - i_{qs} - i_{ql} \qquad (4.4\text{-}3b)$$

Rearranging equation (4.4-3) yields

$$\frac{dv_{ds}}{dt} = \omega_a v_{qs} - \frac{1}{C}(i_{ds} + i_{dl}) = \omega_a v_{qs} - \frac{1}{C} i_{ds} - \frac{v_{ds}}{CR} \qquad (4.4\text{-}4a)$$

$$\frac{dv_{qs}}{dt} = -\omega_a v_{ds} - \frac{1}{C}(i_{qs} + i_{ql}) = -\omega_a v_{ds} - \frac{1}{C} i_{qs} - \frac{v_{qs}}{CR} \qquad (4.4\text{-}4b)$$

Equations (4.4-4), together with equations (3.2-4a), (3.2-5), (3.2-36) - (3.2-38) and (4.3-1) - (4.3-2) constitute the model for transient analysis of loaded operation of a self-

excited induction generator.

4.5 Model of a double-cage induction generator and three-phase capacitor bank for no-load self-excitation simulation

The d-q axis double-cage induction machine model given in Chapter 3 is used for simulation of self-excitation with a three-phase capacitor bank. The saturated double-cage induction machine model with stator and rotor currents selected as state-space variables is given in arbitrary reference frame with equations (3.3-30) - (3.3-34). Saturation dependent inductances are defined by (3.3-25). The steady-state magnetising inductance and dynamic inductance are given in (3.3-27). Magnetising flux and magnetising current are given by (3.3-15) - (3.3-16). The electromagnetic torque is defined in (3.3-5a). A three-phase capacitor bank is connected in parallel to the machine stator terminals. The additional differential equations that describe the capacitor bank are the same as those for the single-cage induction generator, equation (4.3-3).

4.6 Simulation results

4.6.1 No-load self-excitation of a single-cage induction generator

Self-excitation of single-cage induction generator is at first simulated under no-load condition with reactive power being supplied by a three-phase capacitor bank. The induction generator operates at constant speed and there is no load connected to the machine terminals. The single-cage induction machine parameters used in the simulation are given in Appendix. The parameters required in the model are calculated from standard no-load and locked rotor tests. Magnetising curve of the machine, $\psi_m = f(i_m)$, is determined from motoring no-load test and is given in Appendix, in a form of analytical expression arrived at by means of least-squares fitting of the experimental data. As the saturated machine model requires dynamic inductance, the function $L = d\psi_m / di_m = f(i_m)$ is required and also given in Appendix. The magnetising curve, steady-state magnetising inductance and dynamic inductance as function of magnetising

current are shown in Figure 4.6.1 (in terms of rms values). It can be seen from Figure 4.6.1 that variation of the steady-state saturated magnetising inductance differs considerably from the variation of dynamic inductance. Therefore, the inductance L_{dq} which describes the cross-saturation effect is not zero and omission of cross-saturation would lead to incorrect simulation results.

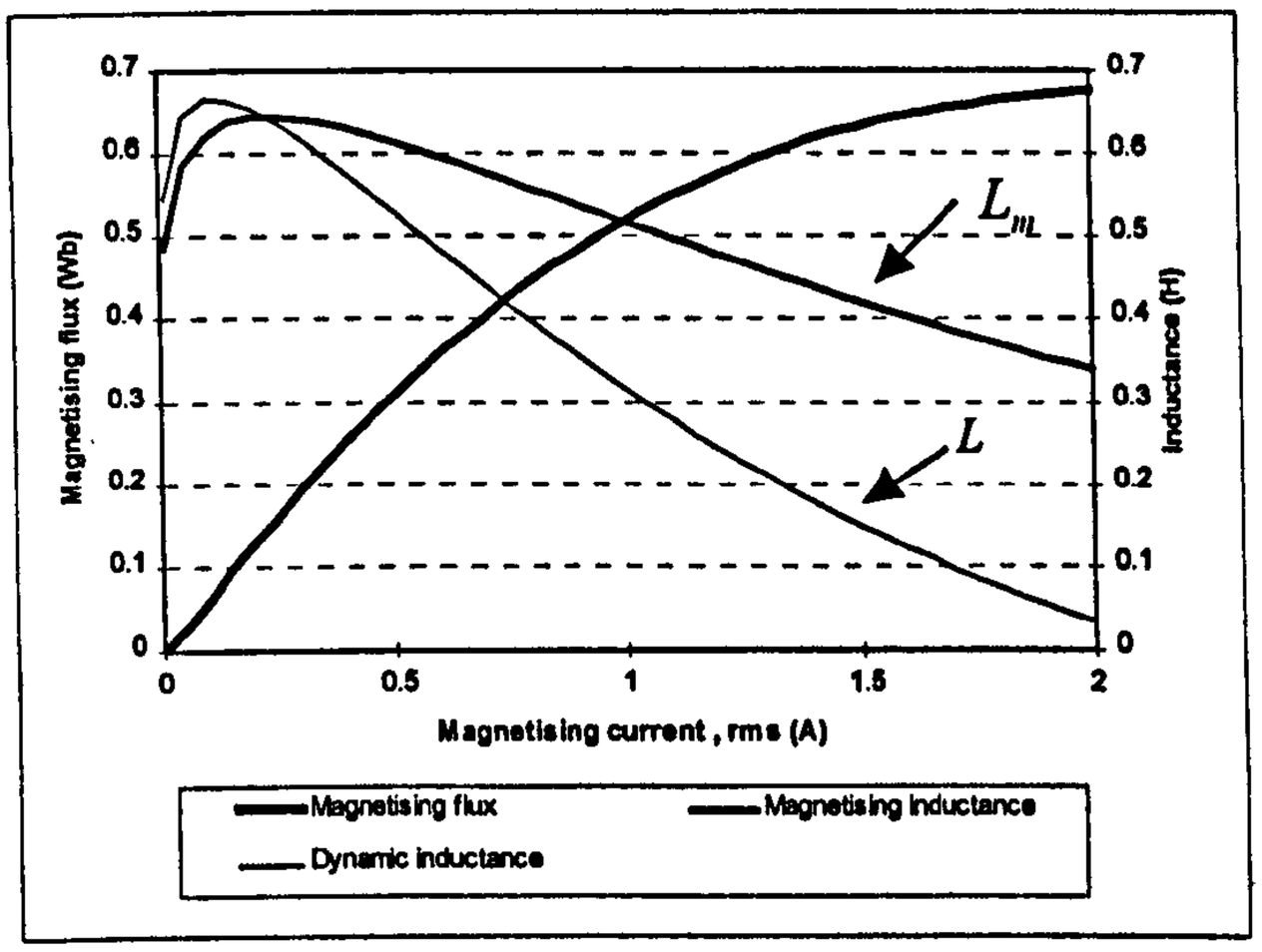

Figure 4.6.1 Magnetising curve, magnetising inductance and dynamic inductance of the single-cage induction machine

The capacitor bank is connected in star, in parallel to the machine terminals and the per-phase capacitance is 25 μF. This value provides steady-state no-load operation in the rated point of the magnetising curve. The rotational speed of the induction generator is kept constant and is equal to the synchronous 50 Hz speed. The d-q axis equations of the induction machine model are rearranged into state-space form,

$$\frac{d[x_{dq}]}{dt} = [A]^{-1}[v_{dq}] - [A]^{-1}[B][x_{dq}] \qquad (4.6\text{-}1)$$

In order to initialise self-excitation, an initial non-zero value of the magnetising current is needed, which is obtained experimentally by running the machine at constant speed and measuring the remanent voltage. The values of the magnetising current are calculated from equations (4.3-1) and (4.3-2) at each computation step. The non-linear functions of magnetising flux and dynamic inductance are then entered, the steady-state

saturated magnetising inductance and dynamic inductance are thus calculated. New values of the inductances L_{dd}, L_{qq} and L_{dq} are calculated from equation (3.2-37) and matrices [A] and [B] are updated. Matrix [A] must be inverted and matrix multiplication $[A]^{-1}[B]$ must be performed at each computation step. Figure 4.6.2 shows voltage, current and torque build-up during self-excitation, obtained by simulation. Voltage and current reach steady-state after approximately 0.85 s. Steady-state peak phase voltage is slightly above 311 V, indicating that the machine operates near the rated 220 V_{rms} phase-to-neutral voltage. Waveforms of current and voltage build-up are the same. Frequency of voltage and current is slightly below 50 Hz in steady-state as the machine generates active power required to cover copper losses in stator and rotor windings. Torque value in steady-state is therefore negative and around -0.62 Nm.

4.6.2 Loading transients of a single-cage induction generator

Loading transient of the single-cage induction generator is simulated next, previous steady-state being the one attained in Figure 4.6.2. A three-phase pure resistive load of 300 Ω per phase is suddenly applied at t = 1.5 s. Figure 4.6.3 shows the load transient response of the induction generator. The stator voltage and stator current decrease when the load is applied. The machine torque develops rapidly and the machine now generates approximately 60% of the rated power. Figure 4.6.3 illustrates one of the major problems in application of capacitor excited induction generators, which is absence of voltage regulation. Any change in loading conditions causes change in the load voltage and it is not possible to provide constant voltage operation for a variable load.

4.6.3 No-load self-excitation of a double-cage induction generator

Double-cage induction generator is studied by simulation in this section. In the induction generator of double-cage construction the two cages are connected by means of end rings. The machine is at first represented with full saturated double-cage machine model. Parameters required in the model are calculated from design data and are listed

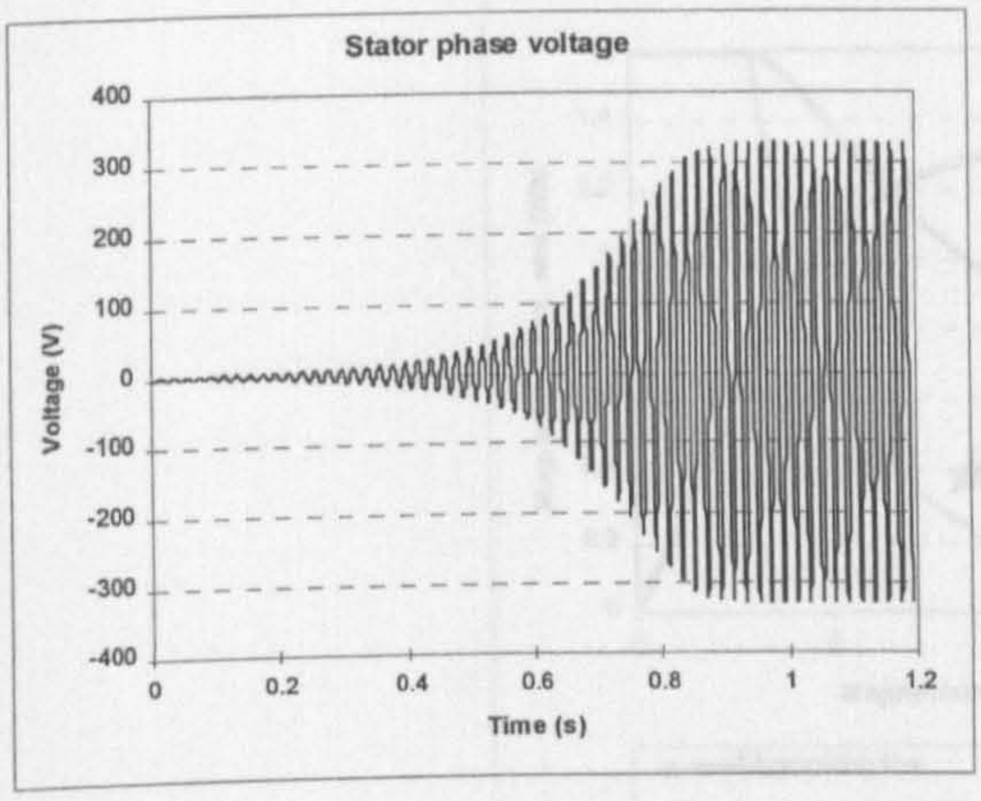

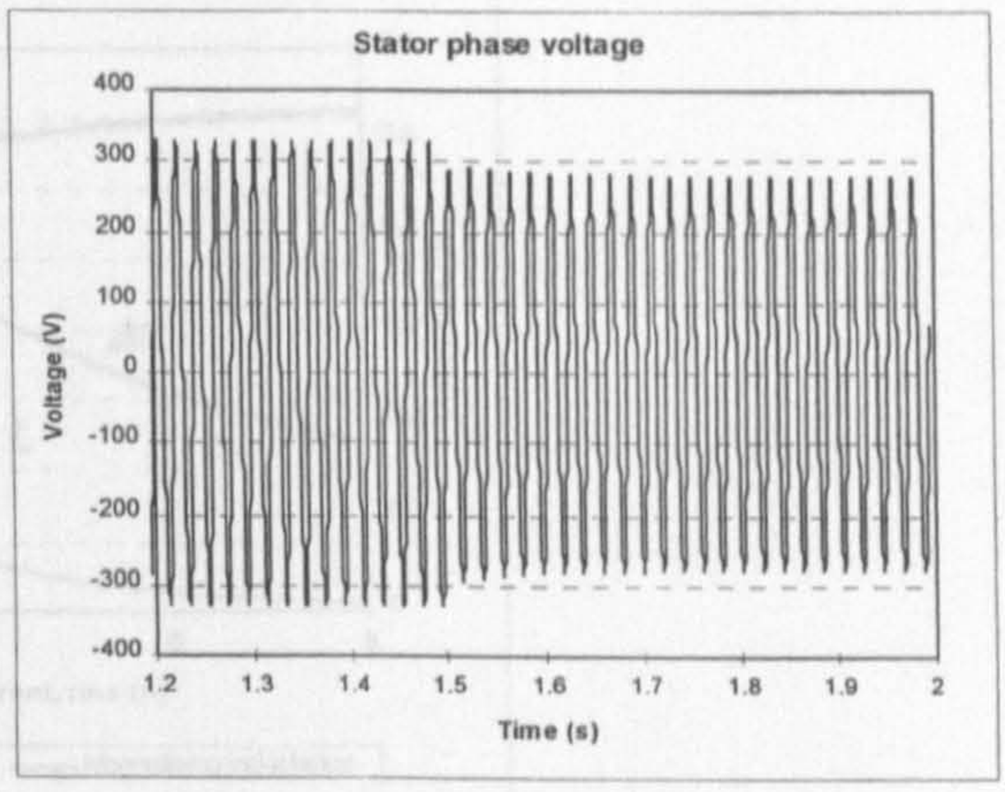

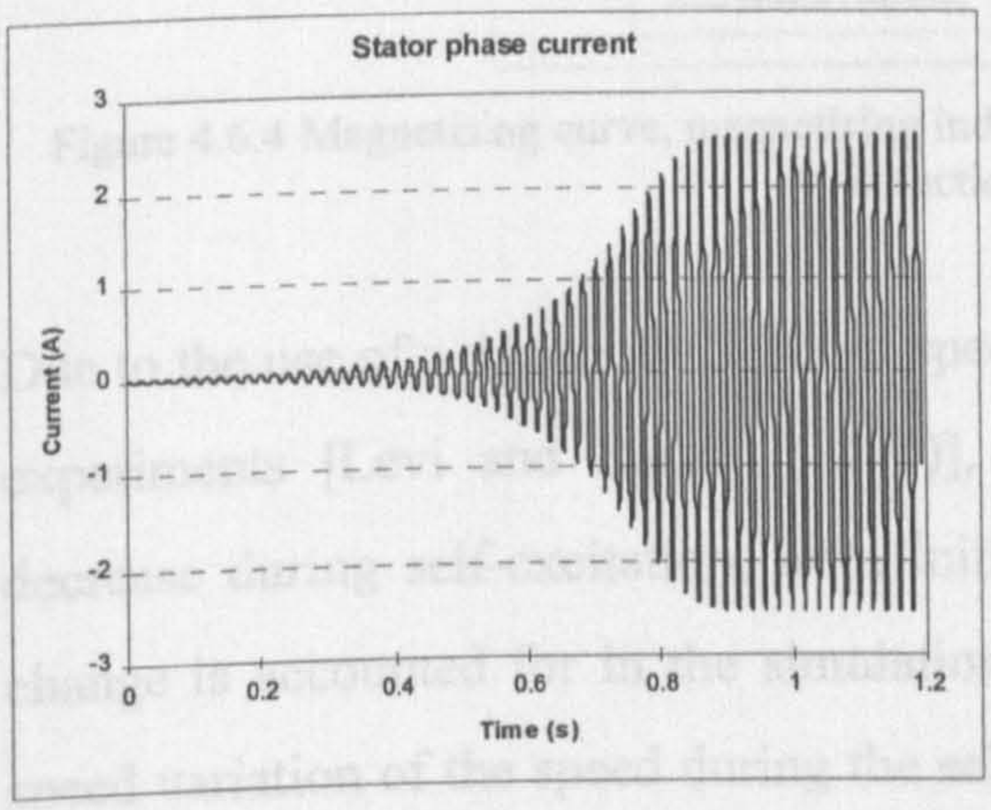

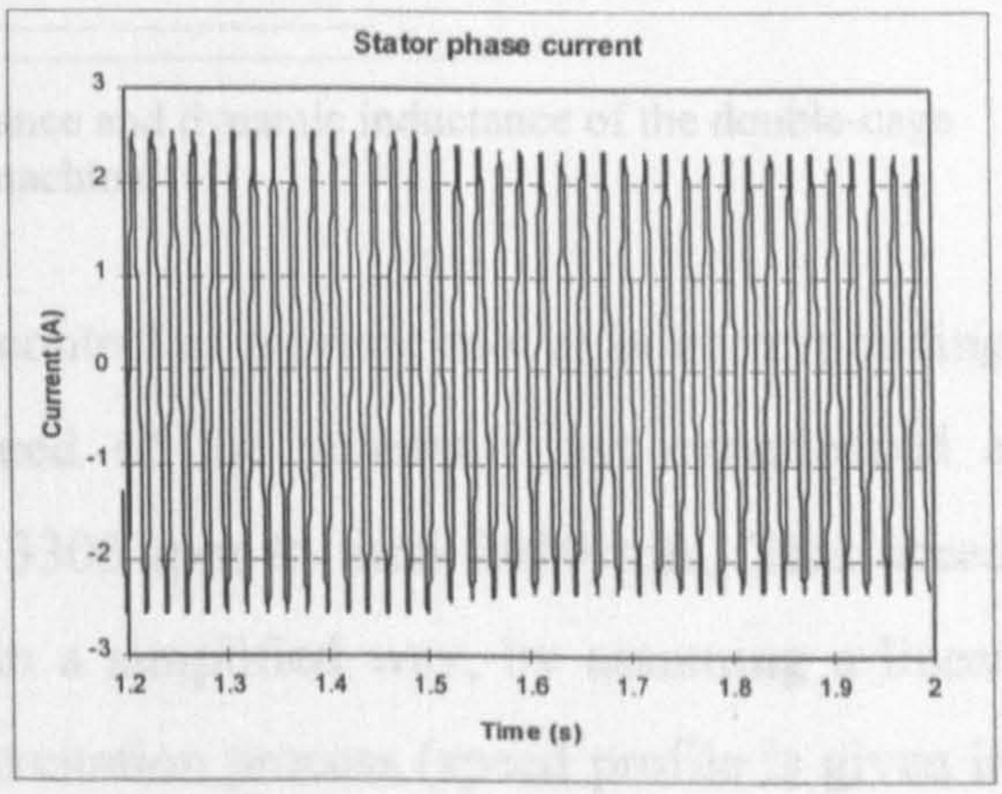

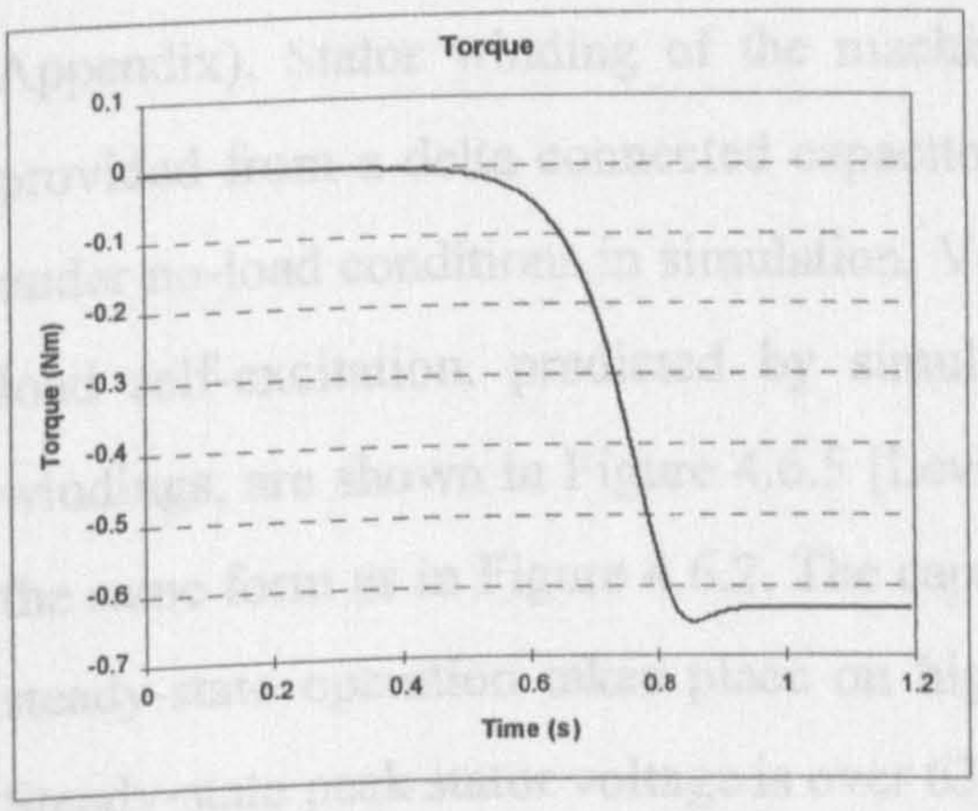

Figure 4.6.2 Voltage, current and torque build-up of a single-cage induction generator

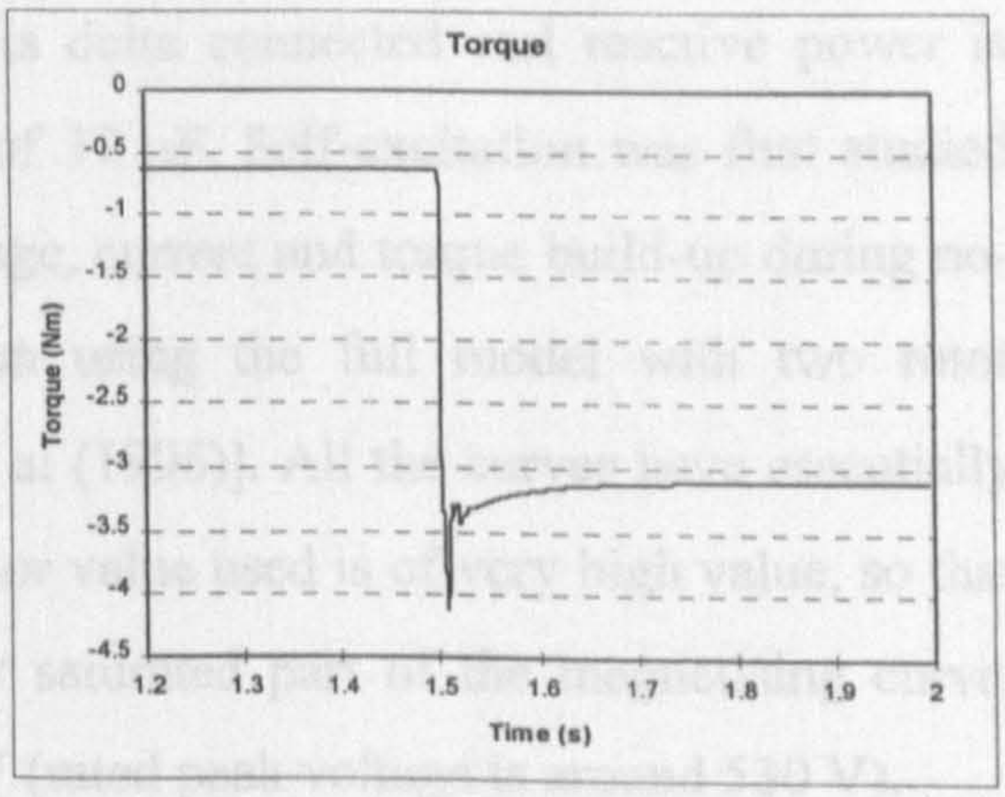

Figure 4.6.3 Loading transient of a single-cage induction generator

in Appendix. Magnetising curve of the machine is determined from motoring no-load test and is given in Appendix. The dynamic inductance as a function of magnetising current is given in Appendix as well. Figure 4.6.4 shows magnetising curve, steady-state magnetising inductance and dynamic inductance, all as functions of magnetising current. Simulation procedure corresponds to the one described in Section 4.6.1.

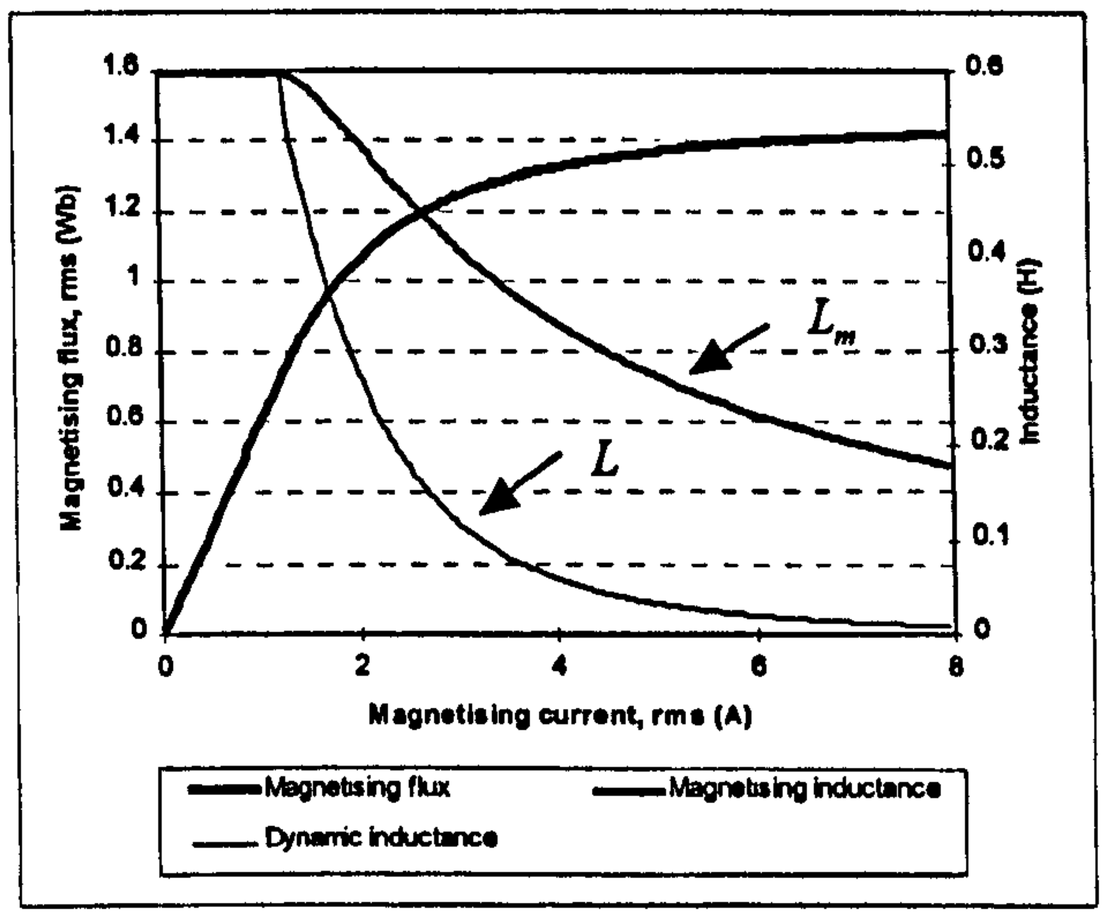

Figure 4.6.4 Magnetising curve, magnetising inductance and dynamic inductance of the double-cage induction machine

Due to the use of a d.c. motor without speed control as a prime mover in corresponding experiments [Levi and Rauski (1993)], speed of the generator has experienced a decrease during self-excitation, from initial 3305 rpm to final 3010 rpm. This speed change is accounted for in the simulations in a simplified way, by assuming a linear speed variation of the speed during the self-excitation process (speed profile is given in Appendix). Stator winding of the machine is delta connected and reactive power is provided from a delta connected capacitors of 37 μF. Self-excitation was first studied under no-load conditions in simulation. Voltage, current and torque build-up during no-load self-excitation, predicted by simulation using the full model with two rotor windings, are shown in Figure 4.6.5 [Levi et al (1996)]. All the curves have essentially the same form as in Figure 4.6.2. The capacitor value used is of very high value, so that steady-state operation takes place on highly saturated part of the magnetising curve. Steady-state peak stator voltage is over 630 V (rated peak voltage is around 530 V).

4.6.4 Loading transients of a double-cage induction generator

Loading transient of the double-cage induction generator is simulated next, previous steady-state being the one reached in Figure 4.6.5. A symmetrical three-phase resistive load of 100 Ω is switched in at t = 1.75 s. Figure 4.6.6 shows the loading transient of the induction generator. Application of the load causes once more reduction in stator

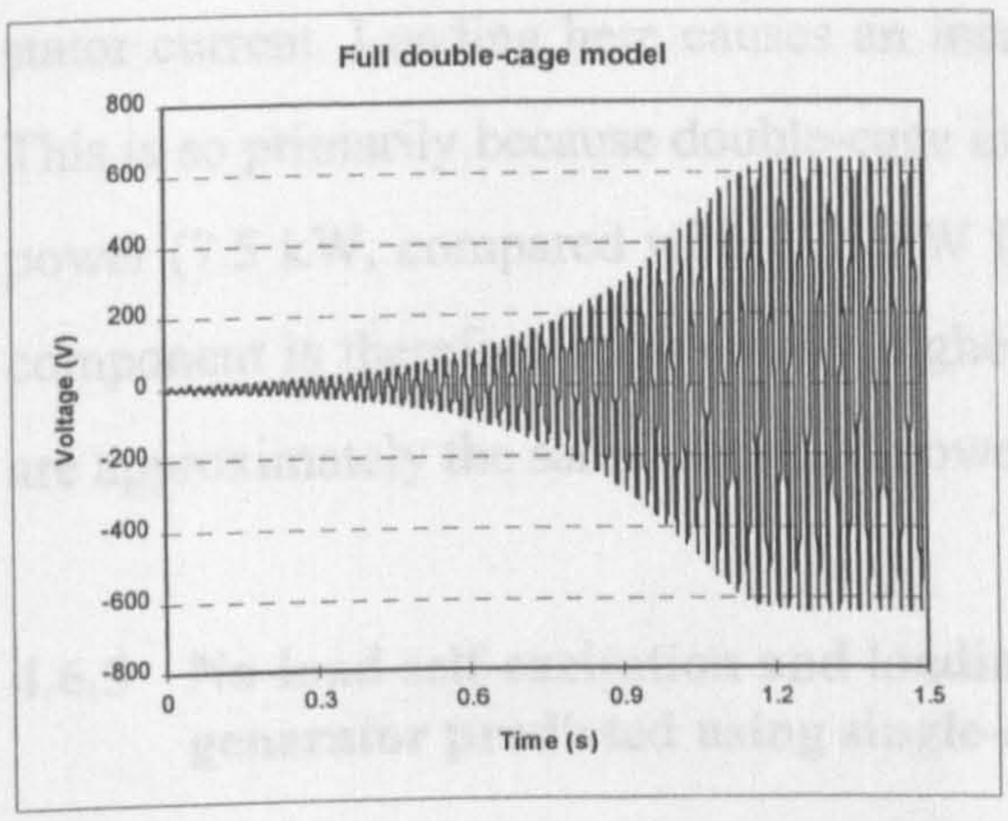

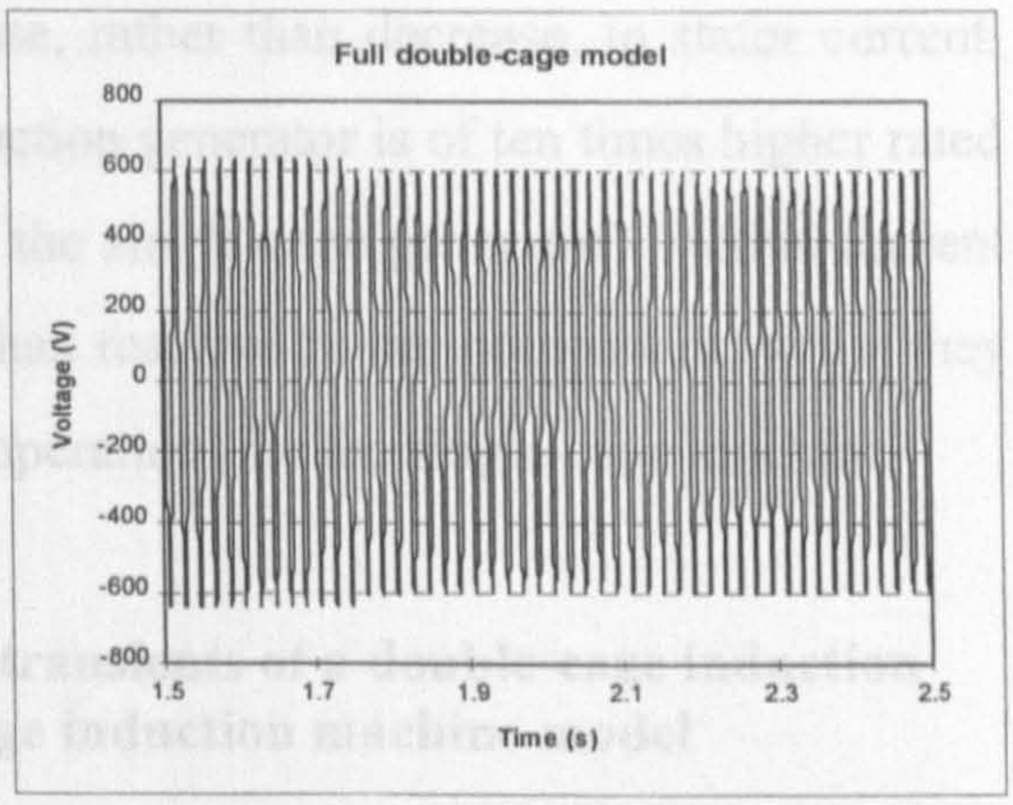

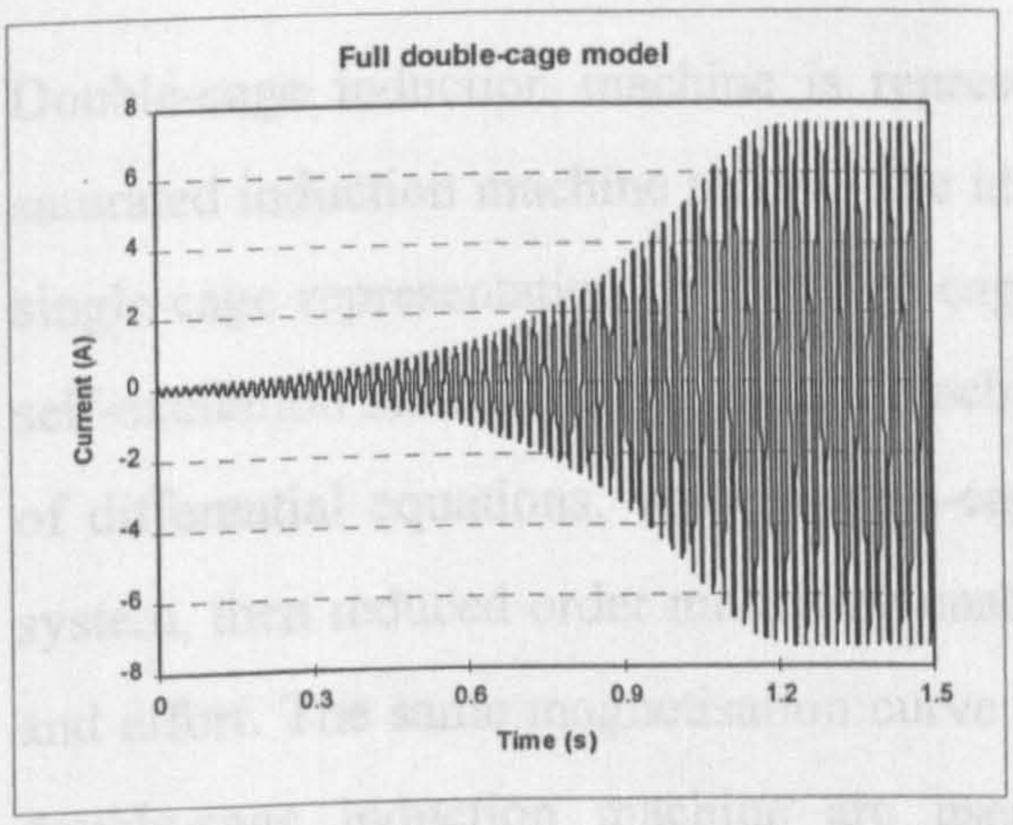

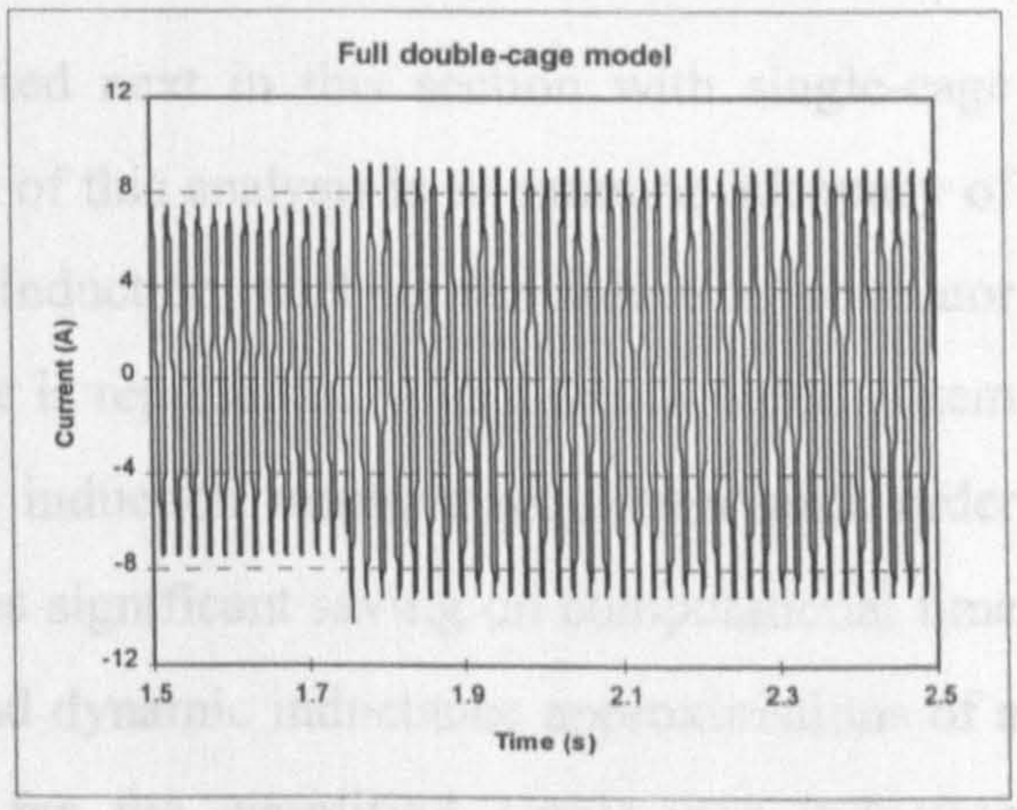

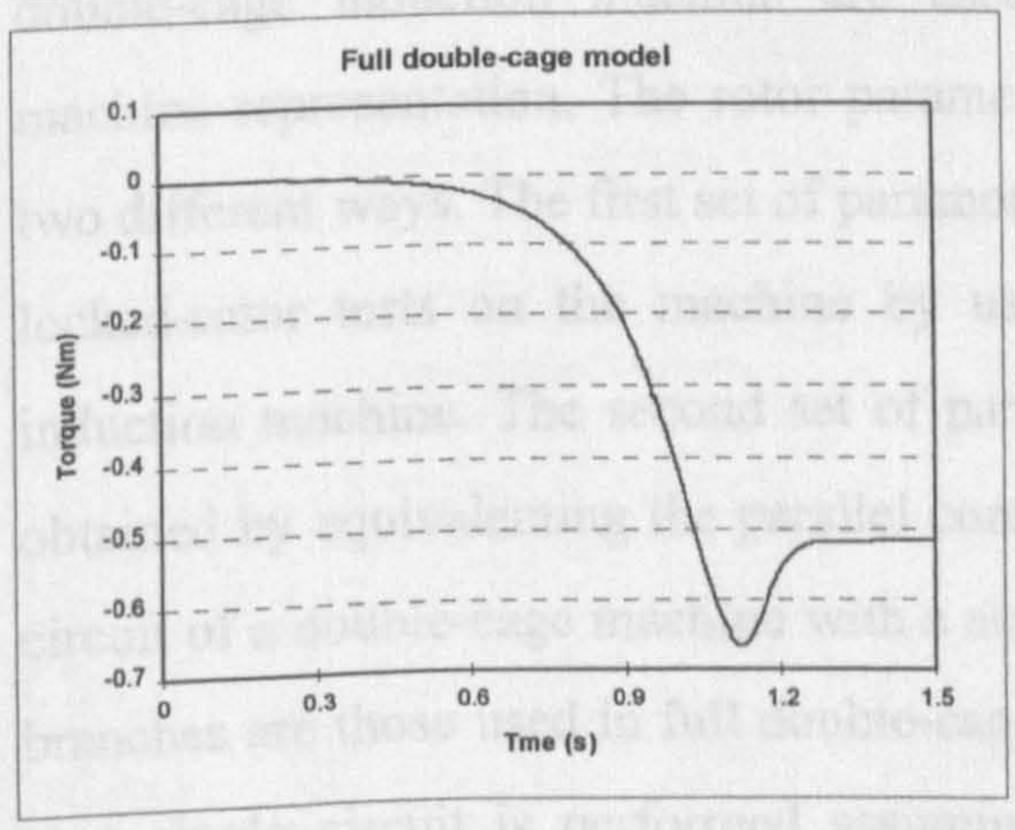

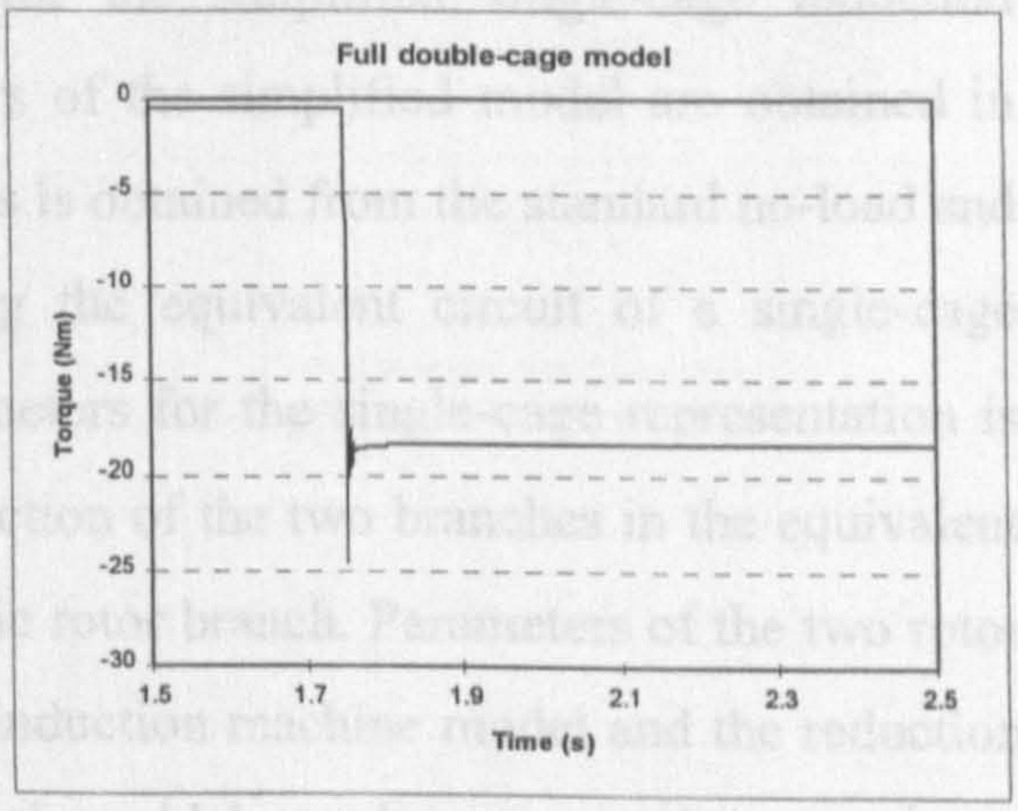

Figure 4.6.5 Voltage, current and torque build-up predicted by full double-cage induction machine model

Figure 4.6.6 Loading transient of a double-cage induction generator

voltage. However, stator voltage decrease is now rather small as the previous steady-state corresponds to operation in the highly saturated region of the magnetising curve (in the case of the single-cage induction generator, previous steady-state was close to rated point on the magnetising curve). One interesting difference, compared with the single-cage induction generator loading transient, can be observed in the waveform of the

stator current. Loading here causes an increase, rather than decrease, in stator current. This is so primarily because double-cage induction generator is of ten times higher rated power (7.5 kW, compared with 0.75 kW for the single-cage generator). Active current component is therefore substantially higher than reactive power component, while they are approximately the same (for rated power operation) for the single-cage machine.

4.6.5 No-load self-excitation and loading transients of a double-cage induction generator predicted using single-cage induction machine model

Double-cage induction machine is represented next in this section with single-cage saturated induction machine model. The idea of this analysis is to examine adequacy of single-cage representation of a double-cage induction machine for induction generator self-excitation study. As single-cage machine is represented with a fourth order system of differential equations, while double-cage induction machine requires a sixth order system, then reduced order modelling enables significant saving on computational time and effort. The same magnetisation curve and dynamic inductance approximations of a double-cage induction machine are used for the simplified single-cage induction machine representation. The rotor parameters of the simplified model are obtained in two different ways. The first set of parameters is obtained from the standard no-load and locked-rotor tests on the machine by using the equivalent circuit of a single-cage induction machine. The second set of parameters for the single-cage representation is obtained by equivalenting the parallel connection of the two branches in the equivalent circuit of a double-cage machine with a single rotor branch. Parameters of the two rotor branches are those used in full double-cage induction machine model and the reduction to a single circuit is performed assuming sinusoidal steady-state conditions at zero speed. Thus both sets of rotor parameters actually represent rotor with 50 Hz parameters. Both sets of parameters are included in Appendix under the sub-headings 'the first set of parameters' and 'the second set of parameters', respectively. Detailed description of calculation of these parameters is given in [Rauski and Levi (1992)].

The same simulation runs are repeated for exactly the same conditions as for the full saturated double-cage model, but this time using the single-cage representation of the induction machine. Current, voltage and torque build-up, obtained with single-cage

representation and the first set of parameters (locked rotor test parameters), are shown in Figure 4.6.7 [Levi et al (1996)] while the load transients are shown in Figure 4.6.8.

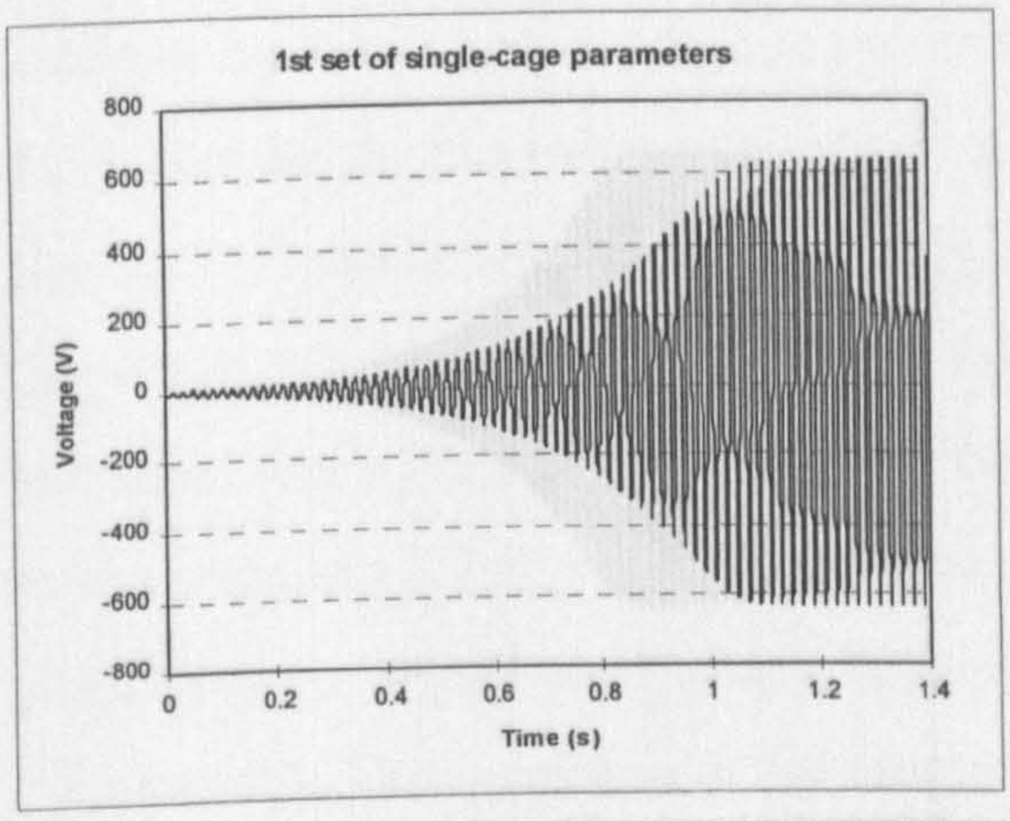

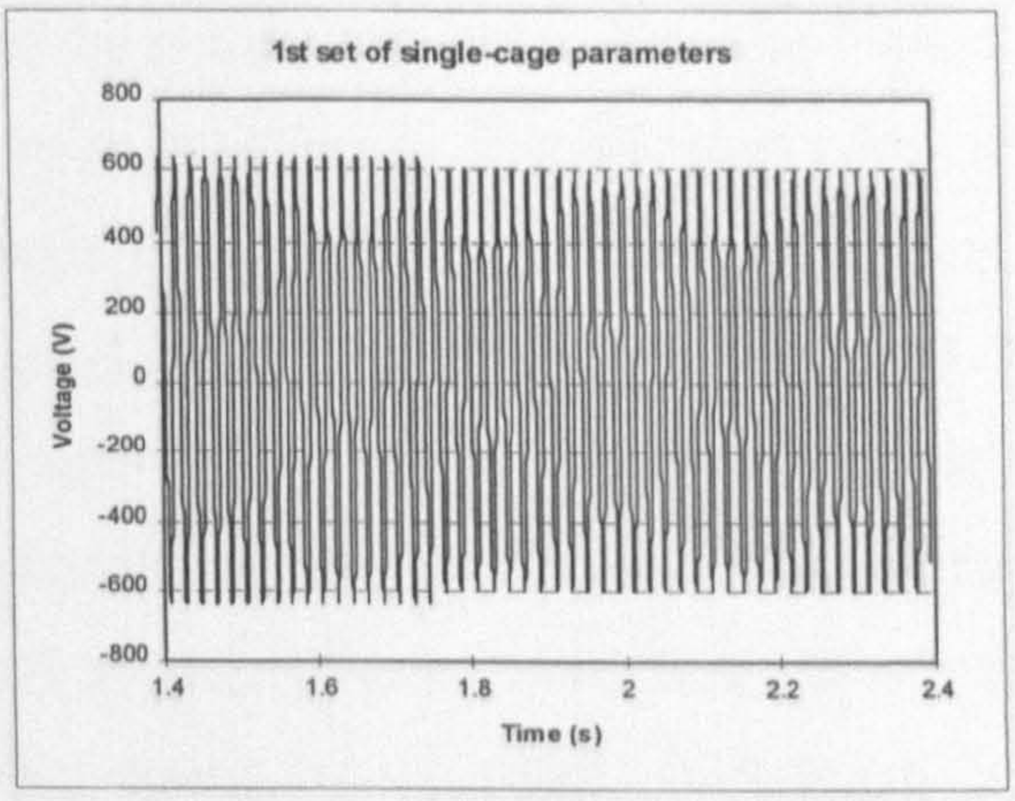

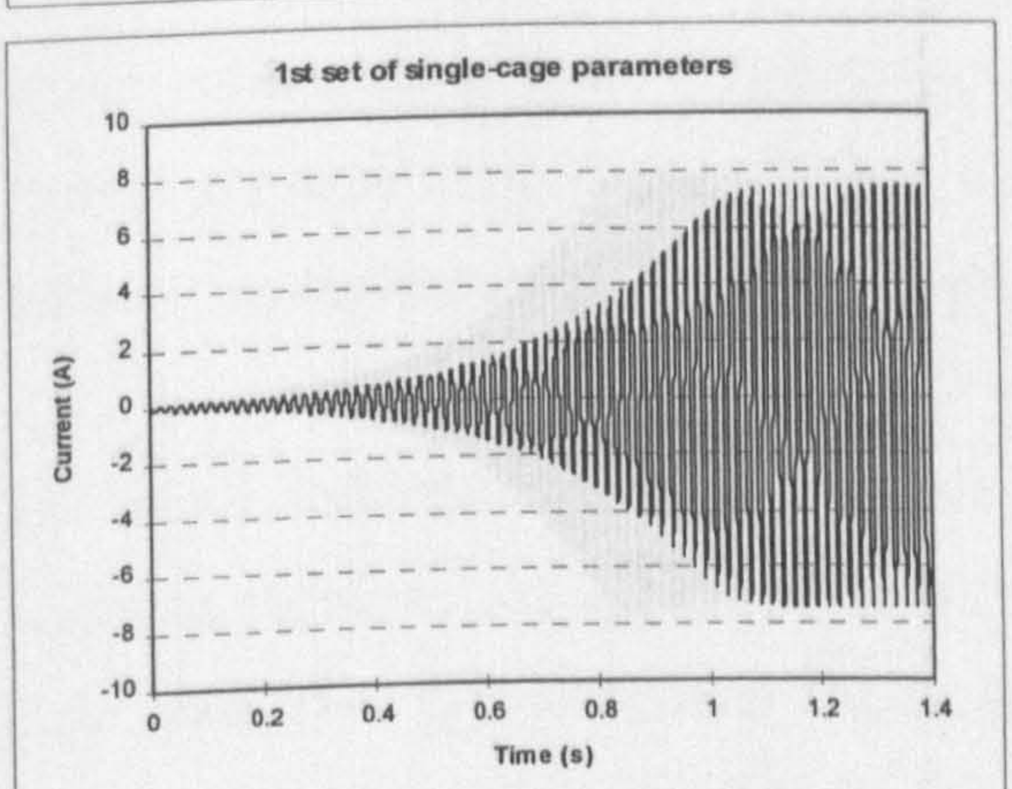

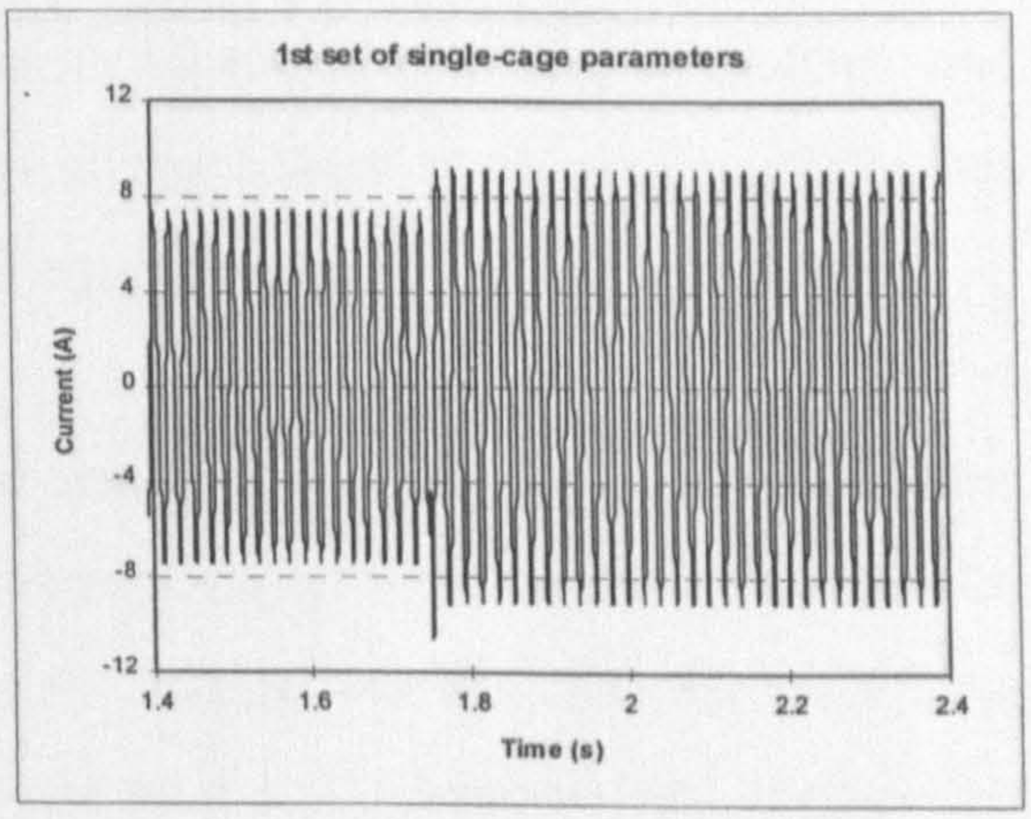

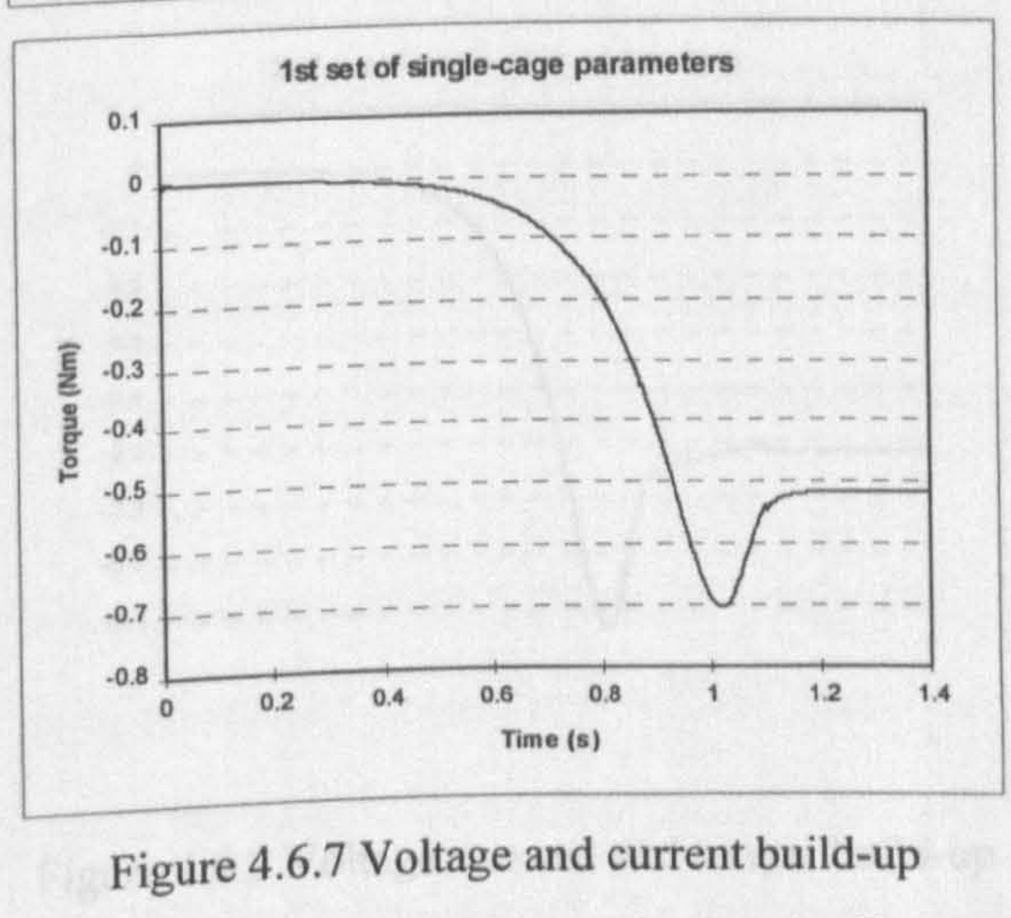

Figure 4.6.7 Voltage and current build-up predicted by single-cage model using the first set of parameters

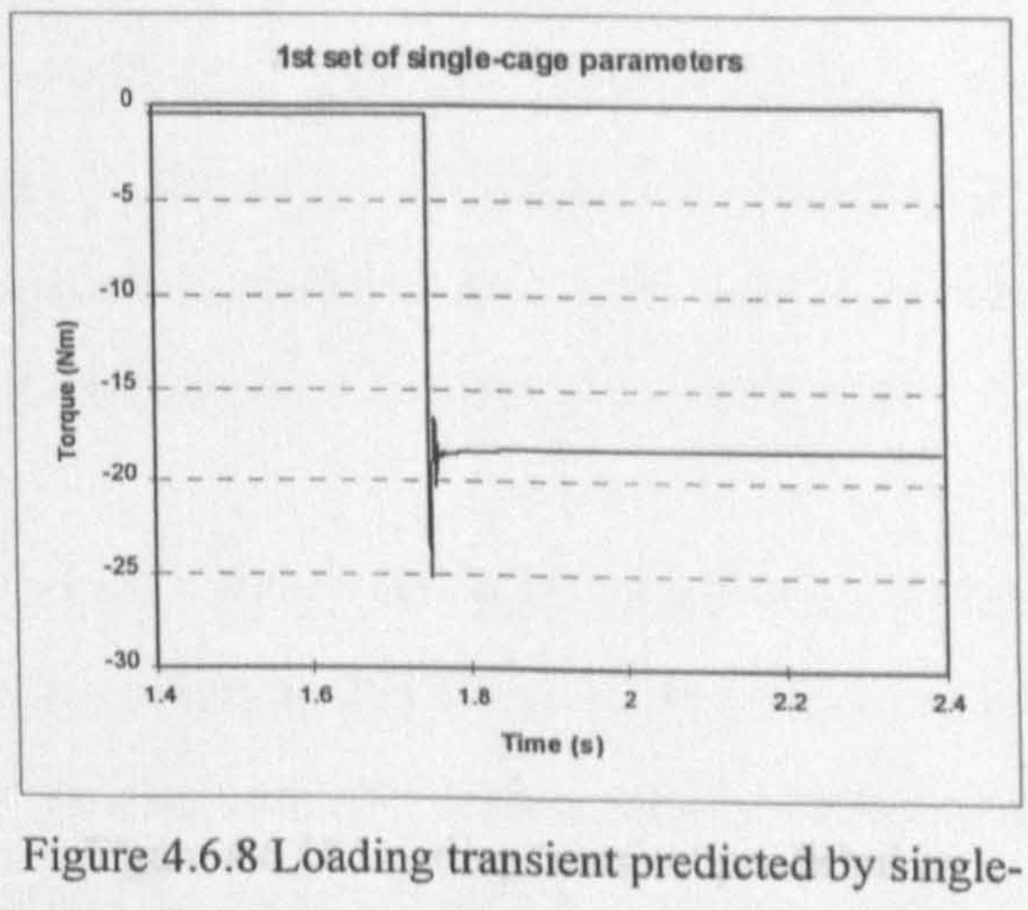

Figure 4.6.8 Loading transient predicted by single-cage model using the first set of parameters

Next, simulation on the basis of the single-cage representation is repeated once more, this time with the second set of parameters. Voltage, current and torque build-up and

subsequent loading transient are shown in Figures 4.6.9 [Levi et al (1996)] and 4.6.10 respectively.

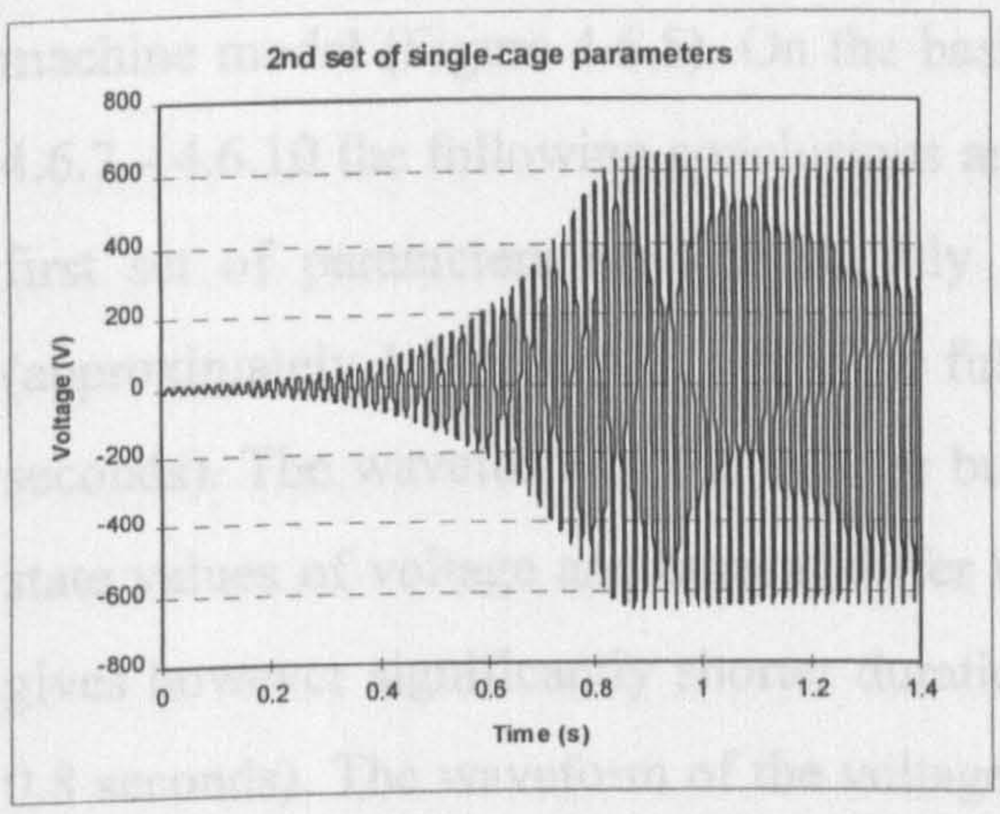

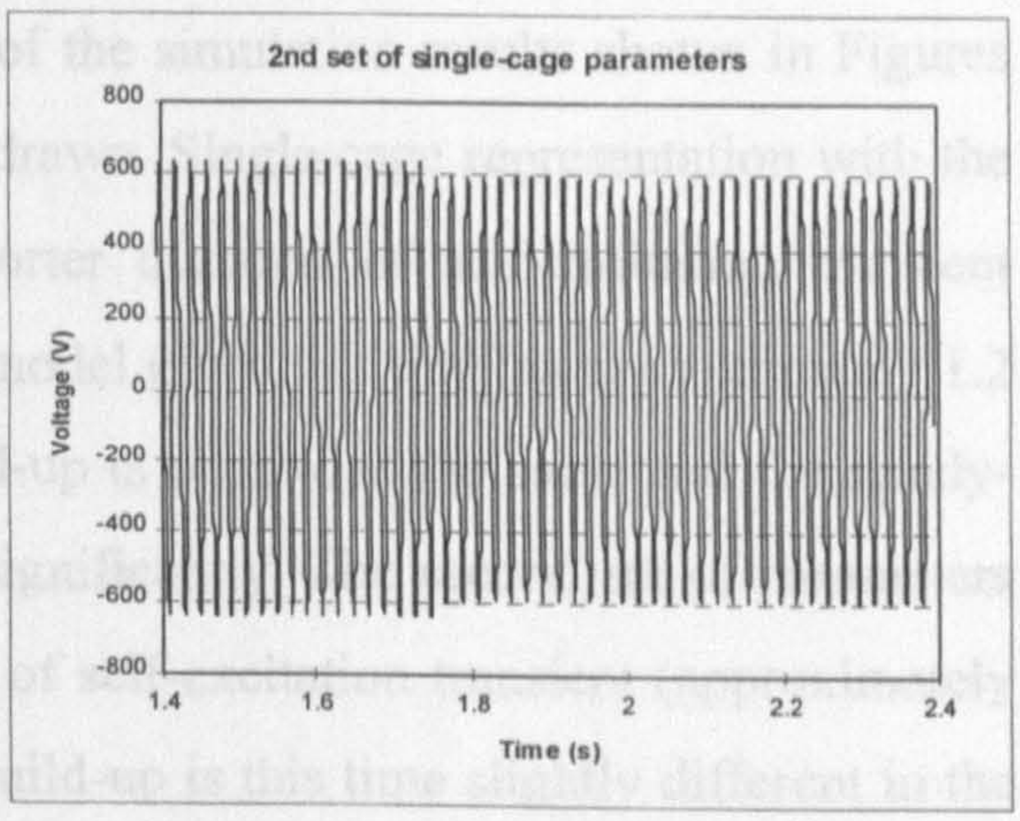

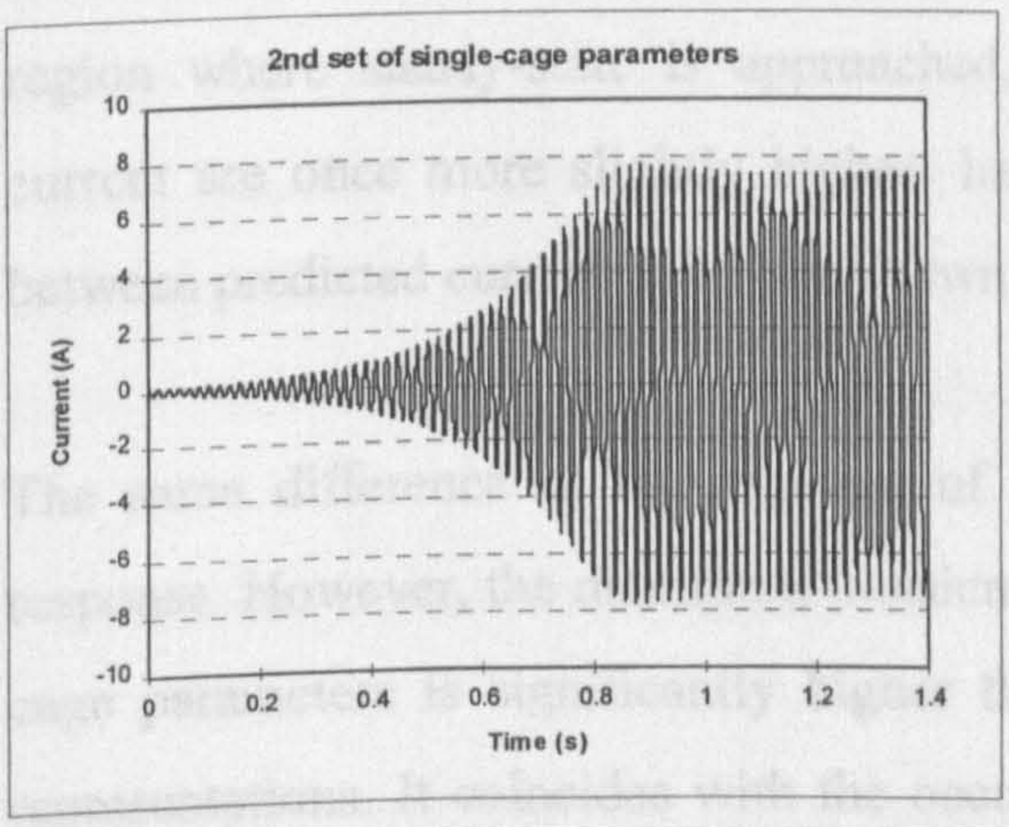

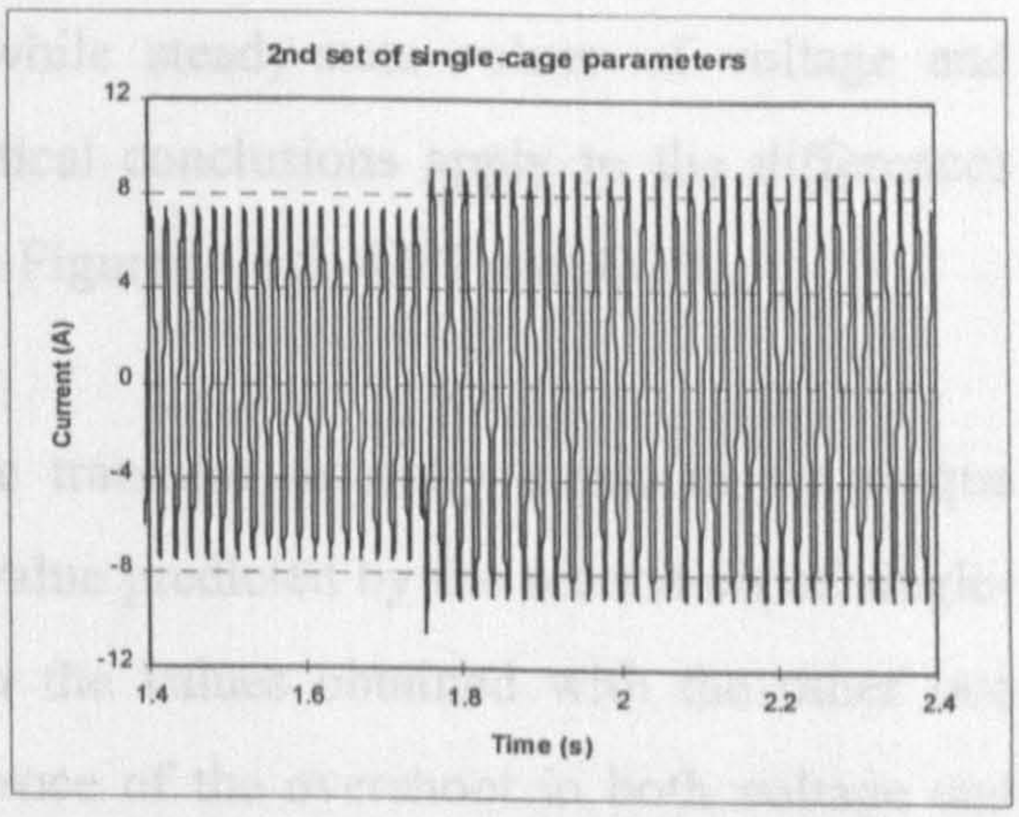

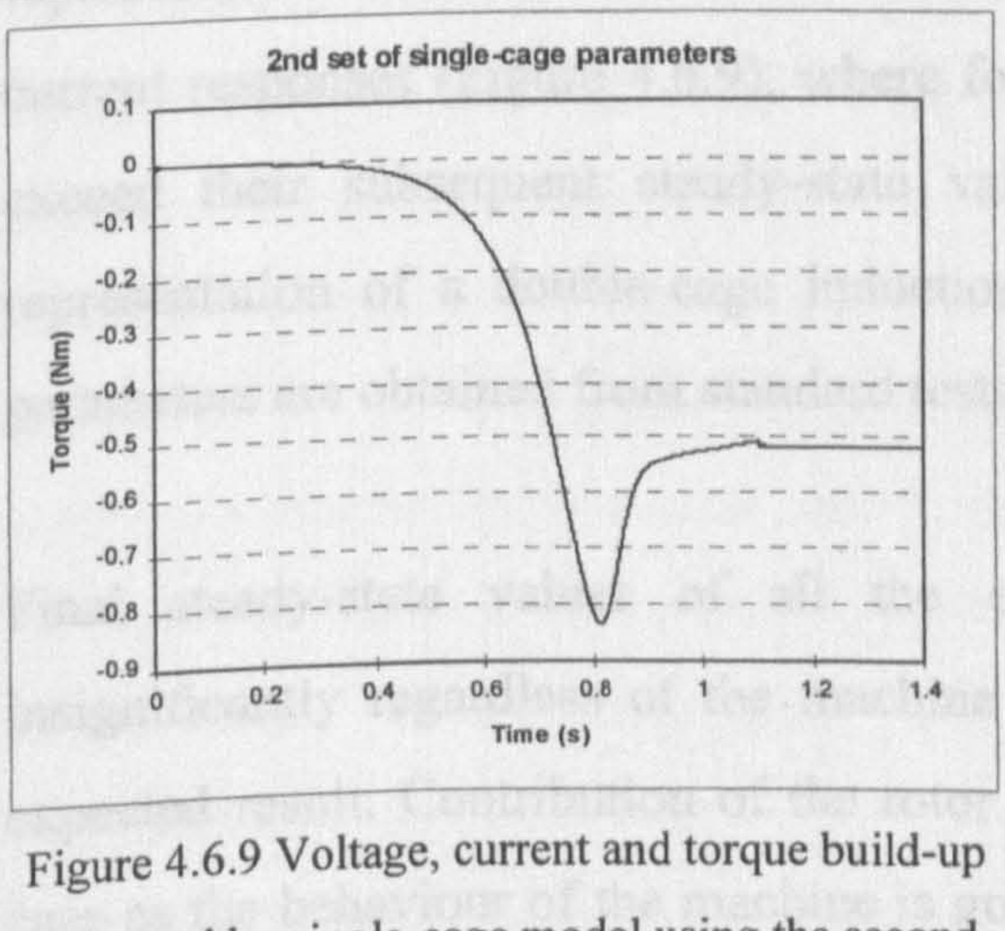

Figure 4.6.9 Voltage, current and torque build-up predicted by single-cage model using the second set of parameters

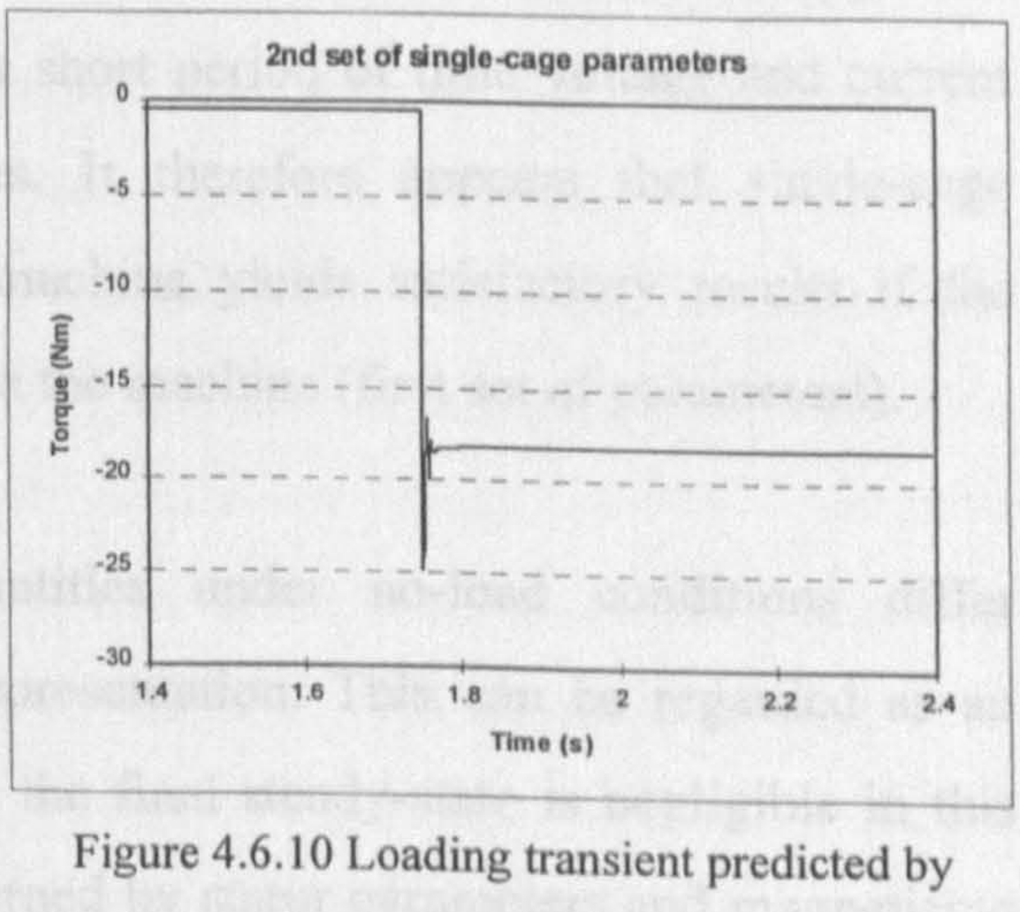

Figure 4.6.10 Loading transient predicted by single-cage model using the second set of parameters

Simulation results of a double-cage induction generator self-excitation obtained with single-cage representation (both the first set and the second set of parameters) are compared with the results obtained by means of the full saturated double-cage induction machine model (Figure 4.6.5). On the basis of the simulation results shown in Figures 4.6.7 - 4.6.10 the following conclusions are drawn. Single-cage representation with the first set of parameters predicts slightly shorter duration of self-excitation transient (approximately 1.08 seconds, while the full model gives this time as approximately 1.2 seconds). The waveform of the voltage build-up is otherwise the same and the steady-state values of voltage and current differ insignificantly. The second set of parameters gives however significantly shorter duration of self-excitation transient (approximately 0.8 seconds). The waveform of the voltage build-up is this time slightly different in the region where steady-state is approached, while steady-state values of voltage and current are once more slightly higher. Identical conclusions apply to the differences between predicted current build-ups shown in Figures 4.6.5, 4.6.7 and 4.6.9.

The same difference in the duration of the transient naturally exists in the torque response. However, the maximum transient value predicted by the second set of single-cage parameters is significantly higher than the values obtained with the other two representations. It coincides with the occurrence of the overshoot in both voltage and current responses (Figure 4.6.9), where for a short period of time voltage and current exceed their subsequent steady-state values. It therefore appears that single-cage representation of a double-cage induction machine yields satisfactory results if the parameters are obtained from standard tests on the machine (first set of parameters).

Final steady-state values of all the quantities under no-load conditions differ insignificantly regardless of the machine representation. This can be regarded as an expected result. Contribution of the rotor to the final steady-state is negligible in this case as the behaviour of the machine is governed by stator parameters and magnetising branch, so that representation of the rotor becomes irrelevant.

4.7 Experimental investigation of induction generator self-excitation

4.7.1 Self-excitation under no-load conditions with star connected capacitor bank

Literature survey indicates that steady-state operation of SEIGs has been covered by extensive experimental investigation. This is however not the case with transient investigation. Experimental evidence with regard to transient behaviour of a SEIG is usually provided only as a proof of correctness of the modelling procedure and simulation results. It is therefore inherently limited in scope. This especially applies to variable speed operation of a capacitor excited induction generator and to the voltage collapse and demagnetisation of the machine that result under certain conditions. The aim of this section is therefore to report on results of an extensive experimental investigation of a SEIG operation. Self-excitation under no-load conditions, with capacitor bank connected in star and in delta, and loading of the generator with and without short-shunt compensation are investigated.

4.7.1.1 Establishment of self-excitation

The induction machine used in the study is 50 Hz, 4-pole, 1.2 kW machine with star connected stator winding. Data of the machine are given in Appendix. A vector controlled induction machine is used as a prime mover. On the basis of the induction machine no-load test it was established that the minimum value of the capacitance should be 15 μF per phase. This value provides full compensation of induction machine's reactive power need and it should yield rated voltage of 240 V at rated synchronous speed of 1500 rpm (i.e. at 50 Hz). However, experimental investigation has revealed that the generator does not self-excite with this capacitor value. The explanation for this is as follows. The machine used in experiments is of older design, with rated operating point on the magnetising curve still in the linear region. Impact of the shape of the magnetising curve on characteristics of a SEIG has been discussed in [Shridhar et al (1993)] under the assumption that rated operating point on the magnetising curve is always in the saturated region. The situation encountered here has not been previously reported. Consequently, the machine operates in saturated region of

the magnetising curve only with voltages that are substantially greater than rated.

Figure 4.7.1 illustrates induction machine's no-load phase to neutral voltage at 1500 rpm (essentially, the magnetising curve), obtained from the standard no-load motoring test, as well as the re-calculated no-load voltage at 1300 rpm (in order to reduce the over-voltage that would otherwise be present, all the experiments are performed at speeds below 1500 rpm). Linearity of the magnetising curve in the vicinity of the rated 240 V voltage (1500 rpm curve) is evident. Capacitor voltage line for capacitance of 15 μF (not shown in Figure 4.7.1) completely overlaps with the magnetising curve and self-excitation does not take place.

Successful self-excitation was achieved at 1300 rpm with star connected capacitors of 23 μF per phase (nominal value; actual capacitance was determined from tests as approximately 21.5 μF). Figure 4.7.1 includes capacitor voltage lines for speeds of 1500 rpm and 1300 rpm (calculated for capacitance of 21.5 μF). Evidently, self-excitation at 1500 rpm would lead to excessive over-voltage. Reasonable voltage is obtained at 1300 rpm and the point labelled as 'operating point' is the one in which the generator operates once when the self-excitation transient is over. Operating flux in this point is approximately 1.25 p.u..

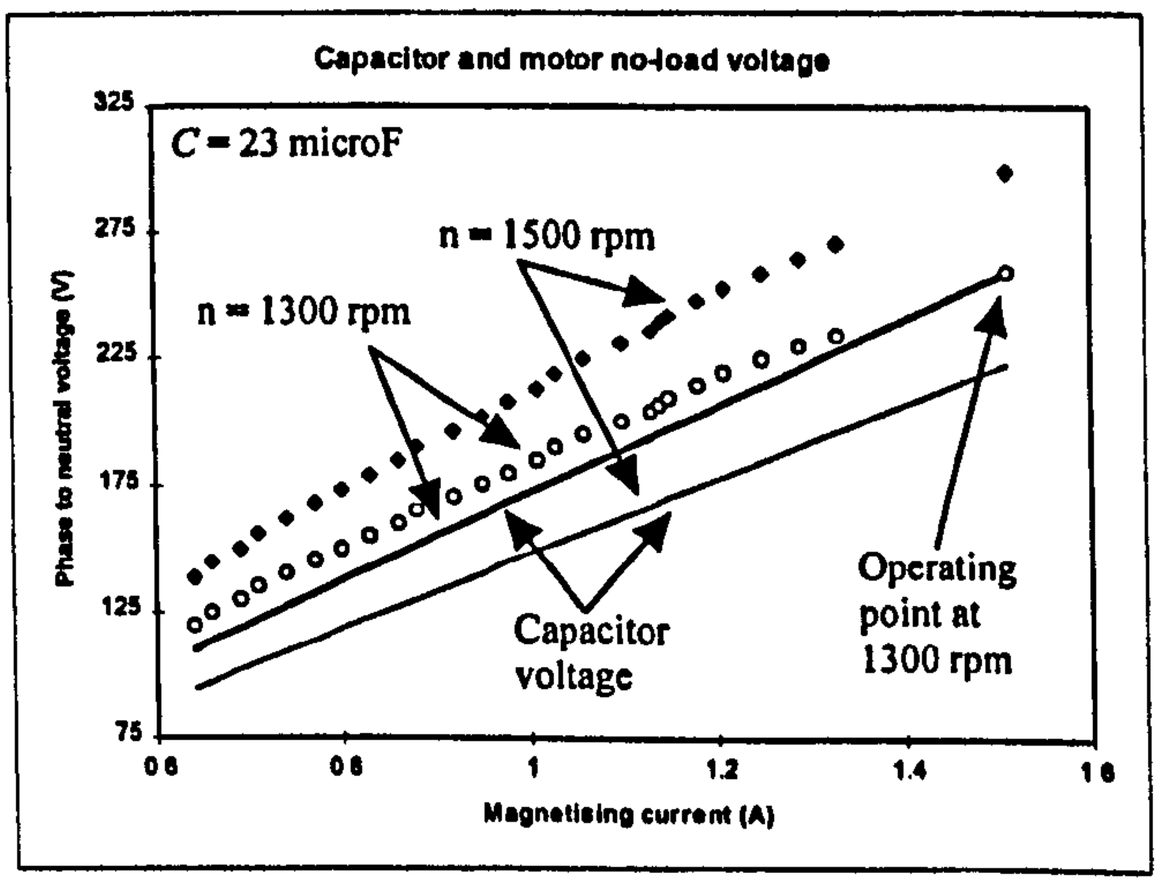

Figure 4.7.1 Capacitor voltage and induction machine no-load voltage for 1500 rpm and 1300 rpm speeds (solid lines: capacitor voltages; circles and squares: induction motor no-load voltages)

Self-excitation is initiated by the virtue of the existence of the remanent voltage in the machine. Figure 4.7.2 illustrates line-to-line remanent (residual) voltage measured at 1500 rpm (50 Hz).

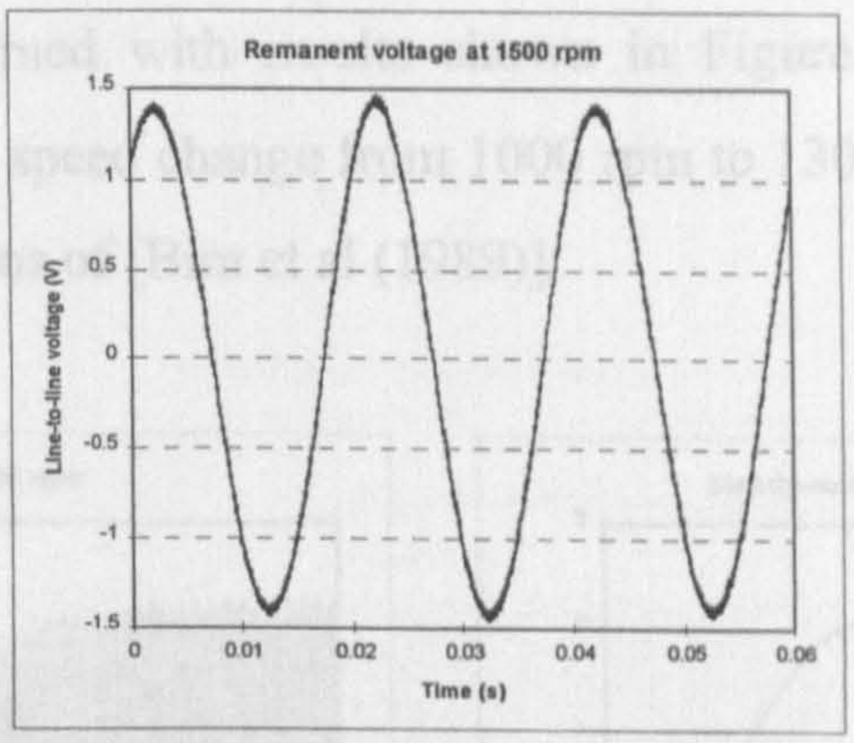

Figure 4.7.2 Remanent line-to-line voltage at 1500 rpm (50 Hz)

Figure 4.7.3 illustrates transient phase to neutral voltage build-up and subsequent steady-state no-load phase voltage at speed of 1300 rpm (43.33 Hz). Corresponding current waveforms are given in Figure 4.7.4 and they closely resemble voltage waveforms.

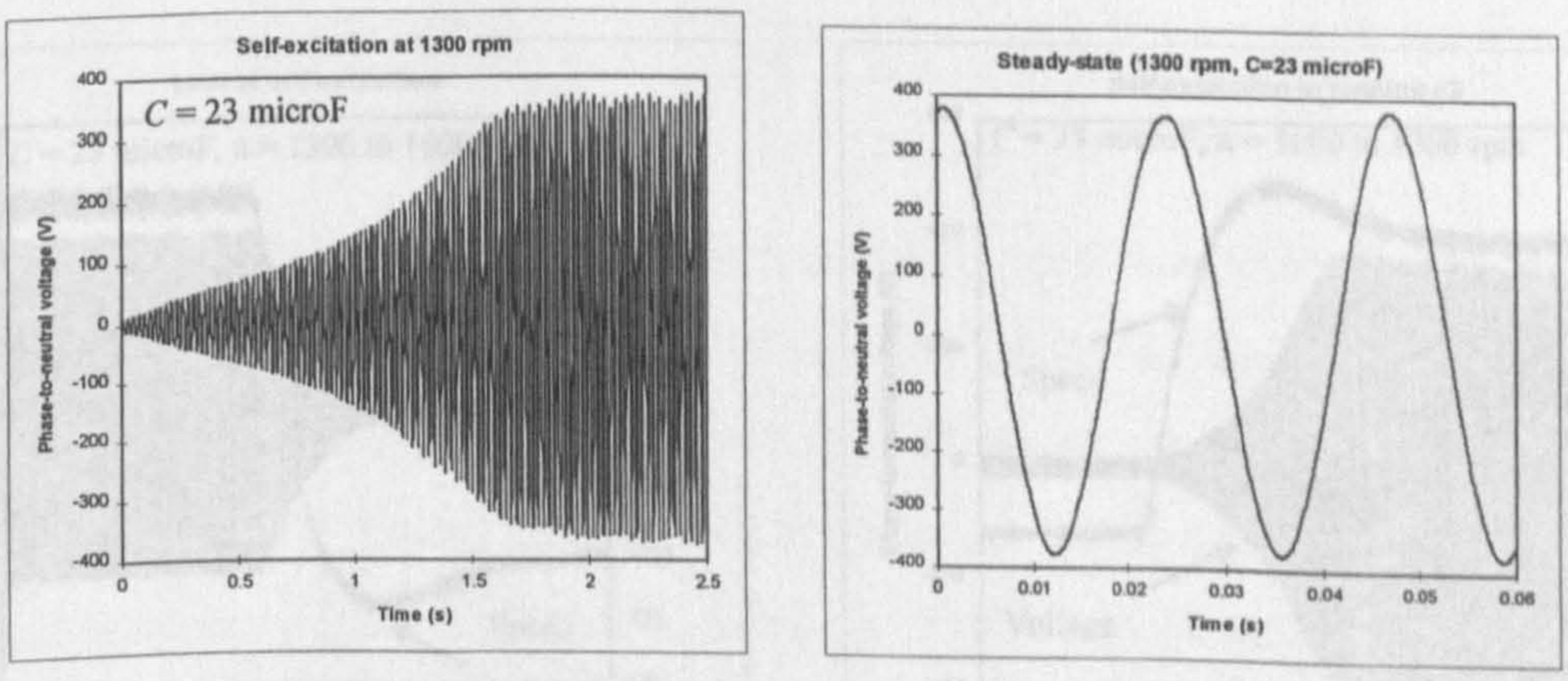

Figure 4.7.3 Phase to neutral voltage during self-excitation transient and subsequent no-load operation at 1300 rpm

4.7.1.2 Variable speed operation

Self-excited induction generator is extremely sensitive to speed variations. If the speed decreases below the threshold of the self-excitation, voltage at machine terminals will

practically disappear. Such a situation is illustrated in Figure 4.7.5, where phase voltage and speed are shown for speed change from 1300 rpm to 1000 rpm. Phase voltage peak value has dropped from approximately 370 V to only 18 V. However, the self-excitation will be re-established once when the speed attains value higher than the self-excitation threshold. This is confirmed with results shown in Figure 4.7.6, where speed and voltage traces that follow speed change from 1000 rpm to 1300 rpm are given, and is in agreement with conclusions of [Bim et al (1989)].

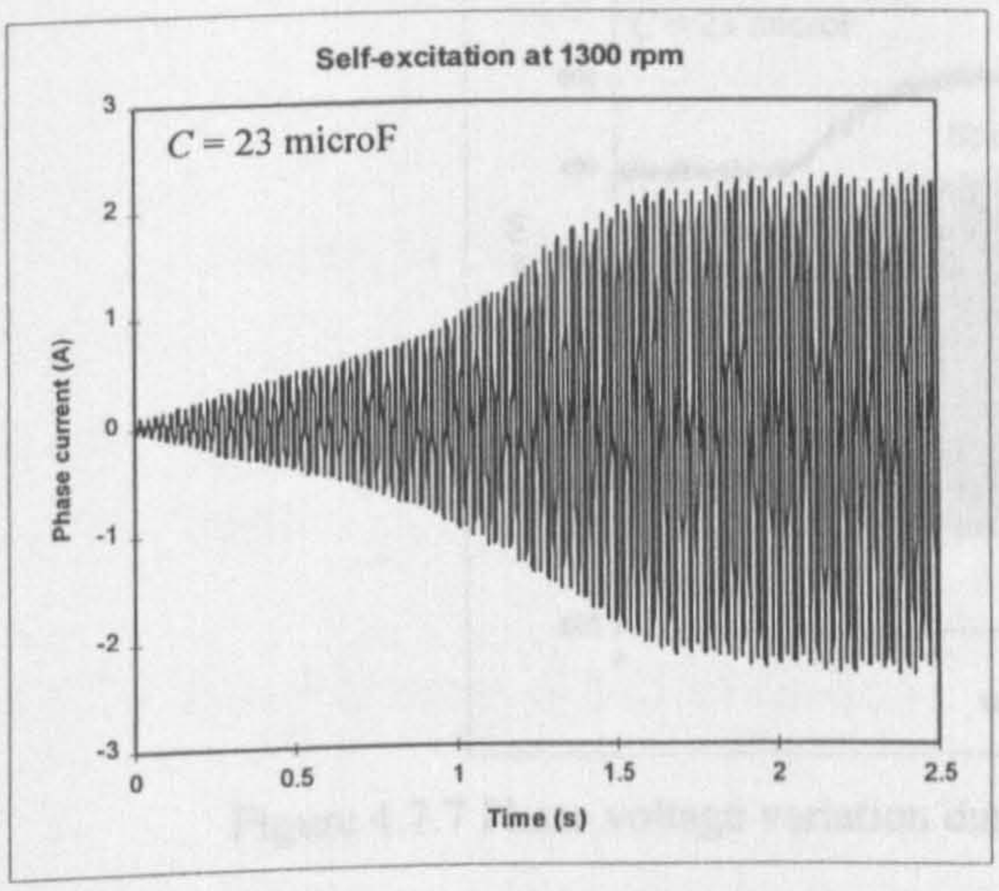

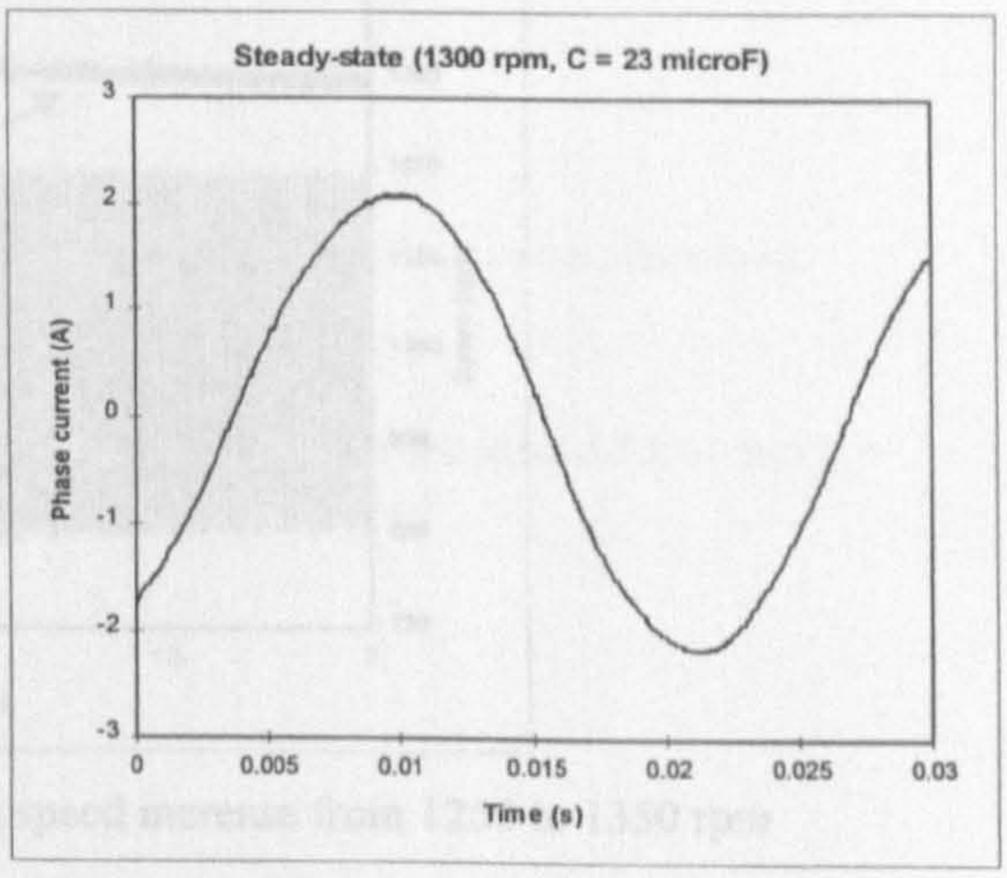

Figure 4.7.4 Phase current during self-excitation transient and subsequent no-load operation at 1300 rpm

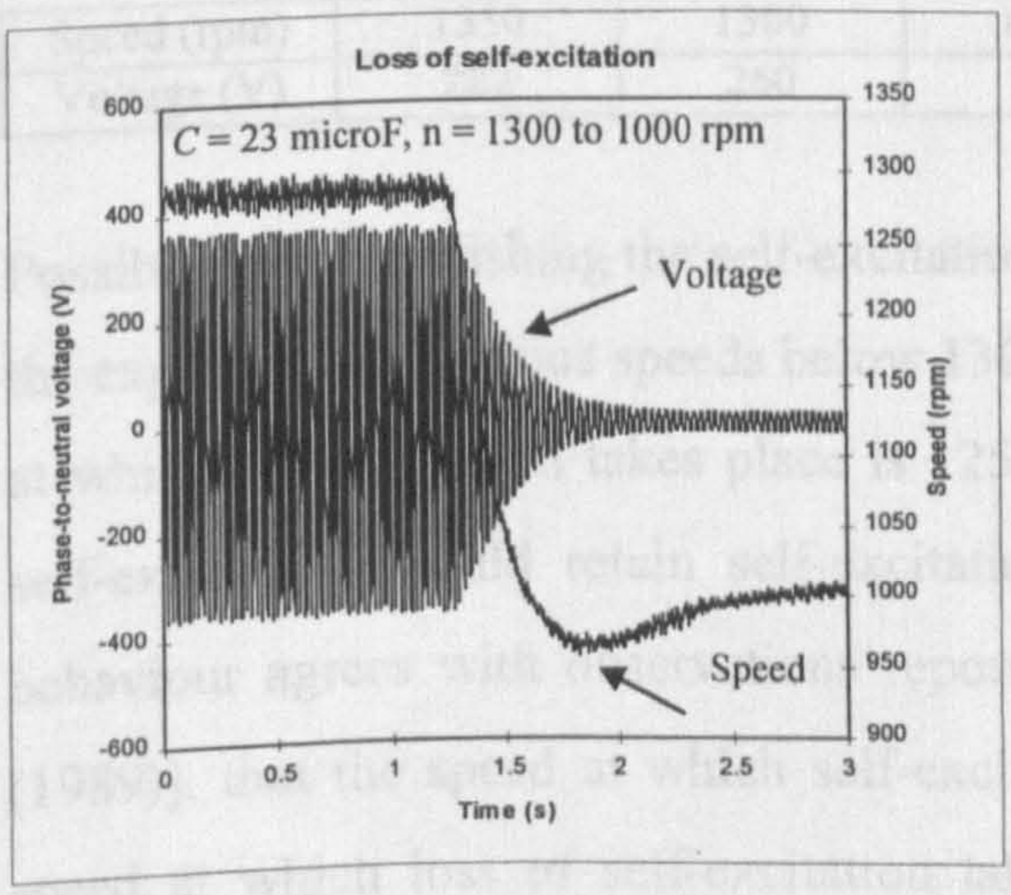

Figure 4.7.5 Loss of self-excitation due to speed decrease from 1300 rpm to 1000 rpm

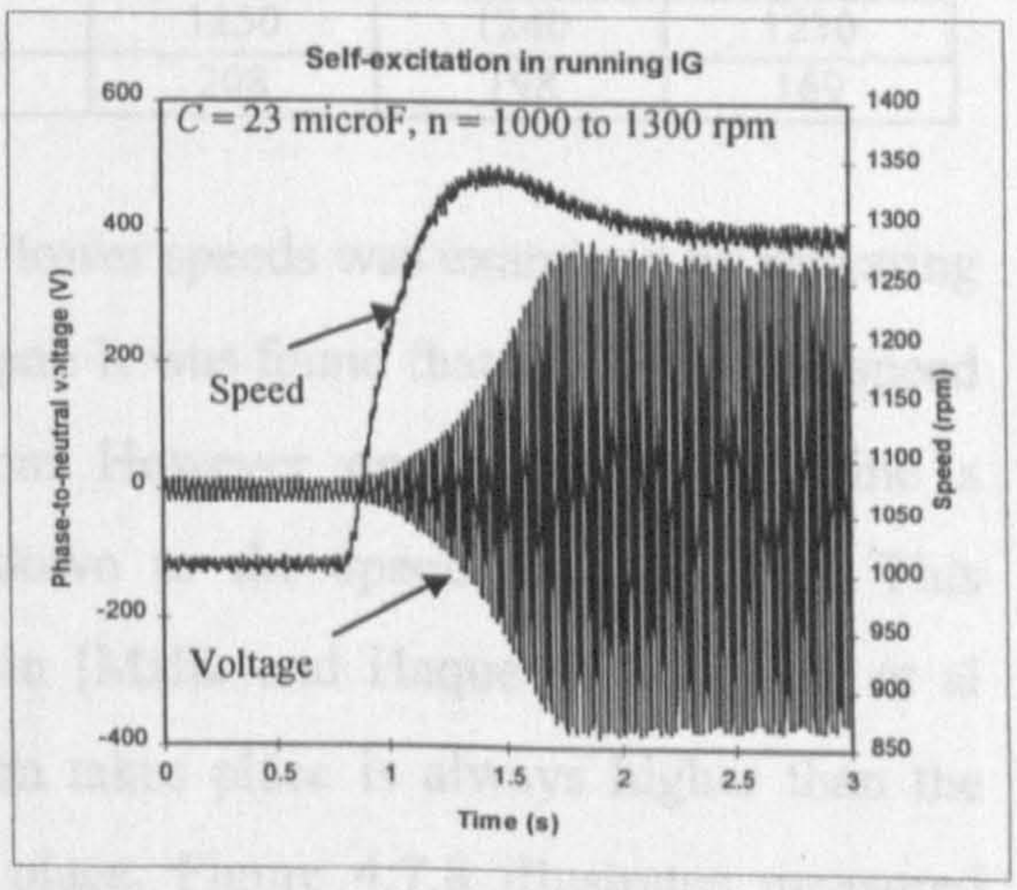

Figure 4.7.6 Re-establishment of self-excitation in a running induction generator with connected capacitor bank

In contrast to the speed decrease, which may extinguish the self-excitation, speed increase leads to occurrence of over-voltage. Even a relatively small change of speed

causes substantial increase in the voltage. Figure 4.7.7 shows traces of speed and phase voltage that were recorded during speed increase from 1250 to 1350 rpm. Taking values at 1250 rpm as the base values, an 8% speed increase has caused 36% increase in the voltage. Table 4.1 shows measured phase to neutral rms voltage for a couple of speeds in the region from 1230 to 1350 rpm and confirms that voltage substantially fluctuates with variation in speed.

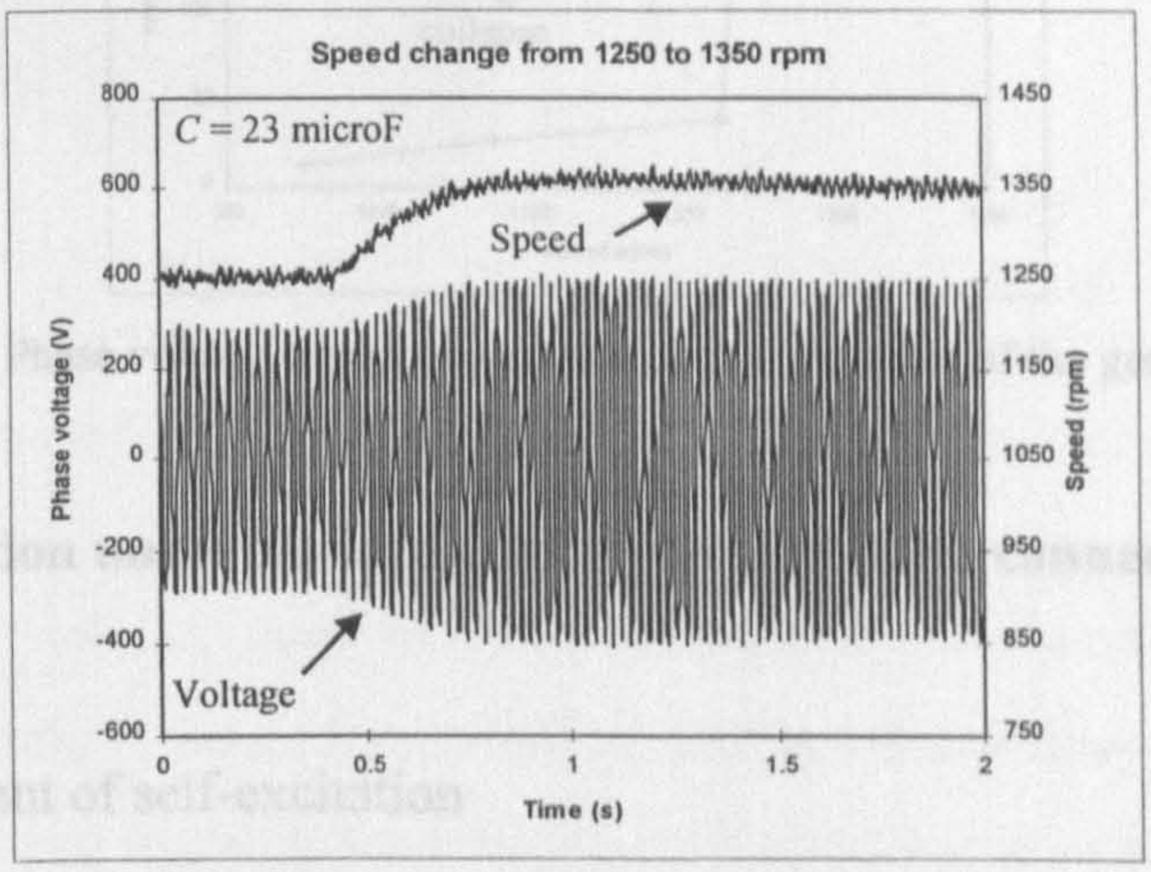

Figure 4.7.7 Phase voltage variation during speed increase from 1250 to 1350 rpm

Table 4.1 Phase voltage rms steady-state values as function of the generator speed

Speed (rpm)	1350	1300	1275	1250	1240	1230
Voltage (V)	282	260	237	208	198	169

Possibility of establishing the self-excitation at lower speeds was examined by repeating the experiment at various speeds below 1300 rpm. It was found that the minimum speed at which self-excitation takes place is 1250 rpm. However, once when the machine is self-excited, it would retain self-excitation down to the speed of 1220 rpm. This behaviour agrees with observations reported in [Malik and Haque (1986), Bim et al (1989)], that the speed at which self-excitation takes place is always higher than the speed at which loss of self-excitation takes place. Figure 4.7.8 illustrates measured phase to neutral rms voltage at various speeds, starting from 1350 rpm and going downwards. It is evident from the figure that the change of no-load voltage in the operating region from 1250 to 1350 rpm is far from linear, as suggested in [Murthy et al (1982), Malik and Haque (1986), Bim et al (1989)]. It should be noted that when the

speed was increased from 1000 rpm upwards, voltage remained essentially equal to the residual voltage until the self-excitation took place at 1250 rpm.

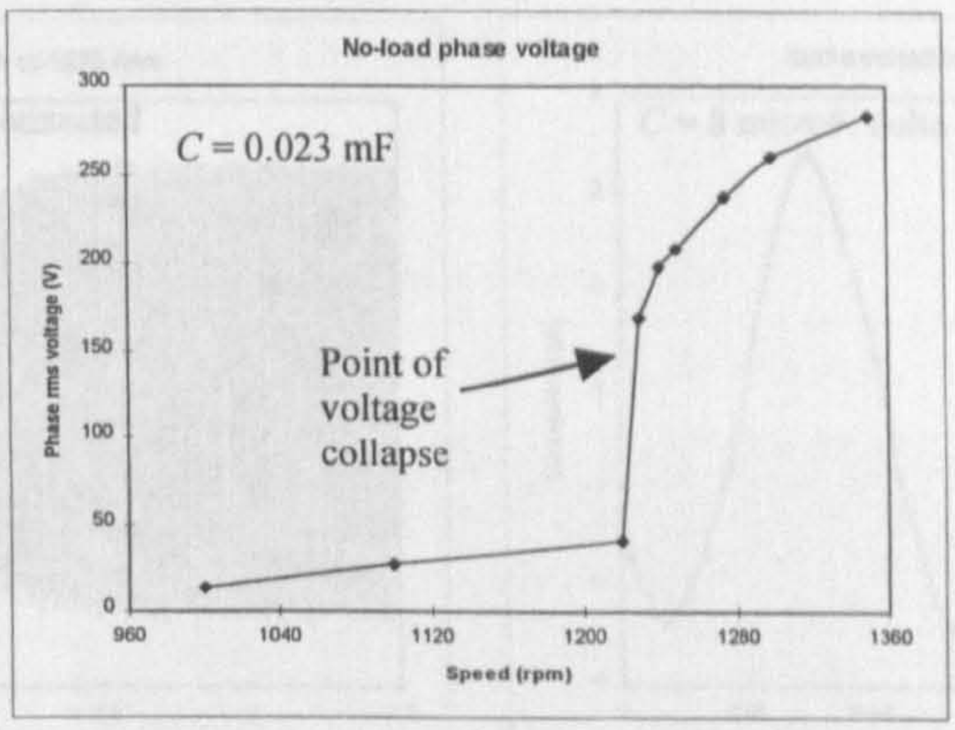

Figure 4.7.8 Phase voltage rms steady-state values as function of the generator speed

4.7.2 Self-excitation under no-load conditions with delta connected capacitor bank

4.7.2.1 Establishment of self-excitation

As is well known, connection of the capacitor bank in delta rather than in star enables achievement of the same self-excitation conditions with three times smaller value of capacitance. Capacitors of 8 μF (approximately 1/3 of the 23 μF value that were used in star connection) are now used and the bank is connected in delta. Figures 4.7.9 and 4.7.10 illustrate self-excitation transient and subsequent steady-state operation at 1275 rpm. Line-to-line voltage and line current are shown, respectively.

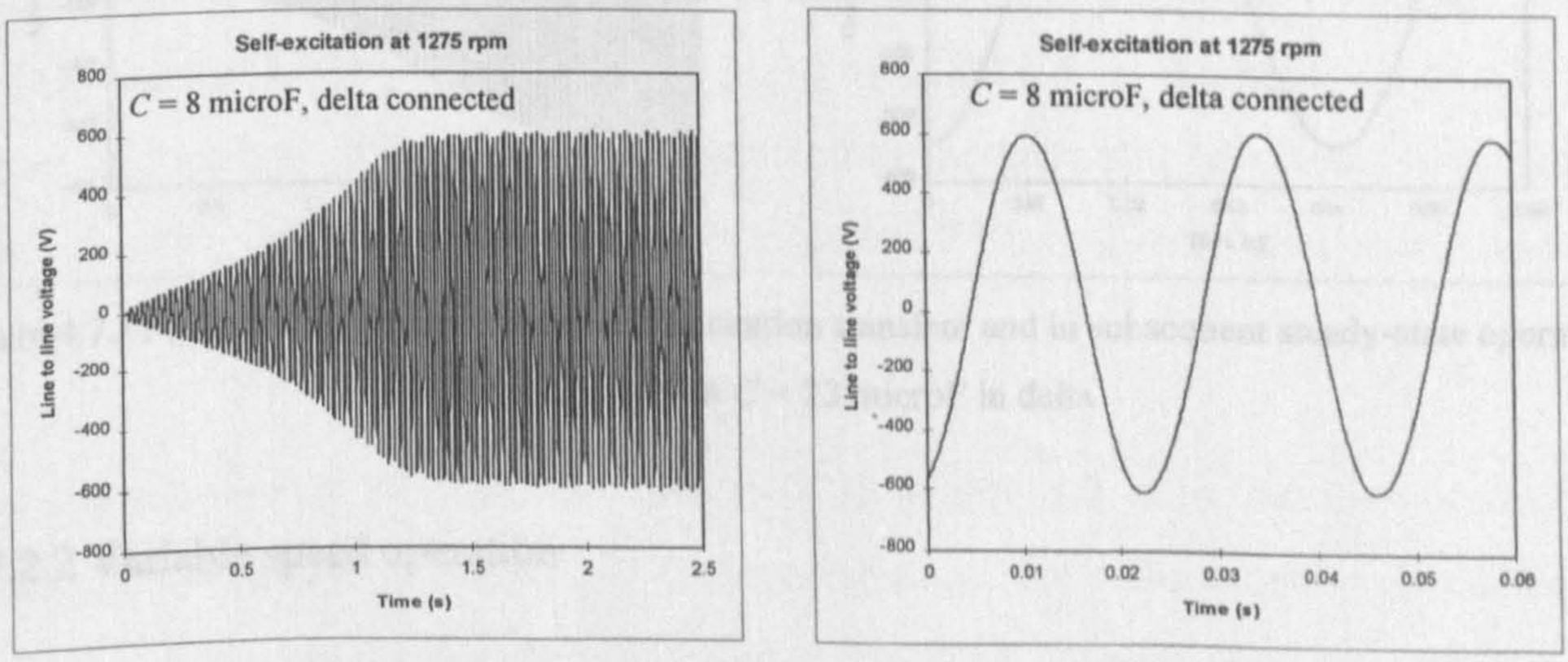

Figure 4.7.9 Line to line voltage during self-excitation transient and in subsequent steady-state operation at 1275 rpm

Once self-excited, the generator will retain self-excitation with this capacitor bank at all speeds higher than 1200 rpm.

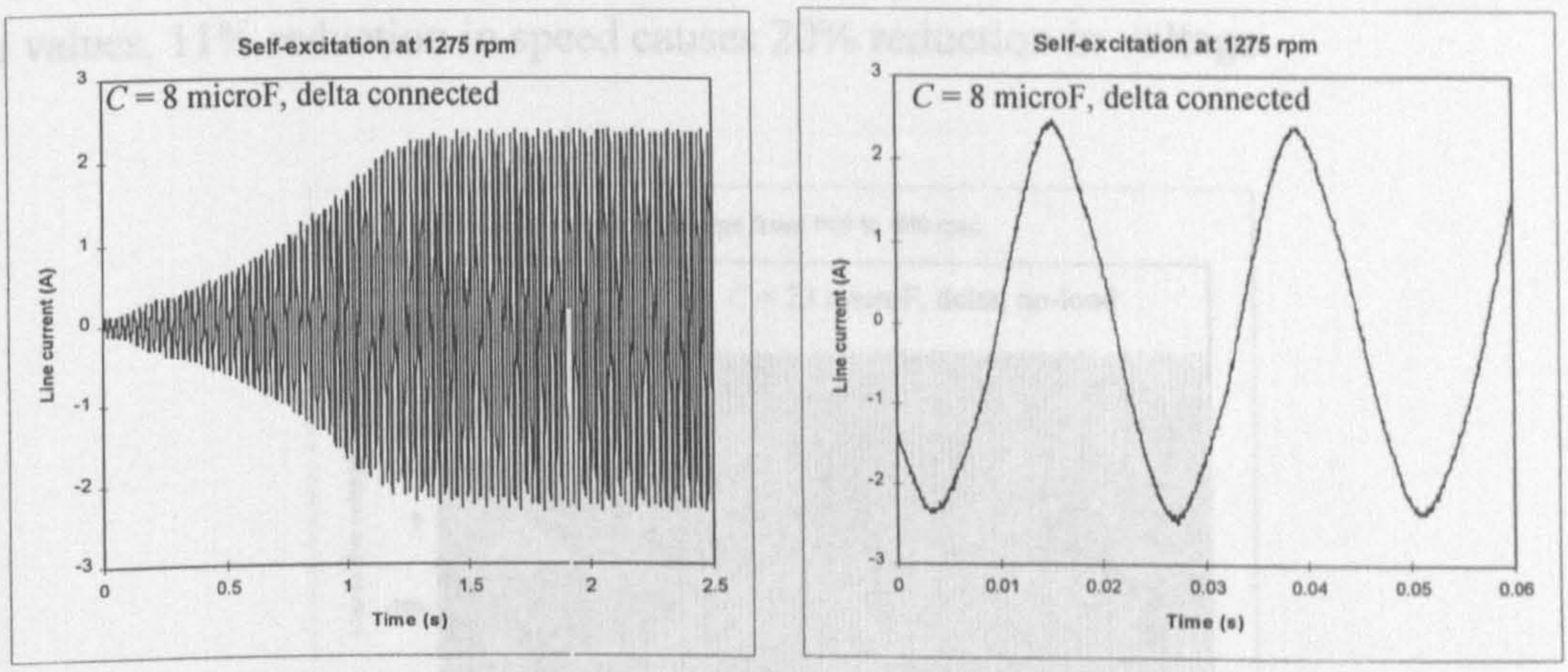

Figure 4.7.10 Line current during self-excitation and in subsequent steady-state operation at 1275 rpm

If capacitors of 23 μF are used in delta connection, the threshold speed for self-excitation significantly reduces. Figure 4.7.11 displays line-to-line voltage during self-excitation transient and in subsequent steady-state operation at speed of 750 rpm, with 23 μF capacitors connected in delta.

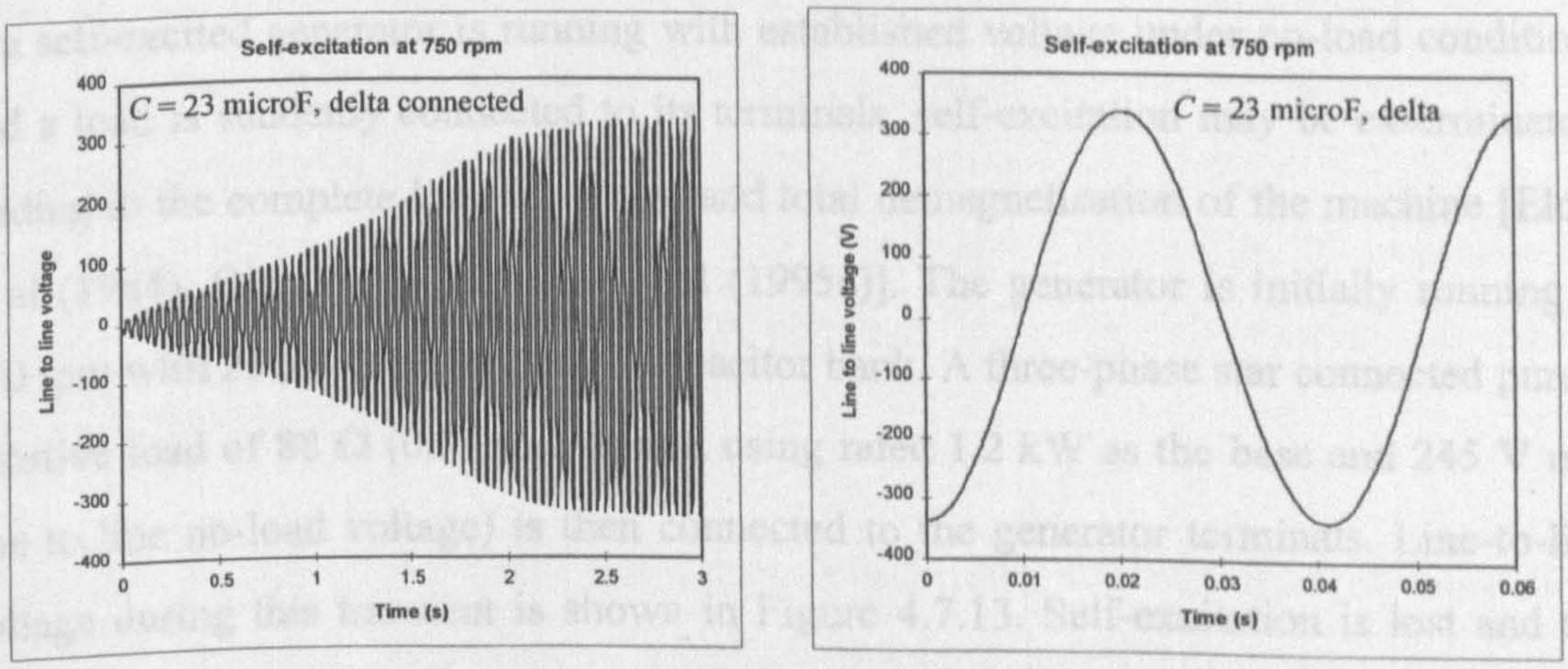

Figure 4.7.11 Line to line voltage during self-excitation transient and in subsequent steady-state operation at 750 rpm with $C = 23$ microF in delta

4.7.2.2 Variable speed operation

Variation of operating speed causes very much the same pattern of induction generator

voltage variation as with star connected bank of capacitors. As an example, Figure 4.7.12 illustrates line to line voltage transient that follows speed change from 900 rpm to 800 rpm, with 23 μF capacitor bank connected in delta. Taking values at 900 rpm as base values, 11% reduction in speed causes 20% reduction in voltage.

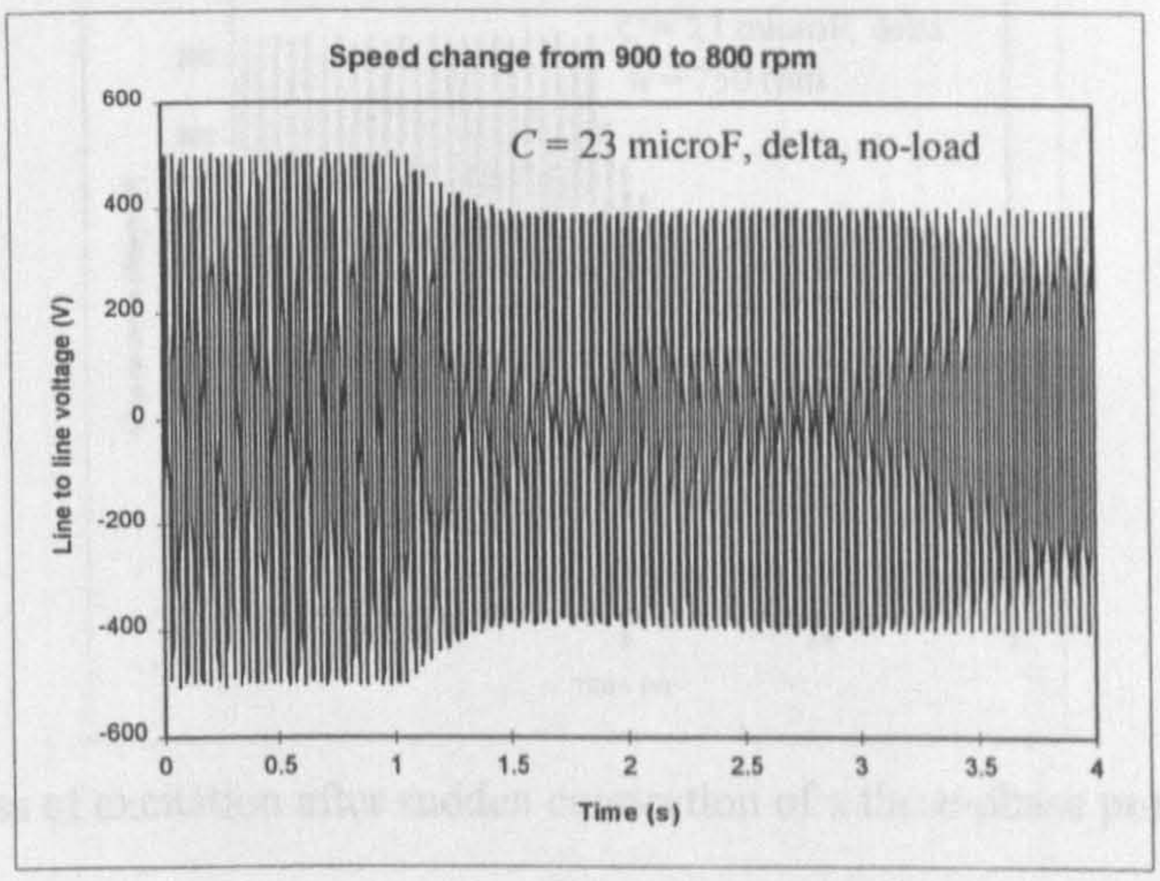

Figure 4.7.12 Line to line voltage transient after speed reduction from 900 to 800 rpm

4.7.2.3 Loss of self-excitation due to step load connection

If a self-excited generator is running with established voltage under no-load conditions and a load is suddenly connected to its terminals, self-excitation may be exterminated, leading to the complete loss of voltage and total demagnetisation of the machine [Elder et al (1984), Ojo (1995), Shridhar et al (1995a)]. The generator is initially running at 750 rpm with 23 μF delta connected capacitor bank. A three-phase star connected purely resistive load of 88 Ω (0.57 p.u. power, using rated 1.2 kW as the base and 245 V rms line to line no-load voltage) is then connected to the generator terminals. Line-to-line voltage during this transient is shown in Figure 4.7.13. Self-excitation is lost and the voltage quickly reduces to zero.

The consequence of the transient illustrated in Figure 4.7.13 is the loss of residual voltage. The machine is completely demagnetised and the self-excitation cannot be re-established any more. Suggestion of [Elder et al (1983)], that the machine will re-excite if the excitation is initiated at sufficiently high speeds, was tested by attempting self-

excitation at speeds up to 1500 rpm, without any success. In order to enable restarting of the self-excitation process it was necessary to recover the residual voltage by connecting the machine to the mains and running it as a motor.

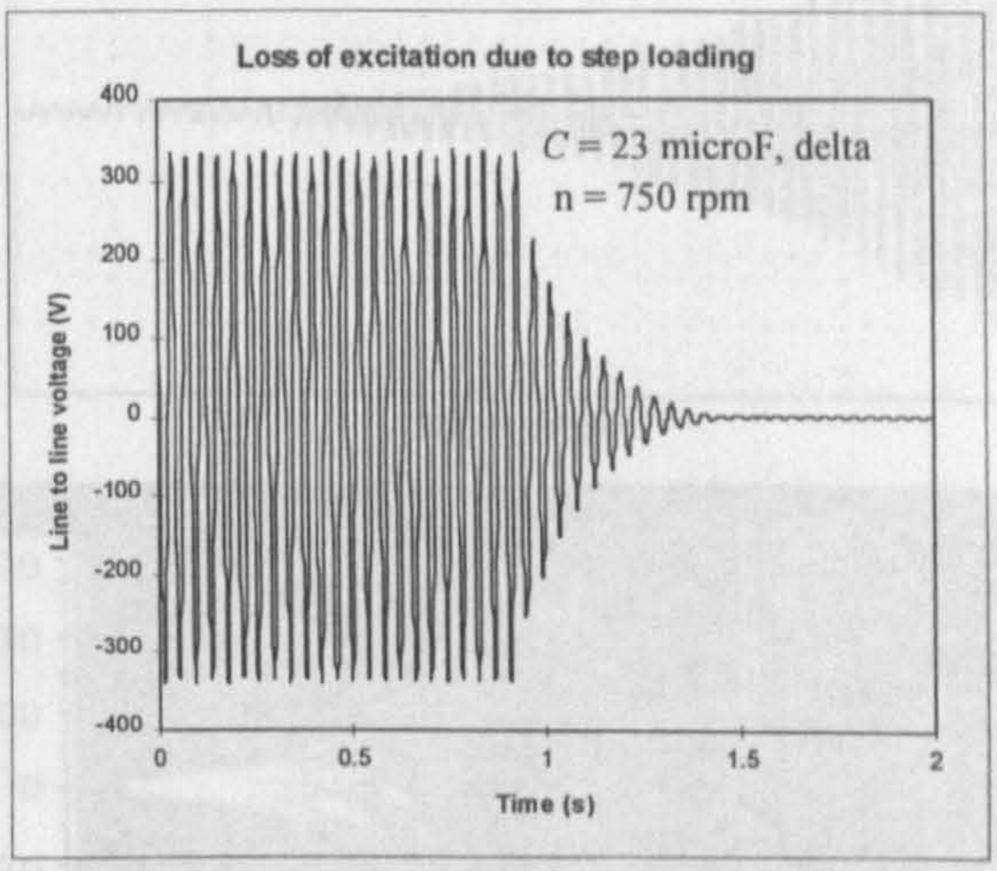

Figure 4.7.13 Loss of excitation after sudden connection of a three-phase purely resistive load

4.7.3 No-load self-excitation of a double-cage induction generator

Voltage and current build-up during no-load self-excitation predicted by simulation using the full double-cage model are given in Section 4.6.3. Experimentally obtained trace of voltage build-up, for no-load self-excitation of the same machine under the conditions specified in Section 4.6.3, is shown in Figure 4.7.14 [Levi et al (1996)]. The approximate duration of the transient is 1.2 seconds. Comparison of experimental voltage build-up with simulation results obtained from the full double-cage model shows good agreement.

Simulation results of a double-cage induction generator self-excitation obtained both with full saturated double-cage induction machine model and with single-cage representation are compared with the results obtained by experiments (Figure 4.7.14). The analysis leads to the conclusion that application of single-cage representation of double-cage induction machines enables sufficiently accurate simulation of self-excitation when rotor 50 Hz parameters, obtained from standard locked rotor test, are used. The only difference appears to be in the predicted duration of the transient, as

single-cage representation gives 10% shorter time interval needed for establishment of steady-state operation.

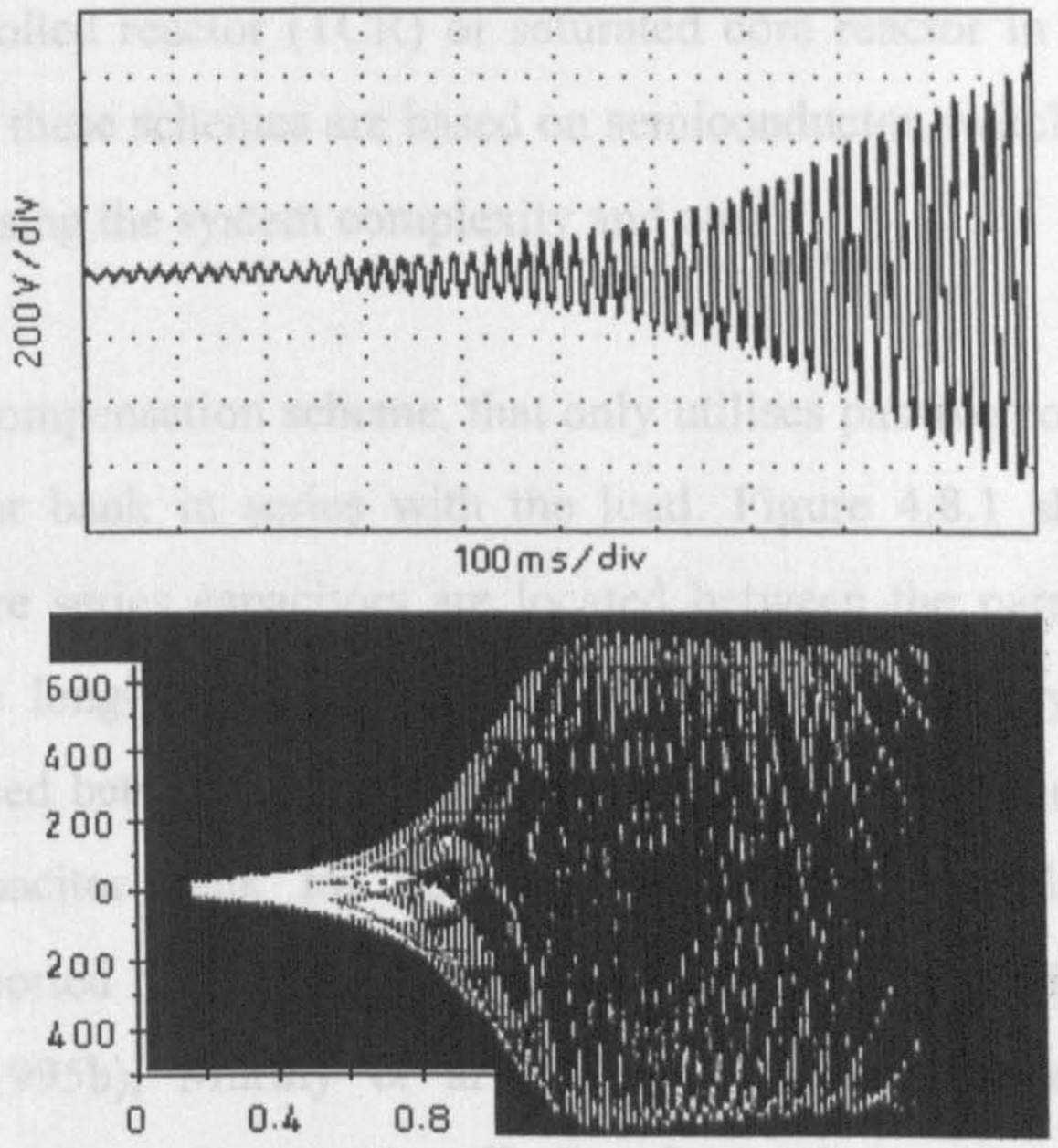

Figure 4.7.14 Experimentally recorded voltage build-up of the double-cage induction generator

The second possibility examined in this chapter, calculation of single-cage parameters from equivalent circuit of the double-cage machine at zero speed, gives rather inaccurate results as duration of the transient is underestimated by 33%. This method of equivalent single-cage rotor parameter determination is thus deemed to be inappropriate.

4.8 Compensation of load voltage variation by means of a series capacitor bank

A self-excited induction generator has a poor voltage regulation characteristic even at constant speeds. For a fixed value of capacitance, the voltage decreases dramatically with increase in load. For a low impedance load, self-excitation will even be lost. In order to avoid loss of excitation after load connection and to compensate for the voltage drop, additional VAr with load increase must be provided. This can be achieved by the use of switched capacitor bank. Additional self-excitation capacitance will be switched in when the load increases. Variable lagging VArs are supplied to the generator by switching in different values of capacitance. However, the control of switched

capacitors is tedious, it is not continuous, and it requires a large number of capacitor banks. Other possible compensation schemes include the use of static VAr compensator, i.e., thyristor controlled reactor (TCR) or saturated core reactor in parallel with fixed capacitor bank. All these schemes are based on semiconductor switches and closed-loop control, thus increasing the system complexity and cost.

A simple voltage compensation scheme, that only utilises passive components, includes additional capacitor bank in series with the load. Figure 4.8.1 shows a short-shunt configuration where series capacitors are located between the parallel capacitor bank and the load. The long-shunt configuration is another possibility, where the series capacitors are placed between the generator terminals and the parallel capacitors. The use of series capacitor bank for voltage compensation of self-excited induction generators was reported by [Basset and Potter (1935), Bim et al (1989), Chan (1995), Shridhar et al (1995b), Murthy et al (1996)]. Both long-shunt and short-shunt compensation methods are found to be effective due to their self-regulating feature and overload capability.

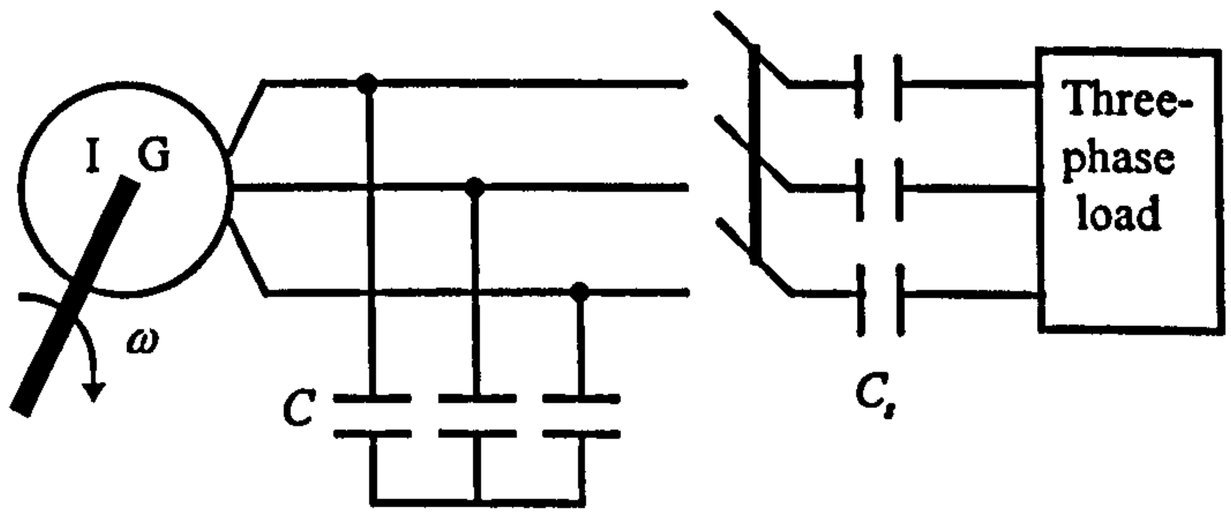

Figure 4.8.1 Scheme of load voltage compensation with a series capacitor bank

4.8.1 Mathematical model

A three-phase capacitor bank is connected in series with a symmetrical three-phase resistive load. Equations which describe the series capacitor bank are

$$\frac{dv_{dc}}{dt} = \omega_a v_{qc} + \frac{i_{dl}}{C_s} \qquad (4.8\text{-}1a)$$

$$\frac{dv_{qc}}{dt} = -\omega_a v_{dc} + \frac{i_{ql}}{C_s} \tag{4.8-1b}$$

where the d-q axis load currents are now

$$i_{dl} = \frac{v_{ds} - v_{dc}}{R} \qquad i_{ql} = \frac{v_{qs} - v_{qc}}{R} \tag{4.8-2}$$

Equations which describe the parallel capacitor bank are the same as before

$$\frac{dv_{ds}}{dt} = \omega_a v_{qs} - \frac{1}{C}(i_{ds} + i_{dl}) \tag{44-4a}$$

$$\frac{dv_{qs}}{dt} = -\omega_a v_{ds} - \frac{1}{C}(i_{qs} + i_{ql}) \tag{4.4-4b}$$

Equations (4.8-1) - (4.8-2), (4.4-4) together with equations of the saturated induction machine form a complete mathematical model for simulation of load voltage compensation of a single-cage self-excited induction generator by means of a series capacitor bank.

4.8.2 Simulation results

The machine model used in the simulation is the saturated single-cage induction machine with winding currents selected as state-space variables, as described in Section 4.3. The capacitance for the parallel capacitor bank is now 30 μF, which is larger than the one used previously. Shorter duration of self-excitation process is achieved in this way. The series capacitor bank with a per-phase capacitance of 100 μF is connected in series with the three-phase resistive load.

Self-excitation starts at synchronous 50 Hz speed under no-load conditions. Switching-in of load and the series capacitor bank follows. Different values of resistors are applied to study the effect of load variations. At t = 1.0 s, a load of 1000 Ω is switched in,

followed by 800 Ω, 600 Ω, 400 Ω, 300 Ω and 200 Ω each at 0.1 seconds intervals. Figure 4.8.2 shows the stator phase voltage, phase current and load voltage. The effect of a series capacitor inserted between the load and the generator is evident from the simulation results. The load voltage regulation is approximately 10% from 1000 Ω load to 200 Ω load (which correspond to approximately 20% of the rated load and full load). The stator phase voltage regulation is about 13% from no-load to full load.

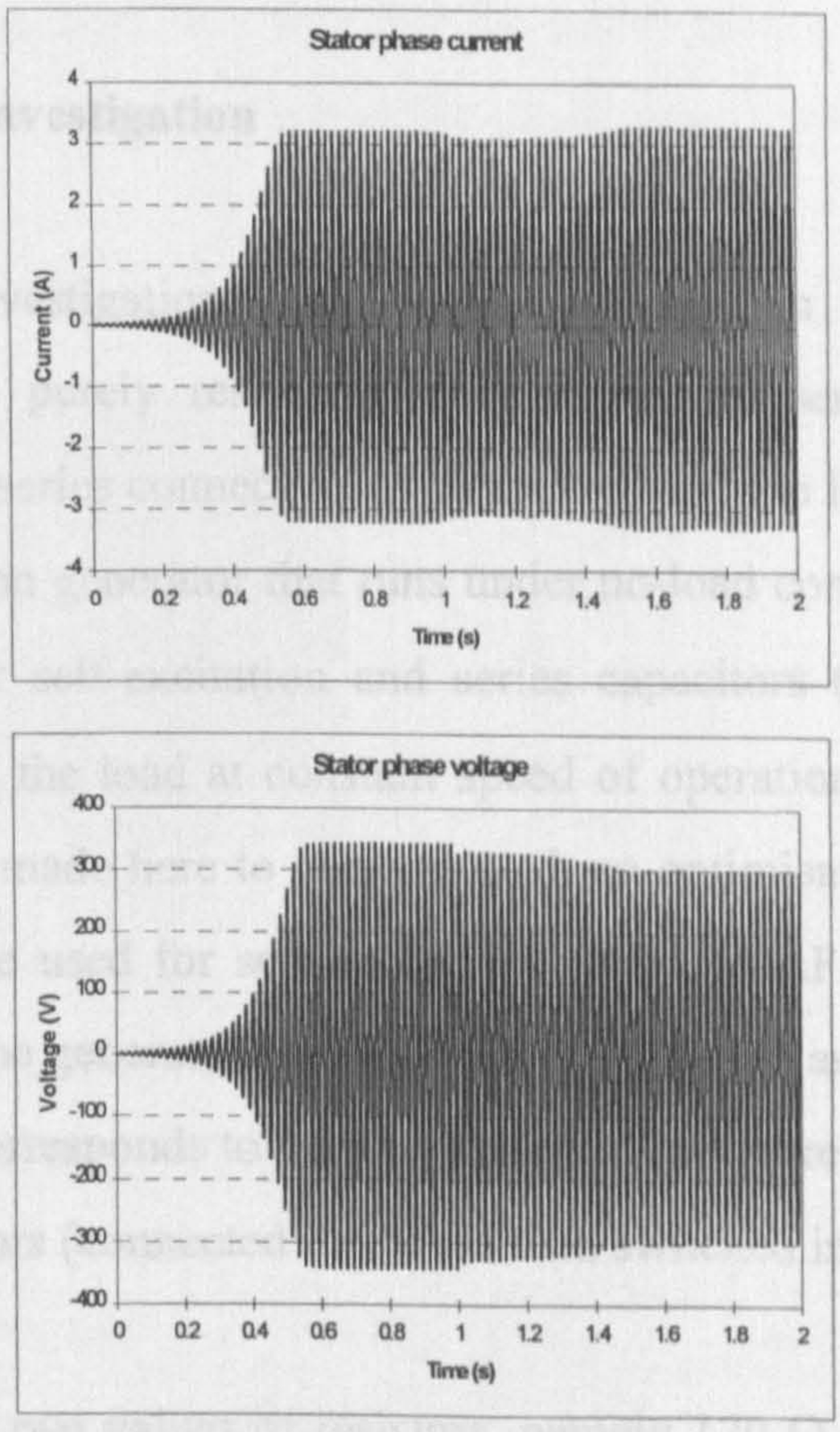

Figure 4.8.2 Load voltage compensation using a series capacitor bank

As the load voltage remains almost constant when the load increases, the series capacitor compensation can increase the power capability of the generator. It can be concluded that for constant speed operation a series capacitor bank provides a simple and effective method for improving the load voltage regulation since there is no control necessary. However, for variable speed operation and/or under different power factor loading conditions, an advanced controlled series compensation scheme reported in [Jain and Singh (1996)] may be used.

4.8.3 Experimental investigation

In the experimental investigation, short-shunt compensation is applied. In this case three-phase load (here purely resistive) is connected in series with a three-phase capacitor bank. Such a series connection of capacitors and the load is then connected to the self-excited induction generator that runs under no-load conditions. Optimisation of the capacitors used for self-excitation and series capacitors (C_s) can enable almost constant voltage across the load at constant speed of operation, regardless of the load value. No attempt was made here to perform such an optimisation. Capacitors of 8 μF (connected in delta) are used for self-excitation, while 15 μF capacitors are used for series compensation. The generator initially runs at 1275 rpm and is self-excited, so that previous steady-state corresponds to the one arrived at in Figure 4.7.9. Series connection of capacitors and resistors (connected in star) is then switched in.

Study is performed for two values of resistors, namely 120 Ω and 80 Ω. Figures 4.8.3 and 4.8.4 illustrate generator transient line to line voltage and load (resistance) transient line to line voltage that result after switching-in of the series connection of 120 Ω resistance and 15 μF capacitor. Figures 4.8.5 and 4.8.6 give the same quantities under the same conditions, when the resistance is 80 Ω. Finally, Figure 4.8.7 shows transient line to line voltage across load (resistance) that follows reduction of speed from 1275 rpm to 1100 rpm, with 80 Ω load.

As can be seen from Figures 4.8.3 - 4.8.6, connection of the resistive load with series capacitance compensation causes an increase in the generator output voltage. Load

voltage is considerably smaller than the generator voltage, as large portion of the generator voltage appears across the series capacitors. Induction generator delivers to the load 0.37 p.u. and 0.315 p.u. power for steady-state operating conditions obtained after transients depicted in Figures. 4.8.3 - 4.8.6, respectively.

Reduction of the speed, Figure 4.8.7, causes reduction of the voltage but self-excitation is preserved, although the final speed is 1100 rpm (self-excitation threshold speed for 8 μF delta connected capacitors was found to be under no-load conditions, as already noted, around 1200 rpm). Indeed, graph of the steady-state load rms line to line voltage

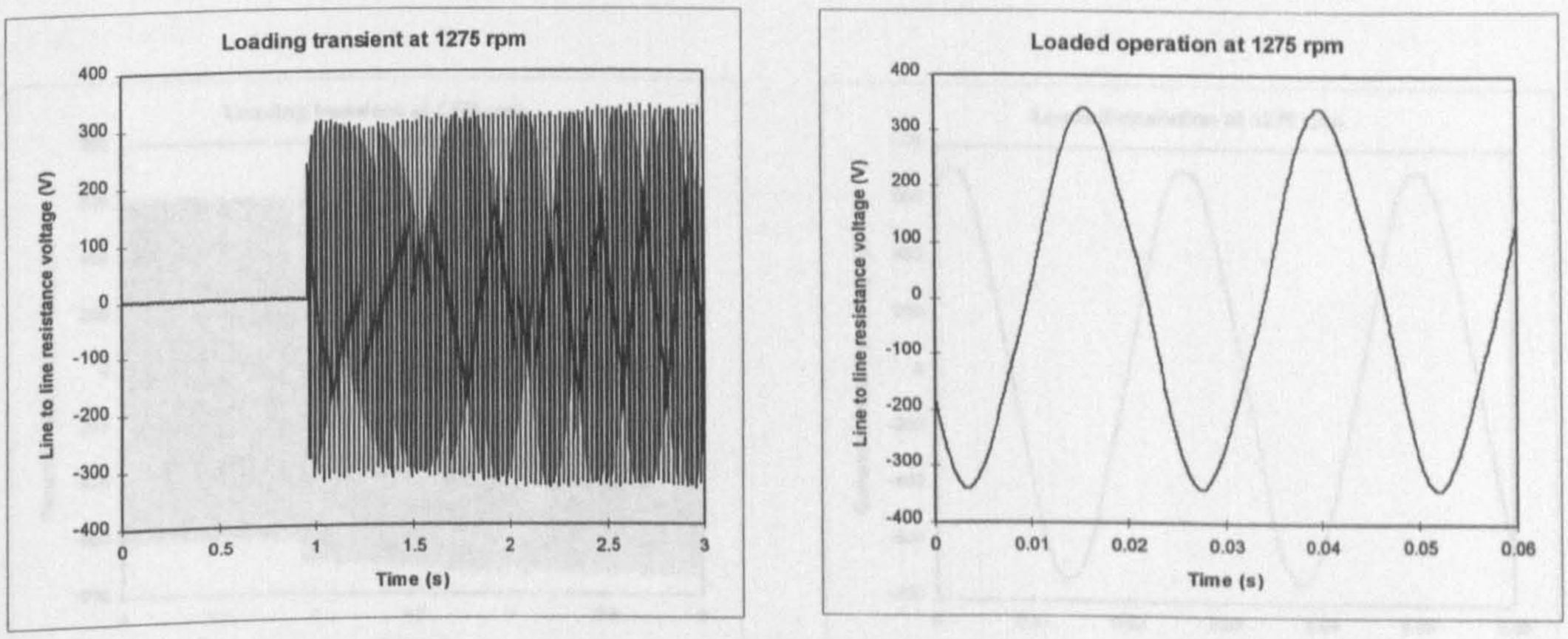

Figure 4.8.3 Line to line voltage across resistance in transient and in steady-state (short-shunt compensation, $C = 0.008$ mF, $R = 120$ ohms, $Cs = 0.015$ mF)

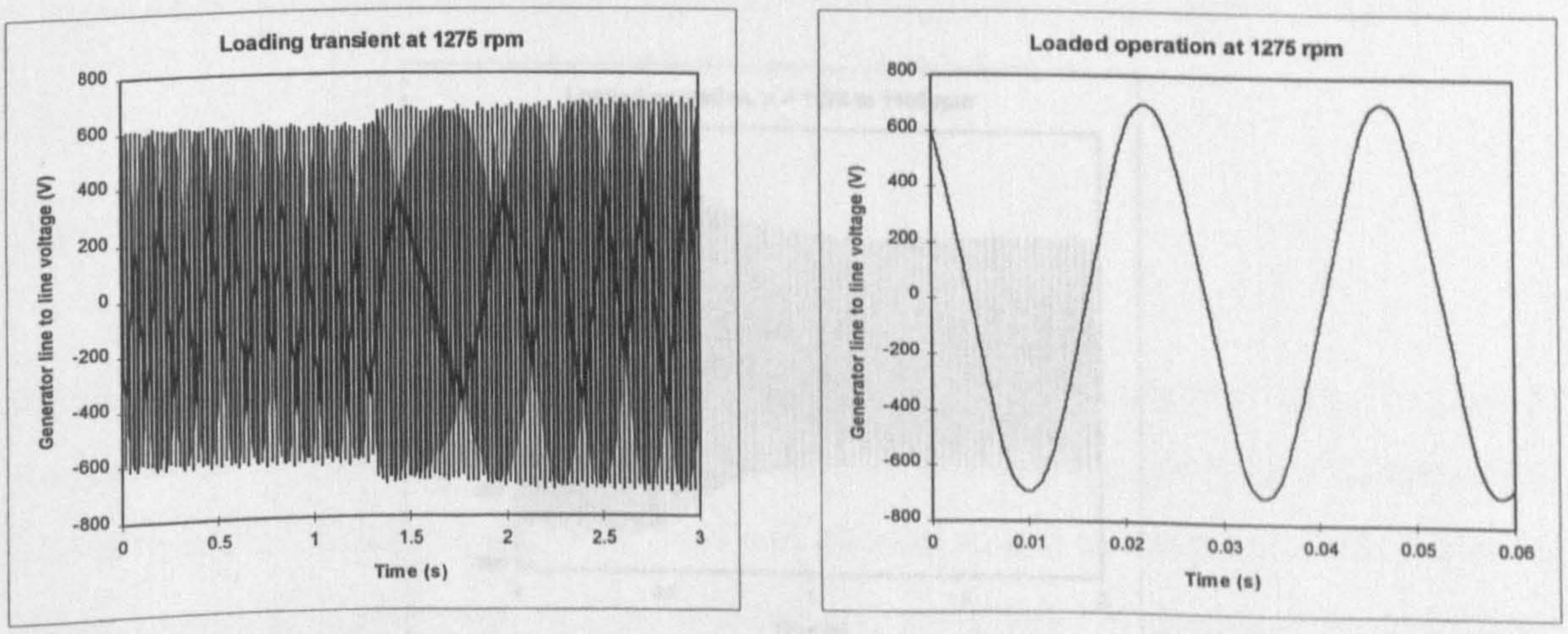

Figure 4.8.4 Generator line to line voltage in transient and in steady-state (short-shunt compensation, $C = 0.008$ mF, $R = 120$ ohms, $Cs = 0.015$ mF)

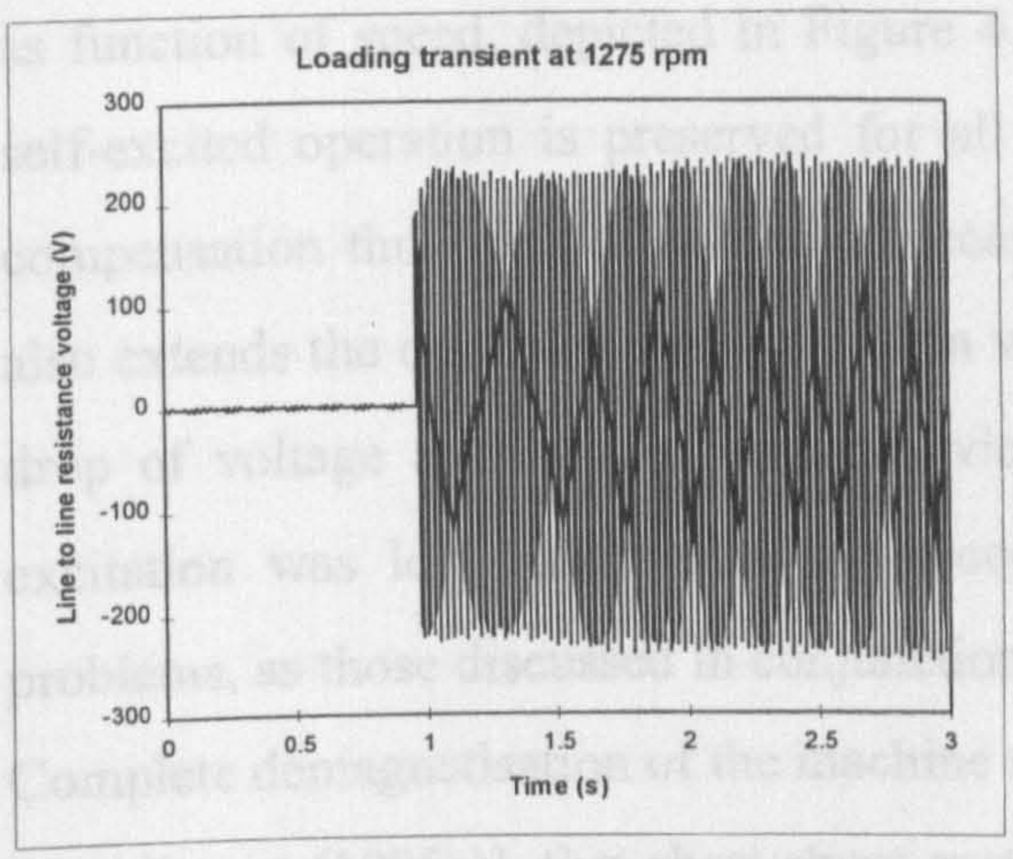

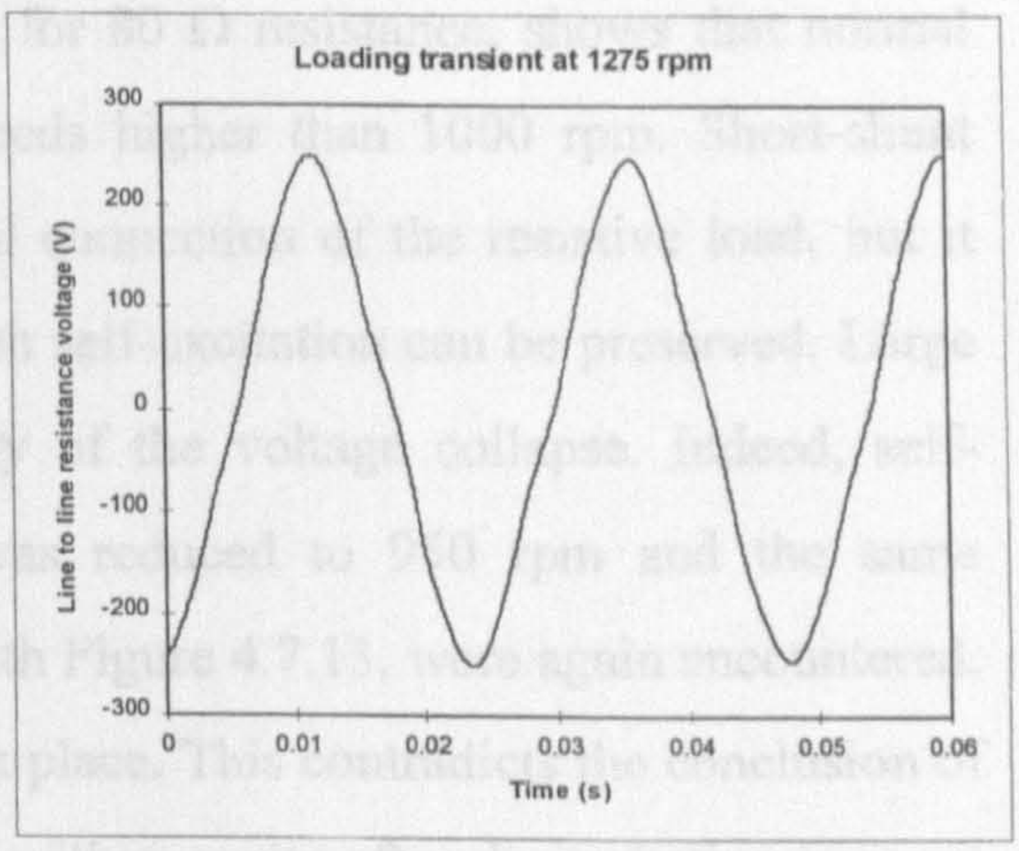

Figure 4.8.5 Line to line voltage across resistance in transient and in steady-state (short-shunt compensation, $C = 0.008$ mF, $R = 80$ ohms, $Cs = 0.015$ mF)

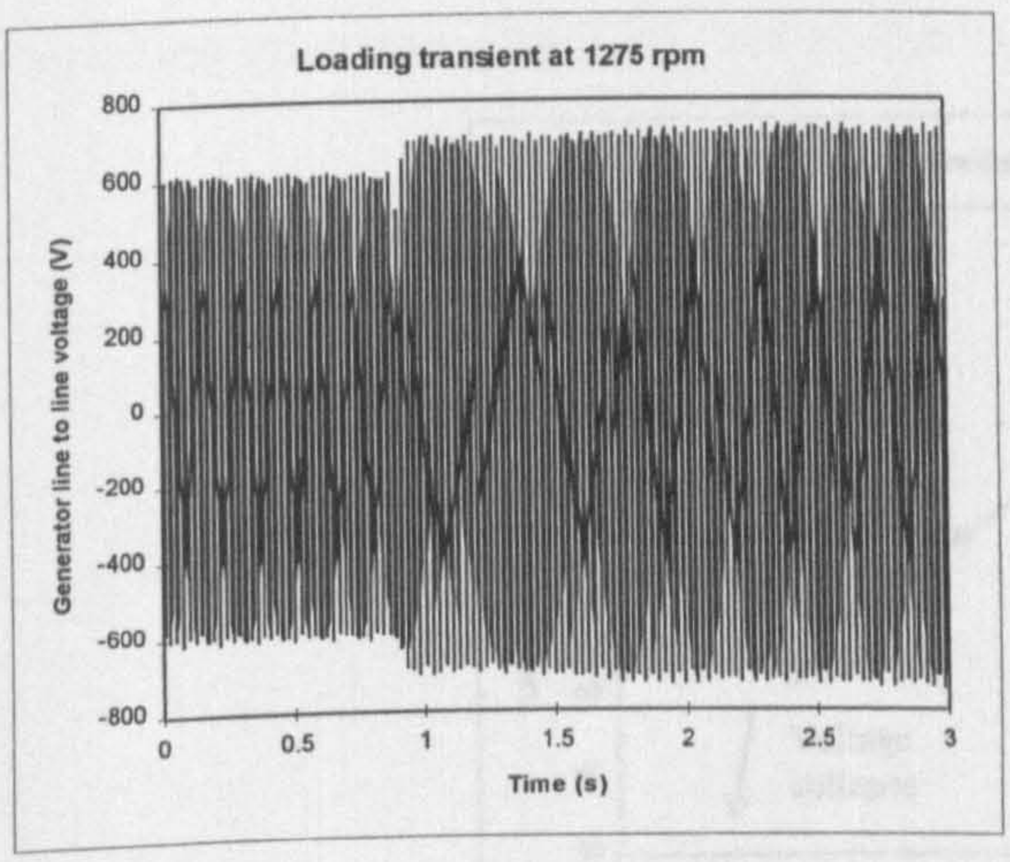

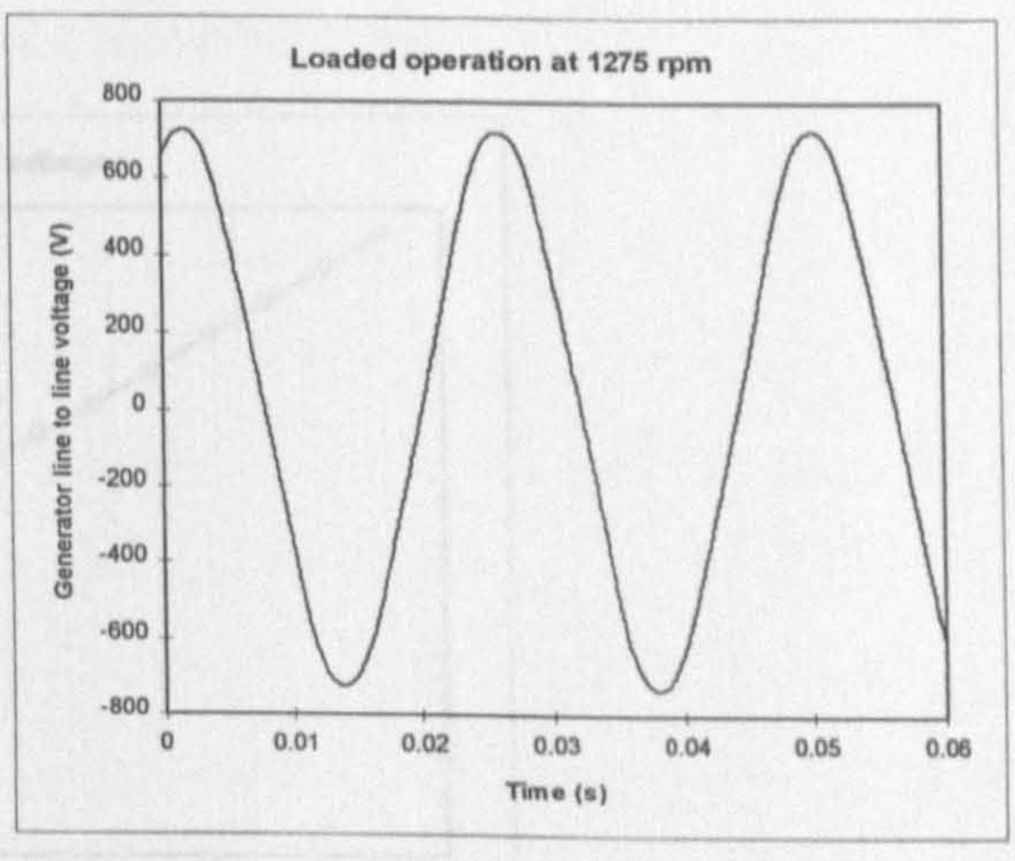

Figure 4.8.6 Generator line to line voltage in transients and in steady-state (short-shunt compensation, $C = 0.008$ mF, $R = 80$ ohms, $Cs = 0.015$ mF)

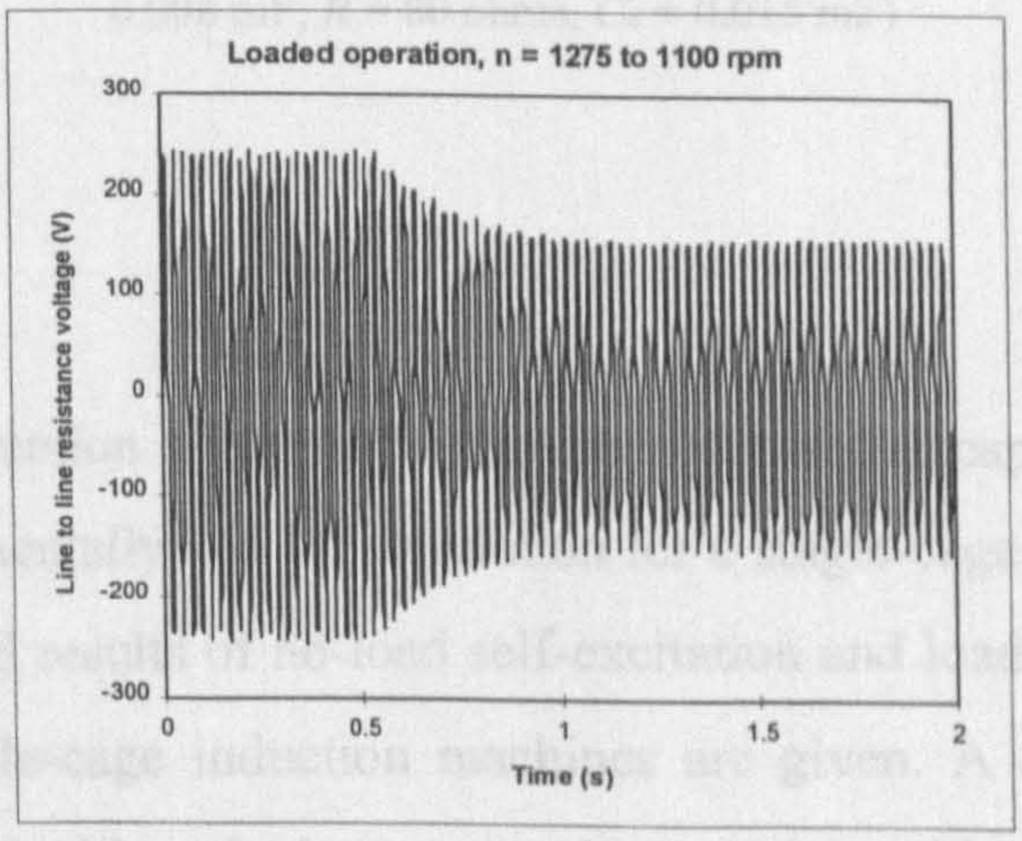

Figure 4.8.7 Line to line voltage across resistance in speed transient (short-shunt compensation, $C = 0.008$ mF, $R = 80$ ohms, $Cs = 0.015$ mF)

as function of speed, depicted in Figure 4.8.8 for 80 Ω resistance, shows that normal self-excited operation is preserved for all speeds higher than 1000 rpm. Short-shunt compensation thus enables not only successful connection of the resistive load, but it also extends the operating speed range in which self-excitation can be preserved. Large drop of voltage at 975 rpm indicates vicinity of the voltage collapse. Indeed, self-excitation was lost once when the speed was reduced to 950 rpm and the same problems, as those discussed in conjunction with Figure 4.7.13, were again encountered. Complete demagnetisation of the machine took place. This contradicts the conclusion of [Shridhar et (1995a)], that short-shunt system will re-excite after de-excitation because combined parallel and series capacitance will manage to dig out what little remanent flux is left.

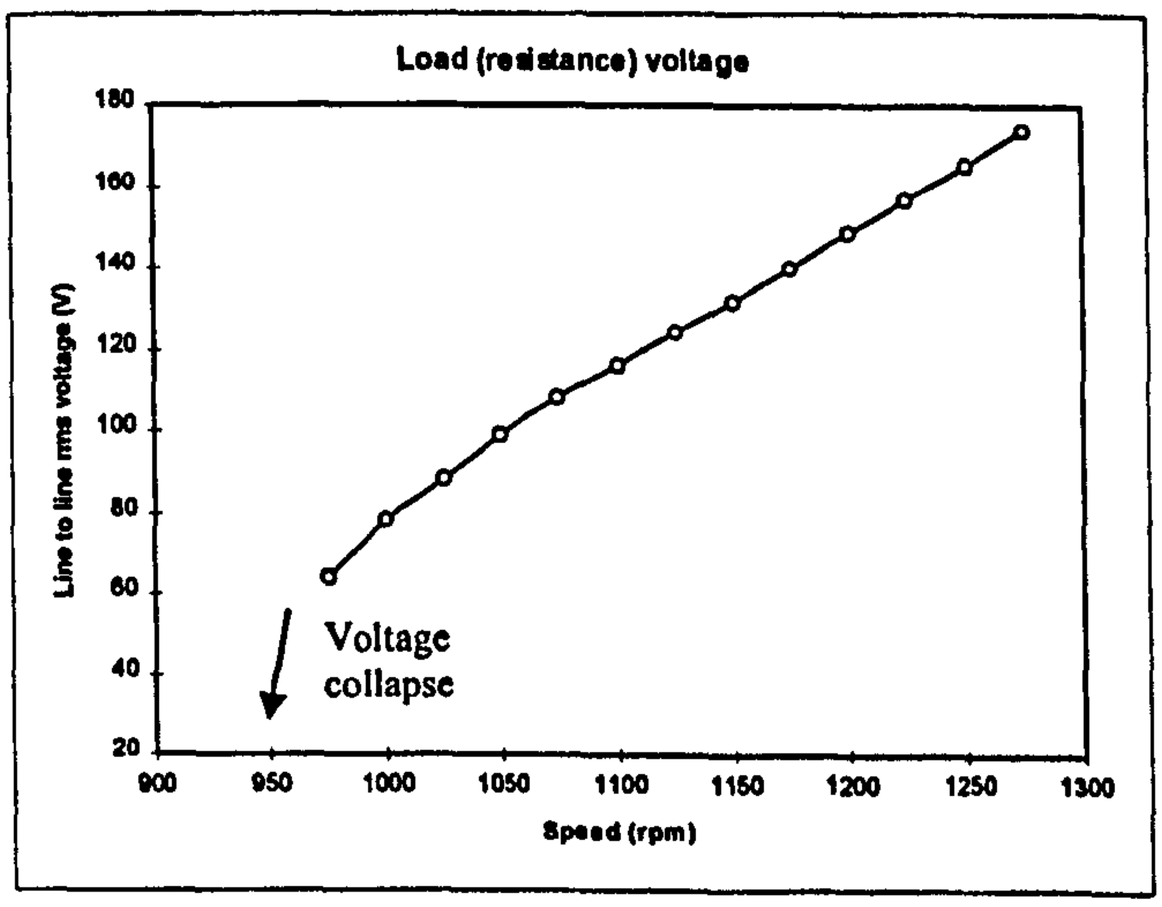

Figure 4.8.8 Steady-state load voltage as function of operating speed (short-shunt compensation, C = 0.008 mF, R = 80 ohms, C_s = 0.015 mF)

4.9 Summary

Self-excitation of induction generator by means of parallel capacitor bank has been analysed both experimentally and by simulation for a single-cage and for a double-cage induction machine and results of no-load self-excitation and loading transients for both single-cage and double-cage induction machines are given. A double-cage induction machine is represented with a single-cage machine model and impact of such a reduced order representation is studied. The results of the study indicate that the major error

introduced by reduced order modelling is inflicted upon the prediction of the time interval required to achieve the steady-state operation. The results are otherwise similar, in terms of both final steady-state and waveform of the voltage build-up. Load voltage variation compensation for stand-alone induction generator using an additional auxiliary series capacitor bank has also been investigated.

Results of an experimental study of dynamic behaviour of a self-excited induction generator with star and delta connected capacitor bank are reported. No-load self-excitation and loading of the generator with and without short-shunt compensation are elaborated. The emphasis is placed on variable speed operation, voltage collapse and situations that result in total demagnetisation. Some of the frequently cited statements regarding operation of a SEIG are shown not to be universally valid.

Chapter 5

MODELLING AND SIMULATION OF A VOLTAGE SOURCE INVERTER (VSI) BASED REACTIVE POWER COMPENSATOR

5.1 Introduction

Previous chapter has examined operation of an induction generator with capacitor bank type of reactive power compensator. Operation of such a scheme is inherently open-loop and therefore leads to substantial variation of the generator flux as function of the operating conditions. In the forthcoming chapters of the thesis (Chapter 6 to 8) a different controllable, reactive power compensator will be used. The compensator is of voltage source inverter type and its control is accomplished by means of PWM. Use of such a compensator will enable substantial improvement in characteristics of the induction generator plant over the case when capacitor bank is used.

The purpose of this chapter is to discuss operation of a PWM voltage source inverter and to explain modelling and simulation of such an inverter using MATLAB/SIMULINK environment.

5.2 Operation and modelling of a PWM voltage source inverter based compensator

Voltage source inverter (VSI) type reactive power compensators, operated in a pulse width modulation (PWM) mode for control of inverter output voltage and frequency, enable very fast control of the inverter so that it reacts to the VAr demand change almost instantaneously. High frequency PWM schemes of VSI compensators can greatly attenuate the current harmonics generated by the compensator itself as the inverter is interfaced with the power system through interconnecting inductors or a transformer. At high switching frequencies, the current harmonics injected into the network are of high frequencies and very small amplitude. The most common method of

PWM is the sinusoidal PWM where three-phase sine reference voltages are compared with a triangular carrier wave of fixed frequency and fixed amplitude. The inverter voltage outputs contain the fundamental component whose amplitude and frequency is equal to the reference sinusoidal signal. By varying the amplitude of the reference sine wave, amplitude of the fundamental output voltage is varied and the reactive power flow is thus adjusted. In order that reactive power can flow from the inverter to the mains, the value of d.c. voltage at the inverter d.c. side has to be sufficiently high so that the fundamental harmonic at the inverter output is greater than the power system voltage. When the fundamental component of the inverter output voltage is higher than the network voltage, reactive current is delivered to the network. When the fundamental component of the inverter output voltage is smaller than the network voltage, reactive current is drawn from the network.

Among PWM techniques that are most frequently used in conjunction with voltage source inverters are sinusoidal PWM, space vector PWM and PWM generated using regular sampling technique. The basic principle of the sinusoidal PWM scheme [Murphy and Turnbull (1988)] is to compare three-phase sine wave references with a high frequency symmetrical triangular carrier wave. The points of intersection determine the PWM switching instants. The modulation index *m*, defined as the ratio of the reference wave amplitude to the carrier wave amplitude, determines the fundamental output voltage. This scheme is usually implemented using analog electronics. Regular sampled PWM technique [Bowes and Mount (1981)] is appropriate for digital hardware and microprocessor implementation. Two types of modulation are possible, namely symmetrical modulation and asymmetrical modulation. In symmetrical modulation, the sinusoidal modulating wave is sampled at regular intervals according to the carrier frequency. A constant level is maintained by a sample-and-hold circuit until the next sampling instant. This results in a sample-hold or amplitude-modulated version of the sinusoidal modulating wave. This digital version of the modulating wave has a constant amplitude while a pulse width is defined and the width of a pulse is proportional to the amplitude of the modulating wave. The space vector PWM method [Van Der Broeck et al (1988), Handley and Boys (1992)] generates three-phase waveforms based on approximation of a rotating reference voltage space vector with those physically

realisable in a three-phase inverter over a period of the carrier frequency. Space vector PWM enables very accurate control of voltage, frequency and phase within one switching cycle.

In sinusoidal PWM, that is adopted here as the PWM strategy, signals are generated using three reference sine waves and a triangular carrier wave. The frequency of the reference sine wave represents the stator frequency of the induction generator. The three reference waveforms are of identical amplitude but each of the sine waves is phase shifted by 120 degrees. The algorithm of sinusoidal PWM is to generate gate signals for the switching devices which turn on the upper switch device when the reference sine wave is higher than the triangular wave and vice visa.

The simulation of PWM VSI based reactive power compensators can be done using either a circuit simulation package or a dynamic system simulation package. Circuit simulation packages are suitable for designing circuit and studying device switching behaviours and they provide interface to printed circuit board layout design. However, they are not intended for designing control systems and studying dynamic system performance. A dynamic system simulation package usually provides interfaces to high level language programming for accelerating simulation speed and for real-time embedded controller designs. For modelling and simulation of a VSI based reactive power compensator with associated control system, a dynamic system simulation package, MATLAB/SIMULINK, is chosen.

5.3 Model implementation in SIMULINK

MATLAB [MathWorks (1992)] is a powerful tool for modelling, analysis and simulation of non-linear dynamic systems. SIMULINK is one of many MATLAB's toolboxes that provides graphical block-oriented interface with MATLAB. SIMULINK includes extensive components in its block diagram library, such as general mathematical functions, transfer function block, integrator, differentiator and many non-linear function blocks (saturation, hysteresis, etc.) so that the user does not need to write the source codes. The hierarchical nature enables custom designed block to be added to

the libraries. C programme can be added if users want to accelerate simulation speed of complex systems. Many numerical methods for integration can be chosen from the control panel, namely, Euler, Adams, Gear and Runge-Kutta 3rd and 5th order. An application programme can be generated, using MATLAB C Compiler, to run on DSPs for real-time control purposes. A dynamic system comprising electro-mechanical devices and their controls can be easily constructed using the built-in functions.

Since the introduction of SIMULINK a considerable effort has been put into development of appropriate models for simulation of electric machines, power electronic converters and variable-speed electric drives. Models of induction machines for mains operation [Houghton and Oghanna (1993)], for three level PWM inverter fed operation [Mathew and Oghanna (1993)] and for vector controlled operation in conjunction with complete control circuitry and power electronic converter [Wade et al (1994), (1997), White and Hinton (1994), (1995), Marino et al (1995)] are already available, as are the models of matrix converters [Zuckerberger et al (1994), (1996), (1997)], complete DC motor based controlled drives [Flinders et al (1993)] and various other power electronic converters [Lai (1994), Teodorescu et al (1995)].

The prevailing approach to inverter modelling in the already existing SIMULINK models appears to be complete idealisation of both the d.c. link circuit and the semiconductor switches in the inverter. PWM voltage source pattern is generated following the appropriate control law, scaled with the constant d.c. voltage value and applied directly to the induction machine terminals [Wade et al (1994), White and Hinton (1995), Marino et al (1995), Zuckerberger et al (1994)]. One of the rare models where the d.c. link circuit is modelled [Teodorescu et al (1995)] however again omits inverter modelling by using the correlation that exists between inverter output three-phase currents and the inverter d.c. link (input) current.

While these simplified approaches are often satisfactory and accurate enough for analysis of induction motor drives with complex control systems, there are a number of PWM voltage source inverter applications where a more detailed inverter and d.c. link circuit models are required. When a PWM VSI is applied as a static reactive power

compensator, supplying either infinite bus-bars or a stand-alone induction generator, the loss in the d.c. circuit and in the inverter determines the amount of real power that has to be supplied to the inverter from the mains (or the induction generator) in order to maintain the approximately constant d.c. voltage at the inverter input. Similarly, if the inverter supplies a static load, losses again should be accounted for. The remainder of this section presents complete SIMULINK models of single-phase and three-phase PWM VSI that account for both d.c. circuit loss and for the inverter conduction losses and are thus well suited for the above listed applications [Liao et al (1996)].

A three-phase PWM voltage source inverter is illustrated in Figure 5.1. The single-phase version of the inverter is obtained by omitting the third leg and by connecting the single-phase load to the output terminals. The inverter configuration shown in the figure closely corresponds to the one utilised in static reactive power compensation. If the inverter is used as a reactive power source for the stand-alone induction generator, then the initial charge on the capacitor is usually from a battery. If the compensator operates on mains, the capacitor has to be pre-charged to the sufficient voltage value prior to its commissioning. A set of three inductors serve as interface between the compensator and the grid. If a transformer is placed between the compensator and the grid, the three inductors correspond to per-phase transformer leakage reactance.

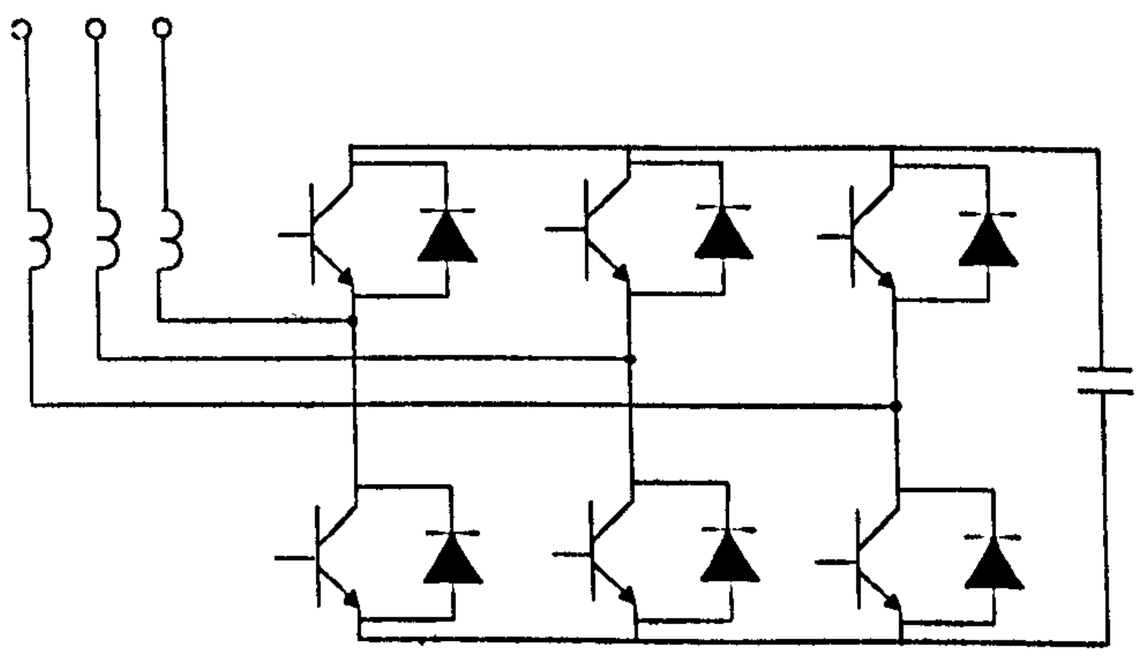

Figure 5.1 Three-phase voltage source inverter

Each of the six power switches in Figure 5.1 is composed of an anti-parallel connection of a diode and a controllable semiconductor which is triggered with PWM signals. Hence it may be regarded as a switch with bi-directional current flow. Such an approach

has already been utilised in switch modelling using SIMULINK [Flinders et al (1993)] and is adopted here. The capacitor in the d.c. circuit is modelled as a lossy one, by connecting a resistance in series with the ideal capacitor [Flinders et al (1993)]. Additionally, the capacitor is pre-charged to the certain voltage level, so that the initial condition is required as well. The SIMULINK model of the lossy capacitor with initial condition is given in Figure 5.2. A three-phase lossy inductor model is required if the inverter operates as static reactive power compensator (Figure 5.1). Similarly, if the inverter supplies static resistive-inductive load, the load can be modelled with a lossy inductor. The lossy inductor (Figure 5.3b) is represented with a parallel connection of an inductor and a resistor. Figure 5.3a shows the resistor model.

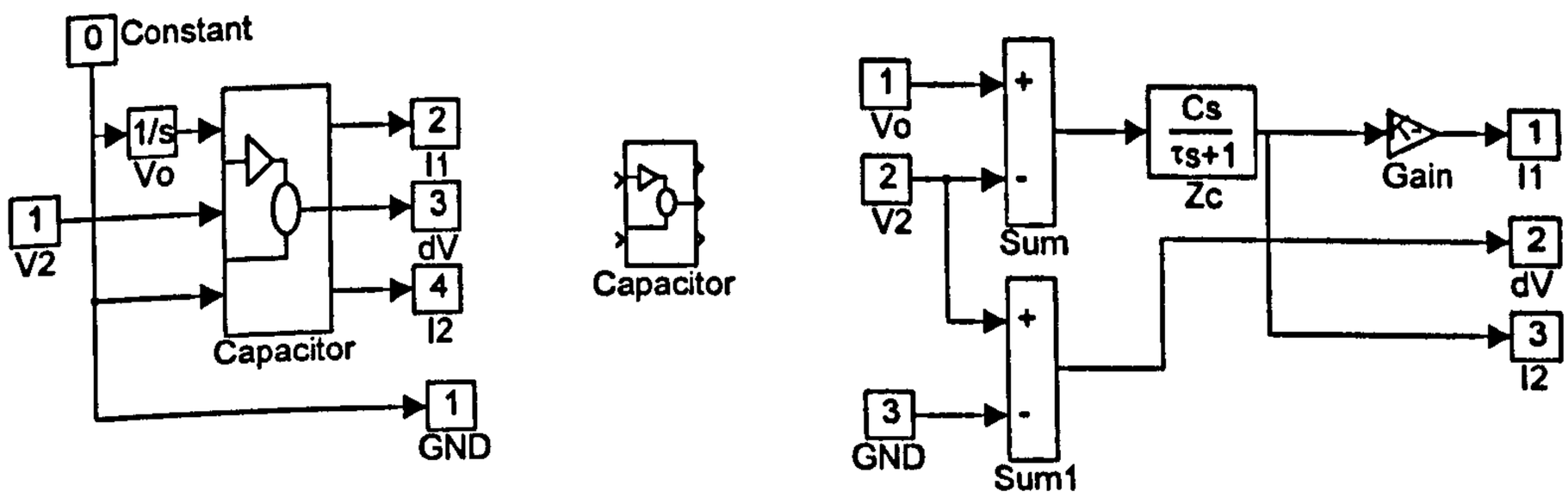

Figure 5.2 Model of lossy capacitor with initial condition

The power switch is modelled as bi-directional to represent the operation of a controllable power semiconductor device with an anti-parallel diode. The resistance of the switch takes one of the two values depending on whether it is on or off. The on and off states are represented by means of appropriate small and very large resistance respectively, so that conduction loss is accounted for. Typically, the order of magnitude of the on-resistance is 0.1Ω, while the off resistance is of the order of 1MΩ. The model of each individual switch is shown in Figure 5.4. The switch function block is used to select the value between the two resistances depending on the gate signals. The gate input is activated by logic levels. When the gate signal is 1, Ron is selected. The switch is therefore in its low impedance state. When the gate signal is -1, Roff is connected. The device is therefore in its high impedance state. This type of switching element modelling results in a linear system.

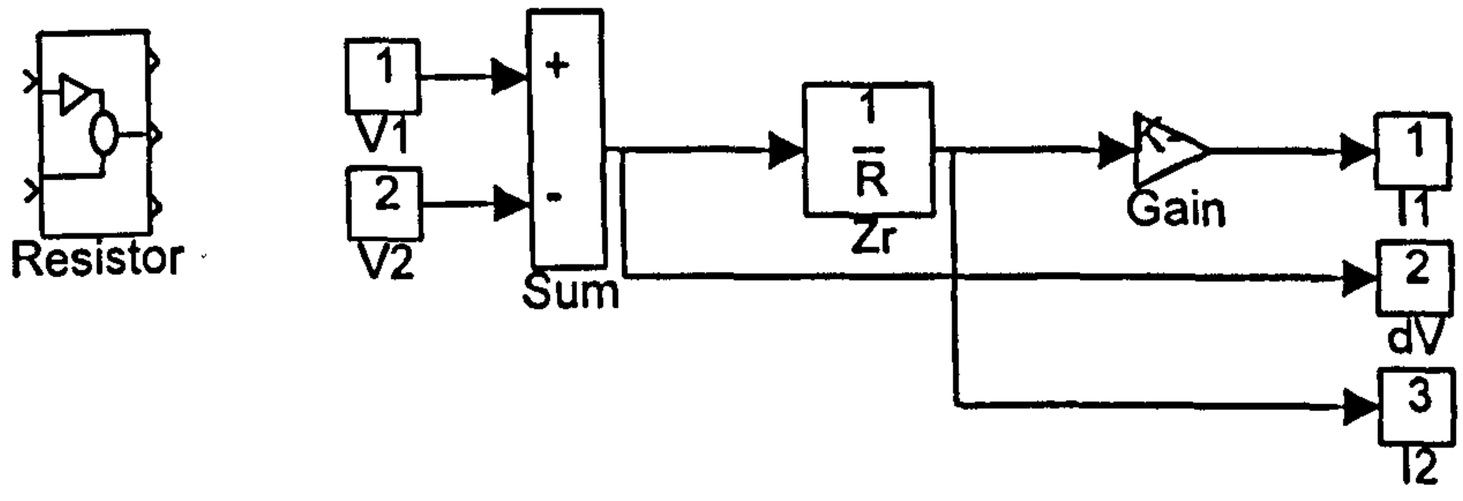

(a)

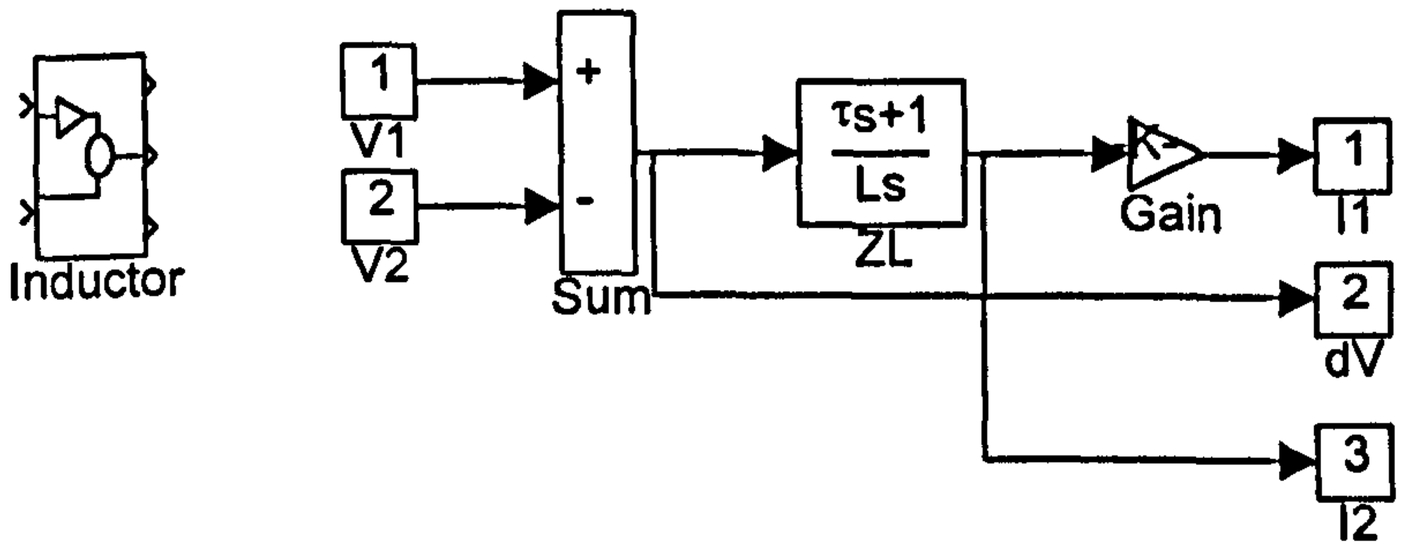

(b)

Figure 5.3 Model of a resistor (a) and of a lossy inductor (b)

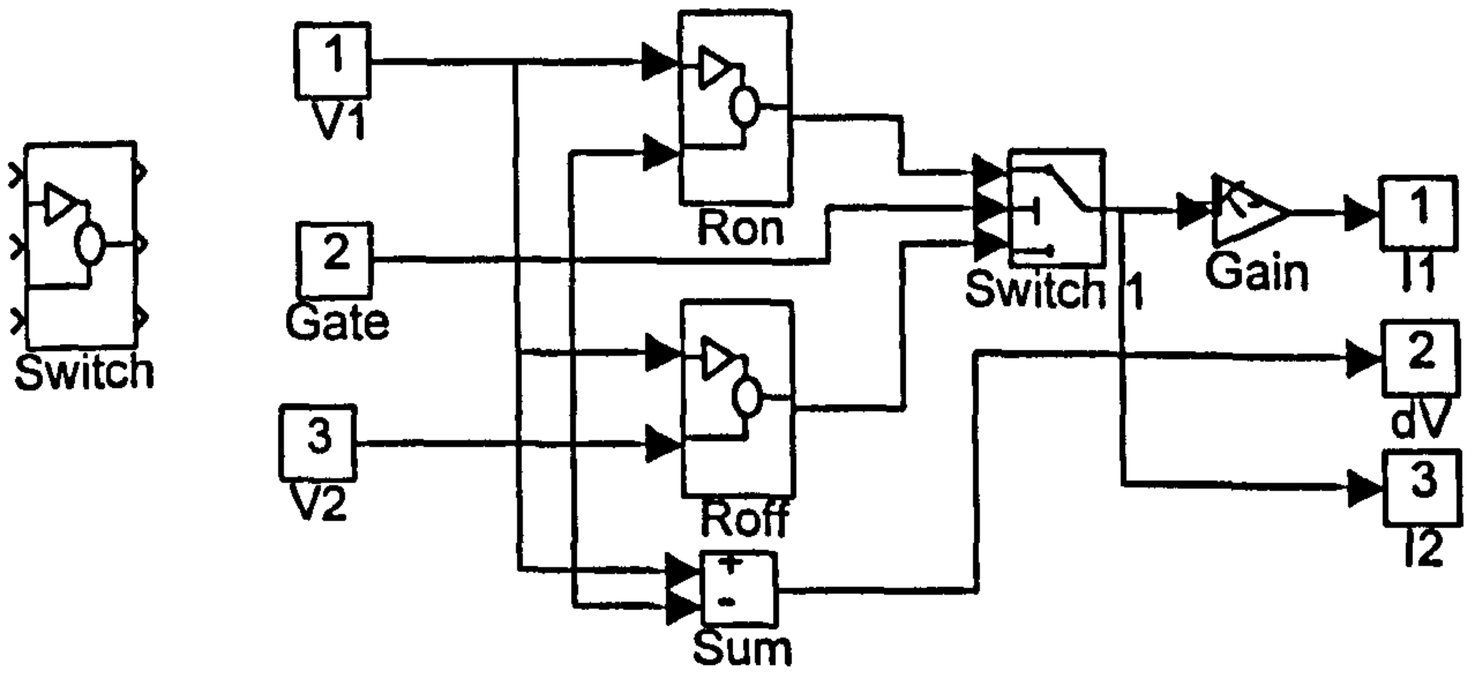

Figure 5.4 Model of a bi-directional switch

All the circuit component blocks have a common feature that the current is a time dependent function of the voltage. The terminal voltages appear at the input side of the block on the left and the terminal currents appears at the output side on the right. Current I1 always connects to the node determining voltage V1 while current I2 connects to the node which in turn determines voltage V2. Sign of current I1 is always

inverse with respect to the sign of current I2 since I1 enters the device while I2 leaves the device. The Kirchhoff's current law is then satisfied.

PWM technique adopted here is the sinusoidal pulse width modulation. The PWM module is built on the basis of signal generator and sine function facilities and its model is given in Figure 5.5. The carrier and the reference frequency are taken in subsequent simulations as 950 Hz and 50 Hz, respectively, while the modulation index is chosen as equal to 0.833.

The PWM patterns are generated using three 120 degrees shifted modulating sine waves and a carrier wave. Each sine wave is compared with the carrier wave and every crossing point determines the triggering instant. Higher the switching frequency, better the output current waveform. In high power and high voltage applications, the loss in the switching devices is a major constraint and this limits the switching frequency to a certain value. The comparator block is written using s-function which links an m-file into a graphical block. The m-file is written in MATLAB. The s-function provides the user with the flexibility to build his own graphical blocks, which can handle continuous, discrete and mixed discrete-continuous simulations. These can be added to standard libraries.

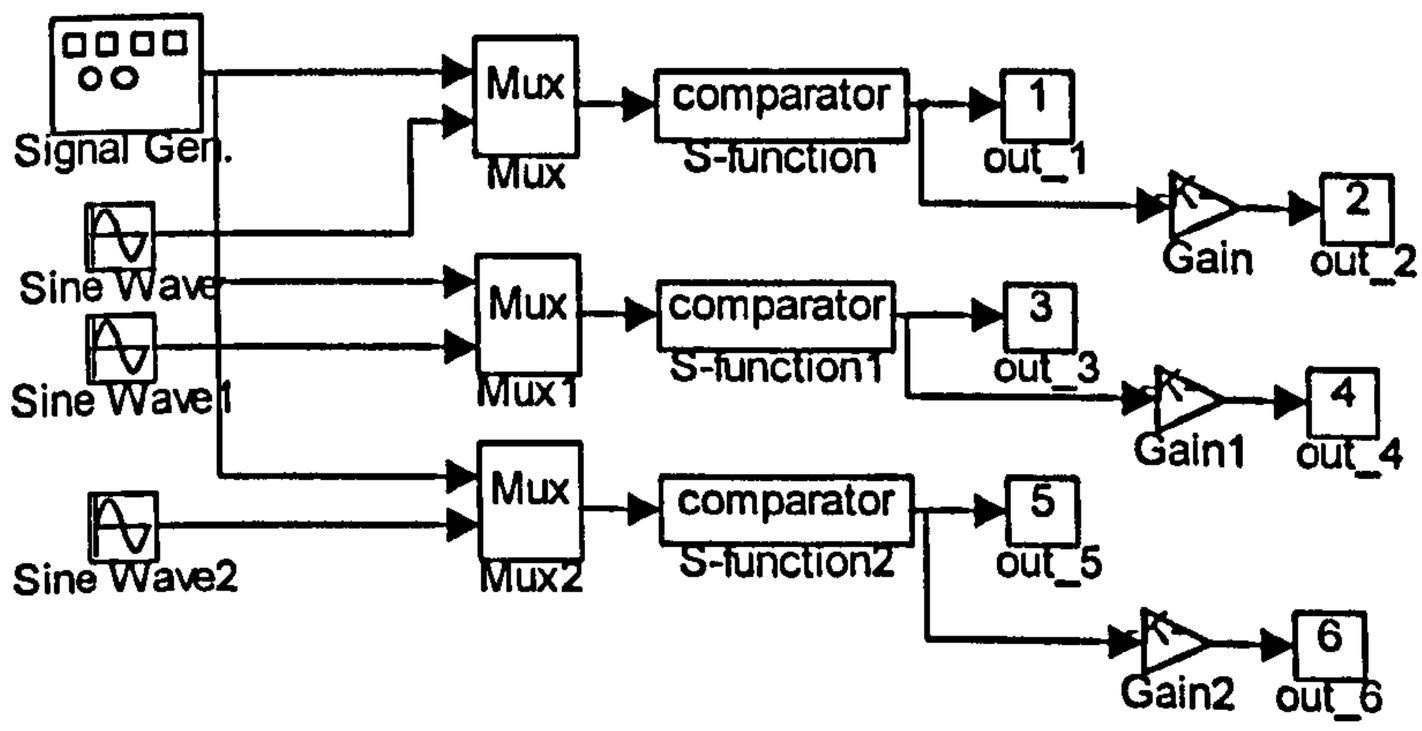

Figure 5.5 Model of three-phase PWM module

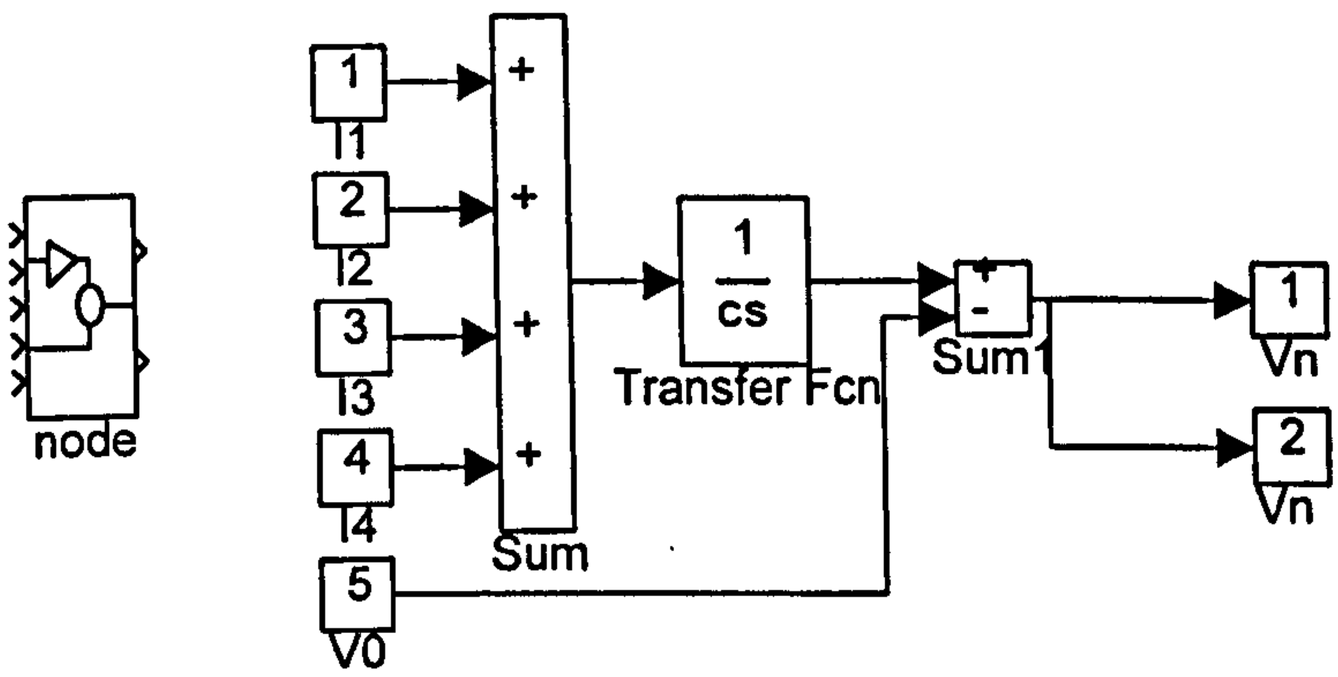

Figure 5.6 Model of a node

In order to connect various components of the model into a complete circuit model, the concept of capacitive node [Flinders et al (1993)] is utilised. A practical circuit will contain circuit capacitances which can be considered as being lumped at the circuit nodes. These nodal capacitances will have a similar effect to those introduced in the simulation model. The capacitive nodes are used as interfaces between different devices. The node sums all the device currents applied to the input of the block and integrates to obtain the nodal voltage at the output of the block. Model of a capacitive node is depicted in Figure 5.6. The value of the node capacitance is usually made very small so that the effect of the node capacitance on the simulation results is negligible.

The inverter is thus modelled with power switches, PWM triggering signals, electrical passive components and capacitive nodes. The Gear numerical integration algorithm is suitable for solving a stiff set of differential algebraic equations formed to model power electronic systems. The Gear numerical integration algorithm is available in SIMULINK.

5.4 Simulation results

On the basis of the blocks described in the previous section, the models of the single-phase and of the three-phase PWM voltage source inverter are built. The models are given in Figure 5.7 and Figure 5.8 respectively. The single phase inverter requires four switches and three nodes, while in the three-phase case six switches and five nodes are

needed. The load at the inverter output is in both models given with a lossy inductor. Simulations therefore apply to the case when a three-phase PWM inverter feeds a static resistive-inductive load [Liao et al (1996)].

Operation of the single-phase PWM inverter is investigated first. The inverter output current is shown in Figure 5.9 when the load of the inverter is a lossy 5mH inductor and the capacitor is pre-charged to voltage equal to 500V. The inverter output voltage and current will reduce as the time goes by, due to the loss in both d.c. circuit and the inverter. This reduction is not observable in Figure 5.9 due to the high value of the capacitance in the simulation. If the load is changed from inductive to purely resistive (1kΩ), decay in the load current and capacitor voltage is illustrated in Figure 5.10 (for the same capacitance and initial capacitor voltage).

Operation of the three-phase PWM VSI with three-phase resistive-inductive load is illustrated next. The value of capacitor in the simulation is taken as one Farad and the capacitor is again pre-charged to 500 volts. Each phase load consists of a 5mH inductor

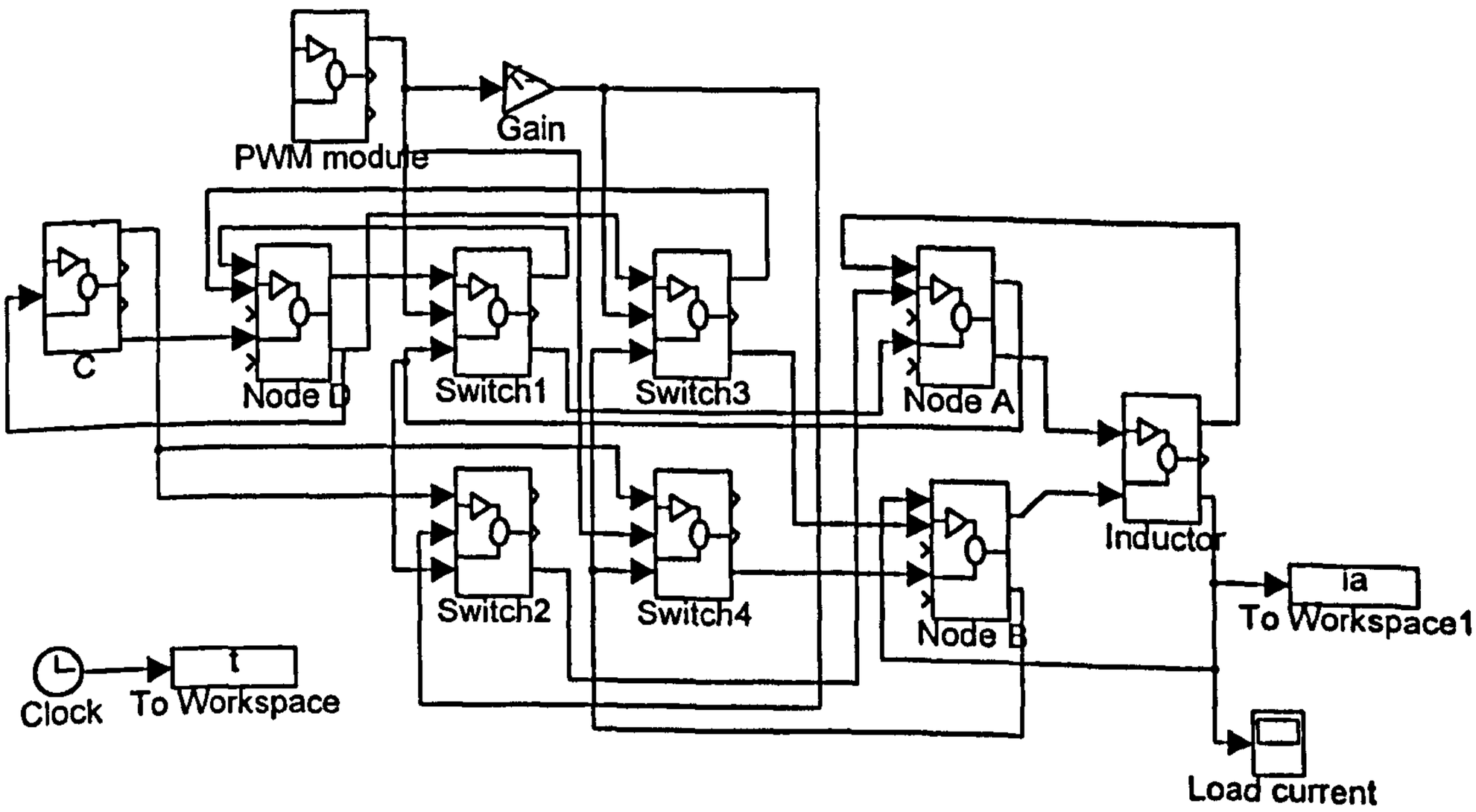

Figure 5.7 Complete SIMULINK model of a single-phase PWM voltage source inverter

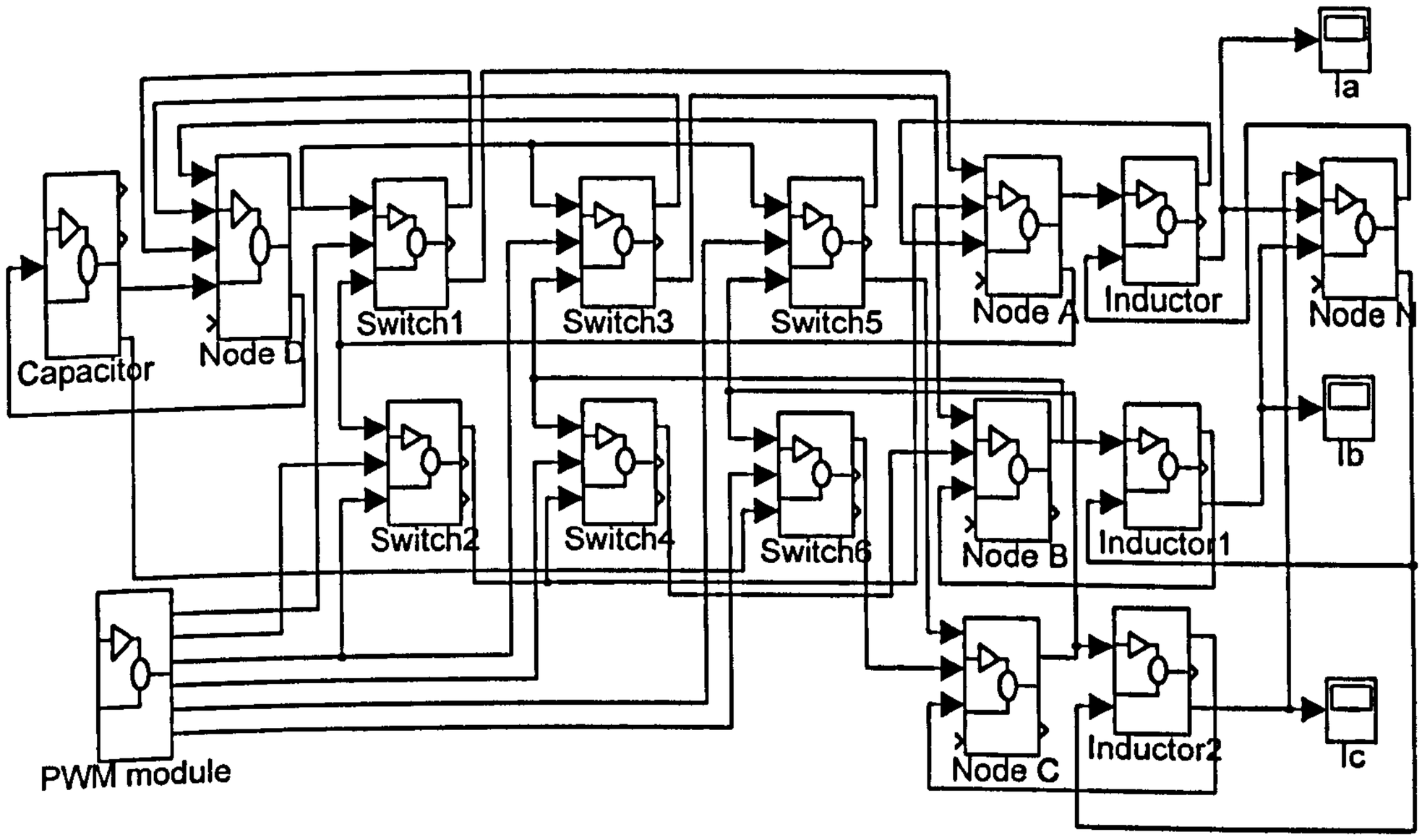

Figure 5.8 Complete SIMULINK model of a three-phase PWM voltage source inverter

in parallel with a 50Ω resistor. All the three inverter output phase voltages and the corresponding three currents in star connected load are displayed in Figure 5.11 and Figure 5.12 respectively.

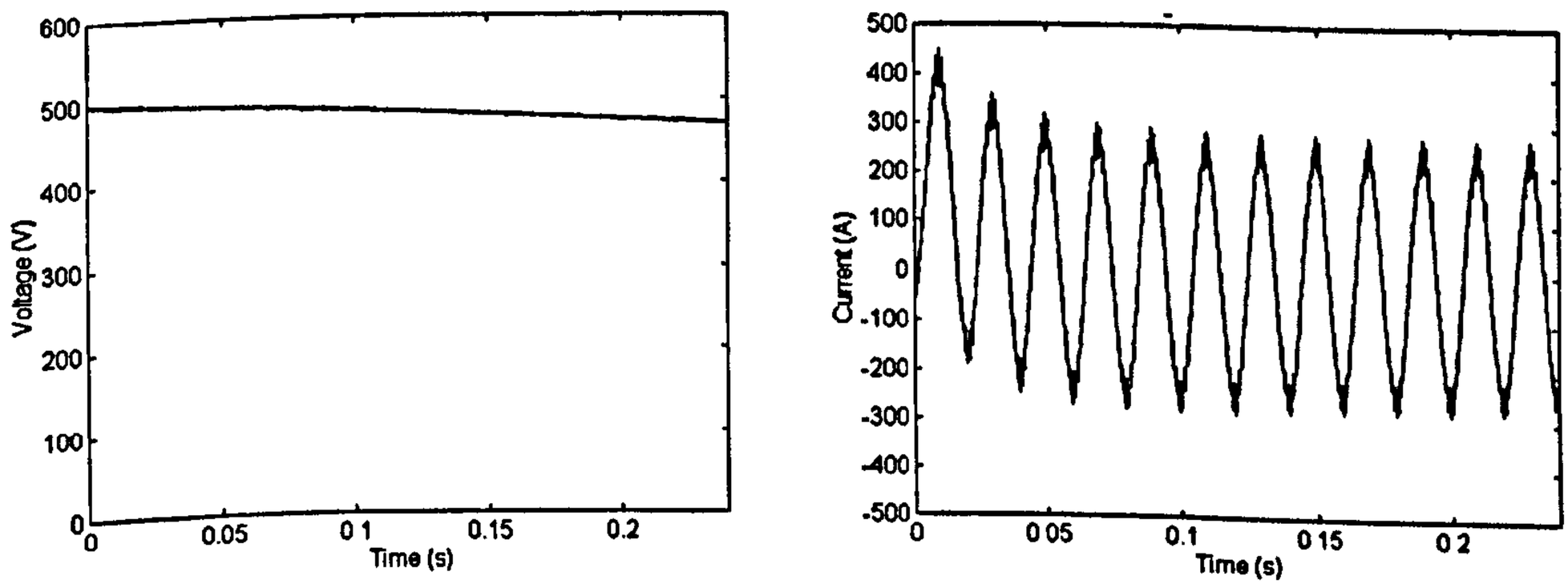

Figure 5.9 Capacitor voltage and single-phase inverter output current with inductive load

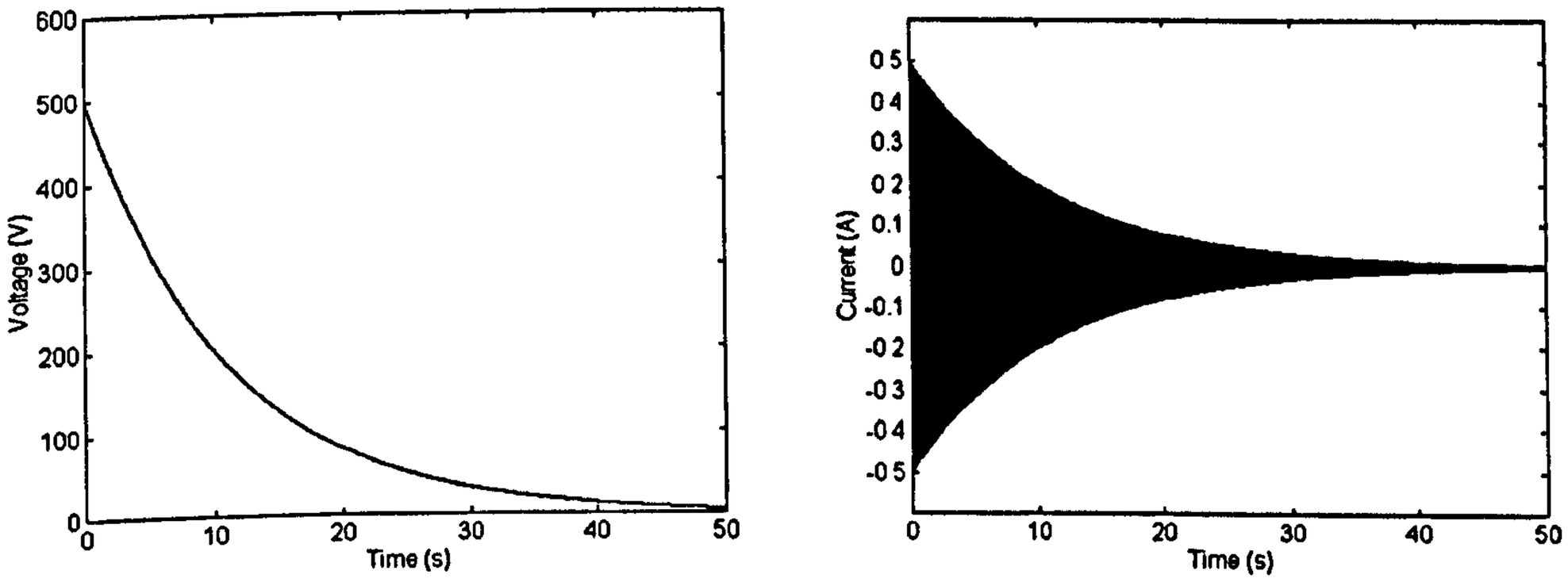

Figure 5.10 Decay of capacitor voltage and single-phase inverter output current for purely resistive load

5.5 Summary

Modelling and simulation, using SIMULINK package, of static reactive power compensator based on a PWM voltage source inverter is presented. Simulation results of operation a single-phase and a three-phase PWM voltage source inverter for different operating conditions are shown. Presented simulation results verify that developed SIMULINK models of single-phase and three-phase PWM voltage source inverter, that account for loss in the d.c. circuit and the conduction loss of semiconductor switches, are correct and well-suited for analysis of PWM VSI based static reactive compensators and for analysis of PWM VSI fed static loads. It is possible to apply the models in analysis of an induction machine fed from a PWM VSI and in simulation of an induction generator with static reactive power compensation.

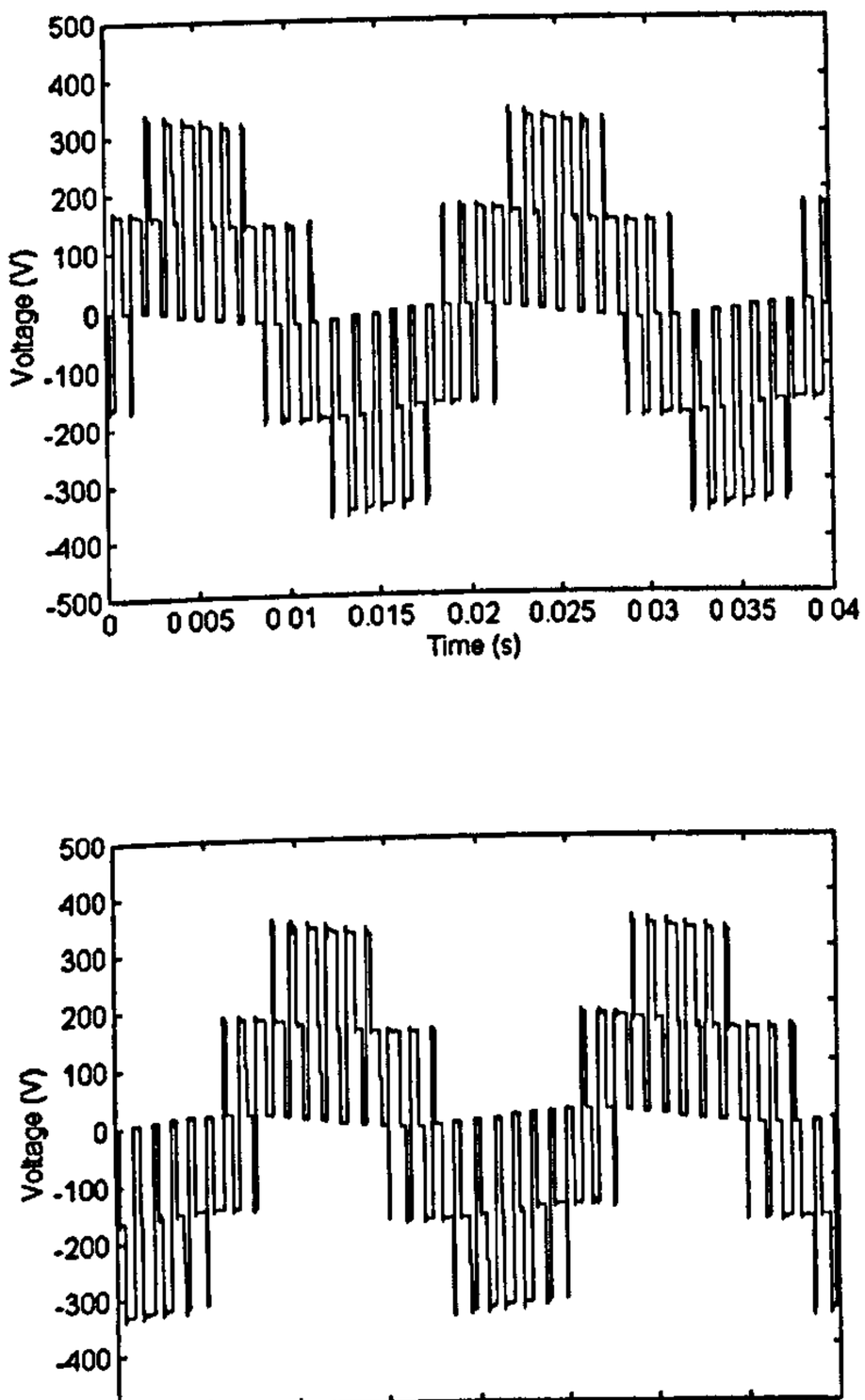

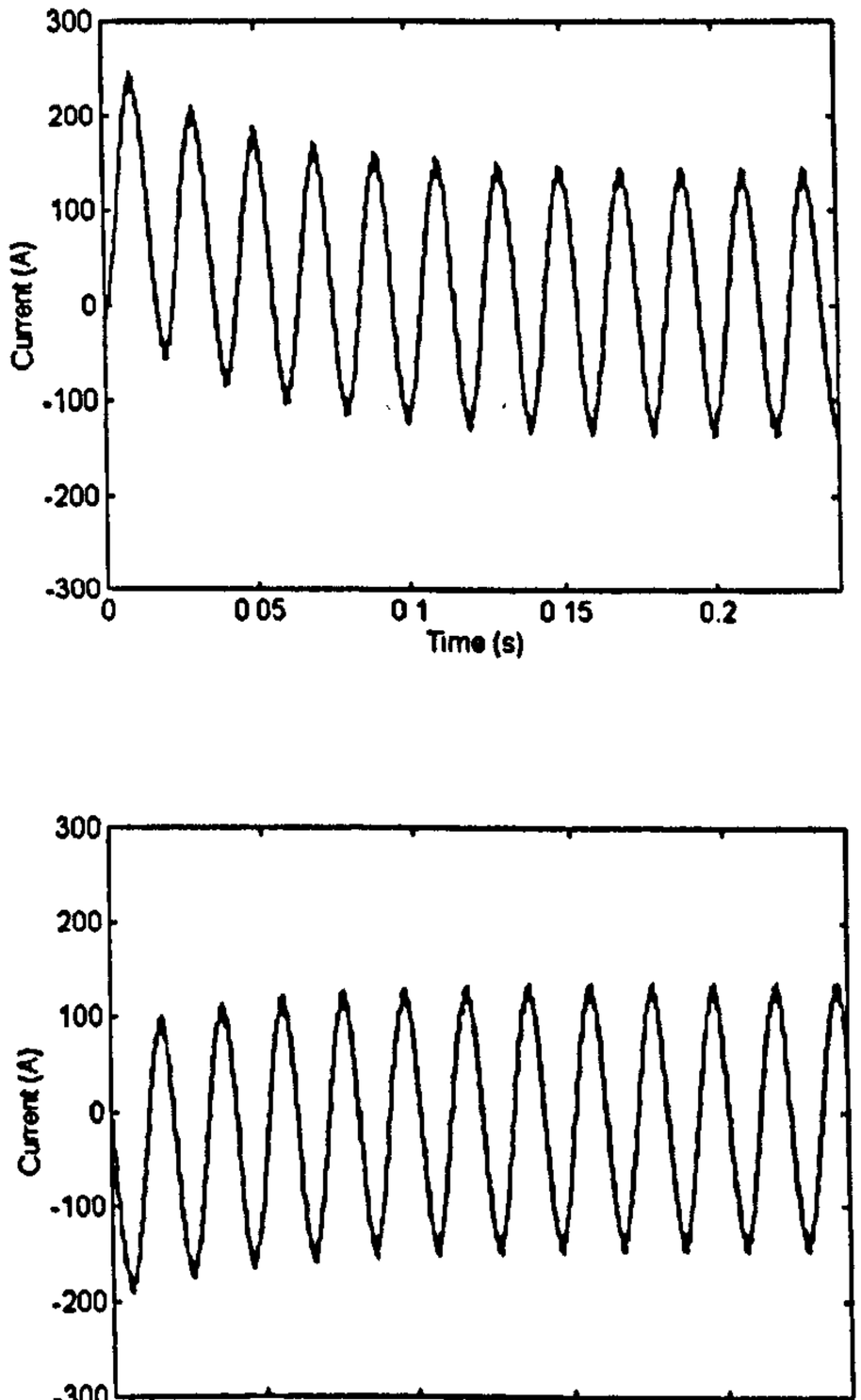

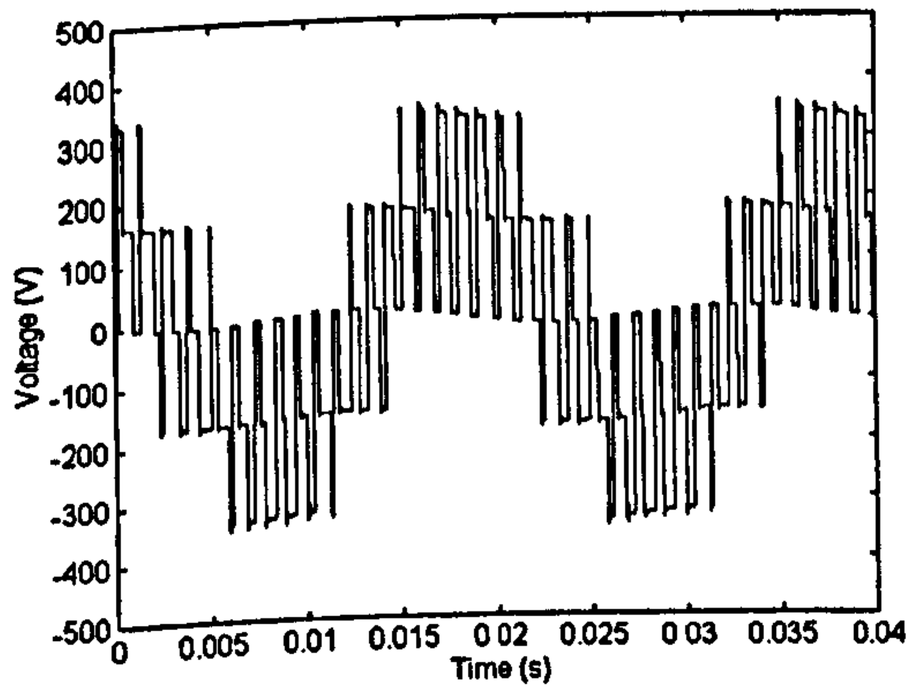

Figure 5.11 Output phase voltages of the three-phase inverter for inductive load

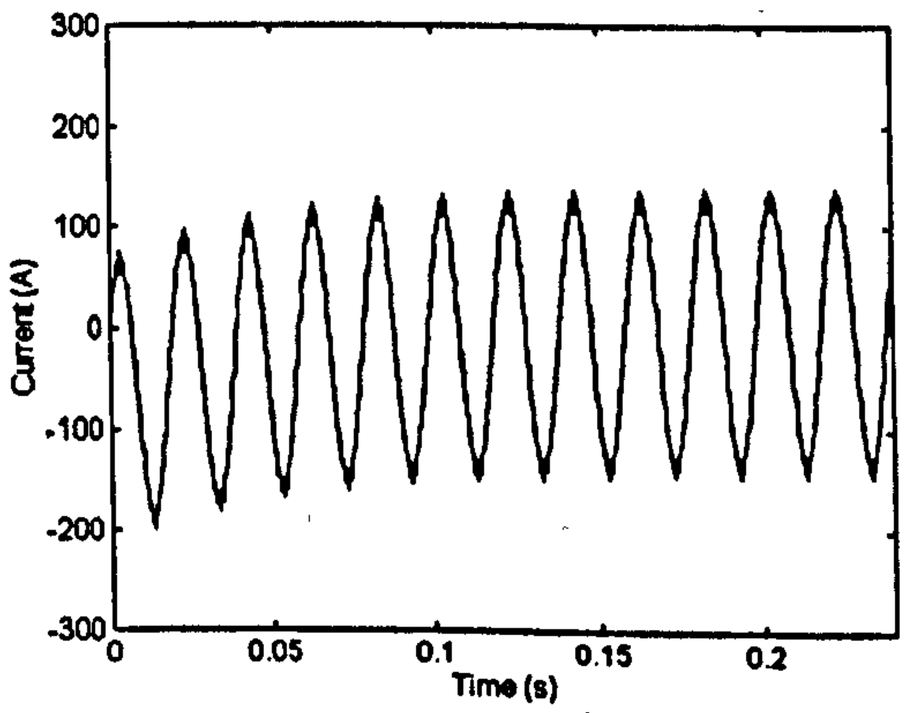

Figure 5.12 Output currents of the three-phase inverter for inductive load

Chapter 6

SCALAR CONTROL OF A PWM VSI REACTIVE POWER COMPENSATOR IN STAND-ALONE INDUCTION GENERATOR APPLICATIONS

6.1 Introduction

Stand-alone application of induction generators requires that an appropriate static reactive power compensator is connected in parallel to the induction generator stator terminals in order to magnetise the machine. Utilisation of a capacitor bank connected to the induction generator terminals is the most conventional and the simplest solution of providing external reactive power. Analysis of self-excitation transients using capacitor bank has been reported in Chapter 4 for constant speed operation and examined experimentally for both constant speed and variable speed operation. However, it is not possible to keep the excitation constant for a large speed operating range due to the fixed value of capacitance and self-excitation may be lost, as shown in Chapter 4. As the reactive power is not controlled, the scheme is not suitable for variable speed operation. In the case of variable speed operation, it is necessary to connect in parallel several capacitor banks of different capacitance values. However, the value of capacitance increases with decrease in the rotor speed, thus very large values of capacitance are required at low speeds, making this approach impractical. Other solutions are utilisation of either thyristor controlled reactor based VAr generator or inverter based static VAr compensators.

The advent of power electronic converters has enabled application of inverters for self-excitation purposes. The utilisation of PWM inverters has gained momentum during the last few years and numerous studies have emerged regarding application and control of PWM voltage source inverters as static reactive power compensators in stand-alone induction generator systems. Two approaches to the inverter control may be identified. The first one corresponds to V / f_s control in motoring and relies on utilisation of one of

the PWM techniques, such as sinusoidal PWM [Leplat et al (1996), Bhadra et al (1996)]. It is the purpose of this chapter to analyse this approach. The second approach involves application of vector control principles and the PWM inverter is current controlled, say, by means of hysteresis current controllers [Silva (1993), (1995), Lyra (1995), Jacobina (1996), Colliez (1997)]. The second approach will be studied in detail in Chapters 7 and 8, in conjunction with stator flux oriented control and rotor flux oriented control, respectively.

Analysis of a PWM VSI operation was explained in Chapter 5 and implementation of the model in MATLAB/SIMULINK environment was described. Such a PWM voltage source inverter is in this chapter used as a reactive power compensator for a stand-alone induction generator.

The chapter deals with dynamics of self-excitation process of a static reactive power compensation scheme comprising VSI with sinusoidal PWM and a pre-charged capacitor at the d.c. side. Scalar control of inverter in an open-loop manner is investigated. Self-excitation under no-load conditions, transient after sudden load application from no-load operation, and dynamics accompanying the speed change, are simulated using TUTSIM and discussed.

6.2 Sinusoidal PWM with scalar control of frequency

The self-excitation scheme in which reactive power is provided by a voltage source inverter with sinusoidal PWM is depicted in Figure 6.2.1. A pre-charged capacitor is connected at the d.c. side of the inverter. The resistor, connected in parallel to the d.c. side capacitor, is used to model losses in the inverter and in the d.c. circuit. The sinusoidal pulse width modulation technique is applied. The inverter is controlled by comparing a high frequency triangular wave with three-phase sinusoidal reference waves. The control signals for the inverter are modulation index m and stator frequency. Modulation index follows V / f_s = constant law and takes the value of unity at rated frequency (50 Hz). Stator frequency is in this study treated as an independent input so that system is simulated for operation under open-loop conditions. In practice it is

necessary to provide measurement of rotor speed and form stator frequency by adding rotor speed to the slip speed controller output [Bhadra et al (1996)]. Slip speed controller often has as input the error between reference d.c. voltage and measured d.c. voltage and this method of closed-loop control attempts to provide operation with constant d.c. voltage. It is applicable when the system supplies a d.c. load that requires constant voltage.

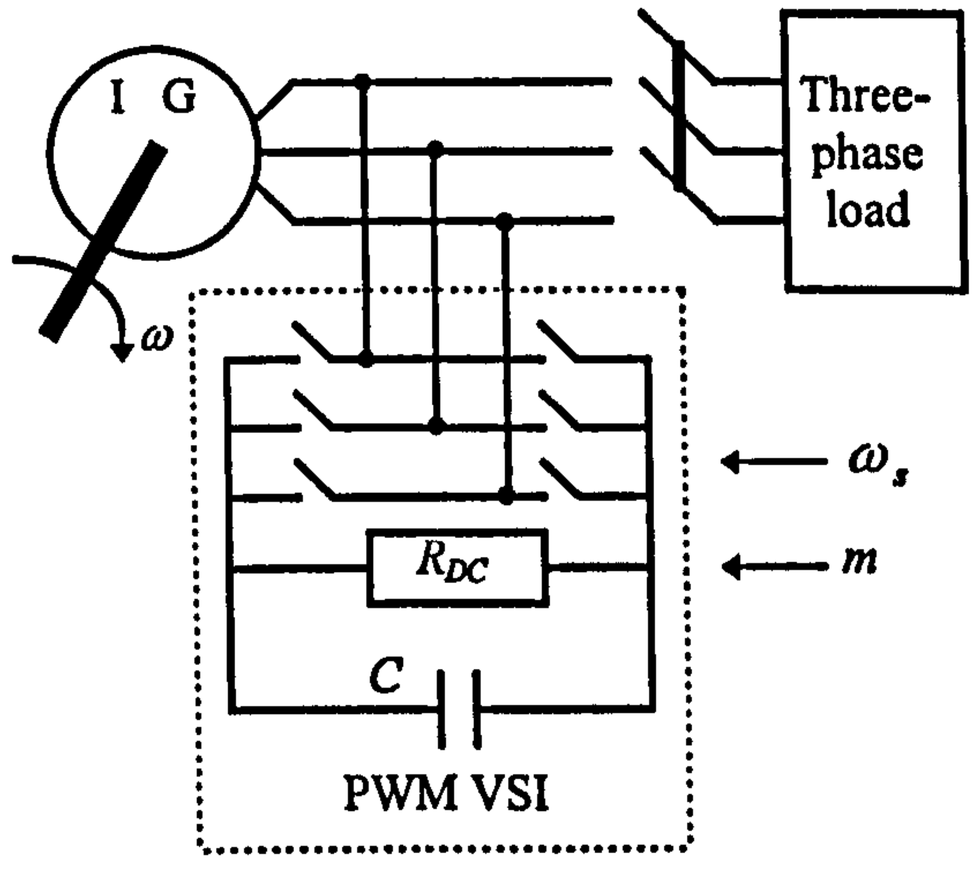

Figure 6.2.1 Self-excitation scheme based on VSI with sinusoidal PWM

The ratio between frequency of the triangular carrier wave and frequency of the reference sine wave is chosen as nineteen. Modulation index is the ratio between peak value of the reference sine wave and the peak value of the triangular carrier wave. As the purpose of scalar control of induction machine is to keep stator flux at approximately constant level, stator frequency of the induction machine has to vary when the supply voltage varies in order to keep the ratio of V / f_s constant. Modulation index m is here defined as the ratio between stator frequency and the base frequency and is equal to unity at rated 50 Hz frequency.

Figure 6.2.2 shows a simplified model of an induction generator without load, supplied by an ideal inverter. It is assumed that inverter is infinitely fast as switching devices switch on or off instantaneously.

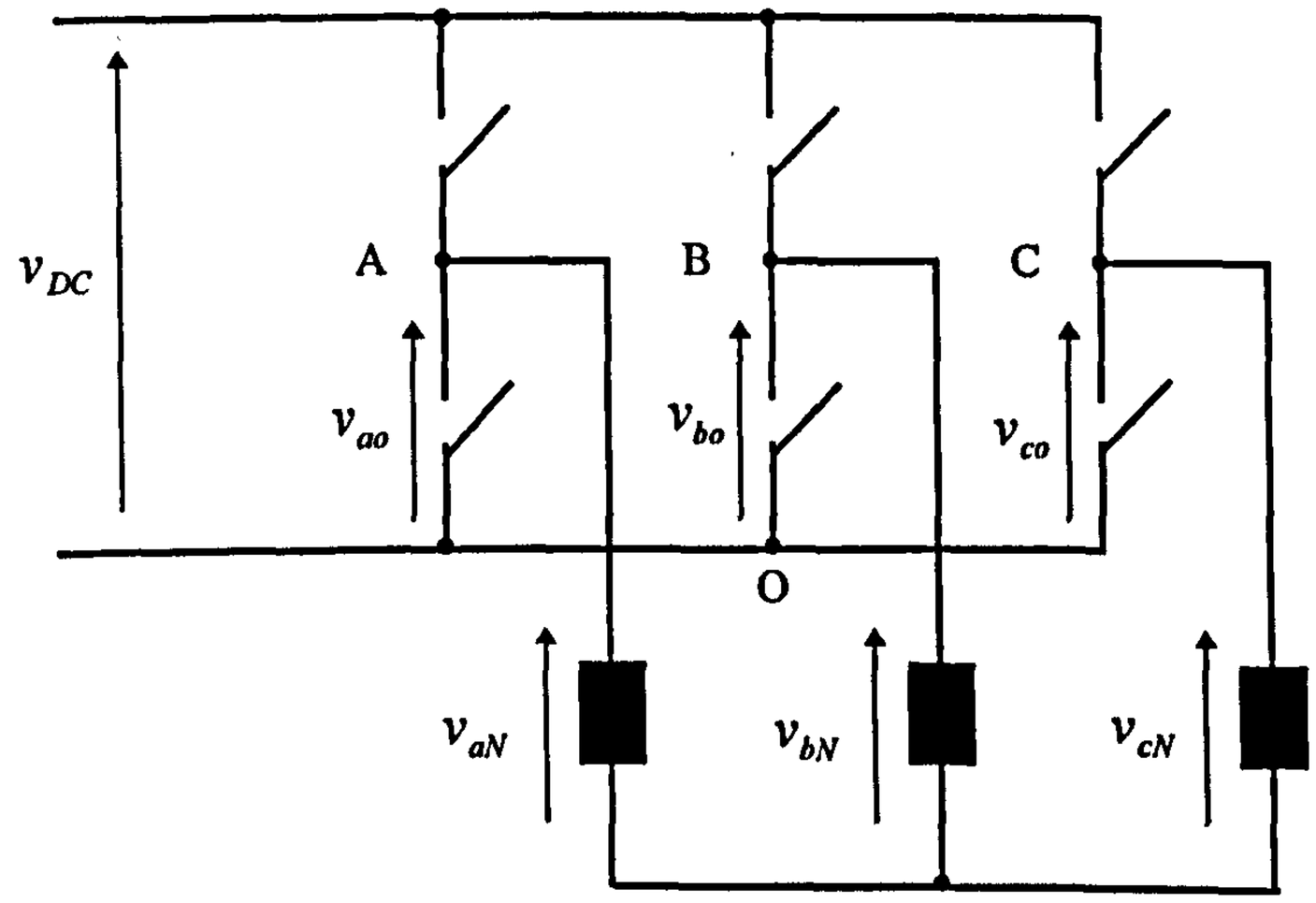

Figure 6.2.2 Star connected induction machine supplied by an ideal inverter

The inverter output voltage, i.e., the induction generator phase voltages, are obtained from the inverter leg voltages as follows [Krause et al (1995), Murphy and Turnbull (1988)]:

$$v_{aN} = \frac{1}{3}(2v_{ao} - v_{bo} - v_{co}) \tag{6.2-1}$$

$$v_{bN} = \frac{1}{3}(2v_{bo} - v_{c0} - v_{ao}) \tag{6.2-2}$$

$$v_{cN} = \frac{1}{3}(2v_{co} - v_{ao} - v_{bo}) \tag{6.2-3}$$

The induction machine line-to-line voltages are obtained as

$$v_{ab} = v_{ao} - v_{bo} \tag{6.2-4}$$

$$v_{bc} = v_{bo} - v_{co} \tag{6.2-5}$$

$$v_{ca} = v_{co} - v_{ao} \tag{6.2-6}$$

The leg voltages are obtained according to the switching scheme of the inverter. Any of the leg voltages equal either v_{DC} or zero (v_{DC} if upper switch is closed and zero if lower switch is closed). If S_a, S_b and S_c are switching functions for phase A, B and C,

respectively, then the leg voltages can be expressed as

$$v_{ao} = S_a v_{DC} \tag{6.2-7}$$

$$v_{bo} = S_b v_{DC} \tag{6.2-8}$$

$$v_{co} = S_c v_{DC} \tag{6.2-9}$$

Therefore, stator phase voltages can be expressed as follows:

$$v_{aN} = \frac{v_{DC}}{3}(2S_a - S_b - S_c) \tag{6.2-10}$$

$$v_{bN} = \frac{v_{DC}}{3}(2S_b - S_c - S_a) \tag{6.2-11}$$

$$v_{cN} = \frac{v_{DC}}{3}(2S_c - S_a - S_b) \tag{6.2-12}$$

6.3 Simulation approach

The main purpose of computer simulation is to test and verify design concept prior to actual hardware implementation. Simulation is beneficial in situations where the actual system is too expensive and time-consuming to build. Because the dynamic model of induction machines is complex due to nonlinearities of the system, it is necessary to simulate the whole system containing the machine and the controllers before building the actual system. Each new control strategy involved in such a system must be thoroughly studied by simulation and dynamic performance evaluated in detail before making a prototype. Different machines can be simulated simply by changing the model parameters. Changing the values of parameters or exploring a new concept or operating strategy can often be done more quickly in a simulation than conducting a series of experimental studies on an actual system. It is important to select a proper tool for successful and efficient design. In the development of computer programs for a stand-alone power generation system, it was realised that a versatile tool for dynamic system simulation was needed. User written program using high level language takes excessive time to implement and debug. The user has to develop his own numerical routines such

as integration algorithm for solving differential equations. Some existing simulation packages allow model to be entered in a block diagram form using pre-written blocks from a library. Development of user-written source code is unnecessary with these packages. SIMULINK is one of such powerful packages and its applicability has been demonstrated in Chapter 5. A similar package, TUTSIM, is chosen as a dynamic system simulation package for the remaining chapters in the thesis. A description of TUTSIM is given in what follows.

TUTSIM is an extremely compact software package since it is written in assembler language. It allows for the fastest possible program execution, thus reducing computation time and memory requirement. TUTSIM is a dynamic system simulation package which allows a model to be built from a library of mathematical blocks. Blocks are classified as source blocks, conditional blocks, mathematical functions, history blocks, logic blocks, special functions, z-blocks and thermodynamic property blocks. The user can develop new customised blocks using C and FORTRAN languages. One further advantage of the use of TUTSIM is its ability to link various model files together into a single model file. This allows a modular approach to modelling large systems. Individual modules, like inverter and induction machine models, can be modelled separately in a range of blocks including comments and parameters and saved as macros. These macros can be imported by other programs to simulate various simple and complex systems.

A model in TUTSIM is described by block statements that are stored in a file. A model entry consists of a sequential calling of four edit processes, namely Structure Entry, Parameter Entry, Plotblock Entry and Timing Entry. The model structure is a list of blocks, identifying the block number, type and interconnections, which is entered from the keyboard, block by block. Each block statement occupies a line which contains the block number, block name and input connections from other blocks. A block is usually entered first by the block number, followed by the block name and finally input connection from other blocks. Unlike the graphical representation of a block in SIMULINK, blocks are not visualised in TUTSIM. The user may view the model parameters and connections by the list command. Blocks are listed in a compact format

as:

PARAMETER; BLOCK NUMBER; TYPE; INPUT CONNECTIONS...

The number of inputs to a block varies from block to block. The maximum number of inputs for a block is forty. Inputs can be positive or negative. There are no input connections for the source blocks. All the blocks have only one output. The maximum number of blocks in a program is 999 which is more than enough for modelling a complex system like the one being investigated in the thesis. For many types of blocks, parameters need to be entered after the block diagram structure has been entered. If parameter entry is missing, the parameter will be set to default value of zero. After the model parameters have been entered, TUTSIM will request the Plotblock information which specifies which block outputs are to be plotted graphically on screen and the scales for the plots. Finally, timing information is required to be entered as step size and total simulation time. The choice of time step is crucial as numerical accuracy and simulation stability are determined by the time step size. Errors in digital simulation are unavoidable because the number representation in a computer is discrete. Roundoff and truncation are two common sources of digital computation errors. Too large step size can cause numerical instability due to inexact integration. If time step is chosen small enough, many times smaller than the smallest time constant in the system, then the solution will be indistinguishable from a continuous solution. If the time step is too small, there is excessive number of calculations. Each calculation causes appearance of an error. The accumulated roundoff errors may become excessive. In some situations where mathematical models have time constants distributed over a wide range, which results in stiffness numerical problem, it is desirable to use an adaptive time step algorithm. If the step size is predictable, the user may use the Variable Delta Time block. Also the Gear algorithm can be used to dynamically control the step size.

TUTSIM performs error checking to ensure that a block has been entered correctly. For example, it will check if there is an input connection that is not defined or if the type of block does not exist, etc. Feedback system can result in what is known as an algebraic loop, which occurs when the output of a given block is fed back as one of the inputs.

When it occurs TUTSIM will give a warning message. Algebraic loops can be avoided by breaking the input with a block that does not have direct feedthrough of the input and also does not change the system operation. One such block is the algebraic delay block in which output is delayed just one time step. The first order lag block with a very small time constant can also be used to break algebraic loops. If the time constant is set in the same order of magnitude as the simulation time step then it becomes almost unnoticeable.

After all four edit processes of original entry have been completed, dynamic behaviour of the system is examined using time-domain simulation. Parameters can be changed while the program is running. The user can interrupt a simulation run at any time and continue the simulation after parameters have been changed. Simulation results can be graphically displayed on screen or can be printed as numerical table in the output data file for post processing, which can be in an ASCII format or in MALTAB file format. Since the transient response requires many time steps in one cycle and it generally takes several seconds to reach steady-state, simulation results will be far too verbose and involve a massive data file. TUTSIM allows the user to choose an output-interval. It should be noted that the output interval has no effect on the simulation's numerical stability, but that too large an output-interval can yield too fewer data points to interpret the results. TUTSIM has a drawback that maximum of four variables can be plotted for each simulation run, although it can show the last calculated value for any specified block on screen.

As mentioned before, MATLAB/SIMULINK is a general purpose simulation package and any of the models simulated in the remaining chapters by means of TUTSIM can be simulated using MATLAB/SIMULINK, at an expense of slower execution time. According to the author's experience, TUTSIM is at least several times faster than SIMULINK (on the same computer) since it is DOS based package.

6.4 Simulation results

The scheme of Figure 6.2.1, with VSI employing sinusoidal PWM, is investigated under

no-load conditions. Single-cage induction machine is again used for simulation. The d.c. side capacitor is of 100 μF capacitance and is assumed to be pre-charged at 50 V. Size of the capacitor is directly correlated to the required initial capacitor voltage and smaller the capacitor is, higher the initial voltage must be. Stator frequency and modulation index are taken as 49.8 Hz and 0.996, respectively, for constant speed operation at 50 Hz synchronous rotor speed. Figure 6.4.1 shows the d.c. side voltage and stator flux build-up and Figure 6.4.2 shows build-up process of both stator phase current and stator phase voltage.

The stator voltage builds up slowly and it takes about 3.5 seconds to reach steady-state. Since the slip speed is not sufficiently negative, self-excitation cannot be sustained if a load is connected to the generator terminals. In order that the generator can withstand a load, the slip speed should be increased, i.e., the stator frequency has to reduce. Next, the scheme of Figure 6.2.1 is simulated for a sequence of transients: self-excitation is initiated under no-load at 50 Hz synchronous speed at t = 0 s, a three-phase load of 600 Ω per phase is applied in a step-wise manner at t = 0.4 s, speed is reduced from 1 p.u. to 0.8 p.u. in a linear manner in time interval from 0.5 s to 0.6 s and is then brought back to 1 p.u. during time interval from 0.8 s to 0.9 s. Speed and load profiles are shown in Figure 6.4.3. The results in Figures 6.4.4 and 6.4.5 display d.c. side voltage, stator flux, stator current and stator voltage [Liao and Levi (1997)].

Stator frequency and modulation index are set to constant values of 48 Hz and 0.96, respectively, for no-load self-excitation and loaded operation at 50 Hz synchronous speed. During speed transients both stator frequency and the modulation index are varied proportionally to the speed in the same linear manner. As can be seen from Figure 6.4.4, it takes much shorter time interval for the stator voltage to build up as the slip is increased. But stator voltage attains unacceptably high value during initial self-excitation and subsequent transients leading to a stator current that exceeds rated (2.1 A rms) in all the regimes. This is the consequence of very high sensitivity of this scheme to slip and stator frequency [Leplat et al (1996), Bhadra et al (1996)], which are here not adjusted in a closed-loop manner. This indicates at the same time that closed loop control must be employed in this scheme for slip speed if stator over-voltages are to be

avoided [Liao and Levi (1997)]. The trace of stator flux shows that stator flux is kept reasonably constant during speed changes by means of V / f_s = constant control.

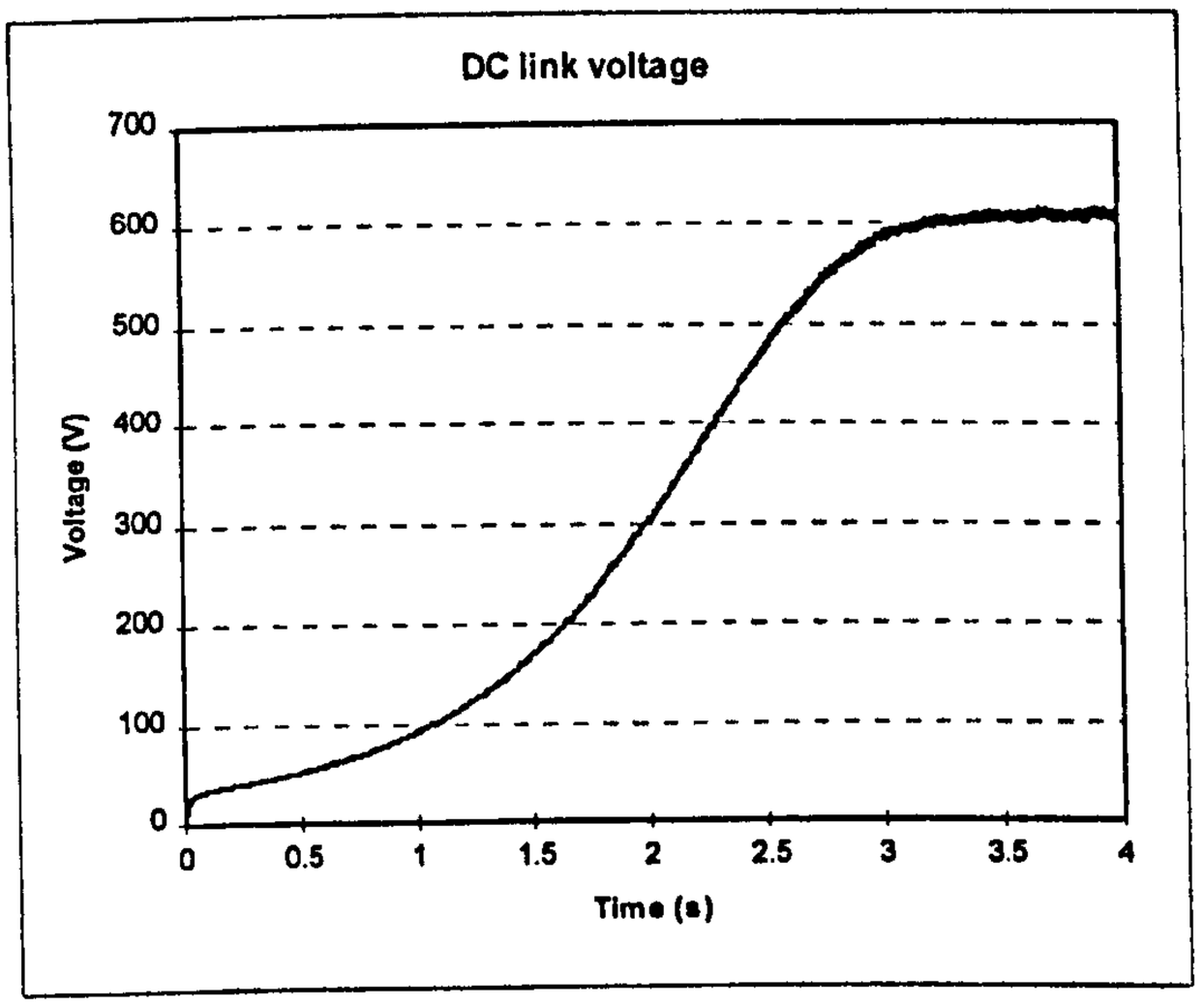

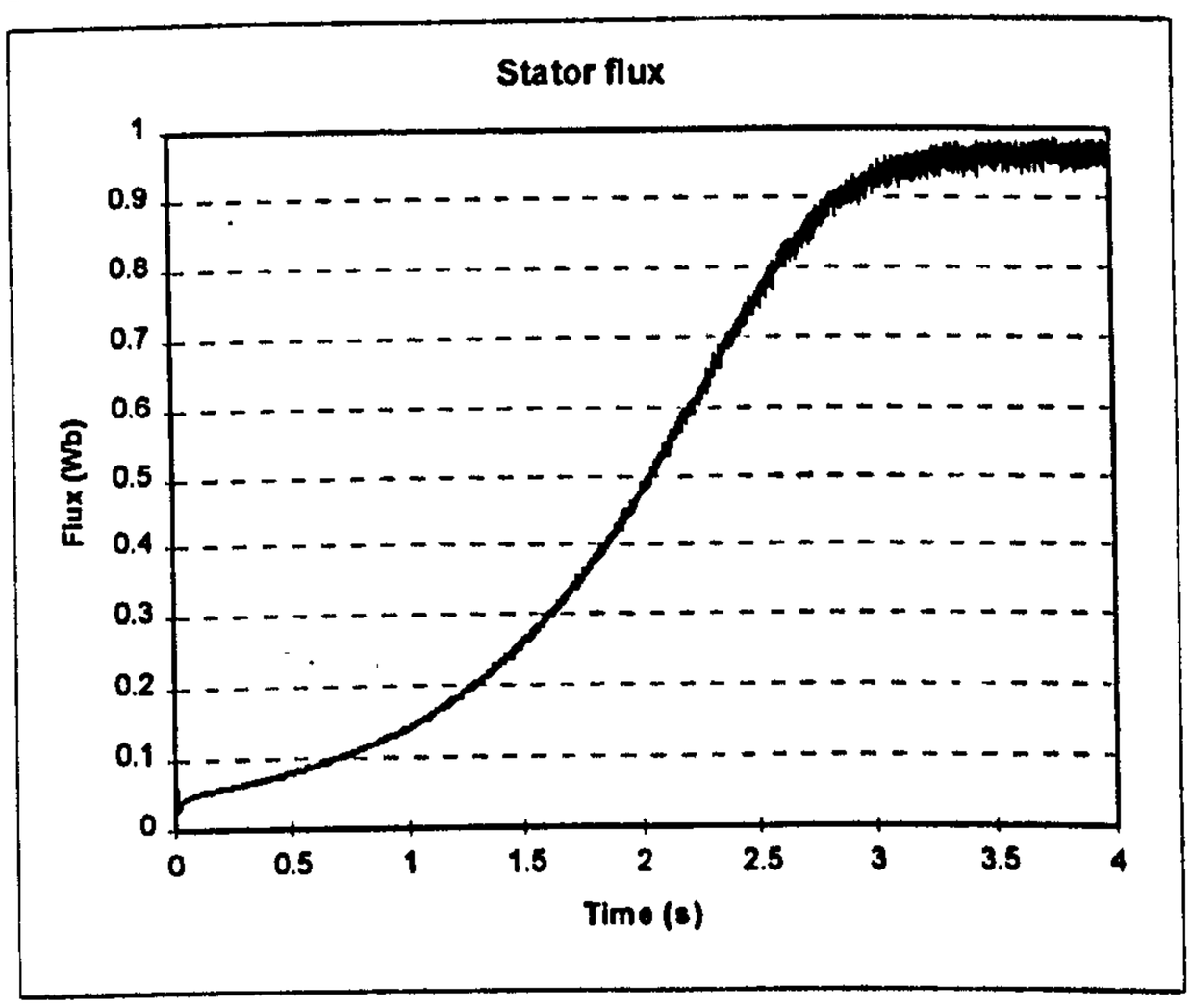

Figure 6.4.1 DC side voltage and stator flux during no-load self-excitation

Figure 6.4.6 shows the machine torque, magnetising inductance and magnetising current. Unlike the results obtained from reactive power compensator using capacitor bank, the induction generator has significant torque ripple due to the use of PWM VSI supply. Stator flux is not kept at desired constant value due to the lack of closed loop control of slip frequency. Magnetising current in the machine depends substantially on loading conditions (it drops from approximately 7 A to less than 5 A when the machine is loaded at t = 0.4 s). Consequently, magnetising inductance experiences substantial

variation as well. It is interesting to note that load application causes reduction in stator current rather than anticipated increase (again a consequence of open-loop frequency control). Thus the losses in the machine significantly reduce and effective change of torque due to load application is very small. As shown in Chapters 7 and 8, all these waveforms will be significantly different when closed-loop vector control is used instead of open loop V / f_s = constant control.

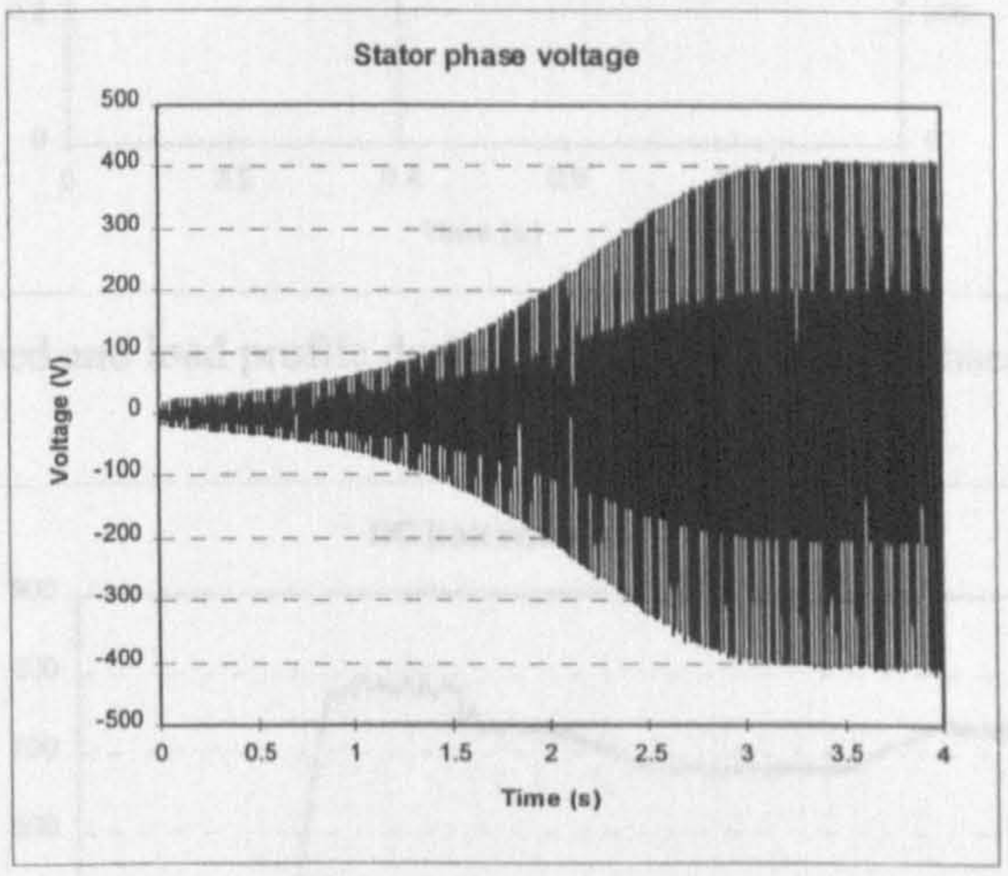

Figure 6.4.2 Voltage and current build-up during no-load self-excitation

6.5 Summary

Dynamics of self-excitation scheme based on a sinusoidal PWM VSI are studied in this Chapter. Self-excitation under no-load conditions, step application of the load and operation with variable speed are simulated for reactive power compensator comprising

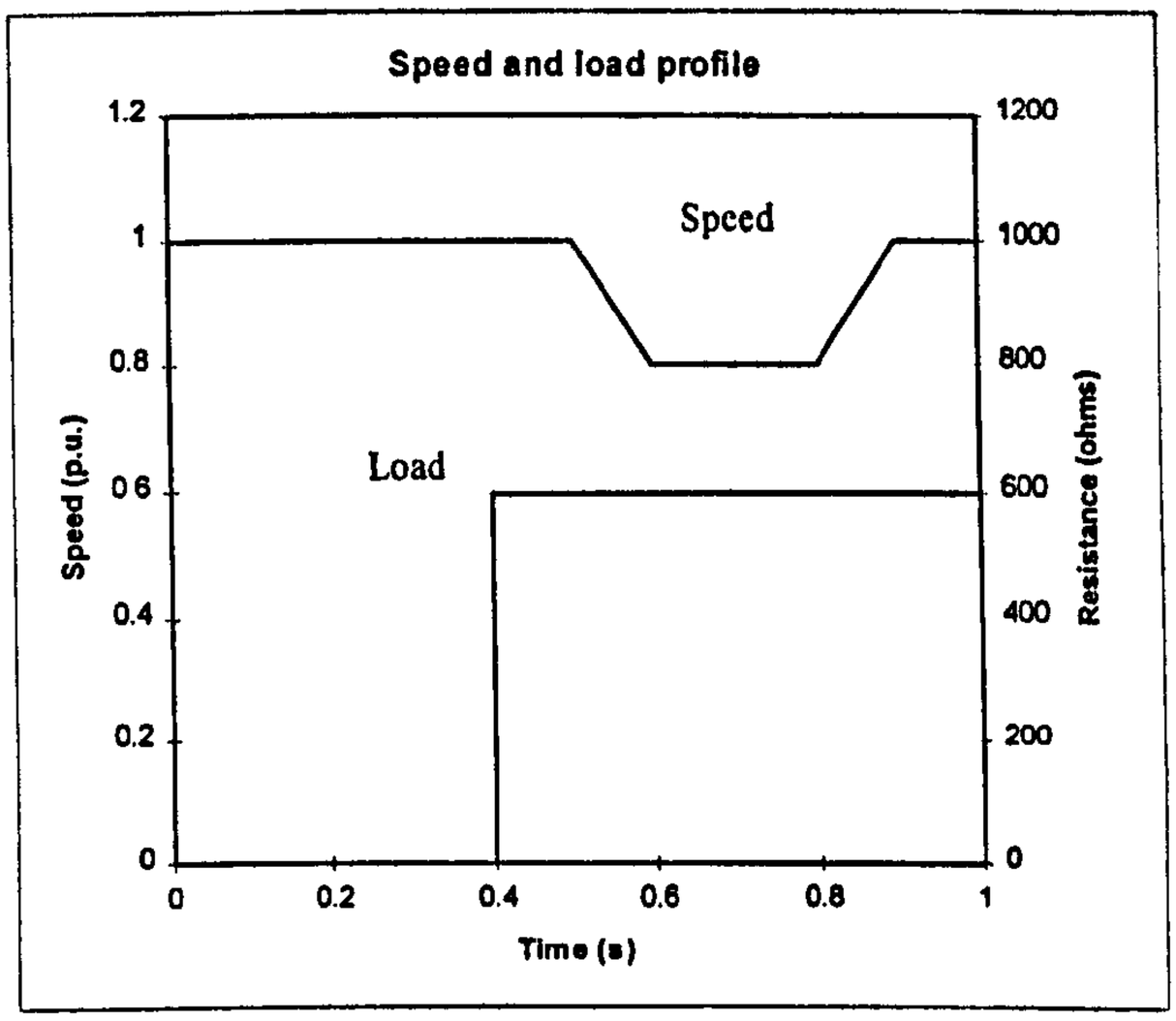

Figure 6.4.3 Speed and load profile during self-excitation and subsequent transients

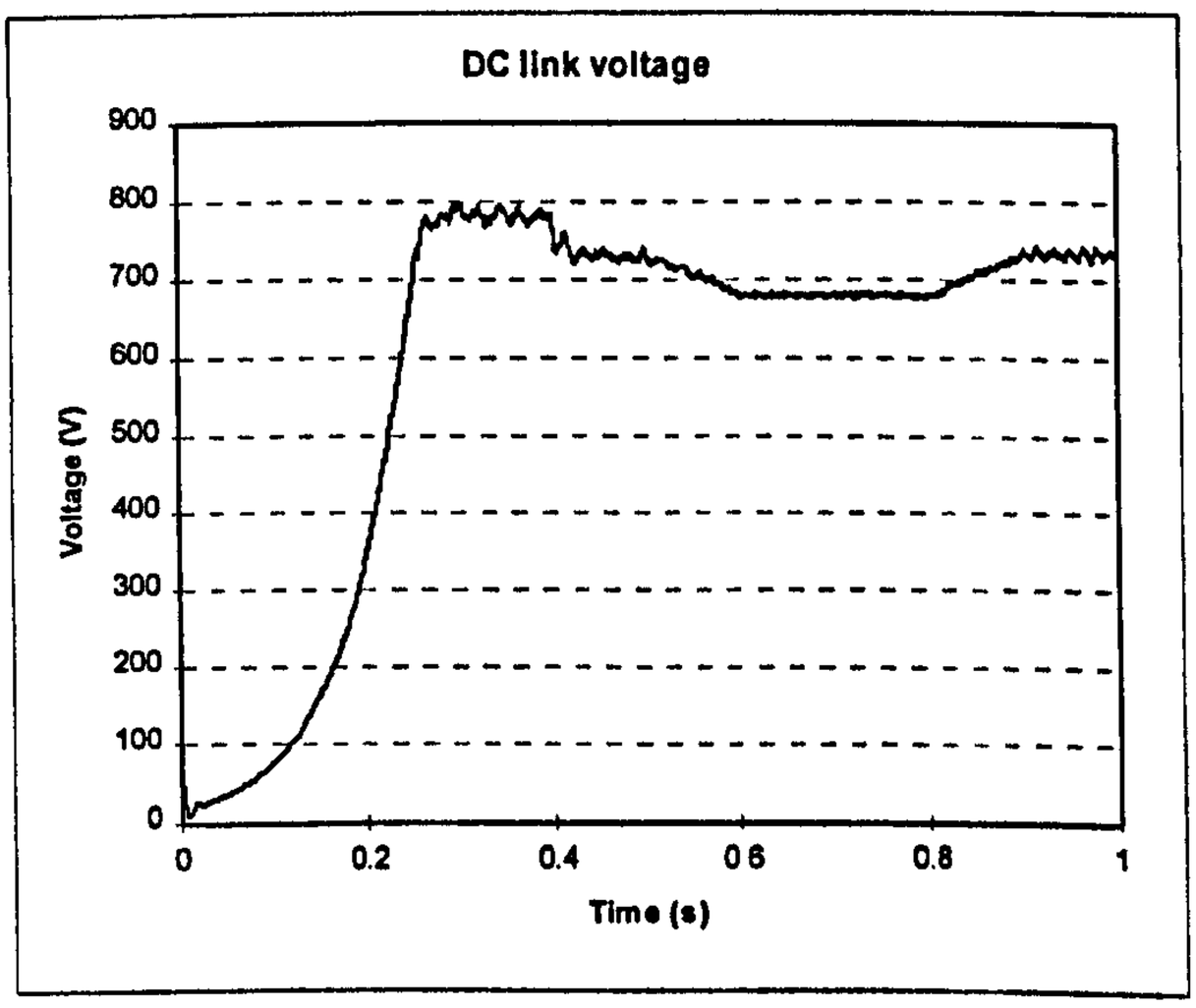

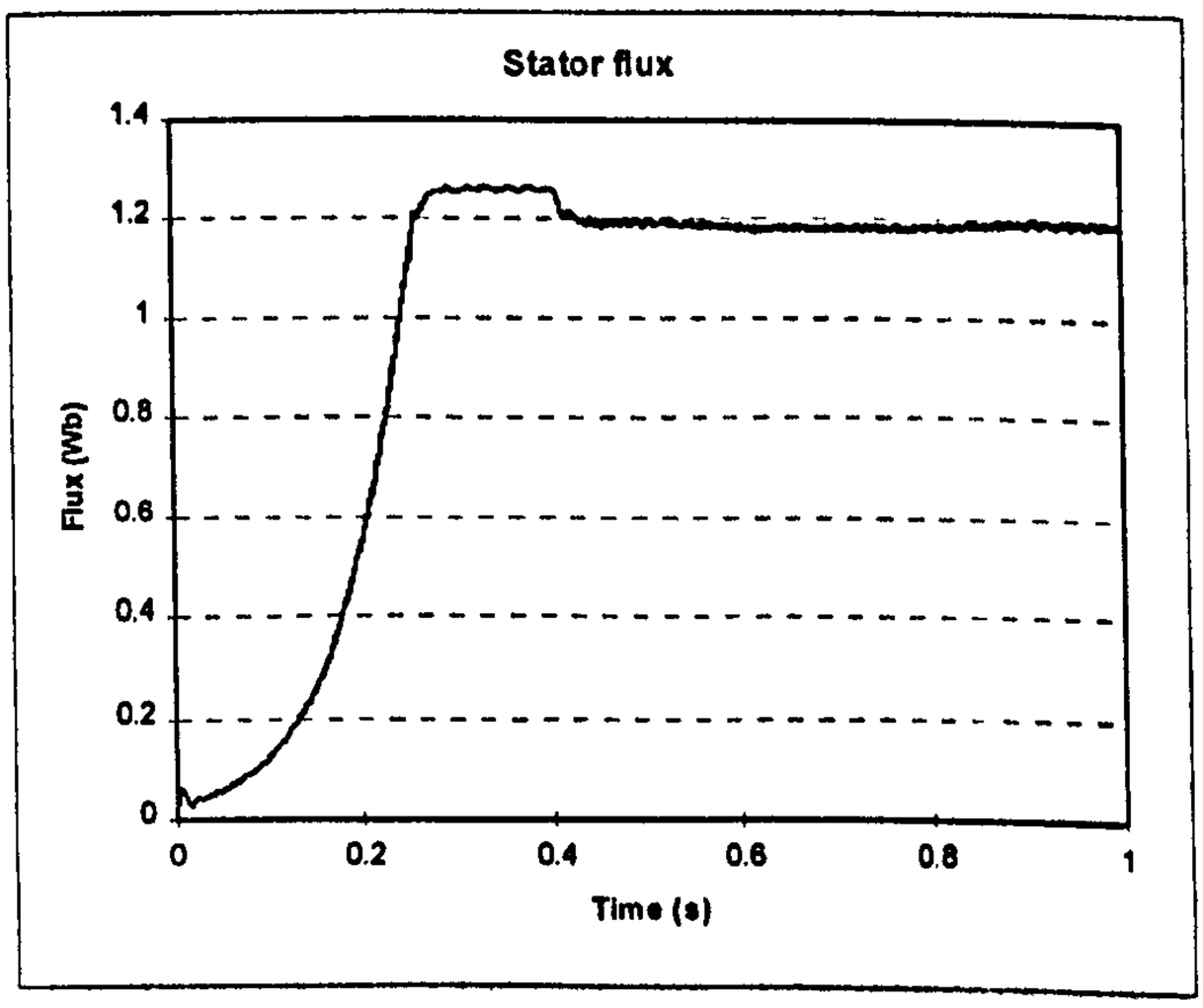

Figure 6.4.4 DC side voltage and stator flux during self-excitation and subsequent transients

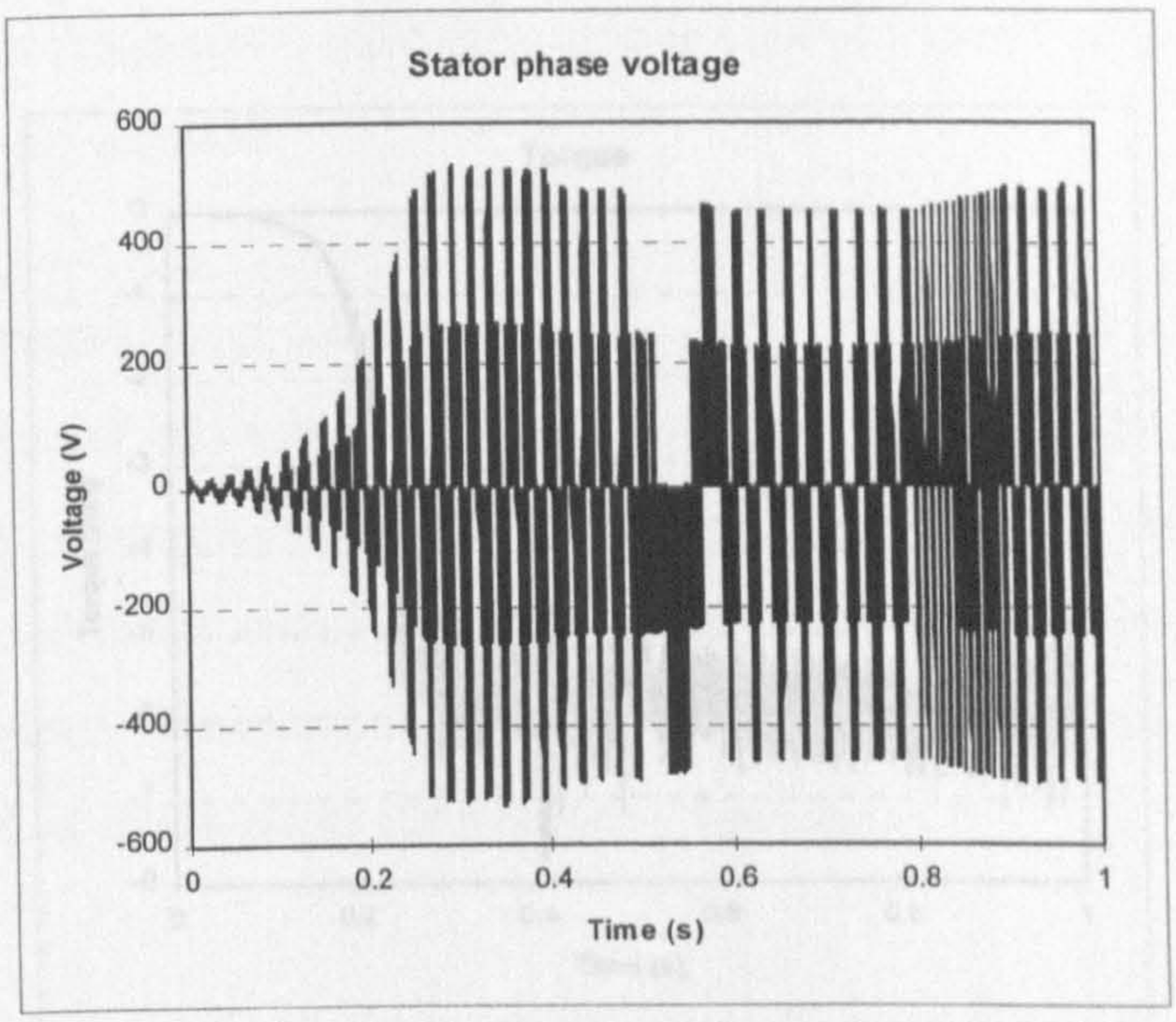

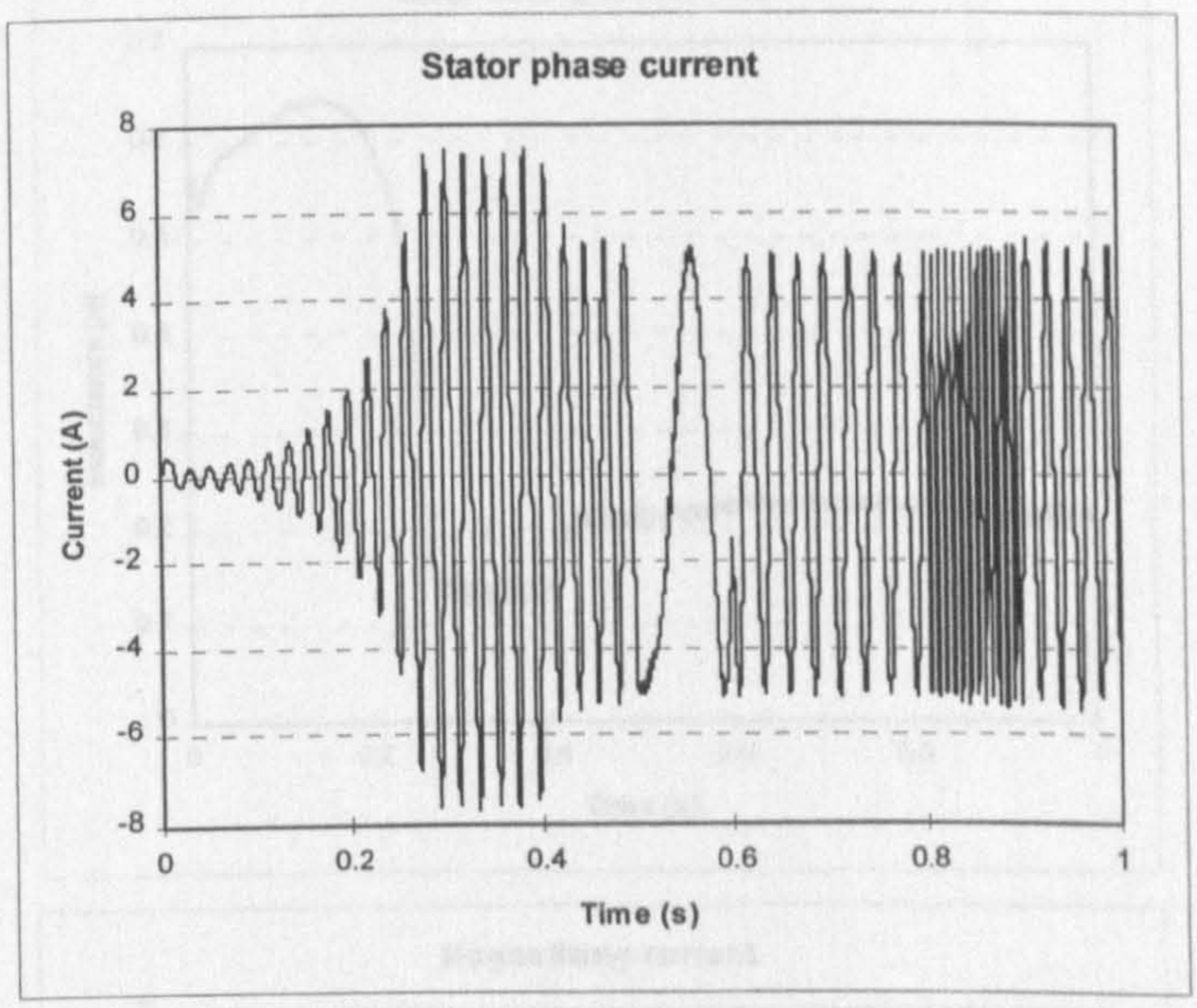

Figure 6.4.5 Stator voltage and current during self-excitation and subsequent transients

voltage source inverter with sinusoidal PWM and V / f_s = constant control. When compared with reactive power compensator comprising three-phase capacitor bank, the scheme with sinusoidal PWM inverter requires relatively higher capacitor value and capacitor must be pre-charged for the self-excitation to take place. But only one capacitor is required instead of banks of wide range capacitors in the case of compensator using switched capacitor banks. Stator flux in the scheme with sinusoidal PWM and V / f_s = constant control is reasonably constant during speed transients but is very sensitive to load application. Furthermore, this scheme exhibits extremely high

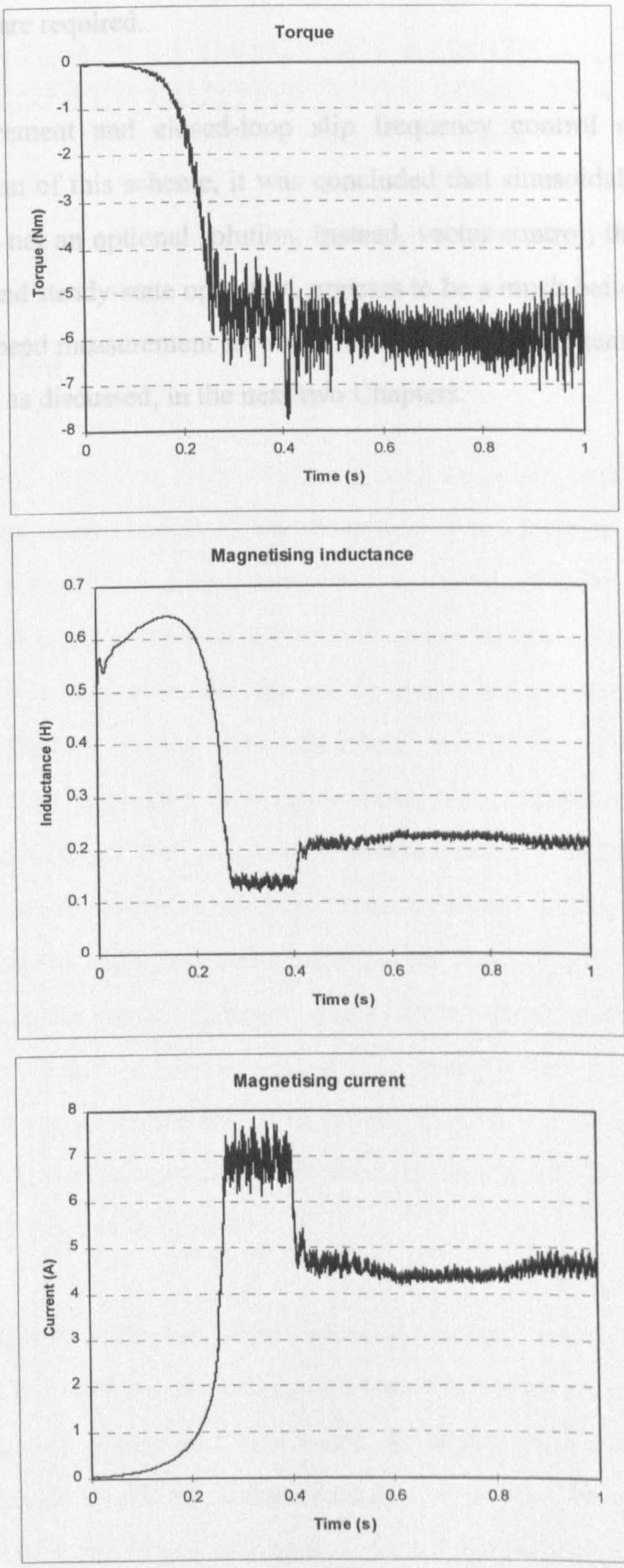

Figure 6.4.6 Machine torque, magnetising inductance and magnetising current during self-excitation and subsequent transients

sensitivity to stator frequency variation so that in practice speed measurement and slip frequency control are required.

As speed measurement and closed-loop slip frequency control are necessary for successful operation of this scheme, it was concluded that sinusoidal PWM method of inverter control is not an optional solution. Instead, vector control, that enables control of both dynamic and steady-state operation, appears to be a much better solution. Vector control requires speed measurement as well. However, control system structure is much more complicated as discussed, in the next two Chapters.

Chapter 7

VECTOR, STATOR FLUX ORIENTED, CONTROL OF A PWM VSI REACTIVE POWER COMPENSATOR FOR A STAND-ALONE INDUCTION GENERATOR

7.1 Introduction

Utilisation of scalar controlled PWM VSI as a reactive power compensator has been described in the previous chapter. If an attempt is to be made to operate induction generator with constant flux during transients, including variable speed operation, capacitor banks and scalar controlled PWM VSI cannot be used. As the static reactive power compensator is intended to provide self-excitation and constant flux operation of the induction generator during both transient and steady-state operation, the compensator has to be controlled in an appropriate, more complex manner. Currently available control techniques, that enable independent control of induction machine flux and torque and that are widely applied in induction motor drives, are usually called vector control methods. Field oriented control (stator flux, air gap flux and rotor flux oriented control) enables the development of high performance variable speed induction motor drives. The theory of vector control is nowadays well established as far as induction motor drives are concerned [Vas (1990), Boldea and Nasar (1992), Novotny and Lipo (1996)]. However, applications of vector control methods in conjunction with induction generator are relatively new.

Vector control relies on utilisation of the induction machine model, which assumes that all parameters in the machine are constant. Parameter variations caused by magnetic saturation, temperature change and iron losses are neglected. Since parameters in the machine vary, detuned operation of the machine will occur. The amount of detuning depends on operating conditions and applied vector control schemes. Compensation schemes for detuned operation of induction machine rely on either modern control

techniques or improved induction machine models.

For a stand-alone induction generator, vector control technique applied to the control of PWM voltage source inverter enables an independent control of the active power and reactive power flow in the induction machine. The methods applied so far are the stator flux oriented control and the rotor flux oriented control. Orientation of the reference frame along stator flux vector has been discussed in [Silva and Lyra (1993), Lyra et al (1995), John et al (1995)]. Schemes with orientation along rotor flux vector are found in [Jacobina et al (1996), Colliez (1997)]. When vector control is applied, PWM VSI static reactive power compensator is current controlled, with current control being executed either in stationary reference frame [Silva and Lyra (1993), Lyra et al (1995)] or in rotational reference frame [Jacobina et al (1996)]. Both direct and indirect methods are used for flux space vector position calculation. Regardless of the method of current control employed and regardless of the flux space vector along which orientation is performed, information on instantaneous flux space vector spatial position is crucial for correct operation of the system. Methods used in the past include stator flux position estimation from measured stator voltages and currents [Silva and Lyra (1993)] and rotor flux position estimation using indirect feed-forward approach [Jacobina et al (1996)].

This chapter deals with stator flux oriented control of a PWM voltage source inverter which provides decoupled control of the active and reactive power for a variable speed stand-alone induction generator. Principles of stator flux oriented control as applied in induction motor drives, are at first reviewed. Detailed mathematical modelling of the components of the induction generator system under consideration is described next. The saturated induction generator is modelled in a synchronous reference frame, with stator current and stator flux d-q axis components as state-space variables. Hysteresis current control technique is adopted for the control of the PWM VSI compensator with current control executed in stationary reference frame. Estimation of stator flux is performed using measured generator stator voltages and stator currents. Simulation results of dynamics of self-excitation process under no-load conditions and subsequent transients for step load application and speed variations below and above base speed are presented.

7.2 Principles of stator flux oriented control as applied in induction motor drives

Rotor flux oriented control of induction machines used to be the natural choice for high performance drives, due to relative simplicity of the control scheme compared to stator and air gap flux orientation. The need for realisation of rather complex decoupling circuit [Erdman and Hoft (1990), Ho and Sen (1988), Vas (1990)] excluded in the past stator and air gap flux oriented control from practical implementations. However, these orientation methods are gaining recently more and more attention, due to rapid advancement in development of high-speed low-cost microprocessors. In particular, stator flux oriented control has been recently studied in detail and successfully applied in conjunction with current fed induction machines [Xu et al (1988a), Xu et al (1988b)].

As a mean for dealing with different operating conditions in induction motor drives in the best possible way, the universal field oriented (UFO) controller has been suggested [De Doncker and Novotny (1988)]. It is capable of operating with orientation along any of the three flux space vectors in the machine in either direct or indirect mode. If the air gap flux is sensed, direct orientation along air gap flux becomes advantageous, compared to stator or rotor flux oriented control [De Doncker et al (1990)]. For such an operation UFO controller can be applied in conjunction with induction machine with tapped stator windings, which enable reliable flux measurement [De Doncker and Profumo (1989)]. Indirect control is performed in low speed range, while direct control takes place for frequencies above certain value.

The principles of stator flux oriented control and the decoupling circuit, necessary for realisation of stator flux oriented control, are derived from constant parameter induction machine model, which can be given in an arbitrary reference frame in terms of space vectors as (Section 3.2 of Chapter 3)

$$\underline{v}_s = R_s \underline{i}_s + \frac{d\underline{\psi}_s}{dt} + j\omega_a \underline{\psi}_s \qquad (3.2\text{-}1)$$

$$0 = R_r \underline{i}_r + \frac{d\underline{\psi}_r}{dt} + j(\omega_a - \omega)\underline{\psi}_r \qquad (3.2\text{-}2)$$

$$\underline{\psi}_s = L_s \underline{i}_s + L_m \underline{i}_r \qquad \underline{\psi}_r = L_r \underline{i}_r + L_m \underline{i}_s \tag{3.2-3}$$

Space vectors, present in equations (3.2-1) - (3.2-3), are defined as

$$\underline{\psi}_s = \psi_s e^{j(\phi_s - \theta_s)} \qquad \underline{\psi}_r = \psi_r e^{j(\phi_r - \theta_r)} \qquad \underline{i}_r = i_r e^{j(\varepsilon_r - \theta_s)} \tag{7.2-1}$$

$$\underline{\psi}_s^s = \psi_s e^{j\phi_s} \qquad \underline{\psi}_r^s = \psi_r e^{j\phi_r} \qquad \underline{i}_r^s = i_r e^{j\varepsilon_r} \tag{7.2-2}$$

where superscript "*s*" identifies space vectors in stationary reference frame and the inductances present in (3.2-3) are stator, rotor and magnetising inductance. Angles $\varepsilon_s, \varepsilon_r, \phi_s, \phi_r$ represent instantaneous angular positions of the stator current, rotor current, stator flux and rotor flux space vectors, respectively, with respect to the stationary stator phase 'a' magnetic axis. Space vectors are composed of real (d-axis) and imaginary (q-axis) parts (components). Correlation between space vectors in arbitrary reference frame, space vectors in stationary reference frame and phase variables is established through the following equations:

$$\underline{v}_s = \underline{v}_s^s e^{-j\theta_s} \tag{7.2-3}$$

$$\underline{i}_s = \underline{i}_s^s e^{-j\theta_s} \tag{7.2-4}$$

$$\underline{v}_s^s = \frac{2}{3}(v_a + \underline{a} v_b + \underline{a}^2 v_c) \tag{7.2-5}$$

$$\underline{i}_s^s = \frac{2}{3}(i_a + \underline{a} i_b + \underline{a}^2 i_c) \tag{7.2-6}$$

where $\underline{a} = e^{j2\pi/3}$.

Electromagnetic torque is expressed in terms of space vectors as

$$T_e = \frac{3}{2} P \operatorname{Im}\{\underline{i}_s \underline{\psi}_s^*\} \tag{7.2-7}$$

where * denotes complex conjugate.

The model given with equations (3.2-1) - (3.2-3) and (7.2-1) - (7.2-7) is utilised further for derivation of stator flux oriented control principles. Current fed machine will be

discussed only. The reason for this is that the resulting control system is complicated enough even for the current fed machine and therefore voltage fed case, which would have asked for even more complex structure of the control system, is of no practical value.

Stator flux space vector is defined in stationary reference frame as

$$\underline{\psi}_s^s = \psi_{\alpha s} + j\psi_{\beta s} = \psi_s e^{j\phi_s} \tag{7.2-8}$$

If the common reference frame is selected as fixed to the stator flux space vector, then the following holds true:

$$\theta_s = \phi_s \qquad \theta_r = \phi_s - \theta \qquad \omega_a = \omega_s \tag{7.2-9}$$

where $\omega_s = d\phi_s / dt$ is the angular velocity of the stator flux space vector. Stator flux space vector, given in an arbitrary frame of reference as

$$\underline{\psi}_s = \psi_{ds} + j\psi_{qs} = \psi_s e^{j(\phi_s - \theta_s)} \tag{7.2-10}$$

becomes real if the d-axis of the common reference frame is fixed to the stator flux space vector

$$\underline{\psi}_s = \psi_{ds} = \psi_s \tag{7.2-11}$$

i.e., stator flux oriented control results if

$$\psi_{qs} = 0 \qquad \frac{d\psi_{qs}}{dt} = 0 \qquad \omega_a = \omega_s \tag{7.2-12}$$

Stator current space vector, given with (7.2-4) in the stationary reference frame, becomes in the stator flux oriented reference frame equal to

$$\underline{i}_s = i_{ds} + j i_{qs} = i_s e^{j(\varepsilon_s - \phi_s)} \tag{7.2-13}$$

Torque equation (7.2-7) yields

$$T_e = \frac{3}{2} P \psi_{ds} i_{qs} \tag{7.2-14}$$

Substitution of (7.2-9), (7.2-11) and (7.2-12) into (3.2-1) and (3.2-2) leads to, taking into account that $i_{dr} = (\psi_{ds} - L_s i_{ds}) / L_m$ and $i_{qr} = -i_{qs}(L_s / L_m)$, the following model in the reference frame fixed to stator flux space vector:

$$v_{ds} = R_s i_{ds} + \frac{d\psi_{ds}}{dt} \tag{7.2-15}$$

$$v_{qs} = R_s i_{qs} + \omega_s \psi_{ds} \tag{7.2-16}$$

$$\psi_{ds} + T_r \frac{d\psi_{ds}}{dt} = L_s i_{ds} + T_r (L_s - \frac{L_m^2}{L_r})[\frac{di_{ds}}{dt} - (\omega_s - \omega) i_{qs}] \tag{7.2-17}$$

$$L_s i_{qs} = (\omega_s - \omega) T_r \psi_{ds} - T_r (L_s - \frac{L_m^2}{L_r})[\frac{di_{qs}}{dt} + (\omega_s - \omega) i_{ds}] \tag{7.2-18}$$

If the leakage coefficient is introduced as $\sigma = 1 - L_m^2 / (L_s L_r)$, equations (7.2-17) - (7.2-18) can be expressed as

$$\psi_{ds} + T_r \frac{d\psi_{ds}}{dt} = L_s (i_{ds} + \sigma T_r \frac{di_{ds}}{dt}) - \sigma L_s T_r (\omega_s - \omega) i_{qs} \tag{7.2-19}$$

$$i_{qs} + \sigma T_r \frac{di_{qs}}{dt} = \frac{T_r}{L_s} (\omega_s - \omega)(\psi_{ds} - \sigma L_s i_{ds}) \tag{7.2-20}$$

while torque equation remains the same,

$$T_e = \frac{3}{2} P \psi_{ds} i_{qs} \tag{7.2-14}$$

The equations (7.2-14), (7.2-19) and (7.2-20) fully describe current fed stator flux oriented induction machine. As can be seen from (7.2-19) and (7.2-20), there are cross-coupling terms present in both equations. For example, if the stator d-axis current is held constant in order to achieve constant stator flux operation, any change in stator q-axis current will affect the level of flux. If the decoupled stator flux and torque control is to be achieved, it is necessary to decouple the equations by introducing decoupling circuit. This fact presents the principle shortcoming of the stator flux oriented control and explains why rotor flux oriented control is usually preferred.

If the induction machine is fed from voltage source, then apart from (7.2-19) and (7.2-20) equations (7.2-15) and (7.2-16) have to be considered as well. In order to realise decoupled flux and torque control with voltage fed machine, two decoupling circuits are needed - the first one for decoupling equations (7.2-19) and (7.2-20) and the second one for decoupling equations (7.2-15) and (7.2-16). Therefore all the existing realisations of stator flux oriented control utilise current fed induction machine.

Equations (7.2-19) and (7.2-20) can be easily rearranged to the following form ($\psi_s = \psi_{ds}, \omega_{sl} = \omega_s - \omega$):

$$i_{qs} + \sigma T_r \frac{di_{qs}}{dt} = \omega_{sl}\left(\frac{T_r \psi_s}{L_s} - \sigma T_r i_{ds}\right) \tag{7.2-21}$$

$$i_{ds} + \sigma T_r \frac{di_{ds}}{dt} = \frac{\psi_s}{L_s} + \left(\frac{T_r}{L_s}\right)\frac{d\psi_s}{dt} + \sigma T_r \omega_{sl} i_{qs} \tag{7.2-22}$$

which gives decoupler equations

$$i_{ds}^* = \frac{1}{1 + s\sigma T_r^*}\left[(1 + sT_r^*)\frac{1}{L_s^*}\psi_s^* + \sigma T_r^* \omega_{sl}^* i_{qs}^*\right] \tag{7.2-23}$$

$$\omega_{sl}^* = \frac{(1 + s\sigma T_r^*) i_{qs}^*}{\psi_s^* T_r^* / L_s^* - \sigma T_r^* i_{ds}^*} \tag{7.2-24}$$

where $s \equiv d/dt$. The decoupler structure is depicted in Figure 7.2.1, where indirect stator flux oriented induction machine is shown. Alternatively, if direct vector control with

orientation along stator flux is applied, the overall control scheme becomes as shown in Figure 7.2.2. Comparison of the two structures reveals that the only difference is in the presence of flux controller in direct orientation method and in the way in which the angular position of the stator flux is obtained.

Stator q-axis current command and torque command are, from equation (7.2-14), correlated with the following expression:

$$i_{qs}^{*} = \frac{T_e^{*}}{(3P/2)\psi_s^{*}} \tag{7.2-25}$$

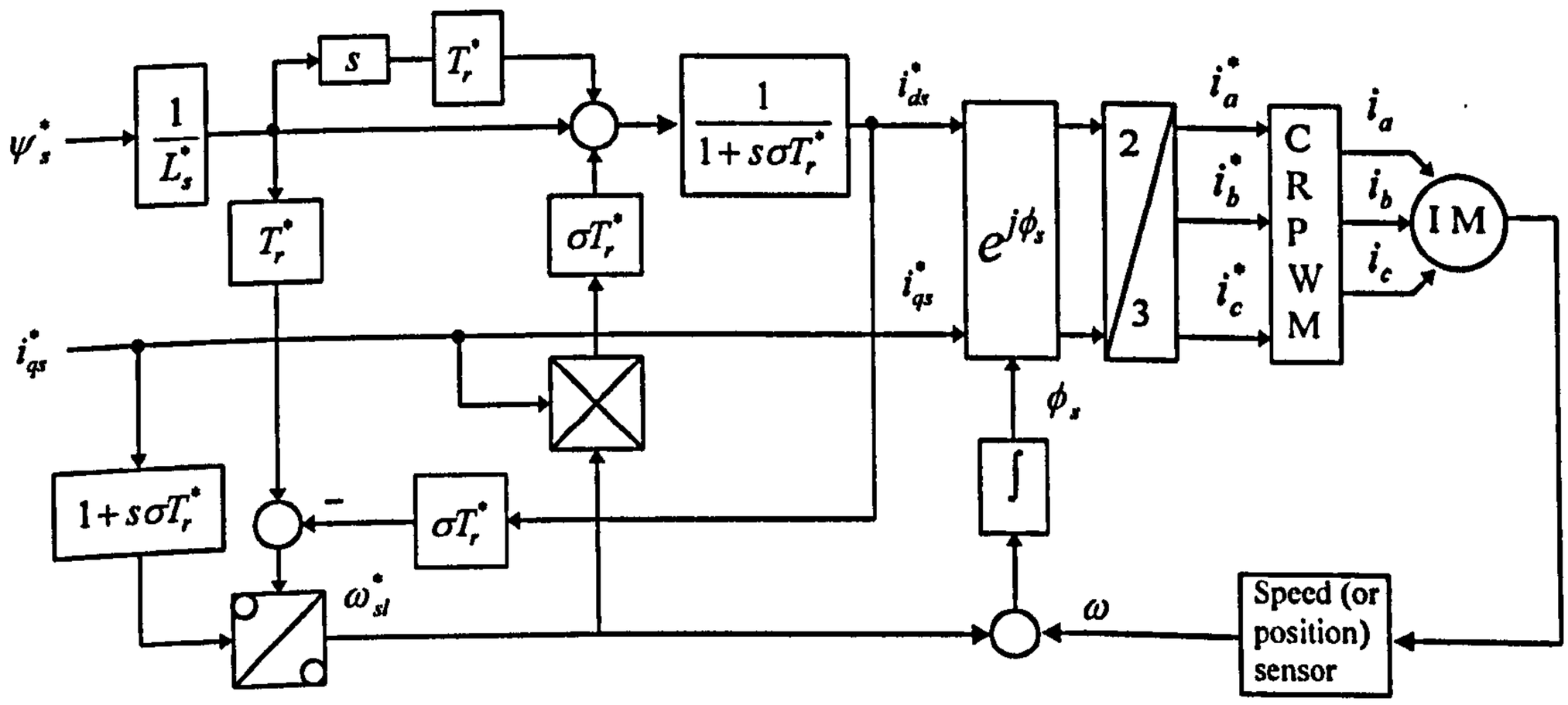

Figure 7.2.1 Indirect stator flux oriented current-fed induction machine with constant parameter decoupling circuit

Thus the q-axis current command is calculated in Figures 7.2.1 and 7.2.2 by utilising the equation (7.2-25) with T_e^* being the output of the speed controller (not shown in Figures 7.2.1 and 7.2.2). If the drive is aimed for constant flux operation only, equation (7.2-25) means simple scaling of commanded torque with a constant.

Figures 7.2.1-7.2.2 clearly indicate the shortcomings of the stator flux oriented control. Even for a current fed machine a decoupling circuit of considerable complexity is needed. This is in heavy contrast with very simple structure of indirect rotor flux oriented current fed induction machine. However, modern DSPs and microprocessors

can easily handle the added complexity of the stator flux oriented control, so that nowadays realisation does not present too much of a difficulty.

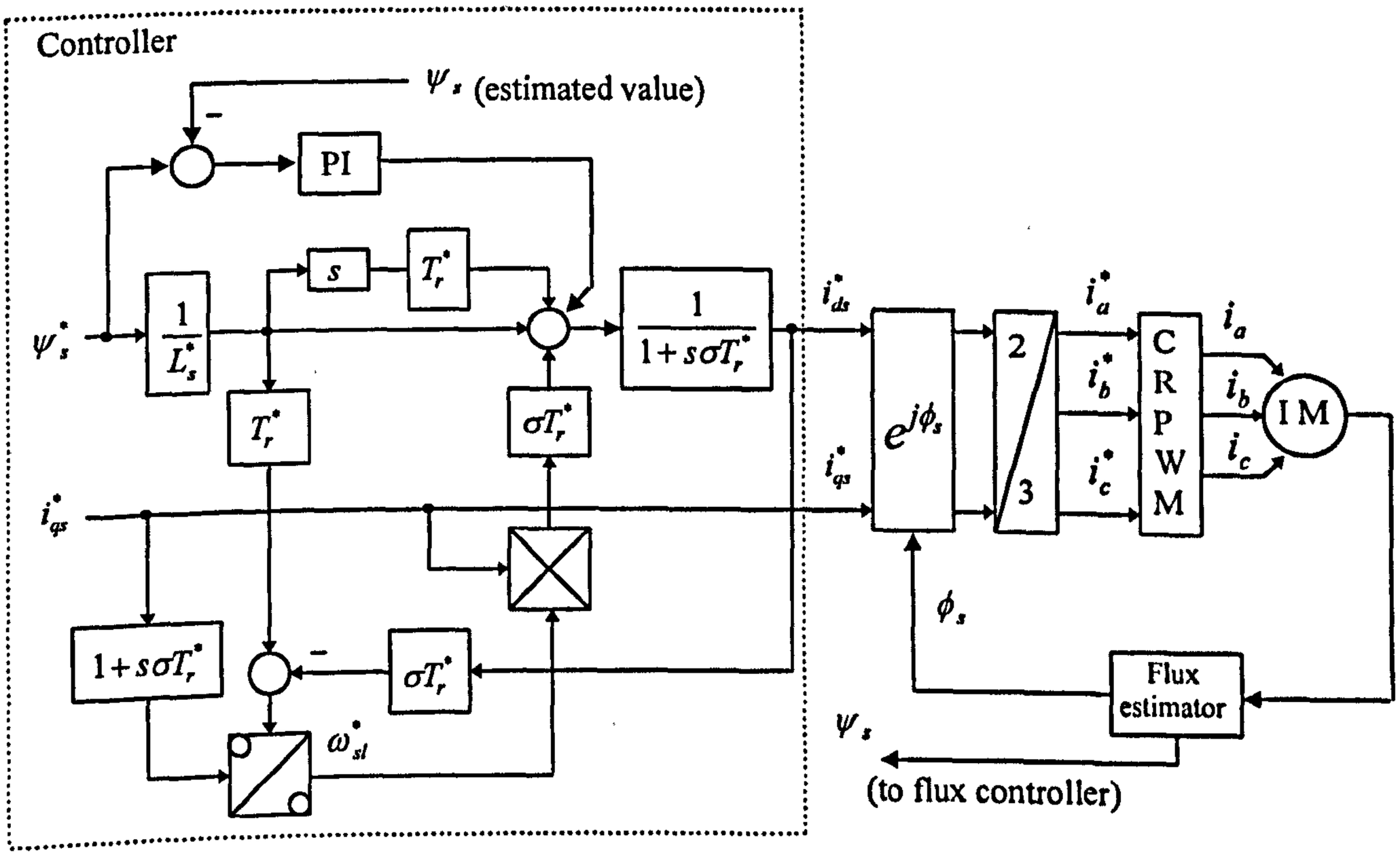

Figure 7.2.2 Direct stator flux oriented current-fed induction machine with constant parameter decoupling circuit

7.3 Current control of a PWM voltage source inverter

Explanation of stator flux oriented control in the previous sub-section assumes that the machine is current fed. Hence the PWM voltage source inverter has to be operated as current controlled source. Principles of current control of a PWM VSI are the same, regardless of whether the inverter is used as supply for a motor drive or as a reactive power compensator for an induction generator. The current controlled PWM voltage source inverter as a reactive power source enables very fast dynamic current response which makes possible use of the vector control technique to control the excitation of the induction generator. Various current control techniques exist nowadays.

All the current control techniques essentially belong to one of two major groups. The first group encompasses all the current control methods that operate in the stationary

reference frame while the second group includes current control techniques with current controllers operating in the rotational frame of reference. If the current control of an induction machine is performed in rotational reference frame, decoupling of stator voltage equations substitutes local current feedback loops in stationary reference frame which suppress influence of stator voltage equations [Harashima et al (1985)].

Current control in stationary reference frame is usually implemented in an analog fashion. The two most common alternatives are hysteresis current controller [McMurray (1984), Lorenz and Novotny (1988), Gaio et al (1988)] and ramp-comparison controllers [Lorenz and Novotny (1988), Gaio et al (1988), Andrieux and Mazenc (1985), Brod and Novotny (1985)]. Approaches with only two controllers in α, β stationary frame of reference are possible. The most pronounced shortcoming of the hysteresis current control is the variable inverter switching frequency over a period of output voltage. Maximum current error equals double the hysteresis band if three independent controllers are applied and neutral is not connected [Brod and Novotny (1985)].

Current control by ramp-comparison controllers, where current error serves as modulating signal which is compared to the triangular wave, leads to deviation of amplitude and phase of phase currents with respect to commanded values and some compensation has to be introduced, the common choice being a PI compensator [Brod and Novotny (1985)]. Another difficulty arises from a possibility that multiple crossing of the carrier may occur if the frequency of the current error becomes greater than the carrier frequency. This can be overcome by adding hysteresis to the controller. The advantage of the ramp-comparison current control with respect to hysteresis current control is fixed and constant inverter switching frequency.

Current control in stationary reference frame asks that current controllers process alternating signals which can be of a large frequency range. Furthermore, controller characteristics in steady-state depend on the operating frequency and machine impedance. These shortcomings can be partially but not completely eliminated by different modifications of the basic current control principles.

At low operating speeds the induced rotational electromotive force in the machine is small and current control enables very good tracking between reference and actual currents, with respect to both amplitude and phase. However at high speeds, due to limited voltage capability of the inverter and finite inverter switching frequency, tracking worsens and an error is met in both amplitude and phase of actual currents compared to reference currents. This feature become very pronounced in the field-weakening region where the inverter operates in the voltage limit. The problem may be solved by removing the current controllers from stationary reference frame into the rotational reference. The outputs of the current controllers then become voltage references in rotational reference frame. If the inverter switching frequency is high enough, decoupling circuit for stator dynamics is usually omitted and the machine is treated as being current fed. In the field-wakening region the machine is essentially fed with square-wave voltages and here the concept of current feeding has to be abandoned. Decoupling circuit is included in the control system and the machine is treated as being fed from a voltage source. The same concept of voltage feeding has to be applied in the base speed range as well if the switching frequency of the inverter is low, this being the case with thyrister inverter that is utilised in conjunction with vector controlled high power induction motors.

Current control in rotational reference frame is well suited to fully digital realisation. The main advantage of this method of current control is that current controllers (most frequently of PI type) process d.c. signals [Lorenz and Novotny (1988), Schauder and Caddy (1982), Rowan and Kerkman (1986)]. As the current control is performed in rotational reference frame, measured currents have to be transformed from stationary to rotational reference frame. When current control in rotational reference frame is applied, different PWM methods may be utilised for creation of the desired voltages at machine terminals. For example, sinusoidal PWM may be selected or voltage space vector modulation may be chosen [Handley and Boys (1990)]. As a separate sub-group, predictive methods of stator current space vector control may be identified. The method described in [Brod and Novotny (1985)] calculates the required voltage space vector in such a way that the current vector error is kept within prescribed boundaries at all times. State of the inverter does not change as long as it is predicted that the current vector

error will remain within defined range. This approach enables minimisation of the inverter switching frequency. The required voltage space vector is created by means of voltage space vector modulation technique, utilising the two neighbouring voltage vectors and the zero voltage vector.

Predictive controller developed in [Kohlmeier and Schroder (1986)] relies on so-called intelligent application of zero voltage space vector but has the drawback as it requires voltage measurement. Another predictive method [Nabae et al (1986)], determines required voltage space vector from positions of the current vector error and counter electromotive force vector. These positions are calculated utilising the current vector error. The method enables maximisation of the speed of response during transients and minimisation of current harmonic content in steady-states. It is independent of machine loading, mean switching frequency is constant and current harmonic content is significantly improved compared to hysteresis current control. An observer may be applied as well for voltage vector calculation [Mayer and Pfaff (1985)], this approach enables very good tracking between reference and actual currents as a predictive feature is included in such a way that influence of time delay needed for processing is eliminated. The predictive controller developed in [Holtz and Stadtfeld (1985)] predicts future trajectory of the current space vector as a function of possible inverter states. The state which minimises switching frequency, while keeping the current vector within prescribed boundaries, is selected as optimal. Double prediction is suggested as a way of eliminating the effect of processing time delay. It should be noted that all the predictive methods significantly complicate the overall control system as numerous additional calculations are required.

Other current control techniques for PWM VSI have recently been introduced [Kazmierkowski (1994)], namely, neural network based current control and fuzzy logic based current control.

Hysteresis current control method is very simple for analog implementation and tends to be the most viable option although the frequency of the inverter varies. In what follows, hysteresis current control by means of three independent current controllers is utilised.

Figure 7.3.1 illustrates the basic concept of this type of current control. This method compares the actual machine current with the reference current signal. The hysteresis comparator outputs the logic signals to gates of the upper or lower inverter switching device. If the current is outside the hysteresis band, appropriate switching of the inverter leg takes place in order to restore the current within the current band limits. The hysteresis band determines the permitted deviation of the actual phase current from the reference current. Standard lockout circuitry is normally incorporated to allow for inverter switch recovery time and thus avoid short circuit across the d.c. link. Actual currents are allowed to deviate from their reference values for the fixed value of hysteresis band. The discrepancy between actual and reference currents will vary in time and will be either positive or negative. The hysteresis controller limits the current error to twice the hysteresis band. The values of the hysteresis band are the same for both positive and negative variation. The state of the appropriate leg of the inverter changes once when the difference between actual and reference current exceeds hysteresis band. Suppose that upper switch in phase *a*, S1, is closed, while the lower switch, S2, is open. This state will be preserved as long as the current error in phase *a*, Δi_a, is within hysteresis band. When the actual current in phase *a* becomes greater than the reference value plus hysteresis band, the upper switch will be opened and the lower switch will be closed. Thus actual current will be forced to reduce and fall once more within the hysteresis band. As the actual current change in time is function of the drive dynamics and operating state, the instants of inverter semiconductor switching cannot be predicted and will vary. Furthermore the switching frequency of the inverter using this method is variable and is dependent on the hysteresis band. It is not constant even over one cycle of the output frequency.

Let the three-phase reference currents be i_a^*, i_b^* and i_c^*, the actual phase currents i_a,i_b, and i_c, and the hysteresis band *H*. The three-phase current errors are obtained as

$$\Delta i_a = i_a^* - i_a, \quad \Delta i_b = i_b^* - i_b, \quad \Delta i_c = i_c^* - i_c. \tag{7.3-1}$$

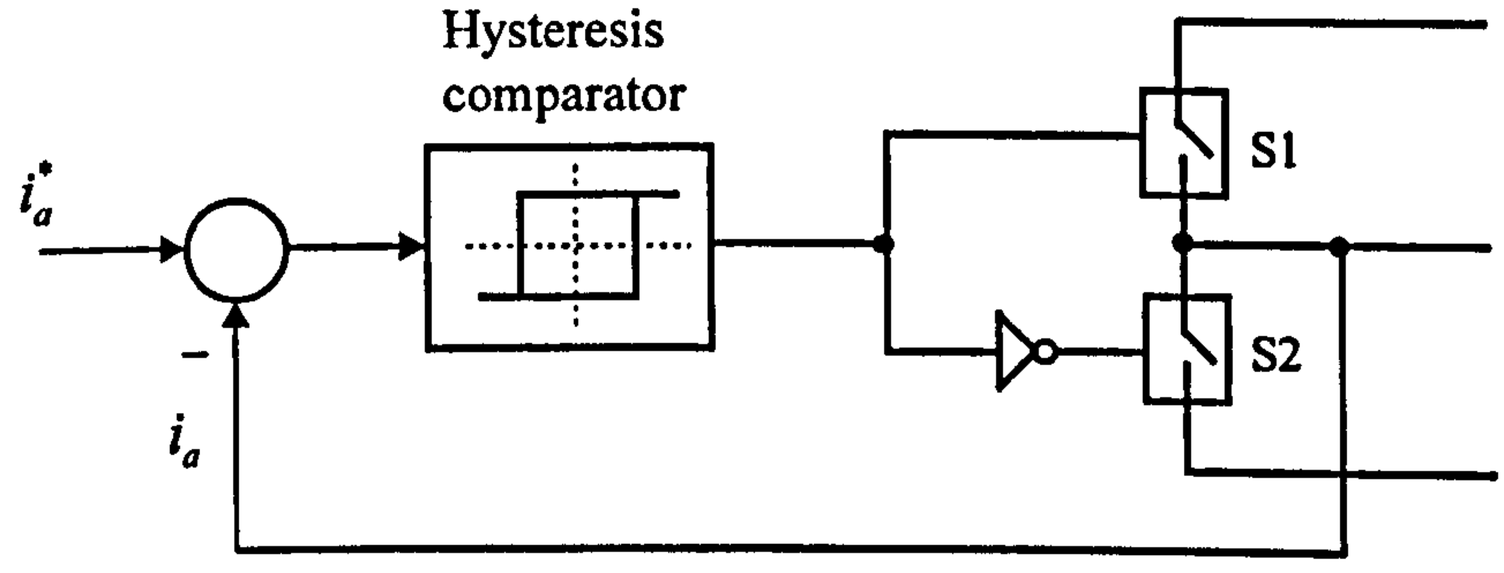

Figure 7.3.1 Hysteresis current controller for phase *a*

The current errors are compared with allowed deviation (hysteresis band *H*). The change of the switching state in each leg will take place only if $|\Delta i_a| \geq H$. Let $i_a^* > 0$ and i_a very small; then

$$\Delta i_a = i_a^* - i_a > 0,\ \Delta i_a < H. \tag{7.3-2}$$

and switch 1 (upper switch) is on, switch 2 (lower switch) is off, hence $v_{ao} = v_{DC}$ (Figure 7.3.2). Switch 1 remains on as long as $|\Delta i_a| < H$. Eventually i_a becomes $i_a^* + H$, i.e.,

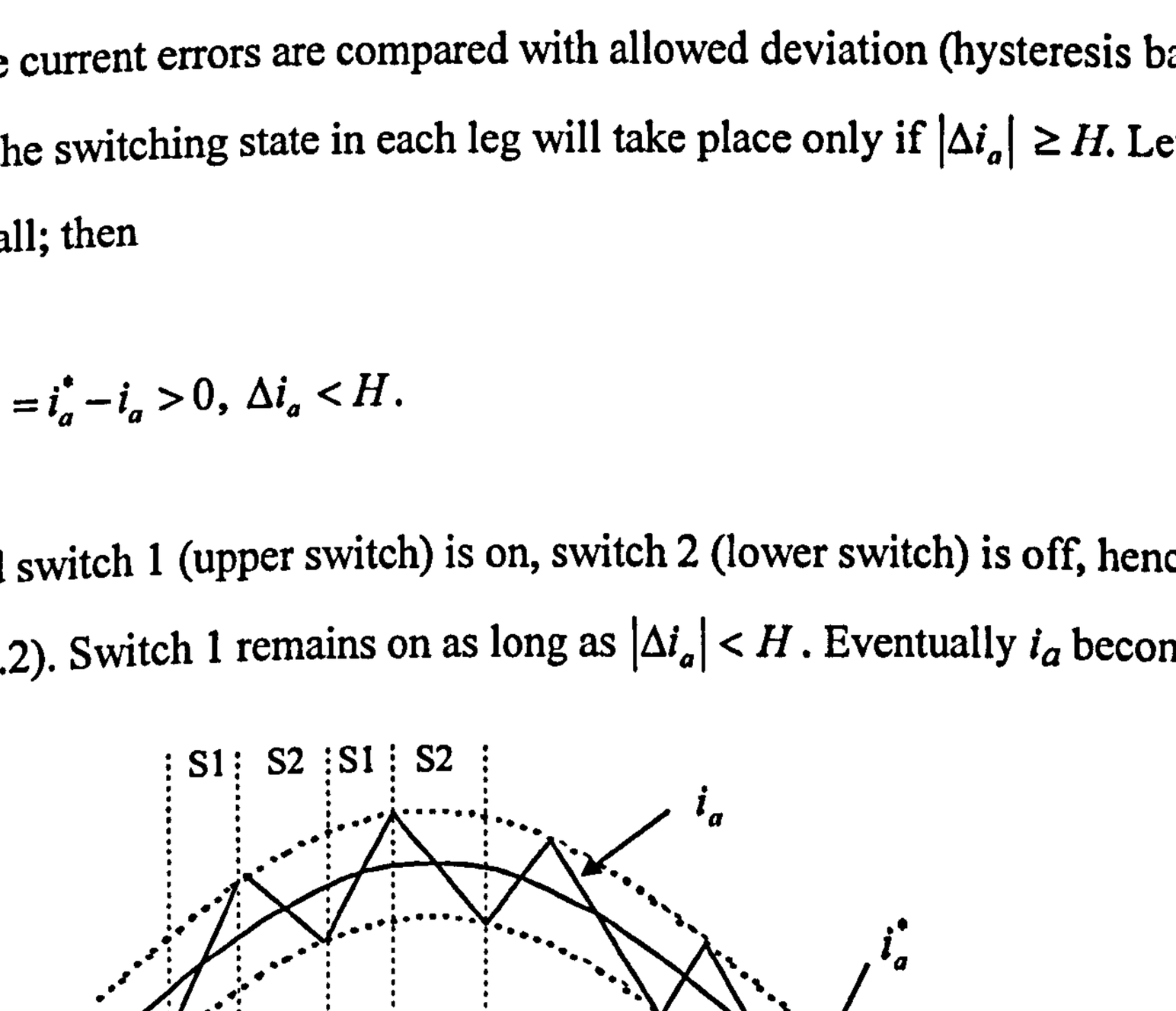

Figure 7.3.2 Switching scheme for phase *a* of the inverter and output voltage of leg *a* with respect to negative d.c. rail of the supply

$$i_a = i_a^* + H, \quad \Delta i_a = -H, \quad |\Delta i_a| = H. \tag{7.3-3}$$

and switch 1 opens, switch 2 closes, $v_{ao} = 0$. The same applies to other two leg voltages v_{bo} and v_{co}.

7.4 Estimation of stator flux space vector

The most simple method to estimate stator flux is to use measured stator currents and measured or reconstructed stator voltages. The only machine parameter that is required is the stator resistance. Stator flux amplitude and position can then be calculated from the measured stator signals. If the machine phase voltages are v_{aN}, v_{bN} and v_{cN} and machine phase currents are i_a, i_b and i_c, then the estimated flux magnitude and transformation angle are calculated by [Xu, et al (1988a)]:

$$\psi_s = \sqrt{\psi_{\alpha s}^2 + \psi_{\beta s}^2} \tag{7.4-1}$$

$$\phi_s = \tan^{-1}\left(\frac{\psi_{\beta s}}{\psi_{\alpha s}}\right) \tag{7.4-2}$$

where the stator flux components in the stationary reference frame are

$$\psi_{\alpha s} = \int (v_{\alpha s} - R_s i_{\alpha s})dt \tag{7.4-3}$$

$$\psi_{\beta s} = \int (v_{\beta s} - R_s i_{\beta s})dt \tag{7.4-4}$$

and

$$v_{\alpha s} = \frac{2}{3}\left(v_{aN} - \frac{1}{2}v_{bN} - \frac{1}{2}v_{bN}\right) \tag{7.4-5}$$

$$v_{\beta s} = \frac{2}{3}\frac{\sqrt{3}}{2}(v_{bN} - v_{cN}) \tag{7.4-6}$$

$$i_{\alpha s} = \frac{2}{3}\left(i_a - \frac{1}{2}i_b - \frac{1}{2}i_c\right) \tag{7.4-7}$$

$$i_{\beta s} = \frac{2}{3}\frac{\sqrt{3}}{2}(i_b - i_c) \tag{7.4-8}$$

Alternatively, stator voltages can be reconstructed from measured d.c. link voltage and switching states of the inverter [John et al (1995)]. It should be noted that this simple stator flux estimator is derived from the linear induction machine model, i.e., constant parameter model. The accuracy of the estimated stator flux depends on the accuracy of the stator resistance. The direct stator flux orientation control is particularly suitable for the control of induction machine operated at high speeds as the stator flux can be estimated accurately because the stator resistance voltage drop is relatively small compared to the amplitude of the stator voltage. At very low speeds, the integration of the voltage is sensitive to the offset voltage of the voltage sensors and the stator resistance may vary due to temperature changes, thus this direct stator flux estimation method may yield unsatisfactory results.

7.5 Stator flux oriented control system for the induction generator

The outlay of the stand-alone variable-speed induction generator system under consideration is shown in Figure 7.5.1. Three-phase load is assumed to be either purely resistive or combined resistive-inductive. The reactive power compensator is required to provide reactive power for the generator and for the load when it is of resistive-inductive nature. Power circuit of the compensator is the well-known six-switch three-phase topology (parallel connection of a controllable semiconductor and an antiparallel diode is shown in Figure 7.5.1 as a simple switch). The capacitor at the inverter d.c. side is of relatively high capacitance and is assumed to be pre-charged to an appropriate voltage, by means of auxiliary equipment that is not shown in the Figure 7.5.1. The resistor, connected in parallel to the d.c. side capacitor, is a fictitious element that does not exist in reality: as inverter switches, capacitor and d.c. link are modelled as loss-less elements, the resistor is used to represent losses that take place in the inverter and in real d.c. circuit.

Direct stator flux oriented control is adopted. Its basic scheme, for an induction motor drive, was shown in Figure 7.2.2. Flux estimator of Figure 7.2.2 is the one described in the previous sub-section. The controller itself has however to be modified in order to adapt the control system to the generating operation. Basic structure of the generating

system is depicted in Figure 7.5.2 and the block that needs to be considered in detailed is the block "vector control algorithm". It is the equivalent of the block contained within dashed lines in Figure 7.2.2 (denoted as "controller") and is shown in Figure 7.5.3. Compared with the control scheme for a motoring application, Figure 7.2.2, there are a number of differences in Figure 7.5.3 that deserve further attention. As far as creation of stator d-axis current reference is concerned, the only difference is that cross-coupling and rate of change of the reference flux are neglected in Figure 7.5.3. Stator flux reference ψ_s^* is an independent input into the vector control block. It is constant and equal to rated stator flux in the base speed region. In the field weakening stator flux reference is reduced inversely proportionally to the speed of rotation. Stator d-axis current reference is thus obtained as PI flux controller output and it controls reactive power flow in the system. Major changes are however present in creation of the stator q-axis current reference. Stator q-axis current reference in a drive is obtained from a speed controller. However in a generating system speed is an uncontrollable input. The role of the speed controller is therefore assigned to the d.c. voltage controller and this branch controls active power flow in the system. Another important difference regards multiplication of the stator q-axis current reference by -1 and it reflects the need for active power flow from the generator to the converter d.c side when difference between reference and actual d.c. voltage is positive. Finally, decoupling is not introduced in q-axis branch either. As already mentioned, decoupling circuit is usually omitted when inverter switching frequency is sufficiently high. This is exactly the case considered here and omission of the decoupling circuit is justified on this ground.

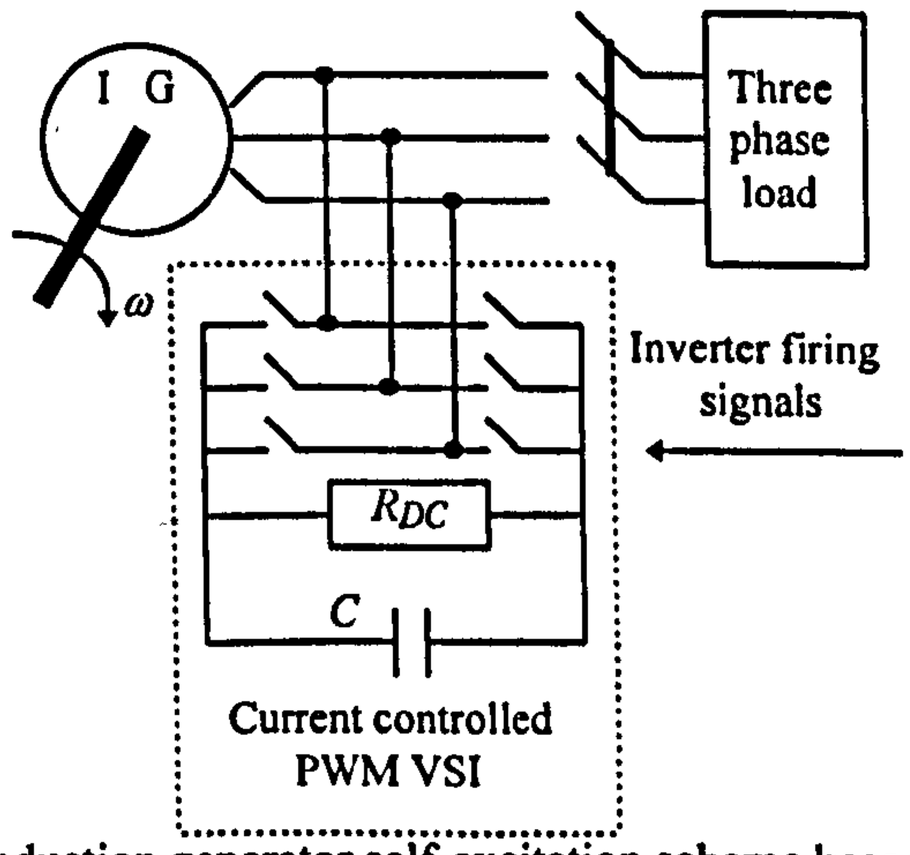

Figure 7.5.1 Induction generator self-excitation scheme based on PWM VSI

The configuration of the system in Figure 7.5.2 indicates that rotor speed, d.c. voltage across the capacitor, stator currents and stator voltages have to be measured. The inverter is now operated as current-controlled source, where inverter firing signals are obtained from the closed-loop current control algorithm. The current references i_a^*, i_b^* and i_c^* are obtained from the stator flux oriented control algorithm. The measured induction generator phase currents are used for both vector control algorithm and for current control algorithm while the measured rotor speed of the machine, d.c. voltage across capacitor and stator phase voltages are used in the vector control algorithm. Alternatively, stator phase voltages may be reconstructed from measured d.c. voltage and inverter switching functions as already explained. Current control is performed in stationary reference frame using hysteresis current controllers, section 7.3. The hysteresis current controllers compare the three-phase currents i_a,i_b and i_c with the three-phase reference currents i_a^*, i_b^* and i_c^*, and determine the on/off states of the inverter switches. The firing signals are thus created on the basis of the errors between phase current references and actual measured stator phase currents of the generator. Outputs of the hysteresis current control block are shown as switching functions S_a,S_b, S_c for each of the three inverter legs.

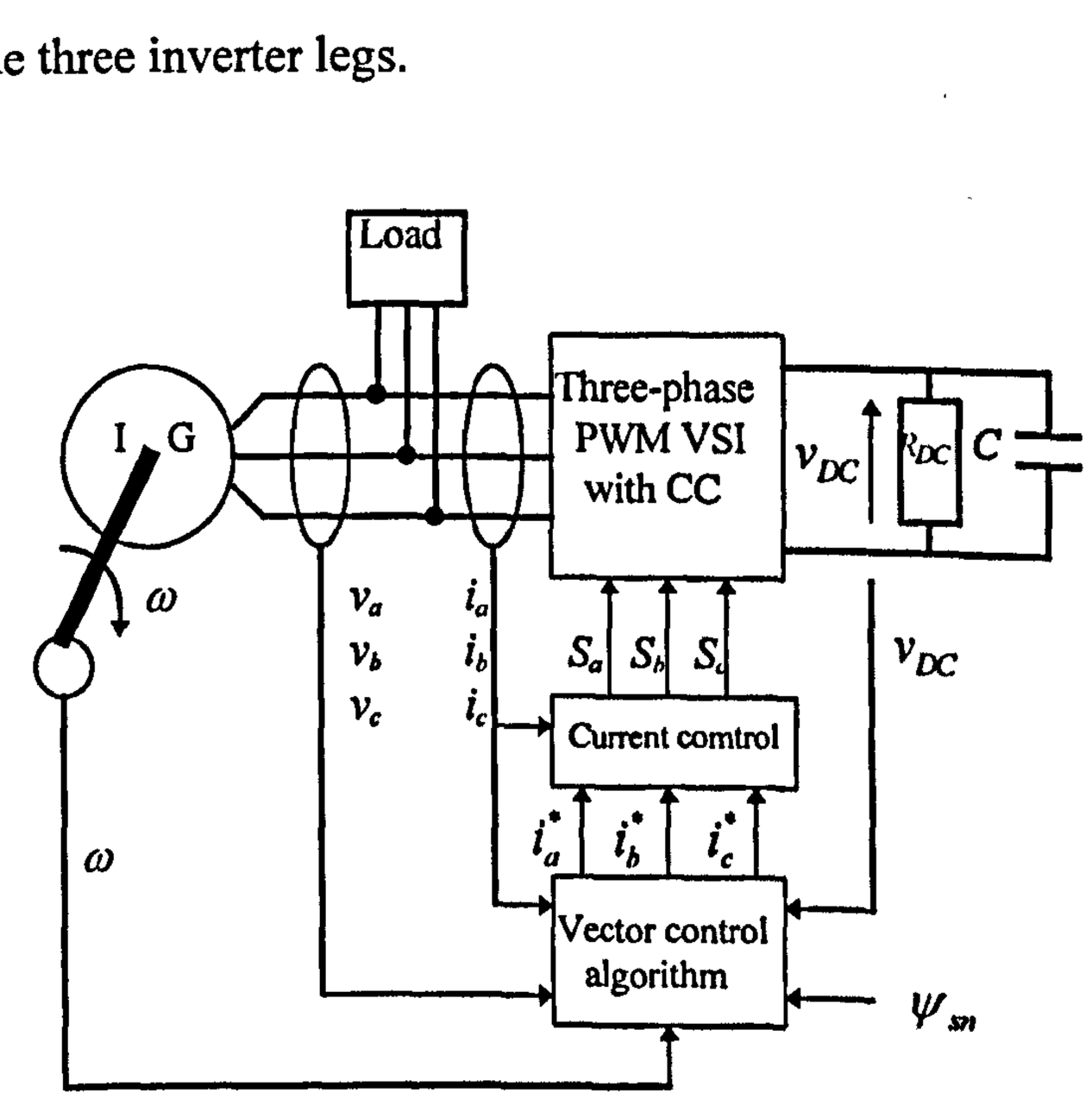

Figure 7.5.2 Configuration of the stator flux oriented control scheme

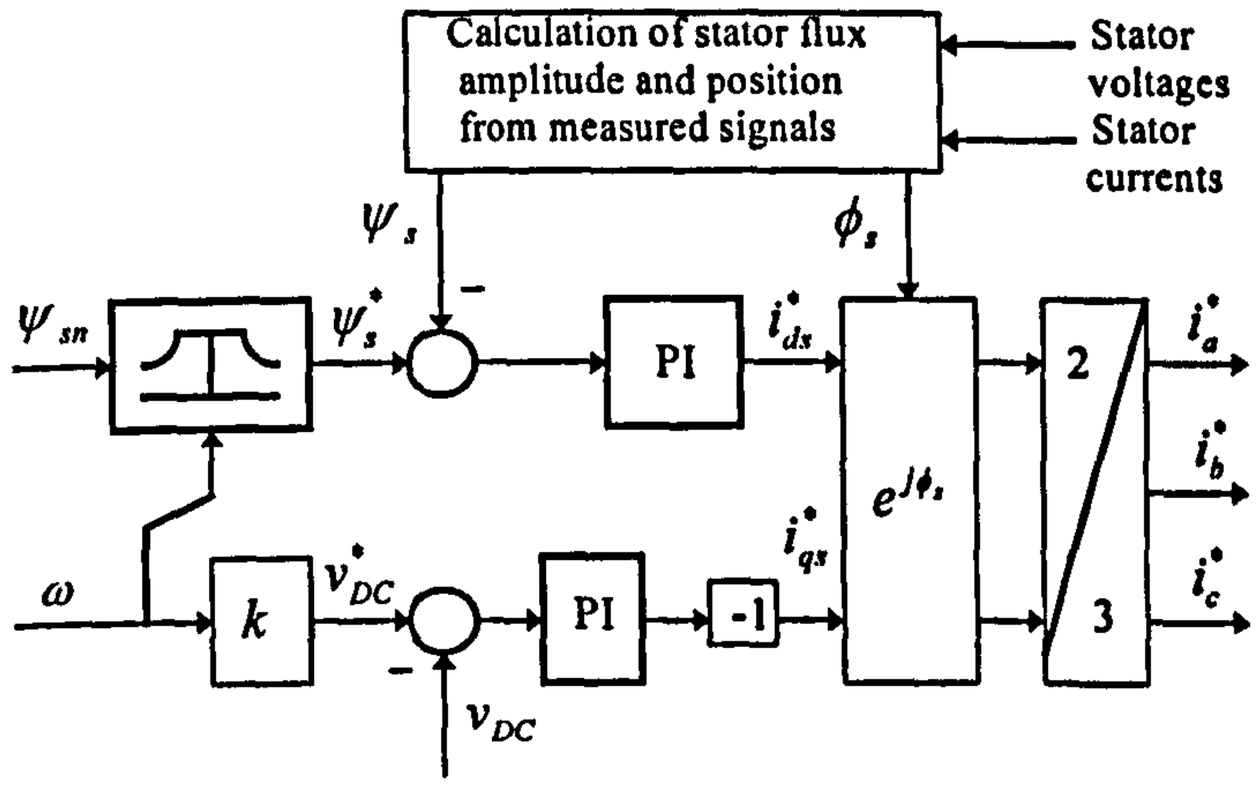

Figure 7.5.3 Outlay of the Block 'Vector Control Algorithm'

7.6 System modelling

The stator flux oriented vector controller does not include axis decoupling and it comprises two control loops. The stator phase current references are generated by the vector control algorithm. The d.c. voltage control loop defines the quadrature component of the reference current i_{qs}^* which represents required active power to maintain the d.c. capacitor voltage level and to cover active power losses in the resistor R_{DC} (i.e., loss in the d.c. circuit and in the inverter). Capacitor voltage reference value v_{DC}^* is proportional to the speed of rotation and is continuously varied in variable speed operation. The reactive component of the reference current, i_{ds}^*, provides necessary excitation and it is obtained from the flux control loop by comparing the reference stator flux and the estimated stator flux of the induction generator. The amplitude and phase angle of the stator flux vector are determined by the flux estimation algorithm and are used for the orientation of the current vector. Calculation of stator flux space vector amplitude and position in Figure 7.5.3 is performed in stationary reference frame, using stator voltage equations. As the operation of the generator takes place at relatively high speeds, sensitivity of this method of flux calculation with respect to stator resistance variation is irrelevant. In both control loops PI controllers are employed to determine the d-q reference currents using the error signals of the d.c. voltage and stator flux.

The induction generator is represented for simulation purposes with a model with stator current and stator flux d-q axis components as state-space variables and main flux

saturation is taken into account. The model is given in Section 3.3.1 of Chapter 3. Co-ordinate transformations between generator phase-to-neutral voltages, determined by the inverter, and d-q axis voltages, and between the generator d-q axis currents and phase currents are given with

$$v_{ds} = \left(\frac{2}{3}\right)\left[v_{aN}\cos 2\pi 50t + v_{bN}\cos\left(2\pi 50t - \frac{2\pi}{3}\right) + v_{cN}\cos\left(2\pi 50t - \frac{4\pi}{3}\right)\right] \quad (7.6\text{-}1)$$

$$v_{qs} = -\left(\frac{2}{3}\right)\left[v_{aN}\sin 2\pi 50t + v_{bN}\sin\left(2\pi 50t - \frac{2\pi}{3}\right) + v_{cN}\sin\left(2\pi 50t - \frac{4\pi}{3}\right)\right] \quad (7.6\text{-}2)$$

$$i_a = i_{ds}\cos 2\pi 50t - i_{qs}\sin 2\pi 50t \quad (7.6\text{-}3)$$

$$i_b = i_{ds}\cos\left(2\pi 50t - \frac{2\pi}{3}\right) - i_{qs}\sin\left(2\pi 50t - \frac{2\pi}{3}\right) \quad (7.6\text{-}4)$$

$$i_c = i_{ds}\cos\left(2\pi 50t - \frac{4\pi}{3}\right) - i_{qs}\sin\left(2\pi 50t - \frac{4\pi}{3}\right) \quad (7.6\text{-}5)$$

The generator is modelled in the synchronously rotating reference frame, $\omega_a = 2\pi 50$, and the selection $\omega_a = 2\pi 50$ is accounted for, indices *a, b, c* identify the three phases and index *N* once more stands for neutral point of the star connected generator's stator winding. The d-q axis voltages v_{ds} and v_{qs} in the synchronous reference frame are treated as the inputs of the generator model. The three-phase currents i_a, i_b and i_c are the model outputs.

Modelling of the d.c. side of the inverter is as follows. Using the notation and current flow definitions of Figure 7.6.1 for the inverter d.c. side, change of d.c. voltage is governed with

$$\frac{dv_{DC}}{dt} = -\frac{i_{DC} + v_{DC}/R_{DC}}{C} \quad (7.6\text{-}6)$$

Total d.c. current i_{DC} can be expressed using inverter switching function as (index *e* identifies compensator phase currents)

$$i_{DC} = S_a i_{ea} + S_b i_{eb} + S_c i_{ec} \tag{7.6-7}$$

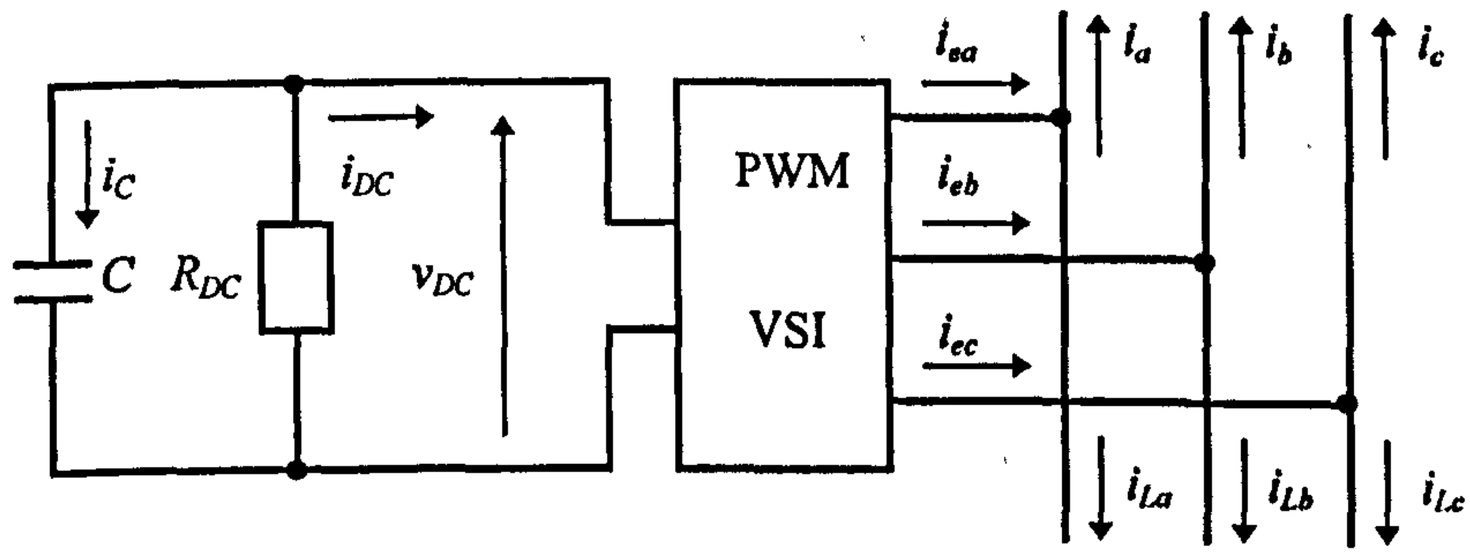

Figure 7.6.1 Current flow directions in the system

Any of the three switching functions takes the value of 1 if upper switch in the given inverter leg is on and lower switch is off, and value 0 if lower switch in the same inverter leg is on, while upper switch is off. Correlation between generator currents, compensator currents and load currents is, from Figure 7.4.4, (load currents are identified with index *L*) given with

$$i_{ea} = i_a + i_{La} \qquad i_{eb} = i_b + i_{Lb} \qquad i_{ec} = i_c + i_{Lc} \tag{7.6-8}$$

The current errors for current control are obtained by comparing the commanded currents with the actual currents; when the current errors are either greater than or less than the allowed deviation (hysteresis band), the change of the switching state in each leg of the PWM inverter will take place, as explained in section 7.3.

Stator phase voltages in terms of inverter switching functions and the d.c. link voltage can be expressed as follows:

$$v_{aN} = \frac{v_{DC}}{3}(2S_a - S_b - S_c) \tag{7.6-9}$$

$$v_{bN} = \frac{v_{DC}}{3}(2S_b - S_c - S_a) \tag{7.6-10}$$

$$v_{cN} = \frac{v_{DC}}{3}(2S_c - S_a - S_b) \tag{7.6-11}$$

Value of the switching function for any of the three inverter legs is determined by the hysteresis current controller of the given phase. Current error in any of the three phases $\Delta i = i^* - i$ is restricted to at most $\pm H$. Twice the hysteresis band is selected in simulations as equal to approximately 3% of the rated peak current of the induction machine (i.e., $2H = 0.1$ A).

Control system is, from Figure 7.5.3, described with the following equations:

$$i_{ds}^* = K_d\left(\psi_s^* - \psi_s\right) + \left(\frac{K_d}{T_d}\right)\int\left(\psi_s^* - \psi_s\right)dt \tag{7.6-12}$$

$$-i_{qs}^* = K_q\left(v_{DC}^* - v_{DC}\right) + \left(\frac{K_q}{T_q}\right)\int\left(v_{DC}^* - v_{DC}\right)dt \tag{7.6-13}$$

where K_d, K_q, T_d and T_q are parameters of the PI controllers in d- and q-branches of the control system, $v_{DC}^* = k\omega$ and $\psi_s^* = \psi_{sn}$ (index n stands for rated values) in the base speed region, while above base speed (identified with index B) stator flux reference is $\psi_s^* = \psi_{sn}\,\omega_B/\omega$. Base speed is taken as equal to rated synchronous speed.

Phase current references are built using estimated stator flux angular position ϕ_s, equation 7.4.2, so that

$$i_a^* = i_{ds}^*\cos\phi_s - i_{qs}^*\sin\phi_s \tag{7.6-14}$$

$$i_b^* = i_{ds}^*\cos\left(\phi_s - 2\pi/3\right) - i_{qs}^*\sin\left(\phi_s - 2\pi/3\right) \tag{7.6-15}$$

$$i_c^* = i_{ds}^*\cos\left(\phi_s - 4\pi/3\right) - i_{qs}^*\sin\left(\phi_s - 4\pi/3\right) \tag{7.6-16}$$

General resistive-inductive passive load is represented in the same reference frame as the generator (i.e., $\omega_a = 2\pi 50$ rad/s) with the following equations:

$$v_{ds} = R_L i_{Lds} + L_L\frac{di_{Lds}}{dt} - \omega_a L_L i_{Lqs} \tag{7.6-17}$$

$$v_{qs} = R_L i_{Lqs} + L_L \frac{di_{Lqs}}{dt} + \omega_a L_L i_{Lds} \qquad (7.6\text{-}18)$$

Another slightly modified system is considered, where a battery, E, connected in parallel with the d.c. capacitor, is used for start-up purpose as shown in Figure 7.6.2. The resistor r_b in series with the battery is used to model the battery internal losses and is assumed to be very small. The diode allows only one current direction in the battery so that no current will be flowing into the battery. The capacitor does not need to be pre-charged in this case. A modification of vector control algorithm is shown in Figure 7.6.3. Only the d.c. voltage controller is altered. The d.c. voltage reference is an independent input and is set to be a constant value. Inversion of the sign of the q-axis current reference i_{qs}^* again accounts for the fact that active power flow is from a.c. to d.c. side of the inverter.

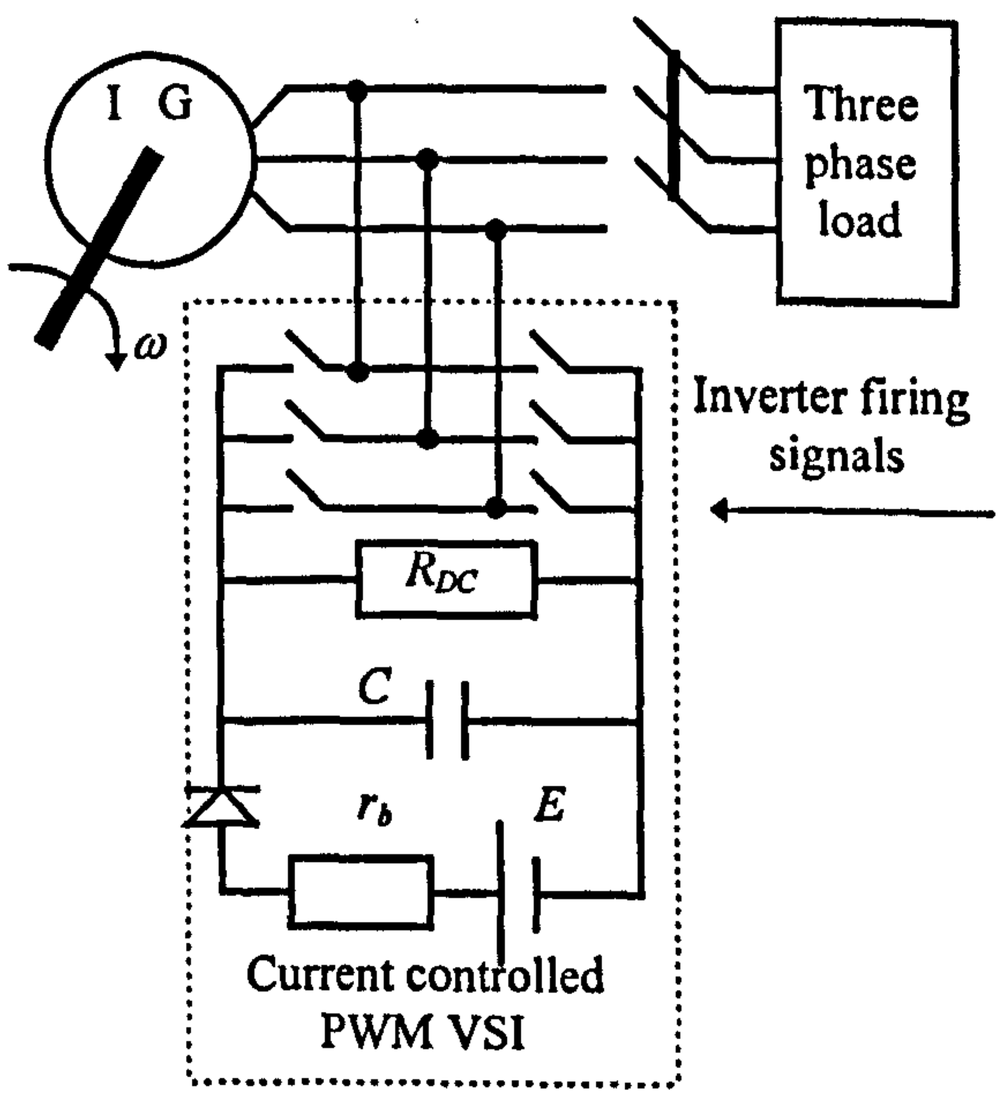

Figure 7.6.2 Induction generator self-excitation scheme based on PWM VSI with start-up battery

The new current flow directions in both d.c. side and a.c. side are shown in Figure 7.6.4. Start-up process supported by the battery is described as follows. As the capacitor voltage is zero initially, the diode turns on. There is a current flowing out of the battery. The total d.c. current i_{DC} can be expressed as

$$i_{DC} = \frac{E - v_{DC}}{r_b} - C\frac{dv_{DC}}{dt} - \frac{v_{DC}}{R_{DC}} \qquad (7.6\text{-}19)$$

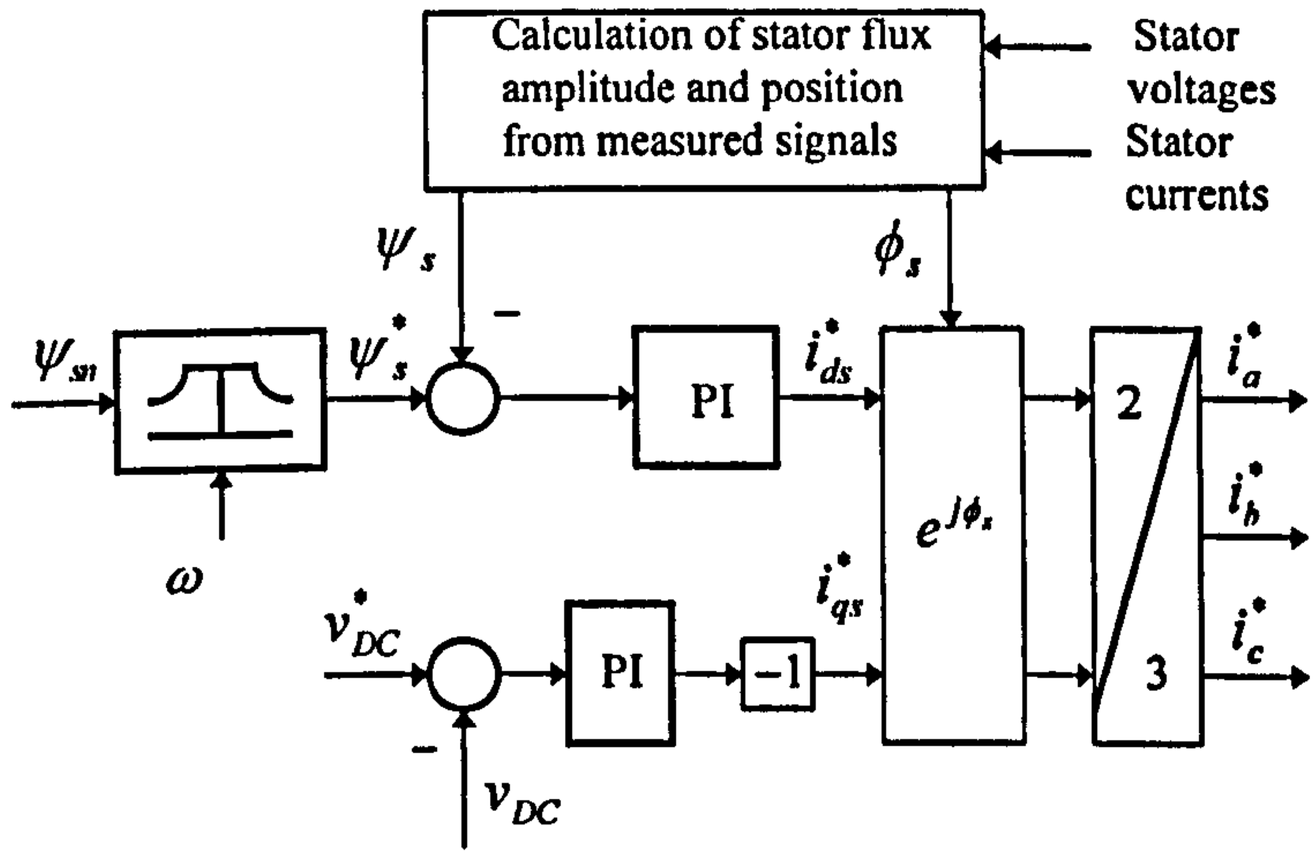

Figure 7.6.3 Modification of the Block 'Vector Control Algorithm' of Figure 7.5.3

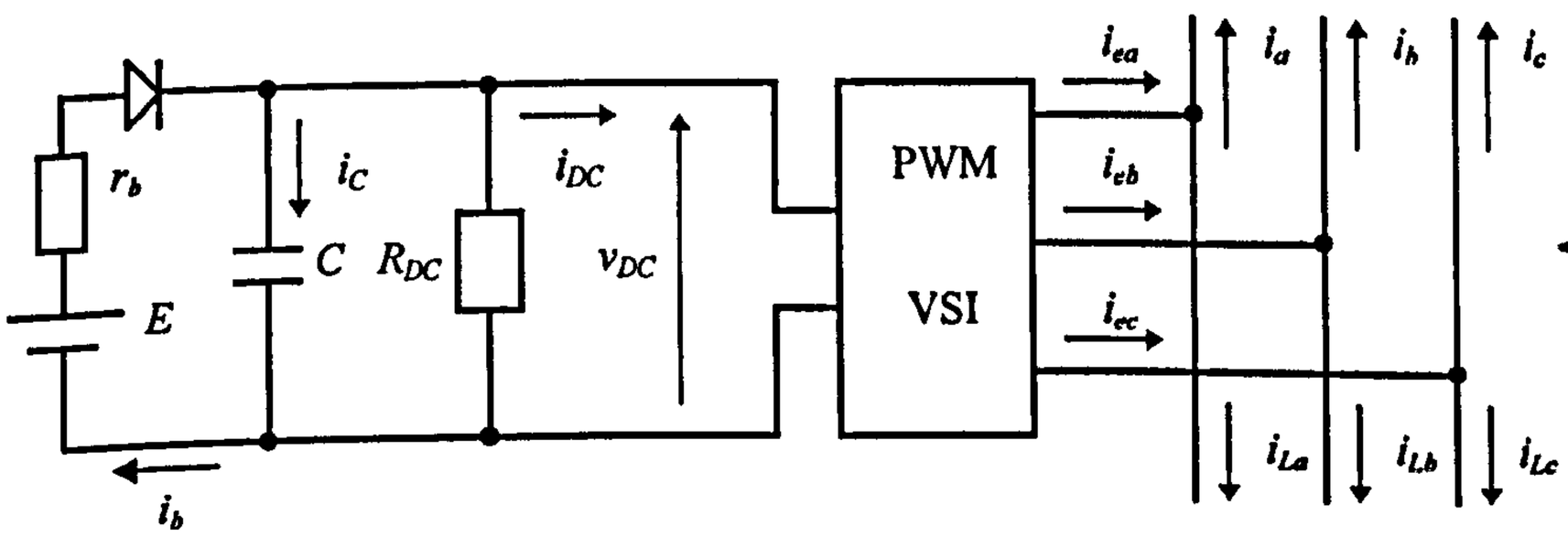

Figure 7.6.4 Current flow directions in the system with start-up battery

The diode remains on as long as the d.c. voltage v_{DC} is smaller than the battery voltage E. Once when d.c. voltage becomes equal to E, the total d.c. current i_{DC} becomes

$$i_{DC} = -C\frac{dv_{DC}}{dt} - \frac{v_{DC}}{R_{DC}} \qquad (7.6\text{-}20)$$

This is equivalent to equation 7.6-6 in which case no current flows through the battery and the capacitor is charged by the active power supplied by the generator. As the a.c. side of the inverter remains unchanged, equations 7.6-7 - 7.6-11 are still valid.

7.7 Simulation of the system

In all the simulations rotor speed is treated as an independent input. The induction generator system of Figure 7.5.1 is simulated using the control system of Figure 7.5.2. The machine used in simulations is again the small 0.75 kW, 50 Hz, 4-pole motor. The d.c. side capacitor is chosen as 250 μF, with initial voltage of 350 V. Self-excitation is initiated under no-load conditions at constant 50 Hz synchronous speed at zero time instant. Next, step application of pure resistive load of 300 Ω (approximately one half of the rated load) per phase follows at time instant t = 1 s. The speed of rotation is then reduced from 1 p.u. to 0.8 p.u. in a ramp-wise manner during time interval from 1.4 s to 1.5 s. The generator operates further with 0.8 p.u. speed and resistive load until the time instant t = 3.5 s is reached. Finally, the speed is brought back to 1 p.u. in time interval from 3.5 s to 3.6 s in a linear manner. The speed and load profile are shown in Figure 7.7.1. Figure 7.7.2 illustrates variation of capacitor d.c. voltage, stator phase voltage, stator phase current, comparison of actual (i.e., from the generator model) and estimated (i.e., from the estimator) value of stator flux, electromagnetic torque and magnetising inductance and magnetising current [Liao and Levi (1997)].

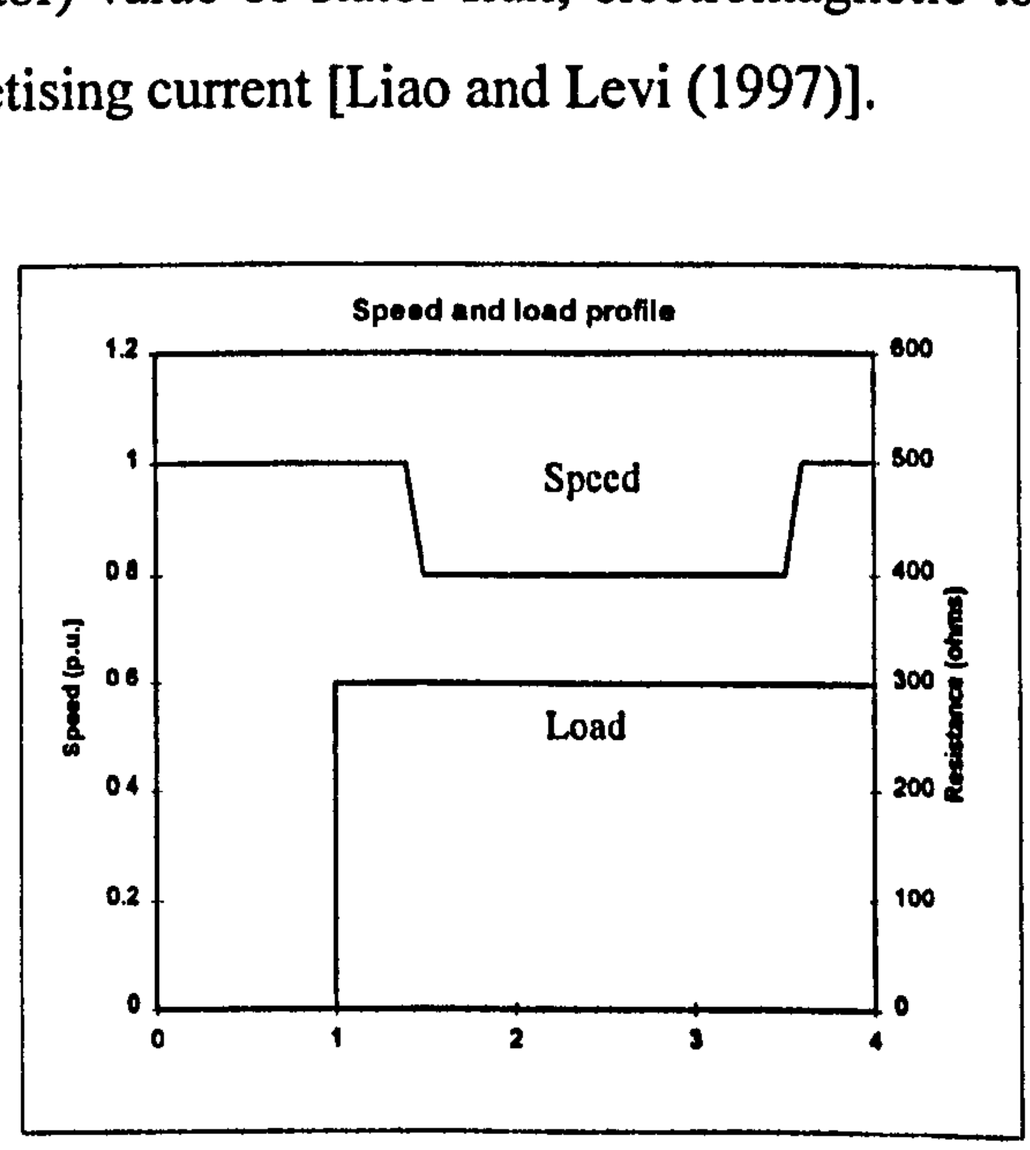

Figure 7.7.1 Speed and load (a.c.) profile for subsynchronous speed operation

When self-excitation is initiated, capacitor d.c. voltage initially experiences large reduction with respect to the pre-charged voltage value, Figure 7.7.2a. However, it quickly recovers and process of excitation is completed within few hundreds of

milliseconds. Application of the load, as well as speed variation, cause transients in both d.c. voltage and stator voltage. The d.c. voltage equals the reference value in steady-state with proper PI controller parameters selected for the d.c. voltage controller. The envelope of stator phase voltage waveform has the same shape as capacitor d.c. voltage waveform. Comparison of actual and estimated stator flux, Figure 7.7.2d, shows that stator flux build-up is very fast and that estimator at all times correctly predicts the value of the stator flux although the estimated value is slightly lower than the actual value when the generator is operated at 0.8 p.u. speed. As stator flux is correctly estimated and controlled, torque change in response to both load application and speed variation is almost instantaneous, Figure 7.7.2e. Figure 7.7.2 thus verifies capability of the control system to maintain constant stator flux operation under all operating conditions.

A similar study is performed once more, this time for operation in the field-weakening region. The machine at first operates under no-load conditions, self-excitation is again initiated at $t = 0$ s at speed of 1 p.u., and load of 300 Ω per phase is applied at $t = 1$ s. Speed change from 1 p.u. to 1.2 p.u. is initiated at $t = 1.4$ s in a linear manner during the 100 ms time interval. Stator flux reference is reduced inversely proportionally to the speed. The speed and load profile described above are shown in Figure 7.7.3. Figure 7.7.4 displays variation of capacitor d.c. voltage, stator phase voltage, generator current, comparison of actual and estimated values of stator flux, torque, magnetising inductance and magnetising current. Once more, the flux estimator correctly tracks the stator flux level in the machine, so that the waveforms of actual and estimated stator flux coincide. The stator harmonic voltage increases due to an increase in the d.c. voltage in the field weakening region. Fundamental component of stator phase voltage remains essentially constant in the field weakening. The increase in torque in the field weakening means that harmonic load losses increase with respect to operation in the base speed region due to the increase in the d.c. voltage. Magnetising inductance significantly increases during operation in the field-weakening region, due to decrease in flux. This is therefore an operating condition that requires representation of the generator with saturated induction machine model.

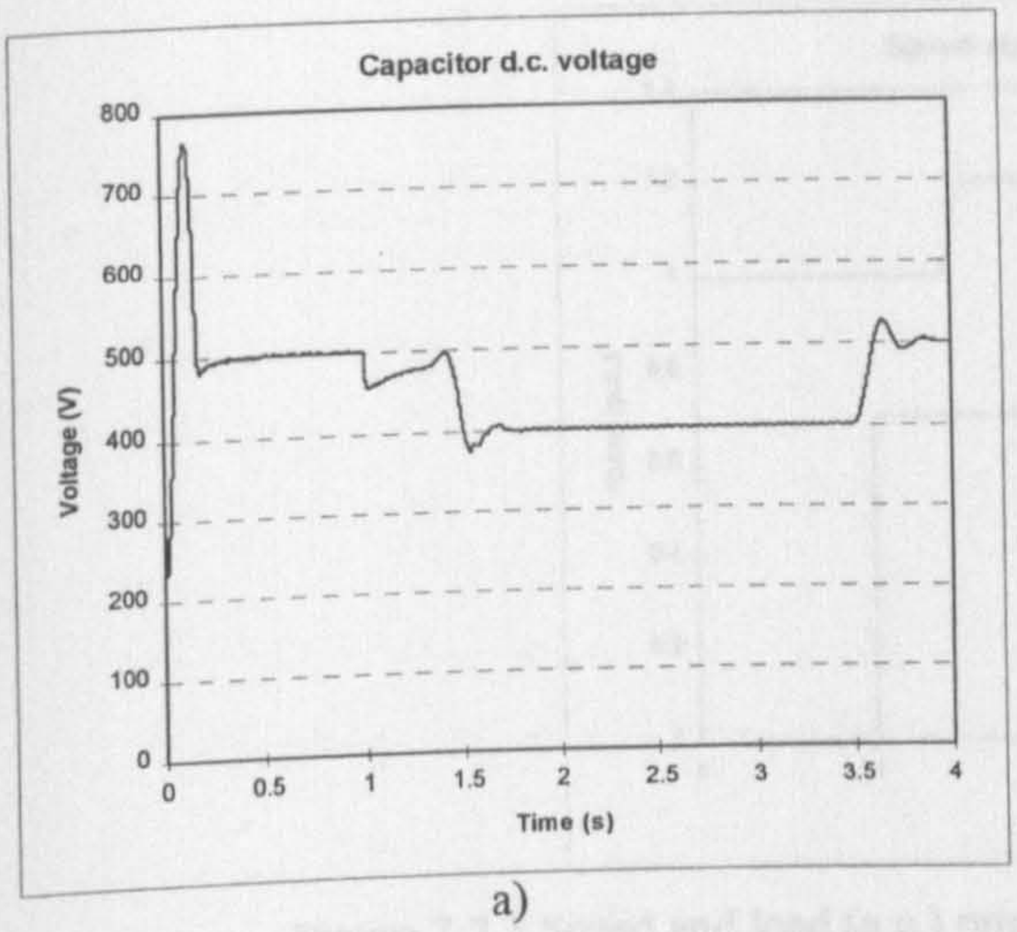

a)

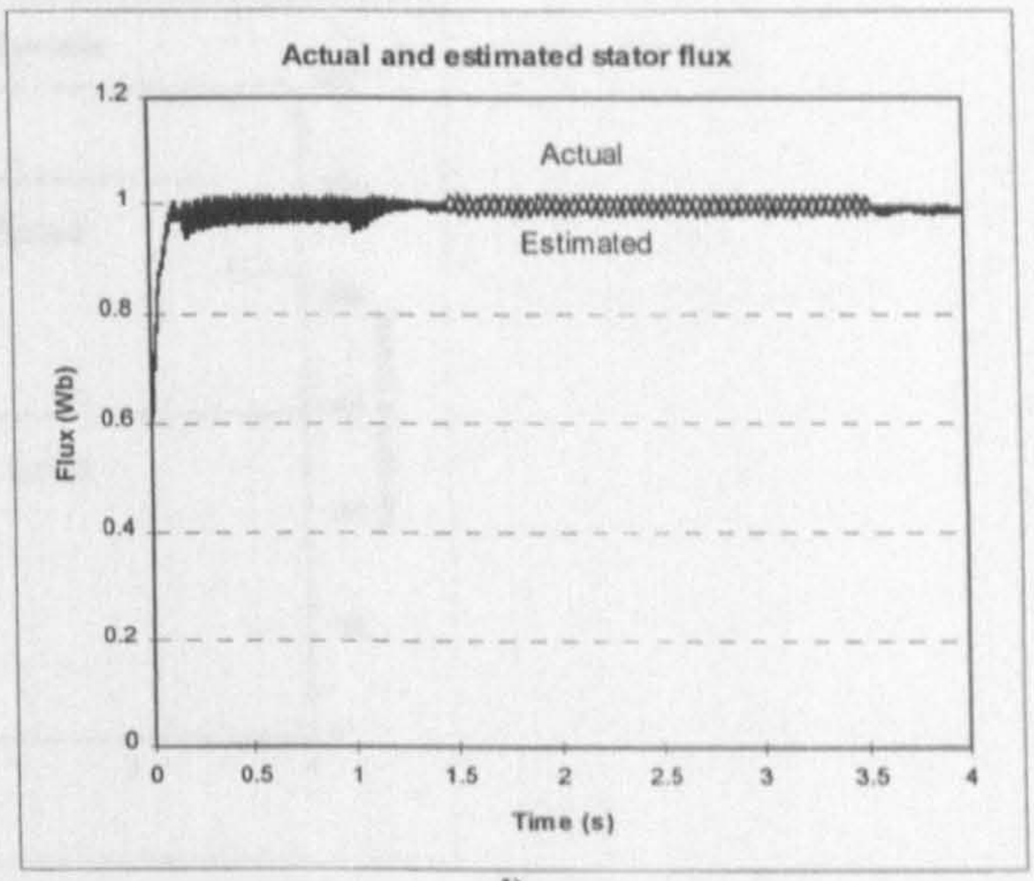

d)

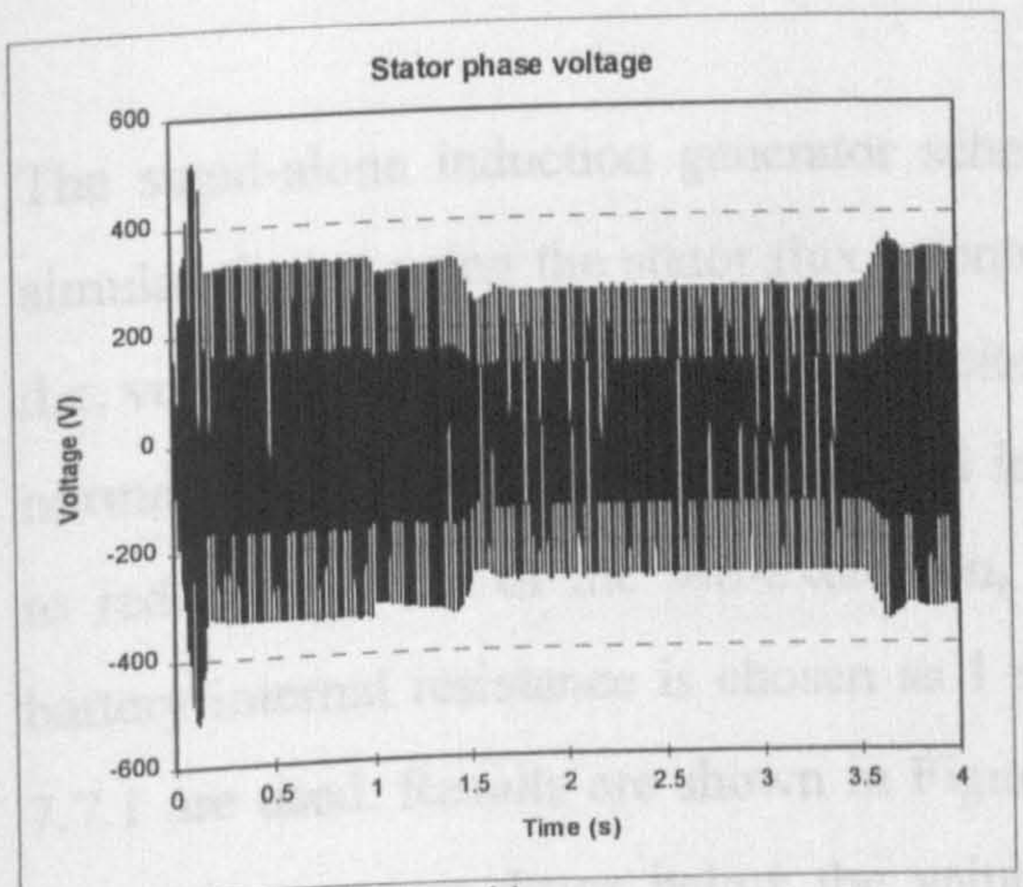

b)

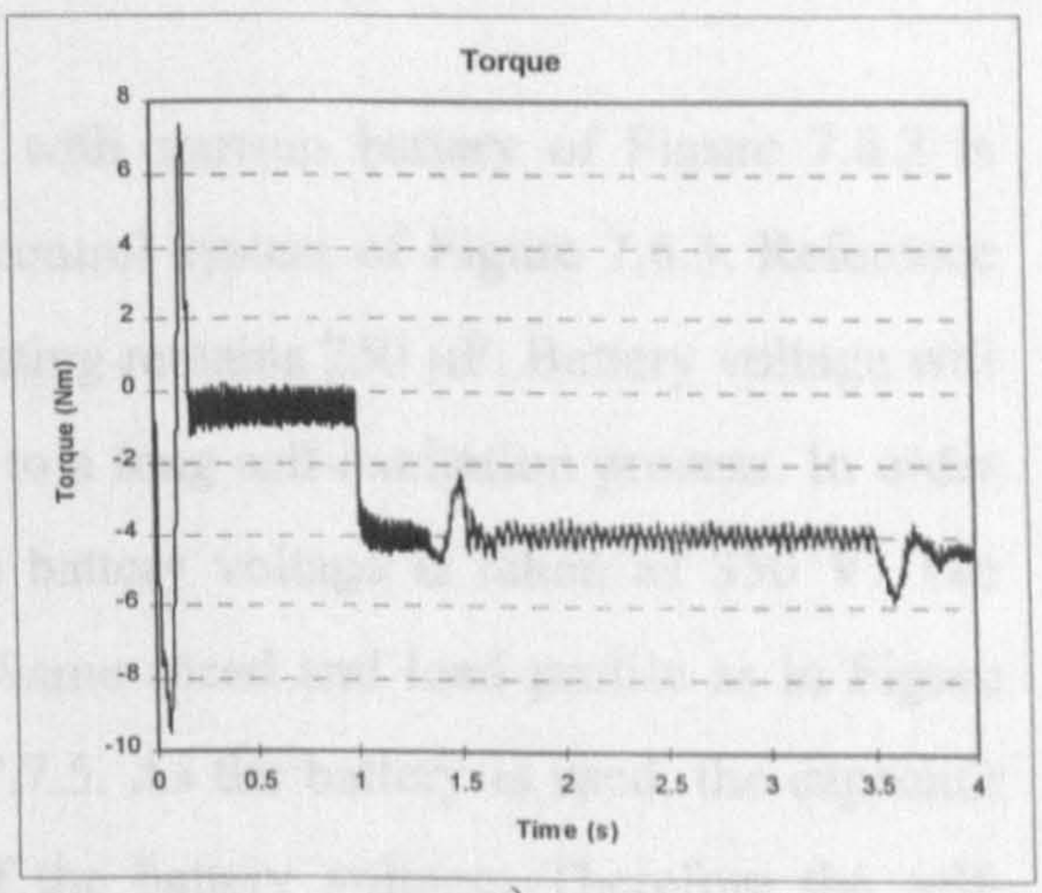

e)

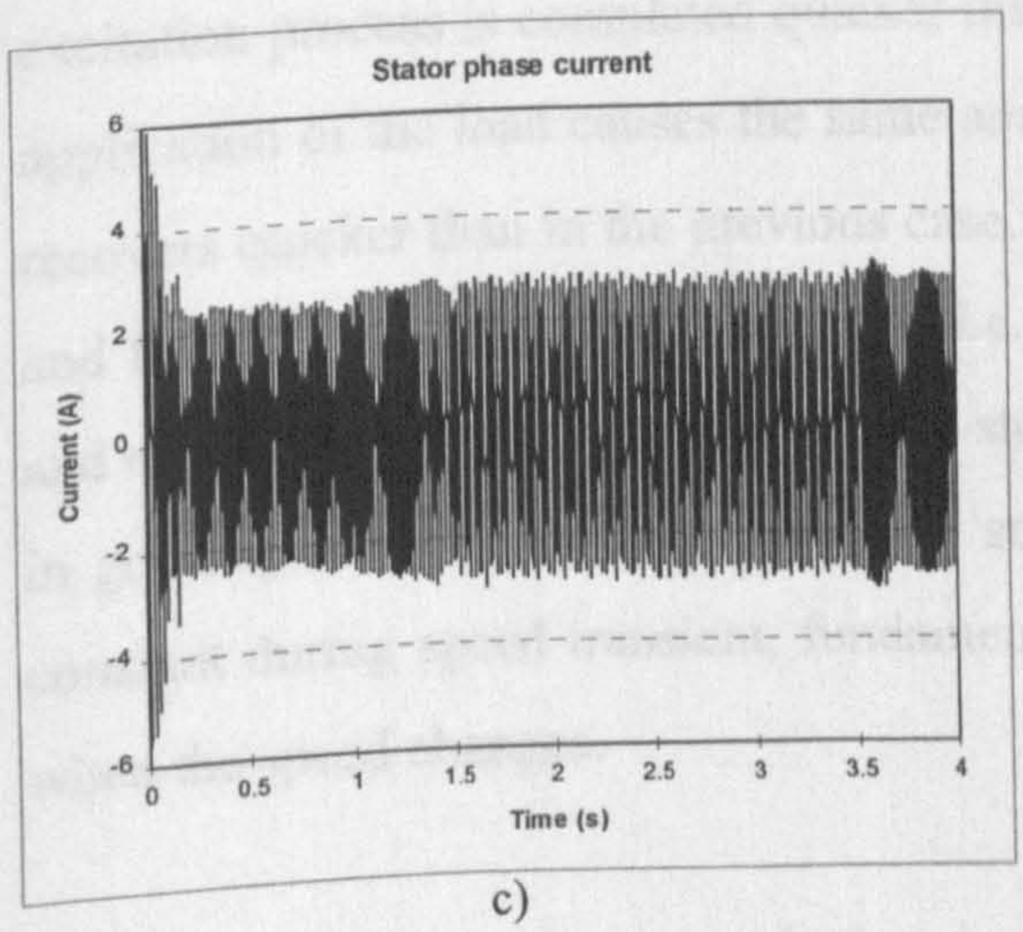

c)

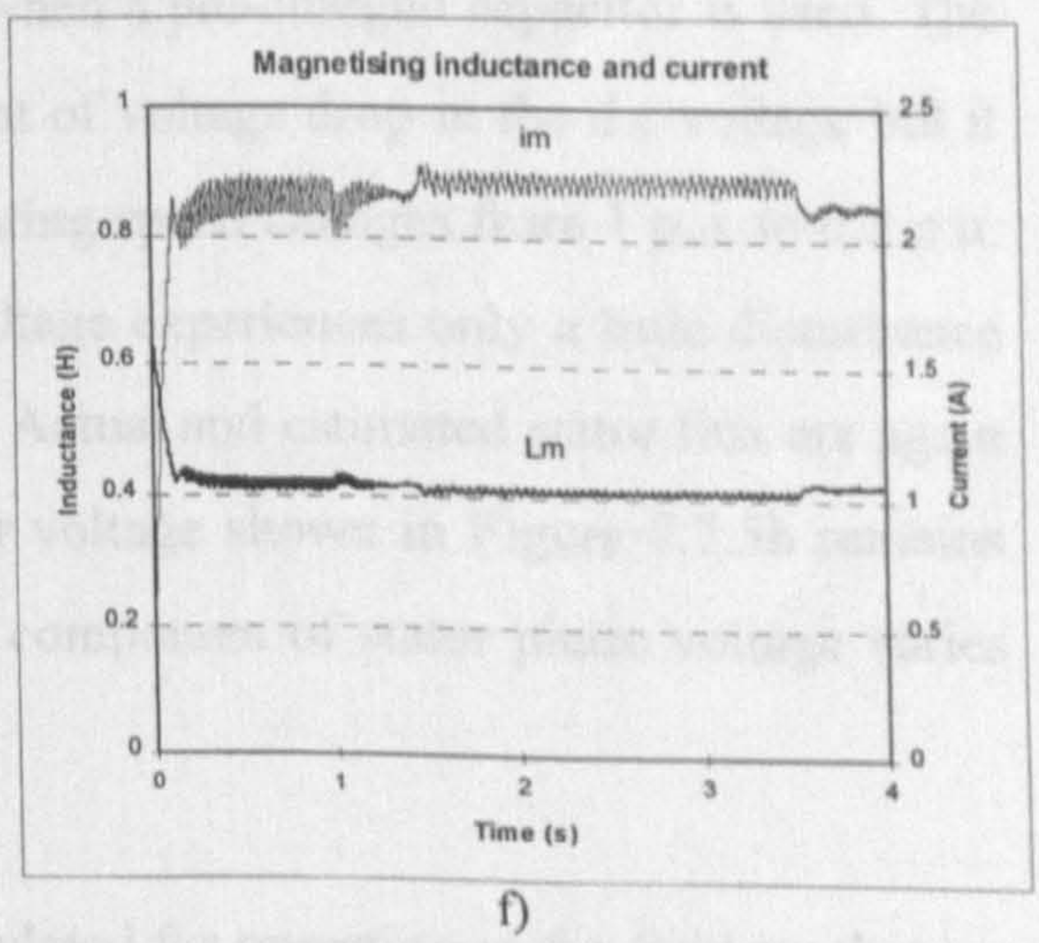

f)

Figure 7.7.2 Self-excitation, step load application and variable speed operation in the base speed region (stator flux oriented control): a) d.c. voltage, b) stator phase voltage, c) stator phase current, d) estimated and actual stator flux, e) torque, f) magnetising inductance and magnetising current

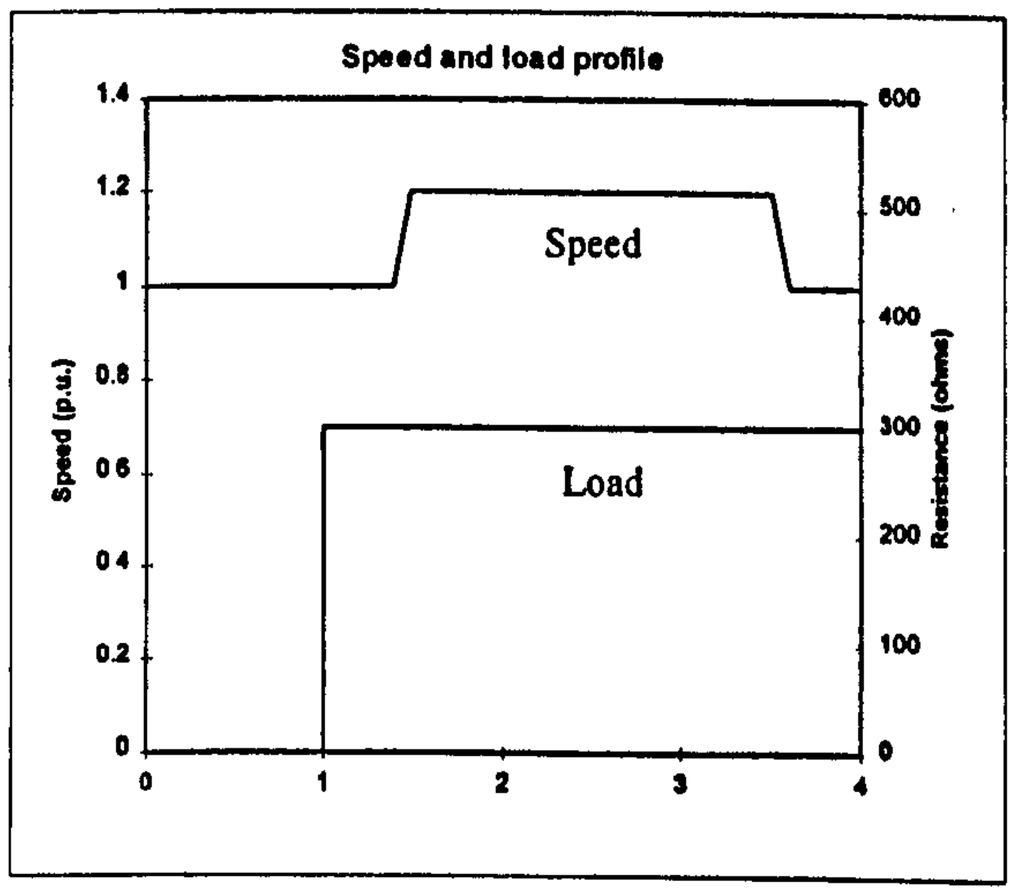

Figure 7.7.3 Speed and load (a.c.) profile for supersynchronous speed operation

The stand-alone induction generator scheme with start-up battery of Figure 7.6.2 is simulated next using the stator flux oriented control system of Figure 7.6.3. Reference d.c. voltage is set to 500 V and the capacitor rating remains 250 μF. Battery voltage will normally be relatively small, which will lead to a long self-excitation process. In order to reduce duration of the self-excitation, the battery voltage is taken as 350 V. The battery internal resistance is chosen as 1 Ω. Same speed and load profile as in Figure 7.7.1 are used. Results are shown in Figure 7.7.5. As the battery is used, the capacitor d.c. voltage never drops below the value of the battery voltage. Therefore the self-excitation process is completed quicker than when a pre-charged capacitor is used. The application of the load causes the same amount of voltage drop in the d.c voltage but it recovers quicker than in the previous case. During speed changes from 1 p.u. to 0.8 p.u. and from 0.8 p.u. back to 1.0 p.u., the d.c. voltage experiences only a little disturbance and equals the reference value in steady-state. Actual and estimated stator flux are again in good agreement. Although generator stator voltage shown in Figure 7.7.5b remains constant during speed transient, fundamental component of stator phase voltage varies when the speed changes.

The above system with start-up battery is simulated for operation in the field-weakening region with speed and load profile given in Figure 7.7.3. Simulation results are given in Figure 7.7.6. Excellent tracking of stator flux is achieved. The transient of the capacitor d.c voltage is the same as the one given in the Figure 7.7.5a. The fundamental

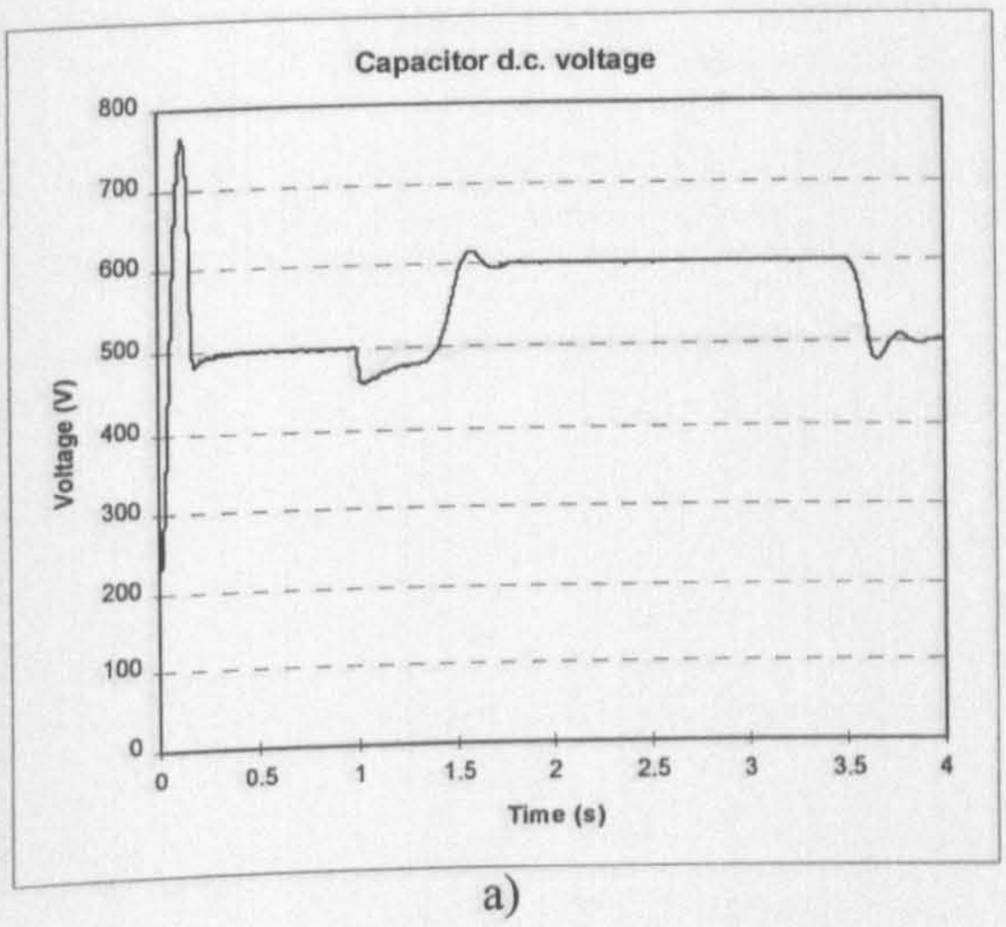

a)

b)

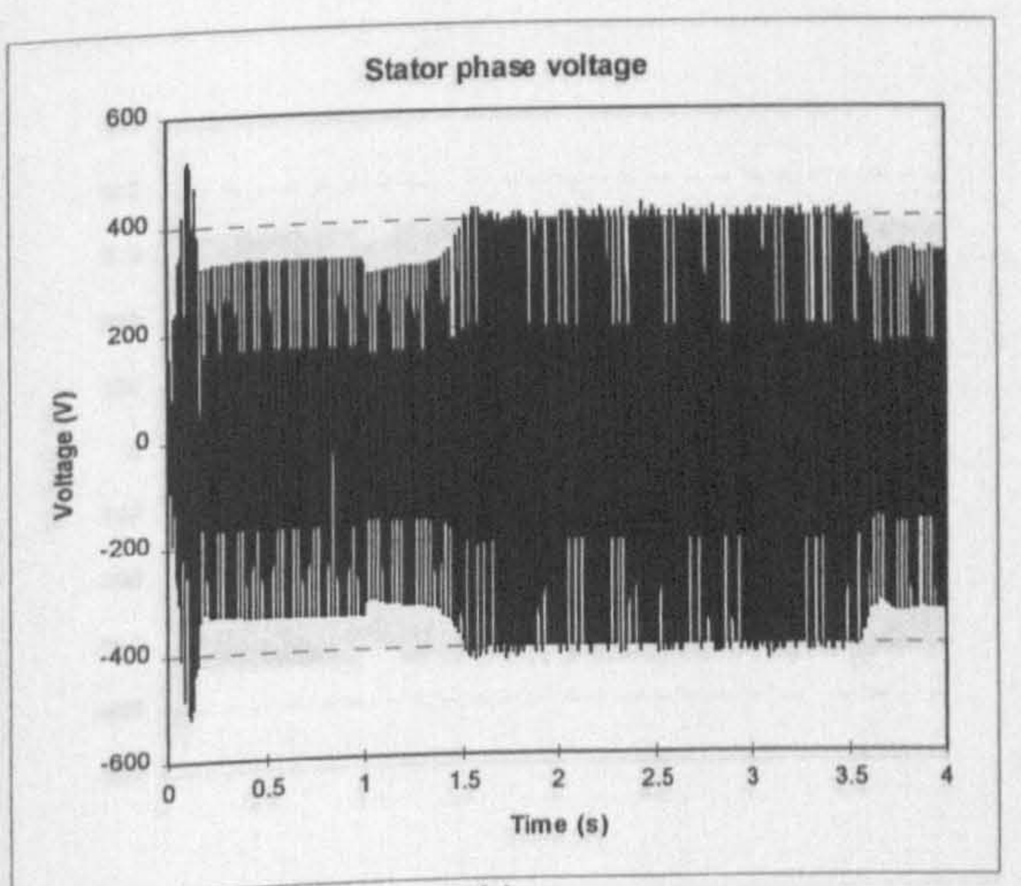

c)

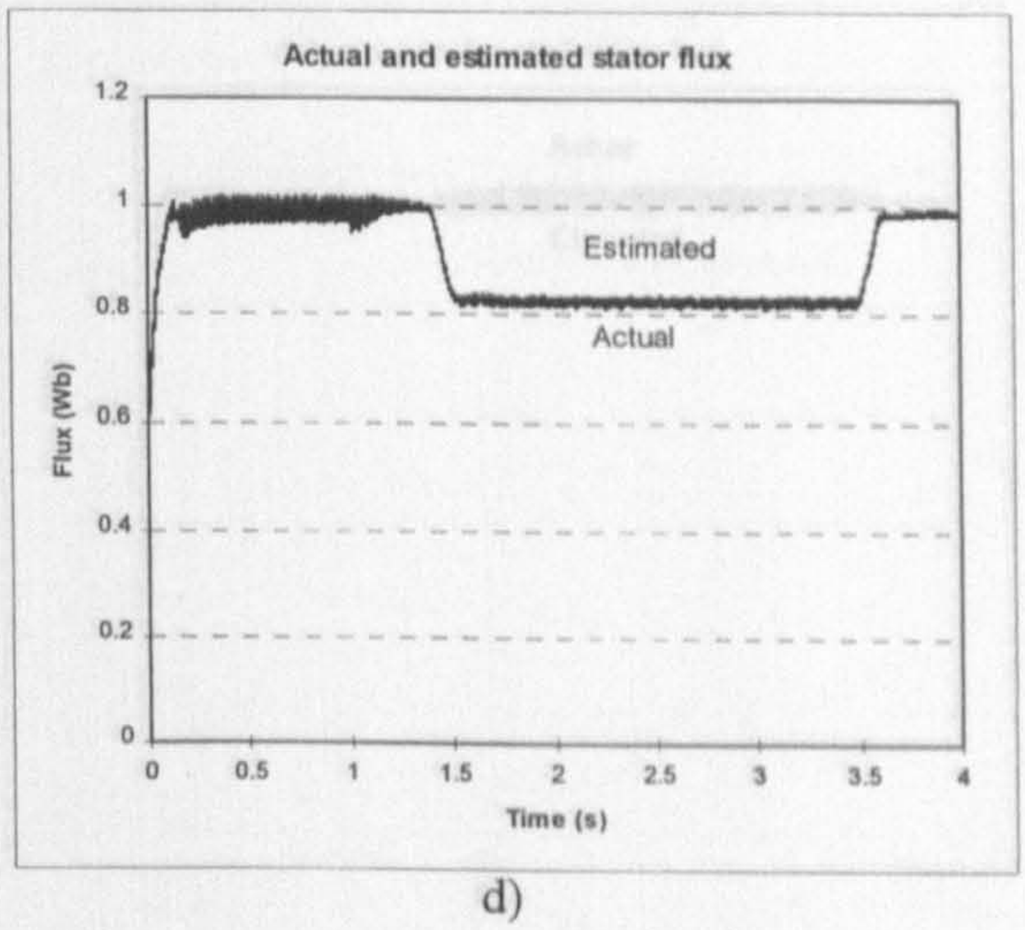

d)

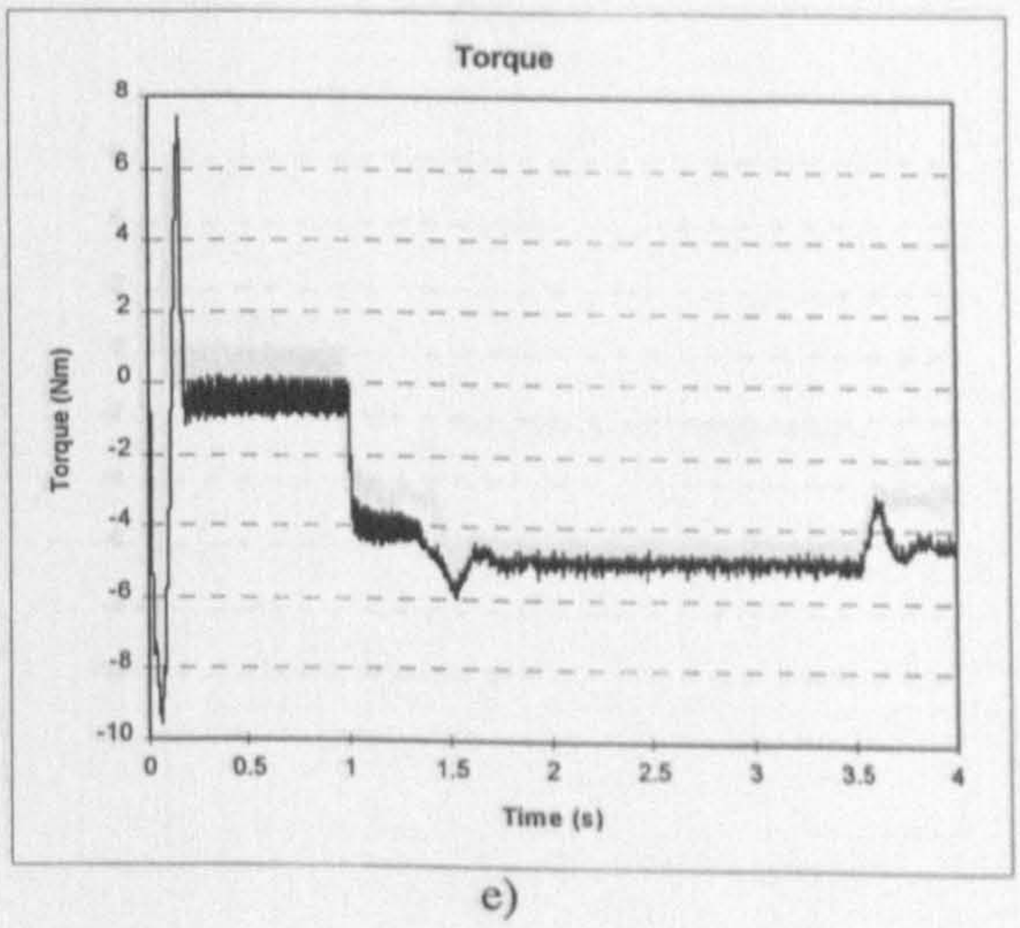

e)

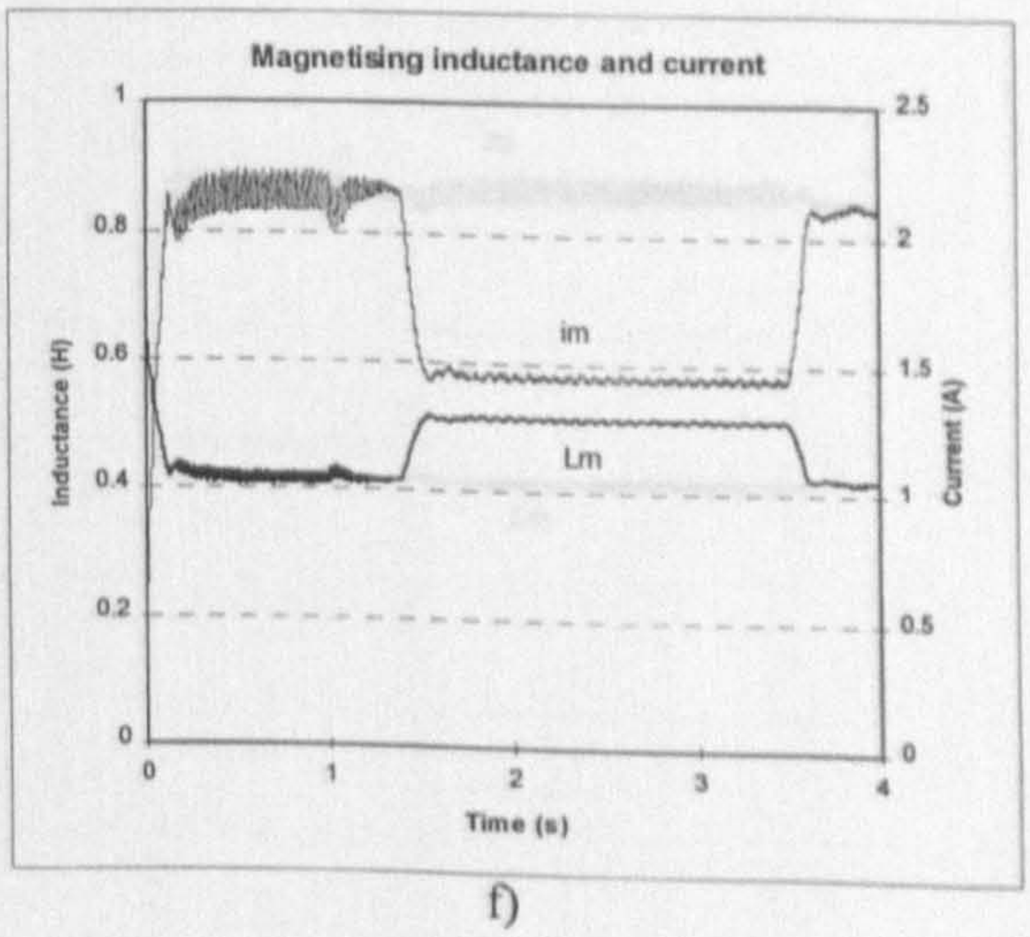

f)

Figure 7.7.4 Self-excitation, step load application and variable speed operation in the field weakening region (stator flux oriented control), trace as in Figure 7.7.2

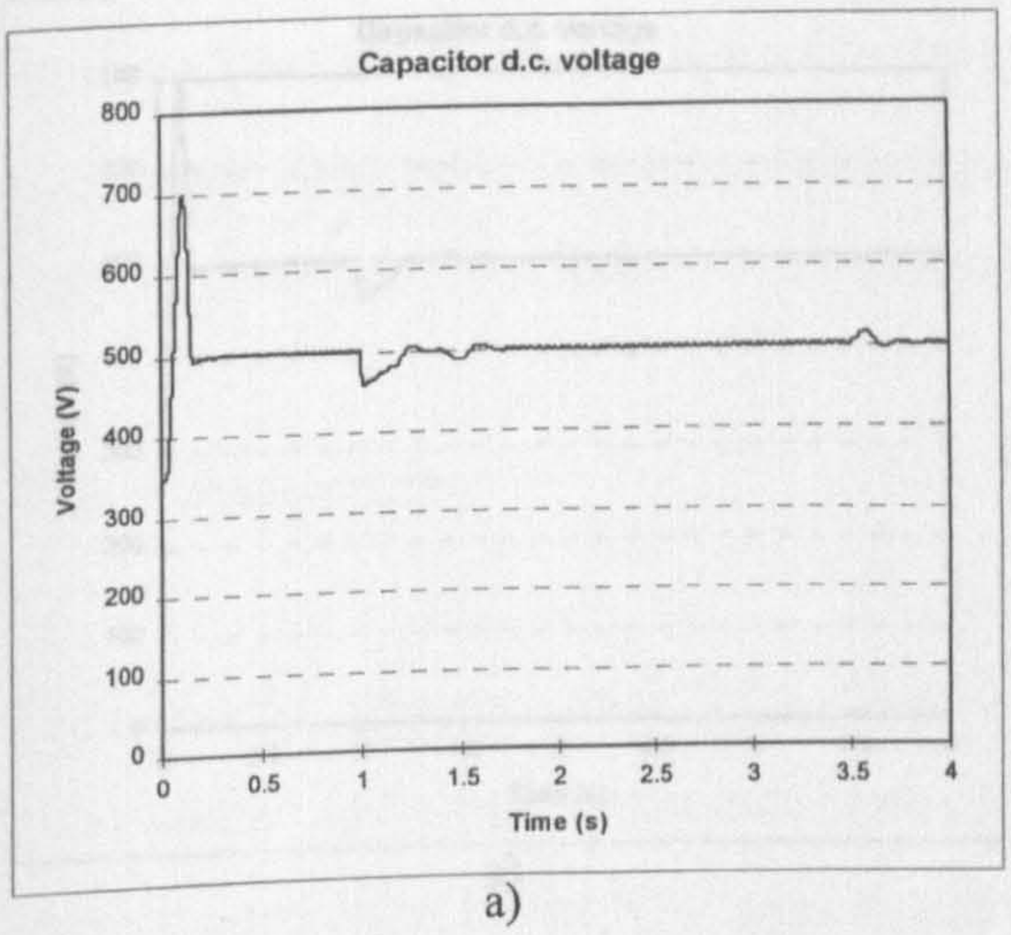

a)

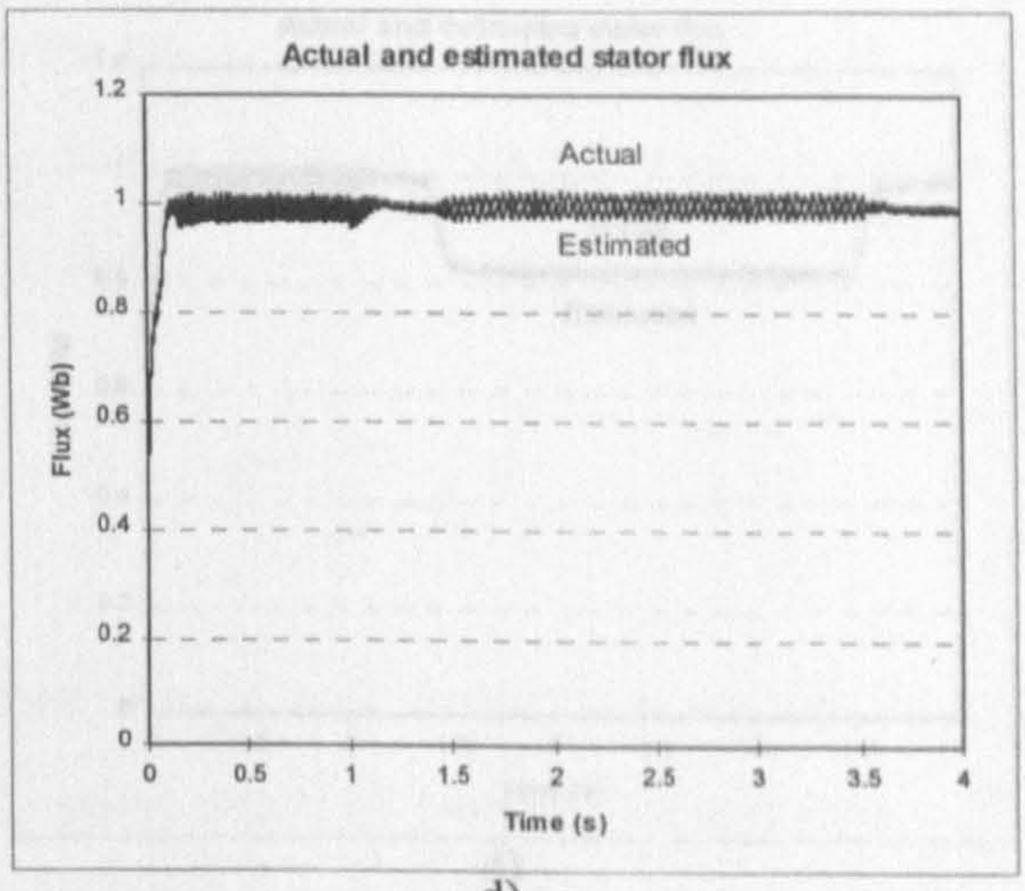

d)

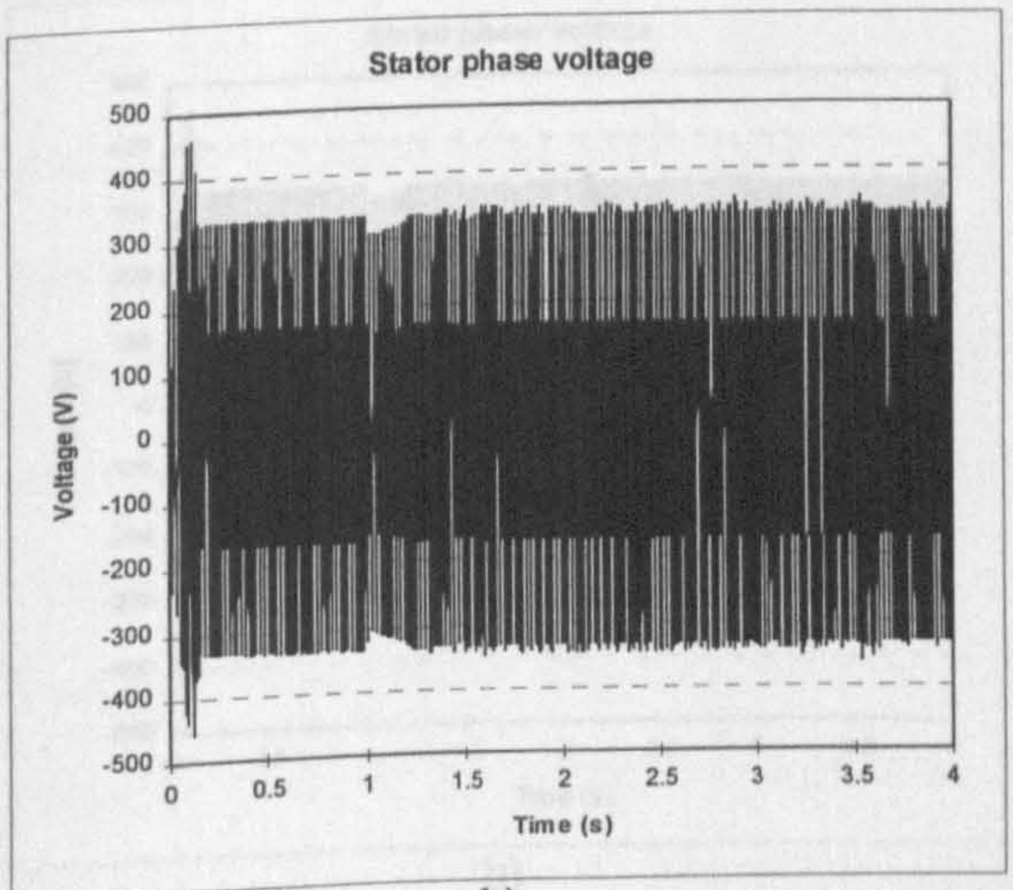

b)

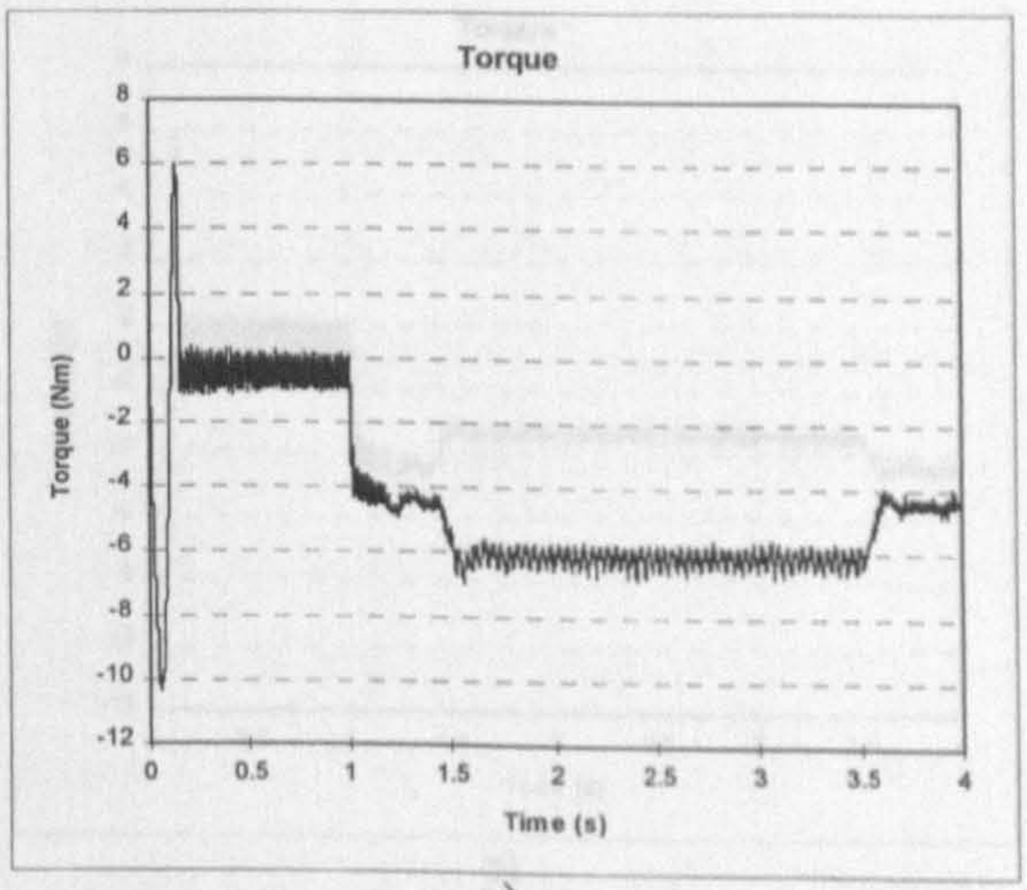

e)

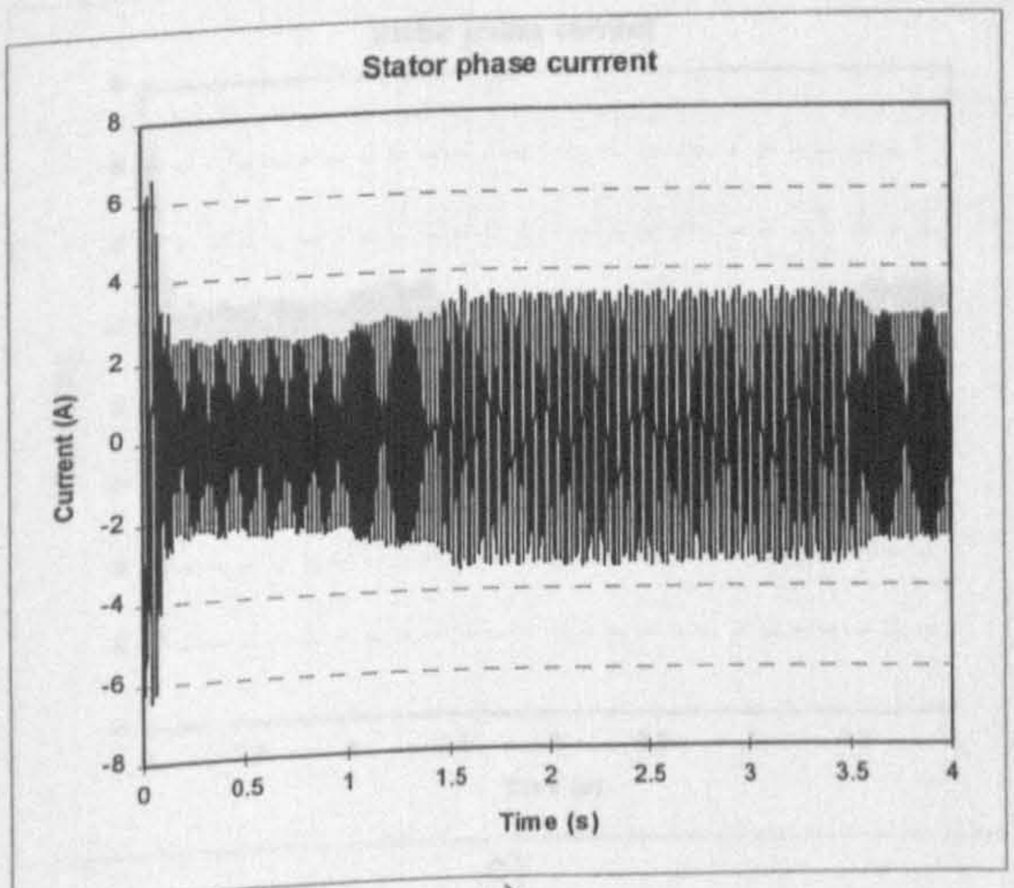

c)

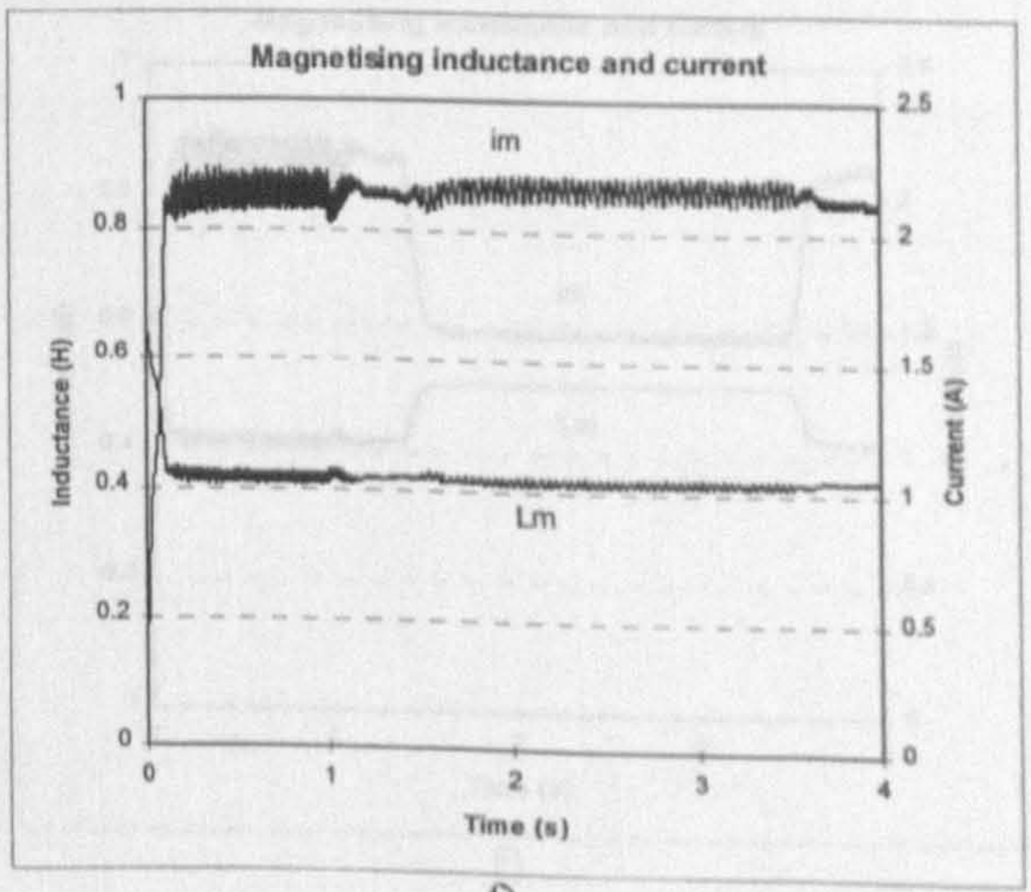

f)

Figure 7.7.5 Self-excitation, step load application and variable speed operation in the base speed region (stator flux oriented control with start-up battery), trace as in Figure 7.7.2

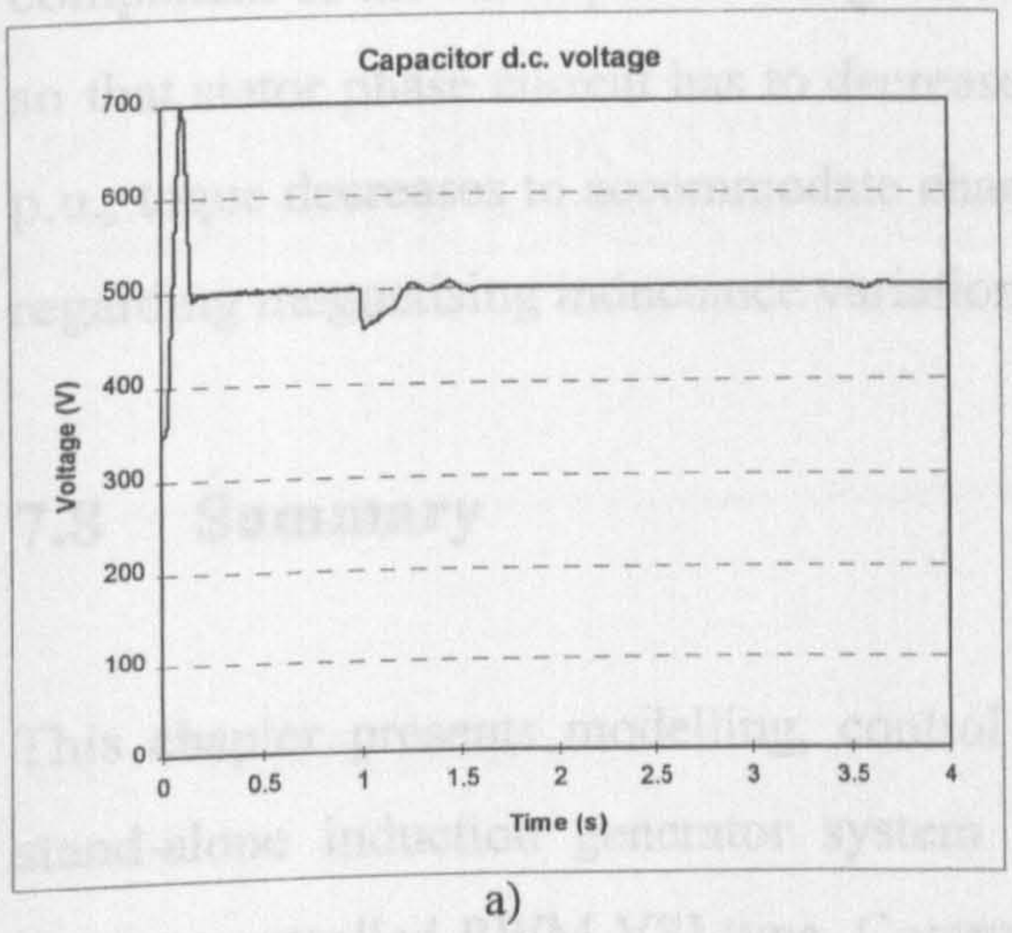

a)

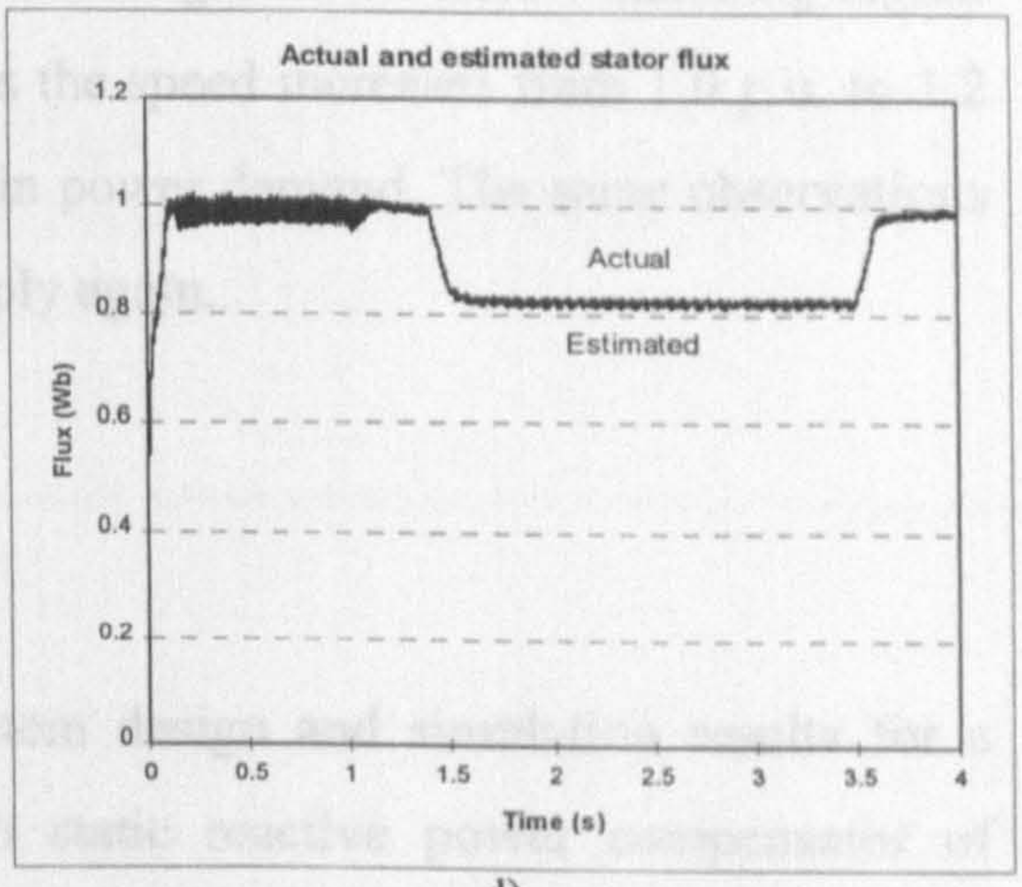

d)

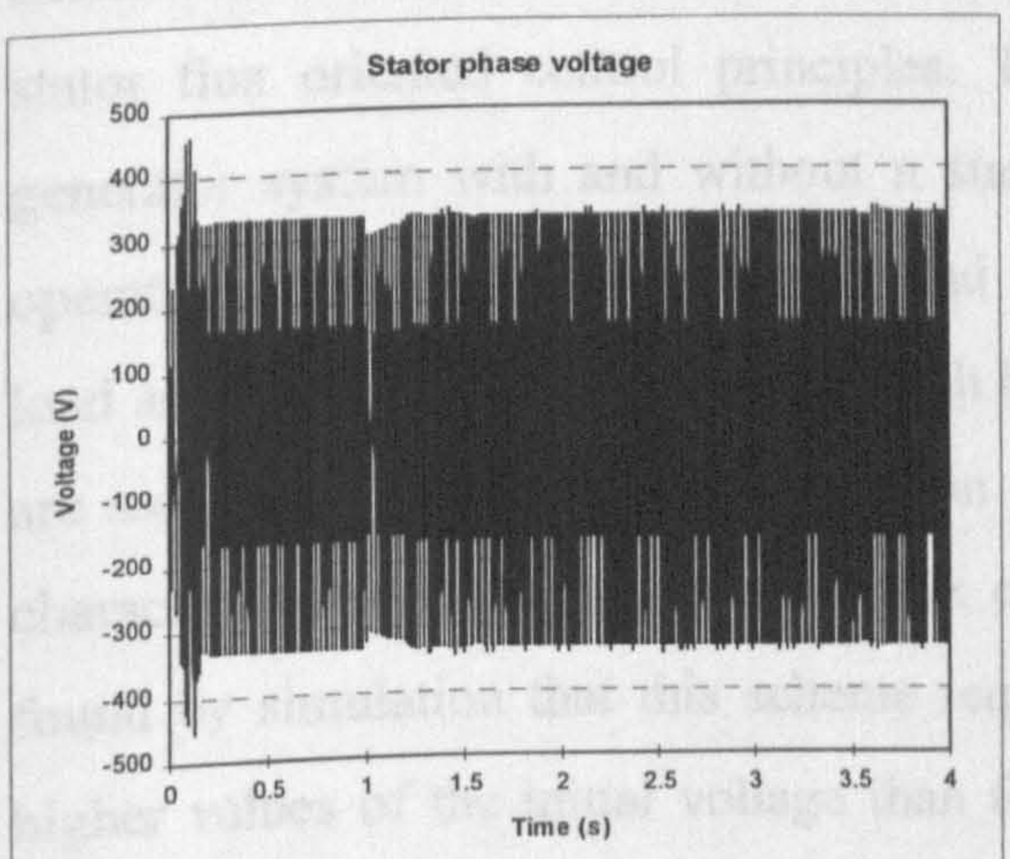

b)

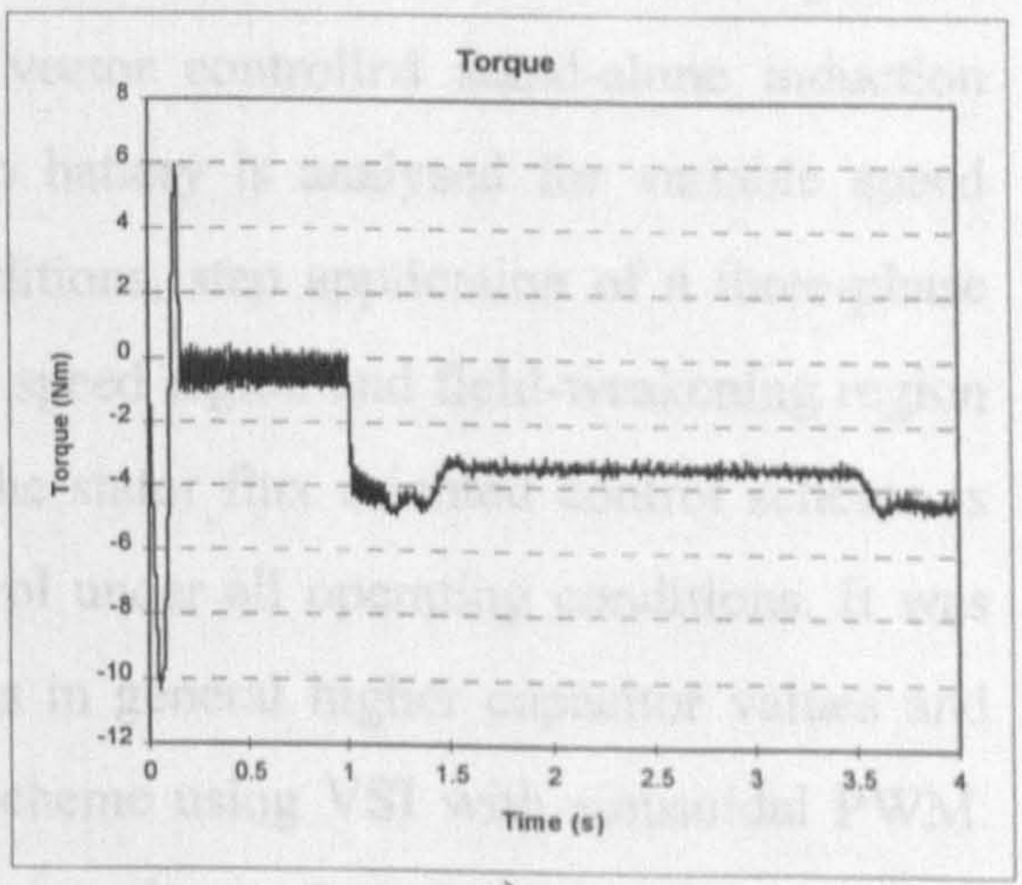

e)

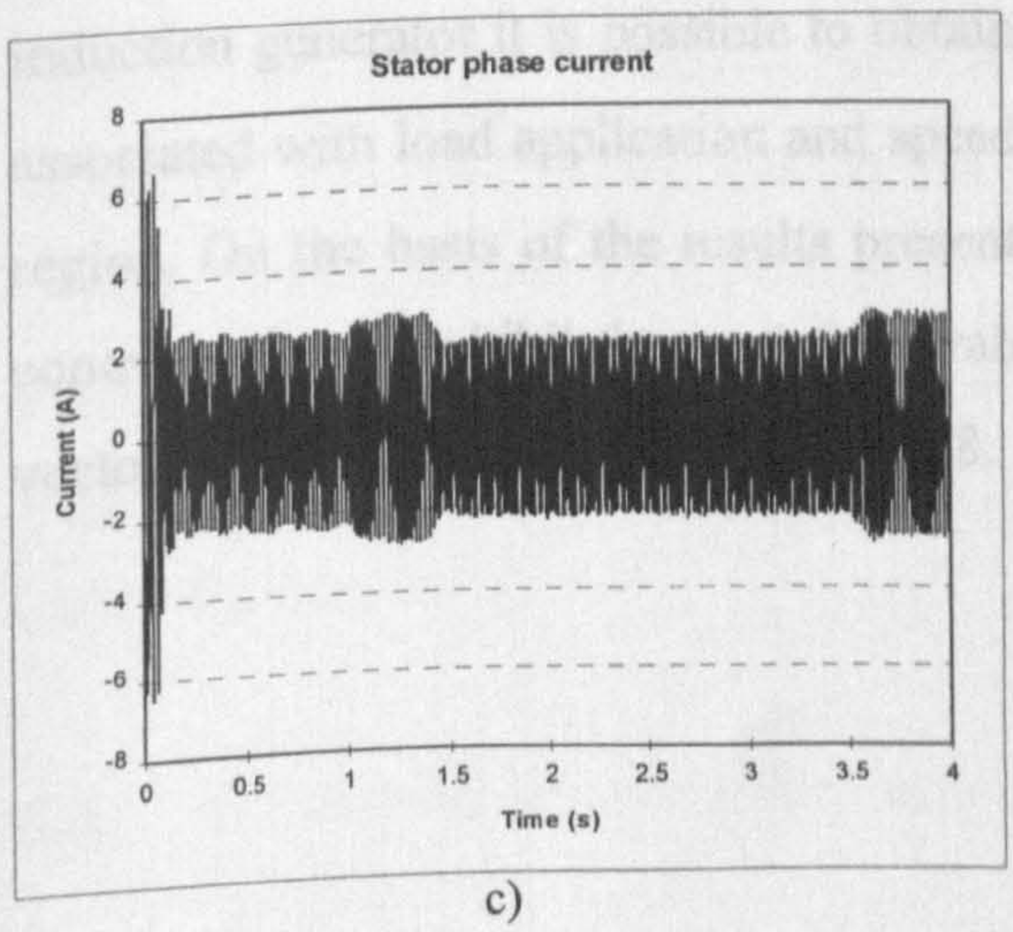

c)

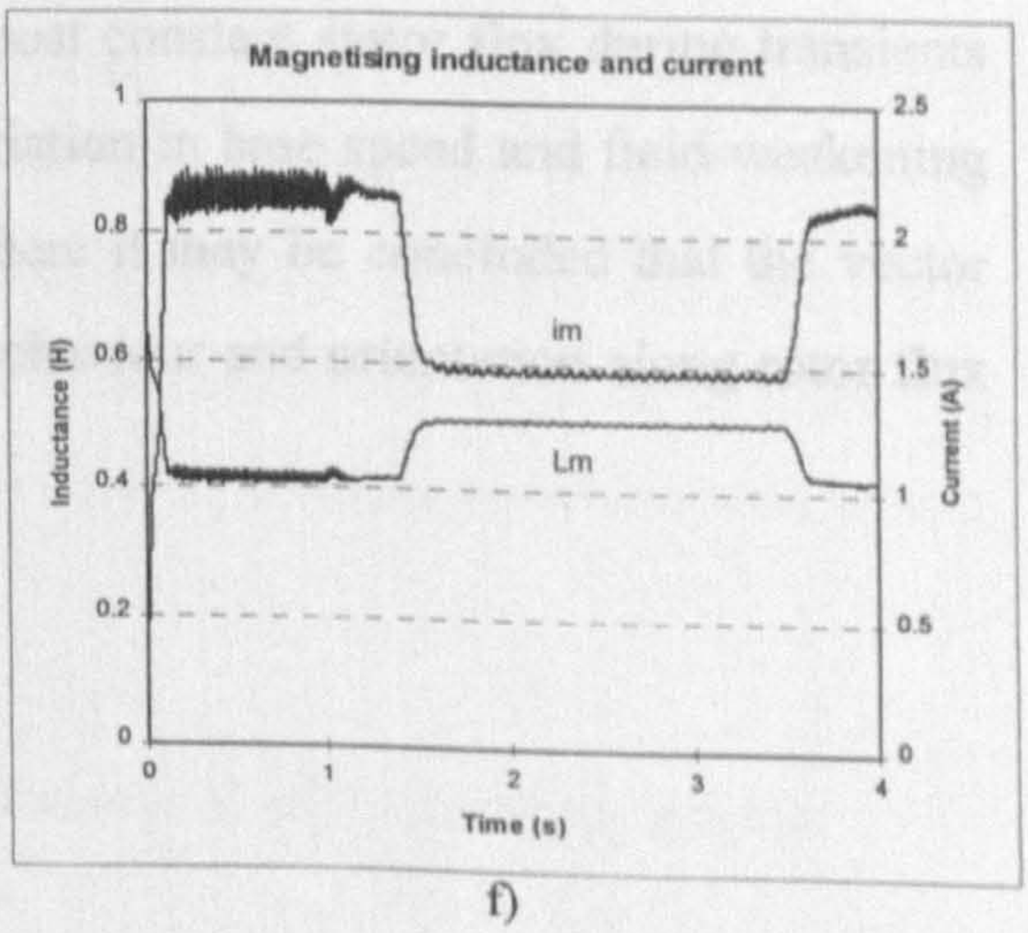

f)

Figure 7.7.6 Self-excitation, step load application and variable speed operation in the field weakening region (stator flux oriented control with start-up battery), trace as in Figure 7.7.2

component of the stator phase voltage remains unchanged in the field-weakening region so that stator phase current has to decrease. As the speed increases from 1.0 p.u. to 1.2 p.u., toque decreases to accommodate change in power demand. The same observations regarding magnetising inductance variation apply again.

7.8 Summary

This chapter presents modelling, control system design and simulation results for a stand-alone induction generator system with static reactive power compensator of current controlled PWM VSI type. Control of the compensator is achieved using direct stator flux oriented control principles. The vector controlled stand-alone induction generator system with and without a start-up battery is analysed for variable speed operations. Self-excitation under no-load conditions, step application of a three-phase load and variable speed operation in both base speed region and field-weakening region are studied by simulation. The operation of the stator flux oriented control scheme is characterised with very good stator flux control under all operating conditions. It was found by simulation that this scheme requires in general higher capacitor values and higher values of the initial voltage than the scheme using VSI with sinusoidal PWM. From the point of view of dynamics, simulation results confirm that in vector controlled induction generator it is possible to obtain almost constant stator flux during transients associated with load application and speed variation in base speed and field-weakening region. On the basis of the results presented here it may be concluded that the vector control schemes exhibit the most favourable behaviour and orientation along rotor flux vector is further investigated in Chapter 8.

Chapter 8

VECTOR, ROTOR FLUX ORIENTED, CONTROL OF A PWM VSI REACTIVE POWER COMPENSATOR FOR A STAND-ALONE INDUCTION GENERATOR

8.1 Introduction

The study presented in Chapter 7 has demonstrated that stator flux oriented control of a PWM VSI reactive power compensator offers a superior performance over scalar control of a PWM VSI in stand-alone induction generator applications. This chapter deals with a variable speed induction generator, aimed at supplying either an autonomous a.c. power system or an autonomous d.c. power system with constant d.c voltage, whose reactive power requirements are again met by a static reactive power compensator of voltage source inverter type. Control of the compensator is now achieved using rotor flux oriented control principles. Induction generator is represented with a saturated machine model with stator current and rotor flux d-q axis components as state-space variables and a novel, saturation adaptive, rotor flux estimator is used to achieve correct field orientation under all operating conditions. Two specific loading situations, load placed at a.c. side of the inverter and load placed at the d.c. side of the inverter, are considered. Dynamics of self-excitation process, step load application, load variation and variable speed operation are simulated. Excellent tracking of rotor flux reference is achieved under all operating conditions, including operation with speeds higher than rated.

8.2 Principles of rotor flux oriented control of induction motor drives

Principles of stator flux oriented control, as applied in motor drives, were reviewed in Section 7.2. This section presents similar review with regard to application of rotor flux oriented control in induction motor drives. Material presented in this section is

nowadays available in many books [Vas (1990), Boldea and Nasar (1992), Novotny and Lipo (1996), Trzynadlowski (1994), Leonhard (1996)]. Mathematical model of a rotor flux oriented induction motor is derived from the general space vector model, given in an arbitrary reference frame with the equations (3.2-1) - (3.2-3) and the electromagnetic torque is expressed in terms of rotor flux space vectors as

$$T_e = \frac{3}{2} P \frac{L_m}{L_r} \mathrm{Im}\{\underline{i}_s \underline{\psi}_r^*\} \qquad (8.2\text{-}1)$$

where * denotes complex conjugate.

As already noted, rotor flux oriented control can be achieved with both current fed and voltage fed induction motor drive. In practice, however, current-fed case is much more common as the resulting control system is simpler. For this reason only the principles of rotor flux oriented control, as applied in conjunction with current fed induction machine, are discussed here. Development of rotor flux oriented control scheme for an induction generator, that is to follow in Section 8.3 of this chapter, assumes that the machine is current-fed. If the machine can be regarded as current fed, stator voltage equation can be omitted from further consideration. It is therefore necessary to consider only rotor voltage equation (3.2-2) and torque equation (8.2-1).

Let the common reference frame be fixed to the rotor flux space vector and moreover, let the d-axis (real axis) of the common reference frame coincide with rotor flux space vector. Then,

$$\theta_s = \phi_r \qquad \theta_r = \phi_r - \theta \qquad \omega_a = \omega_r \qquad \omega_r = \frac{d\phi_r}{dt} \qquad (8.2\text{-}2)$$

Rotor flux space vector becomes real variable in this special frame of reference,

$$\underline{\psi}_r = \psi_{dr} + j\psi_{qr} = \psi_r \qquad (8.2\text{-}3a)$$

i.e., it follows that

$$\psi_{dr} = \psi_r \qquad \psi_{qr} = 0 \tag{8.2-3b}$$

Position of rotor flux and stator current space vectors in the common reference frame fixed to the rotor flux space vector is illustrated in Figure 8.2.1. Taking into account equations (8.2-3), equation (8.2-1) yields

$$T_e = \frac{3}{2} P \frac{L_m}{L_r} \psi_r \operatorname{Im}\{\underline{i}_s\} = \frac{3}{2} P \frac{L_m}{L_r} \psi_r i_{qs} \tag{8.2-4}$$

Torque equation (8.2-4) is of the same form as the torque equation met in DC machine theory and it shows that if the magnitude of the rotor flux is kept on constant value, torque can be independently controlled by stator q-axis current.

In order to accommodate rotor voltage equation to the chosen reference frame, rotor current space vector has to be expressed as

$$\underline{i}_r = \frac{\psi_r - L_m \underline{i}_s}{L_r} \tag{8.2-5}$$

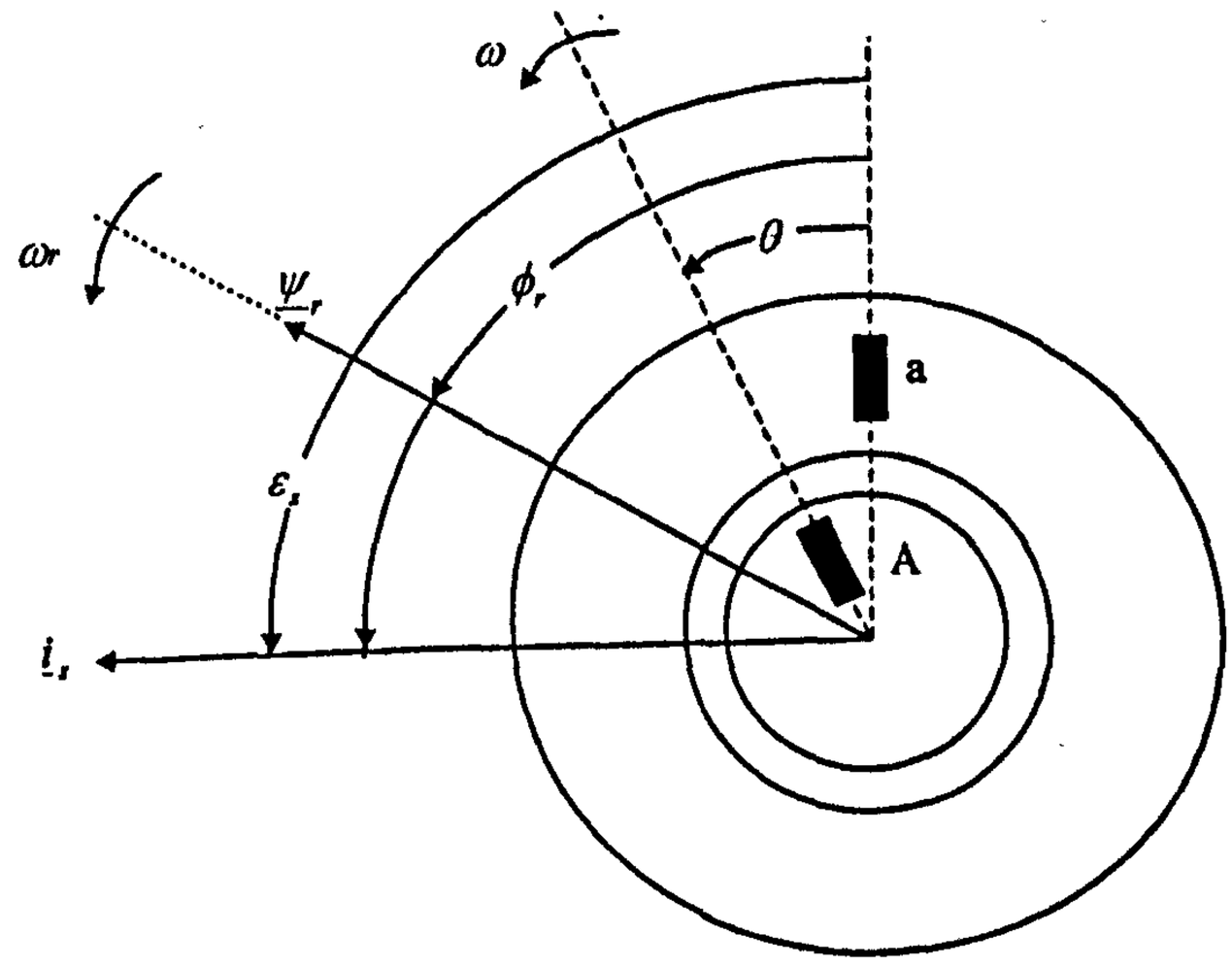

Figure 8.2.1 Illustration of space vectors in common reference frame fixed to the rotor flux space vector

The following rotor voltage equation is obtained by substituting (8.2-5) into (3.2-2):

$$0 = \frac{1}{T_r}\psi_r + \frac{d\psi_r}{dt} + j(\omega_r - \omega)\psi_r - \frac{1}{T_r}L_m \underline{i}_s \tag{8.2-6}$$

where $T_r = L_r / R_r$.

Separation into real and imaginary part yields

$$\psi_r + T_r \frac{d\psi_r}{dt} = L_m i_{ds} \tag{8.2-7}$$

$$(\omega_r - \omega)\psi_r T_r = L_m i_{qs} \tag{8.2-8}$$

Equation (8.2-7) reveals that, in this special common reference frame fixed to the rotor flux space vector, magnitude of rotor flux can be controlled by stator d-axis current and that magnitude of rotor flux is constant if the stator d-axis current is constant. According to equation (8.2-8) angular slip frequency $\omega_{sl} = \omega_r - \omega$ is linearly dependent on stator q-axis current if the magnitude of rotor flux is constant. Consequently, developed torque is proportional to slip frequency. If the stator d-axis current is held constant, torque can be instantaneously altered if it is possible to change stator q-axis instantaneously. Illustration of flux and torque production in a current fed rotor flux oriented induction machine is given in Figure 8.2.2. From Figure 8.2.2 it directly follows that rotor flux amplitude is controllable by stator d-axis current component only. The control system has to operate in rotor flux oriented reference frame if decoupled flux and torque control is to be achieved, while actual machine operates in stationary phase domain. Coordinate transformation is therefore necessary. A schematic representation of a current-fed induction machine with rotor flux oriented control is given in Figure 8.2.3. Block denoted as CRPWM represents current regulated PWM inverter, speed drive is shown, and provision for operation in field-weakening region is included. The configuration of the drive displayed in Figure 8.2.3 corresponds to category of direct orientation schemes. Structures of rotor flux estimators, that provide information regarding rotor flux amplitude and position, as well as a torque estimate, are dealt with in Section 8.4.

Rotor flux oriented control can be achieved by indirect orientation as well, where position of the rotor flux space vector is estimated again on the grounds of induction

machine model in rotor flux oriented reference frame. In order to achieve orientation it

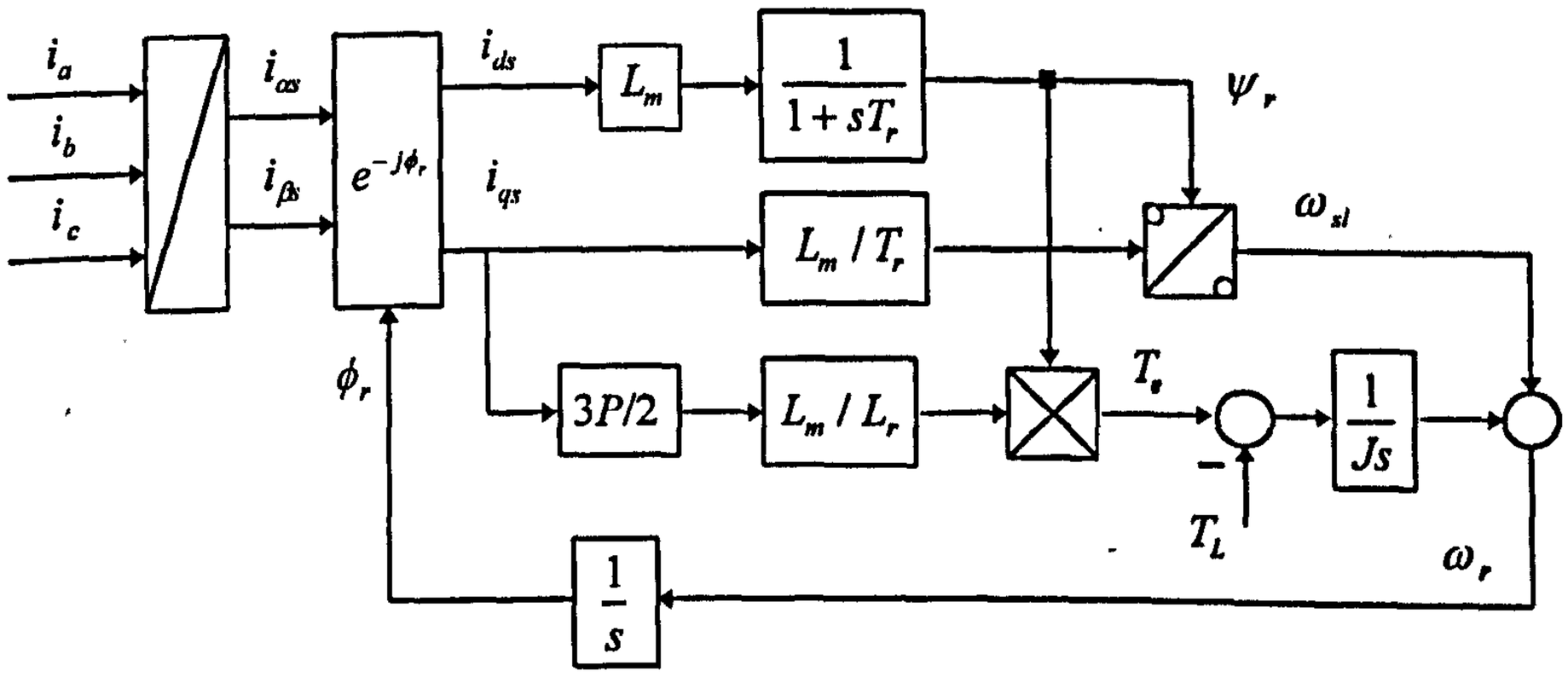

Figure 8.2.2 Block diagram of an ideal current fed rotor flux oriented induction machine (friction torque is neglected and s represents Laplace operator)

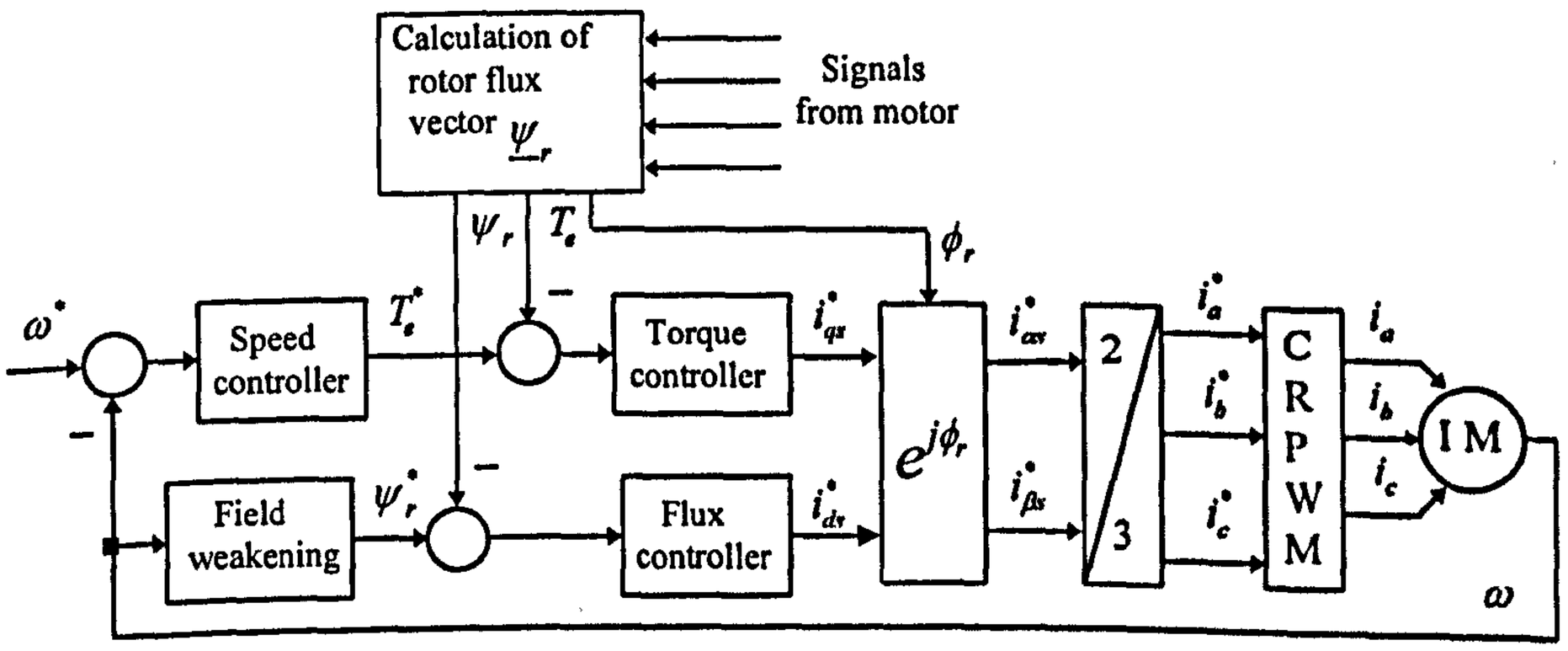

Figure 8.2.3 Current-fed rotor flux oriented induction machine

is theoretically necessary to measure only rotor speed or position. All the other required quantities are calculated in a feed-forward manner, using reference stator d-q axis current values. Indirect vector controlled induction machine is conventionally fed from current-regulated PWM inverter and current control is performed in the stationary reference frame. Indirect orientation relies on equations (8.2-4), (8.2-7), (8.2-8), that are used to determine reference values of stator d-q axis current components and reference angular slip frequency:

$$i_{qs}^* = \frac{2}{3P}\frac{T_e^*}{\psi_r^*}\frac{L_r}{L_m}$$
$$i_{ds}^* = \frac{1}{L_m}(\psi_r^* + T_r\frac{d\psi_r^*}{dt}) \qquad (8.2\text{-}9)$$

$$\omega_{sl}^{*} = \frac{L_m}{T_r}\frac{i_{qs}^{*}}{\psi_r^{*}} \qquad (8.2\text{-}10)$$

$$\phi_r = \int(\omega_{sl}^{*} + \omega)dt$$

Indirect rotor flux oriented controller is illustrated in Figure 8.2.4, where asterisk denotes reference quantities.

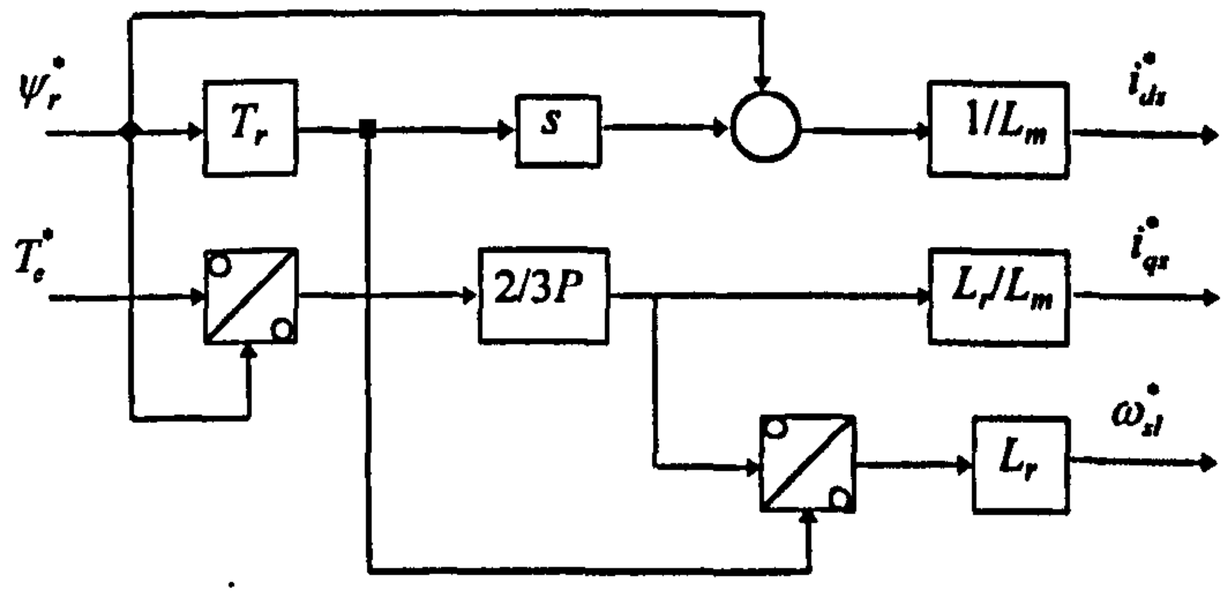

Figure 8.2.4 Principle of indirect rotor flux oriented control of a current-fed induction machine

Prevailing applications are for drives that require operation in the base speed range only. Consequently, only operation in the constant flux region is needed and the scheme can be further simplified. Such a drive is shown in Figure 8.2.5, where due to ψ_r^* = constant, $i_{ds}^* = \psi_r^* / L_m$ is a constant as well. Torque command (or stator q-axis current

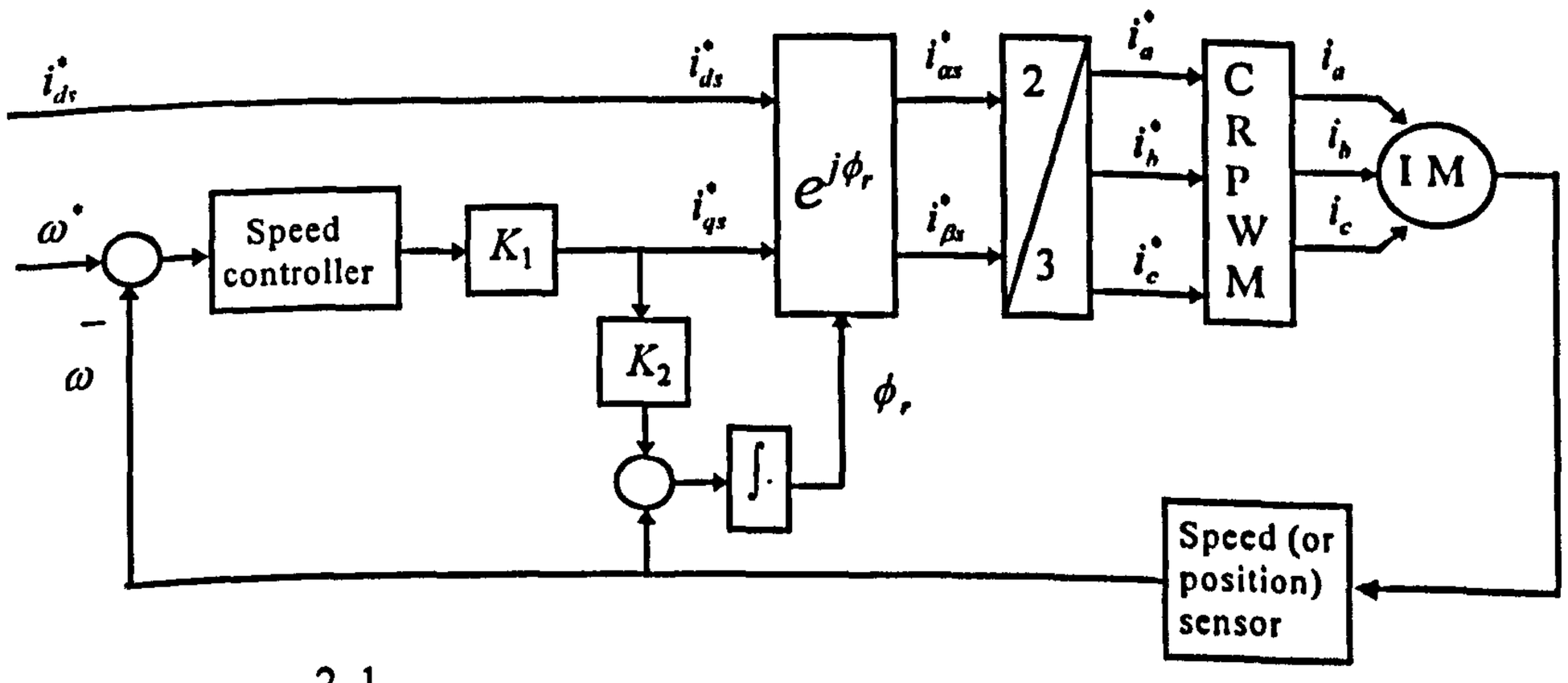

$$K_1 = \frac{2}{3}\frac{1}{P}(L_r / L_m^2)(1 / i_{ds}^*) \qquad K_2 = (1 / T_r)(1 / i_{ds}^*)$$

Figure 8.2.5 Current-fed induction machine with indirect rotor flux oriented control in the base speed region only

command) is obtained as output from the speed controller. Indirect vector control has gained enormous popularity in practical realisations as the overall control system complexity is significantly reduced compared to direct orientation methods.

8.3 Rotor flux oriented control system of an induction generator

Vector controlled induction generator operated in variable speed mode can be used to supply an autonomous power system consisting of either a.c. load [Lyra et al (1995), Miranda et al (1997)] or d.c. load [Silva and Lyra (1993), (1995)]. Rotor flux oriented stand-alone induction generators feeding both a.c. and d.c. loads are studied here and treated separately. In the case of a.c. loads, the generator can be used to supply frequency insensitive loads such as lighting, resistive heating and water pumping, which are connected at the a.c. side of the inverter. The generator can also be used to supply d.c. loads like battery chargers with constant voltage, which are connected at the d.c. side of the inverter. If three-phase 50 Hz constant voltage is required, the second PWM VSI will be connected to the d.c. link [Jones and Smith (1993), Jones and Gilmore (1995)]. It is possible to produce a unity power factor supply at the a.c. side of the second converter. In this case, the d.c. link voltage has to be kept constant over a wide range of speeds in order to provide high quality three-phase sinusoidal supply. This scheme, composed of two PWM VSIs, is however beyond the scope of the research presented here.

8.3.1 Rotor flux oriented induction generator supplying a.c. load

Control of the PWM VSI static reactive power compensator is depicted in Figure 8.3.1. A three-phase a.c. load is connected at the a.c. side of the inverter. Induction generator phase currents are measured and used for both vector control algorithm and for hysteresis current control algorithm. Additionally, rotor speed of the machine and d.c. voltage across capacitor are measured as well and used in the vector control algorithm. Rotor flux reference is an independent input into the vector control block. It is constant and equal to rated rotor flux in the base speed region. In the field weakening rotor flux reference is reduced inversely proportionally to the speed of rotation. Hysteresis current

controllers are the same as those described in Chapter 7. Resistance R_{DC} in this case represents the power loss in the compensator and on the d.c. side of the inverter.

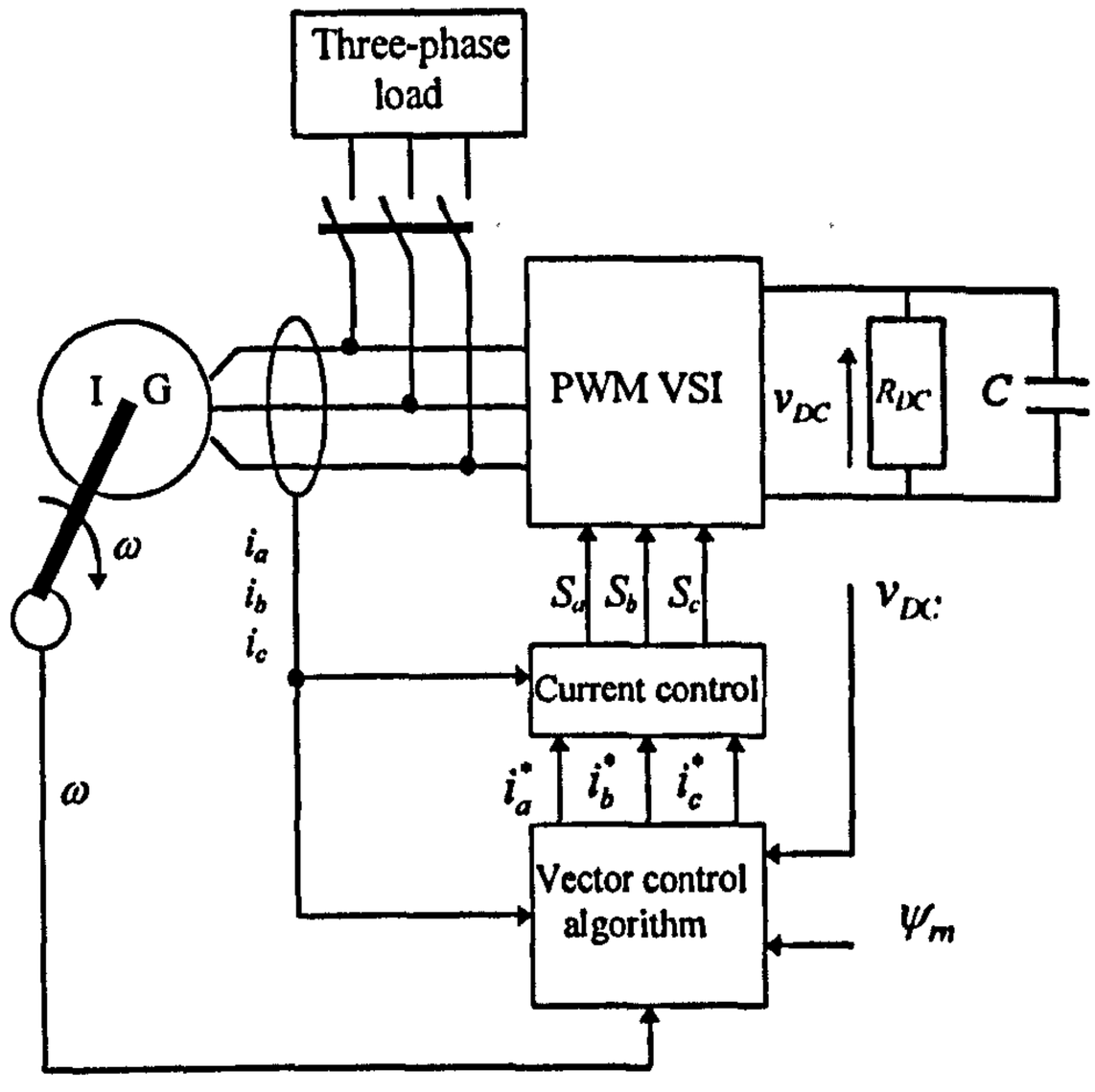

Figure 8.3.1 Configuration of the rotor flux oriented control scheme for an induction generator supplying a.c. load

Vector control algorithm is illustrated in Figure 8.3.2 and it belongs to the group of direct orientation schemes. It consists of two branches that operate in parallel and enable creation of stator phase current references. Compared with the corresponding control scheme for an induction motor drive, Figure 8.2.3, one can notice that rotor flux path remains the same. Current reference for d-axis is thus created in the same way as for a drive system. However, creation of q-axis current reference is now done using a d.c. voltage PI controller instead of a speed controller. This is the consequence of the generating role of the machine in this application. In a motor drive d.c. voltage is determined with mains and hence fixed, while speed is an independent controllable input. In a generating system speed is determined with a turbine and is hence not controllable, while d.c. voltage is, due to absence of the mains, an independent controllable input.

Current reference for d-axis is created by means of closed loop rotor flux amplitude control and it enables excitation of the machine. This control loop controls reactive power flow in the system. The second branch creates q-axis current reference by means

of closed loop control of the capacitor voltage v_{DC}. This control loop enables active power flow from the generator to the d.c. circuit and enables active power loss in resistor R_{DC} (i.e., loss in the d.c. circuit and in the inverter) to be covered. Inversion of the sign of the q-axis current reference accounts for the fact that active power flow is

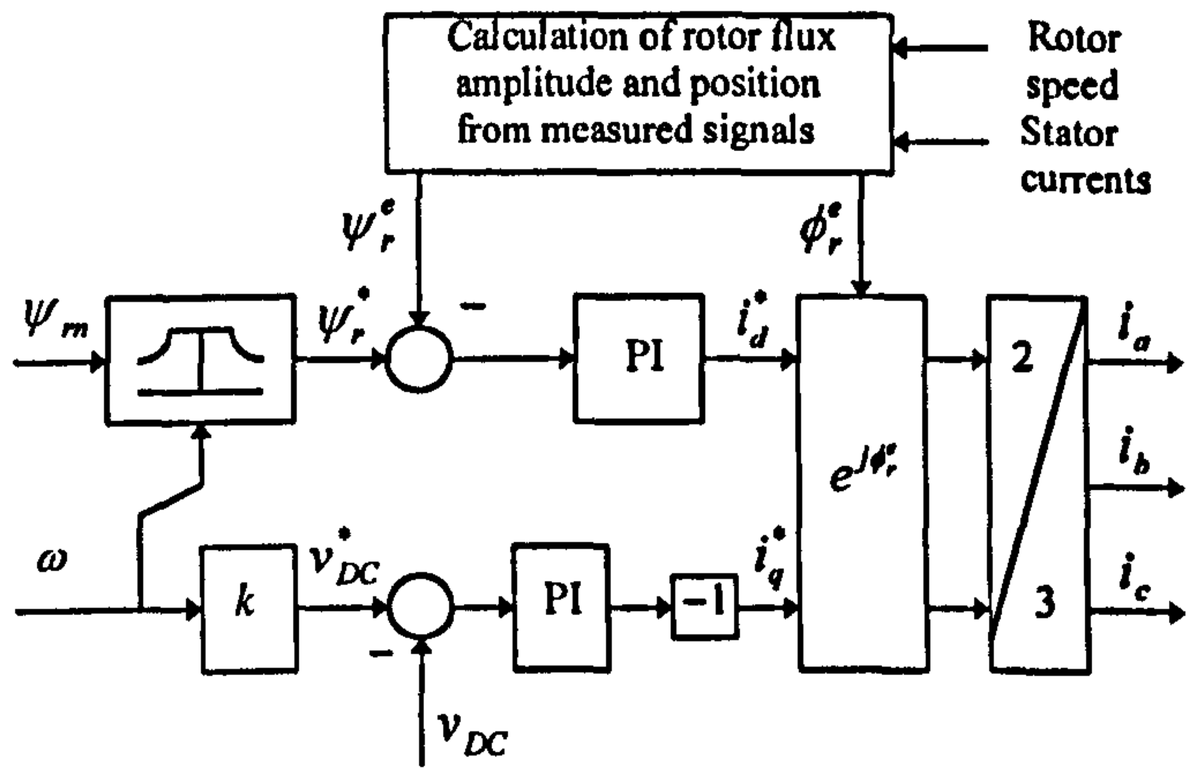

Figure 8.3.2 Outlay of the block 'Vector control algorithm' of Figure 8.3.1

from a.c. to d.c. side of the converter. Capacitor voltage reference value is proportional to the speed of rotation and is continuously varied in variable speed operation. Control system operates in rotor flux oriented reference frame and information about rotor flux space vector instantaneous angular position is obtained from the block 'Calculation of rotor flux and position', whose structure is described in Section 8.5 (superscript e denotes estimated values, while asterisk stands for reference values). It suffices to say for the time being that rotor flux estimation is performed in rotor flux oriented reference frame, from measured stator currents and rotor speed. Rotor flux controller and d.c. voltage controller are both of PI type.

8.3.2 Rotor flux oriented induction generator supplying d.c. load

The outlay of the system is shown in Figure 8.3.3. The load is now connected at d.c. side of the converter (resistance R_{DC}). The PWM VSI provides reactive power for the generator, while generator supplies active power to the load R_{DC}. A battery E is used for start-up purposes. Inverter firing signals are obtained on the basis of closed-loop hysteresis current control algorithm in stationary reference frame. Control scheme of the

PWM VSI static reactive power compensator is depicted in Figure 8.3.4 (battery of Figure 8.3.3 is omitted) and it is essentially identical to the one of Figure 8.3.1, except for the placement of the load.

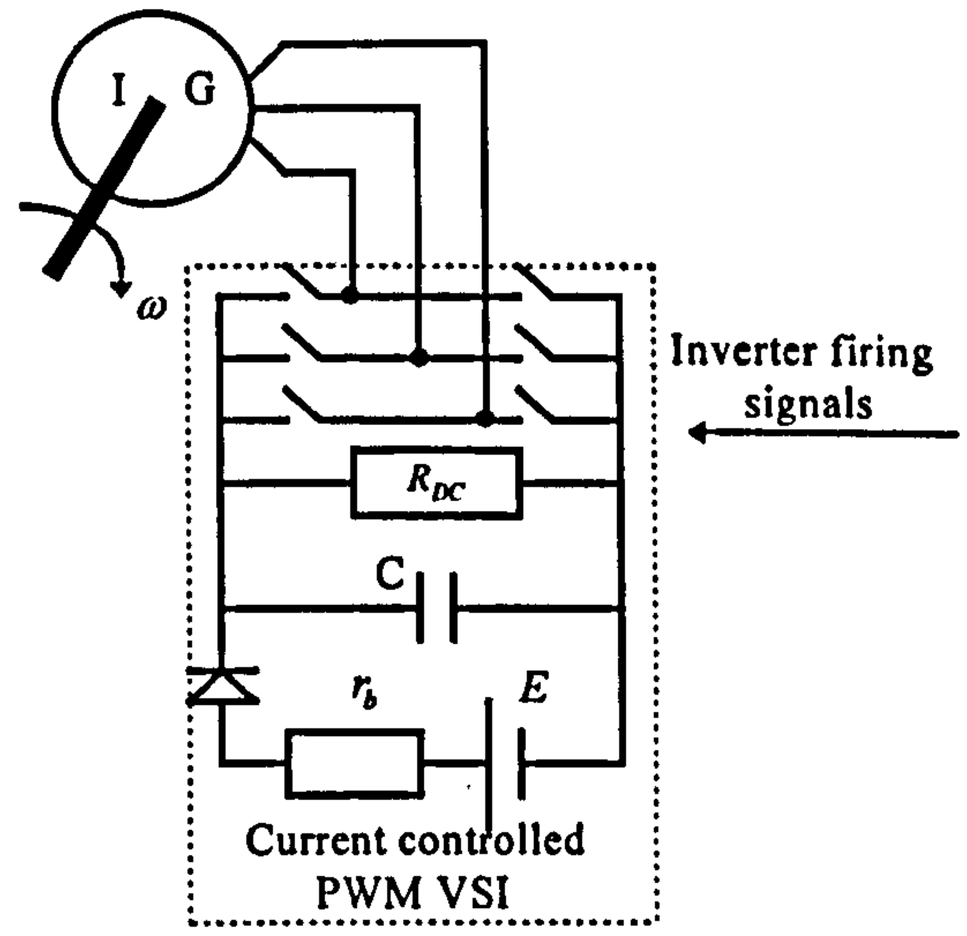

Figure 8.3.3 Induction generator with PWM VSI supplying d.c. load

Vector control algorithm is illustrated in Figure 8.3.5 and it again consists of two branches that operate in parallel and enable creation of stator phase current references. Current reference for d-axis is once more created by closed loop rotor flux amplitude control, in the same way as in Figure 8.3.2. The second branch again creates q-axis current reference by closed loop control of the capacitor voltage v_{DC} . This control loop

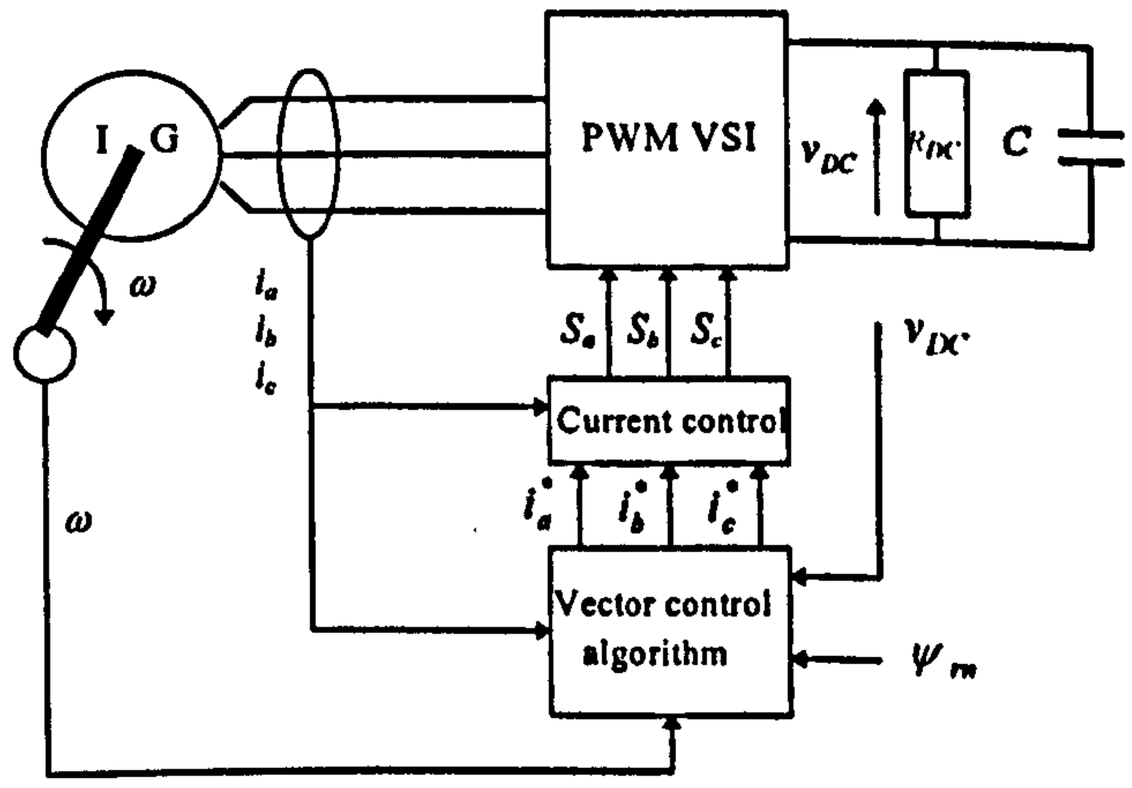

Figure 8.3.4 Configuration of the rotor flux oriented control scheme for an induction generator supplying d.c. load

enables active power flow from the generator to the d.c. circuit and enables supply of generated active power to the resistive load R_{DC}. Structure of this control path however

differs from the one shown in Figure 8.3.2. The role of this part of the control system is to keep d.c. voltage across the load and capacitor at constant value, regardless of the speed of rotation. Required d.c. voltage is therefore constant input into the control system. Output of the PI d.c. voltage controller represents active power demand P^*_{act}, which is divided with measured speed of rotation in order to create an appropriate torque demand [Colliez et al (1997)]]. Torque command is further divided with a signal obtained from the rotor flux estimator, so that stator q-axis current command is created. Inversion of the sign of the q-axis current reference is again included. Rotor flux estimation is performed in rotor flux oriented reference frame, from measured stator currents and rotor speed and the estimator fully accounts for main flux saturation. Detailed description of this estimator is given later in Section 8.5. Estimator additionally provides signal used to create stator q-axis current reference from torque reference in the d.c. voltage control channel.

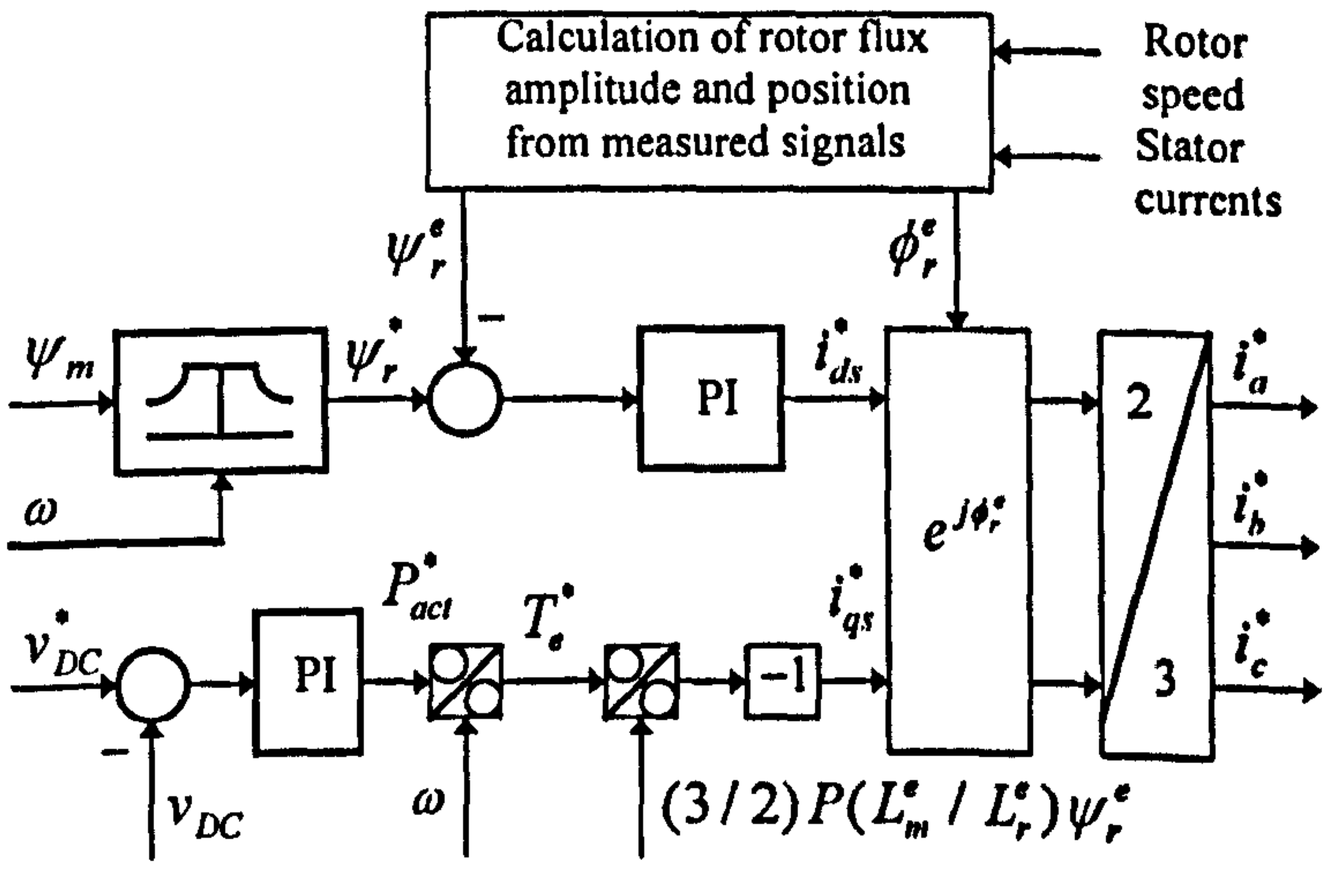

Figure 8.3.5 Block 'Vector control algorithm' of Figure 8.3.4

8.4 Estimation of rotor flux space vector

Numerous rotor flux space vector estimation techniques exist nowadays [Vas (1990), Boldea and Nasar (1992), Novotny and Lipo (1996), Trzynadlowski (1994), Leonhard (1996)]. If the values of stator current components and main flux components in the stationary reference frame, $i_{\alpha s}, i_{\beta s}$ and $\psi_{\alpha m}, \psi_{\beta m}$, are determined from the sensed signals (ψ_m - i_s estimator), magnitude and position of the rotor flux space vector can be

obtained from equation (3.2-3a), taking into account that

$$\psi_{\alpha m} = L_m i_{\alpha m} \qquad \psi_{\beta m} = L_m i_{\beta m} \tag{8.4-1}$$

$$i_{\alpha m} = i_{\alpha s} + i_{\alpha r} \qquad i_{\beta m} = i_{\beta s} + i_{\beta r} \tag{8.4-2}$$

according to the following equations:

$$\psi_{\alpha r} = (1+\sigma_r)\psi_{\alpha m} - L_{\sigma r} i_{\alpha s} \qquad \psi_{\beta r} = (1+\sigma_r)\psi_{\beta m} - L_{\sigma r} i_{\beta s} \tag{8.4-3}$$

$$\psi_r = \sqrt{\psi_{\alpha r}^2 + \psi_{\beta r}^2} \qquad \cos\varphi_r = \frac{\psi_{\alpha r}}{\psi_r} \qquad \sin\varphi_r = \frac{\psi_{\beta r}}{\psi_r} \tag{8.4-4}$$

where $\sigma_r = L_{\sigma r} / L_m$.

Torque equation can be given as a function of the measured variables,

$$T_e = \frac{3}{2} P(\psi_{\alpha m} i_{\beta s} - \psi_{\beta m} i_{\alpha s}) \tag{8.4-5}$$

The advantage of the ψ_m - i_s estimator is that acquisition of the rotor speed or position signal is not needed for the estimation procedure. However, main flux has to be sensed and this requires physical modification of the machine. This method is therefore rarely used nowadays.

The second rotor flux space vector estimation method asks for measurement of stator voltages and stator currents (v_s - i_s estimator). If the stator phase currents and voltages are sensed and transformed into two-phase stationary reference frame, magnitude and position of the rotor flux space vector can be calculated either by means of analog or digital circuitry. Model of an induction machine in stationary reference frame ($\omega_a = 0$) is given from (3.2-1)- (3.2-2) as

$$v_{\alpha s} = R_s i_{\alpha s} + \frac{d\psi_{\alpha s}}{dt} \qquad v_{\beta s} = R_s i_{\beta s} + \frac{d\psi_{\beta s}}{dt} \tag{8.4-6}$$

$$v_{\alpha r} = R_r i_{\alpha r} + \frac{d\psi_{\alpha r}}{dt} + \omega\psi_{\beta r} \qquad v_{\beta r} = R_r i_{\beta r} + \frac{d\psi_{\beta r}}{dt} - \omega\psi_{\alpha r} \tag{8.4-7}$$

$$T_e = \frac{3}{2} P(\psi_{\alpha s} i_{\beta s} - \psi_{\beta s} i_{\alpha s}) \tag{8.4-8}$$

and it, together with flux linkage equation (3.2-3a), suggests the following procedure:

$$\psi_{\alpha s} = \int (v_{\alpha s} - R_s i_{\alpha s}) dt \qquad \psi_{\beta s} = \int (v_{\beta s} - R_s i_{\beta s}) dt \tag{8.4-9}$$

$$\psi_{\alpha r} = (1+\sigma_r)\psi_{\alpha s} - \sigma \frac{L_s L_r}{L} i_{\alpha s} \qquad \psi_{\beta r} = (1+\sigma_r)\psi_{\beta s} - \sigma \frac{L_s L_r}{L_m} i_{\beta s} \tag{8.4-10}$$

$$\psi_r = \sqrt{\psi_{\alpha r}^2 + \psi_{\beta r}^2} \qquad \cos\phi_r = \frac{\psi_{\alpha r}}{\psi_r} \qquad \sin\phi_r = \frac{\psi_{\beta r}}{\psi_r} \tag{8.4-11}$$

where $\sigma = 1 - L_m^2 / L_s L_r$.

Equation for torque calculation (8.4-8) remains unchanged,

$$T_e = \frac{3}{2} P(\psi_{\alpha s} i_{\beta s} - \psi_{\beta s} i_{\alpha s}) \tag{8.4-8}$$

The shortcoming of the above method is that integration is involved, according to Equation (8.4-9). This restricts practical implementations of the estimator to drives which are not aimed for operation with zero speed. Typical limit is frequency value of 3 Hz. Comparative analysis of ψ_m - i_s and v_s - i_s estimators reveals that their behaviour is practically identical at frequencies above 10 Hz, while at low frequencies ψ_m - i_s estimator is advantageous and can be used down to the frequency of 0.5 Hz [Vas (1990)]. Typical applications of v_s - i_s estimator are correlated with drives where speed and position sensors are to be avoided.

The most frequently used method of rotor flux space vector estimation asks for measurement of the stator currents and rotor speed or position (i_s - ω estimator). The main reasons for such a widespread application of this scheme are that there is no need for special construction or modification of the machine, integration is avoided and estimation is operational at zero speed. Estimation of rotor flux space vector by means of measured stator currents and rotor speed (position) utilises the model of an induction machine in rotor flux oriented reference frame. If the common reference frame is fixed

to the rotor flux space vector and d-axis of the common reference frame coincides with rotor flux space vector, then the machine is described, from Section 8.2, with

$$T_e = \frac{3}{2} P \frac{L_m}{L_r} \psi_r i_{qs} \tag{8.2-4}$$

$$\psi_r + T_r \frac{d\psi_r}{dt} = L_m i_{ds} \tag{8.2-7}$$

$$(\omega_r - \omega)\psi_r T_r = L_m i_{qs} \tag{8.2-8}$$

Equations (8.2-7) and (8.2-8) can be rewritten as

$$i_{ds} = (i_{mr} + T_r \frac{di_{mr}}{dt}) \tag{8.4-12}$$

$$\omega_{sl} = \frac{i_{qs}}{T_r i_{mr}} \tag{8.4-13}$$

where $i_{mr} = \psi_r / L_m$ is the equivalent rotor magnetising current.

Spatial position of the rotor flux space vector is determined with

$$\phi_r = \int (\omega_{sl} + \omega) dt \tag{8.4-14}$$

Equations (8.2-4), (8.4-12), (8.4-13) and (8.4-14) are used to calculate estimates of torque, rotor flux amplitude and rotor flux position. Block diagram of the corresponding i_s - ω rotor flux estimator is shown in Figure 8.4.1. Magnetising inductance is assumed

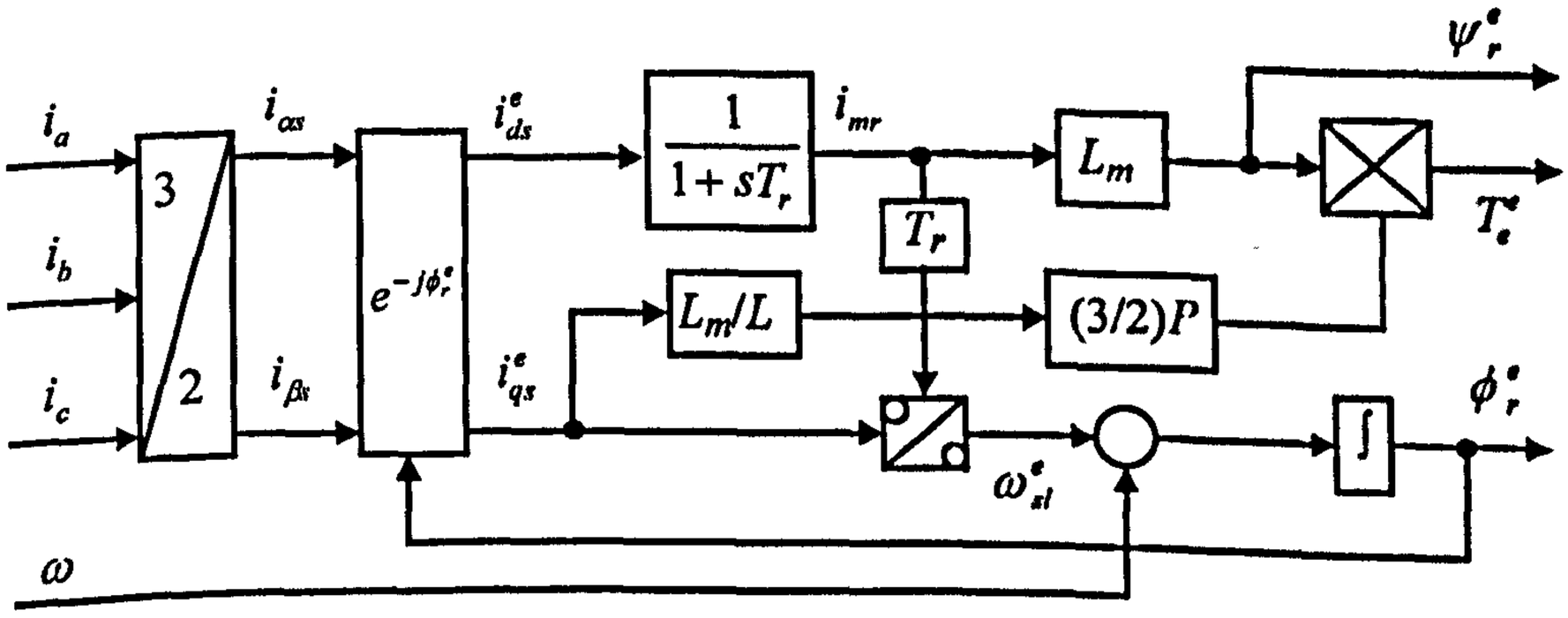

Figure 8.4.1 Rotor flux space vector estimation by means of measured stator currents and rotor speed in rotor flux oriented reference frame

to be constant, so that main flux saturation is neglected. The main disadvantage of this

scheme is that, apart from being sensitive to parameter variations, it requires coordinate transformation of measured stator currents from stationary to rotor flux oriented reference frame. Application of this method therefore requires a total of two coordinate transformations (as opposed to a single coordinate transformation, required for all the other described methods).

8.5 Development of a novel, saturation adaptive, rotor flux estimator

As operation of the generator under variable rotor flux conditions is assumed, it is necessary to utilise a rotor flux estimator that accounts for main flux saturation and therefore provides adaptation to the instantaneous saturation level in the machine. Such an estimator will be capable of providing correct tracking of rotor flux reference under all operating conditions. A model of the saturated induction machine, with state-space variables selected as d-q axis components of magnetising flux and rotor flux, [Levi (1995b)], can be used as a starting point in design of such an estimator. The rotor flux estimator, derived from the model of [Levi (1995b)], is described in [Levi (1994b)], where its capability of providing instantaneous adaptation to the actual saturation level in the machine is verified for the case of a rotor flux oriented induction motor drive. Different approach is however used here and a novel, saturation adaptive, rotor flux estimator is derived.

If stator current d-q axis components and rotor flux d-q axis components are selected as state-space variables, full dynamic saturated machine model can be described by equations (3.2-29), (3.2-30), (3.2-33) - (3.2-35) given in Section 3.2 of Chapter 3. Electro-magnetic torque is given in an arbitrary reference frame with:

$$T_e = \left(\frac{3}{2}\right) P \left(1 - \frac{L_{\sigma r}}{L_r}\right) \left(\psi_{dr} i_{qs} - \psi_{qr} i_{ds}\right) \qquad (8.5\text{-}1)$$

Equation (3.2-33) indicates that explicit terms responsible for dynamic cross-saturation appear only in the stator voltage equations. This property of the model greatly facilitates design of the saturation adaptive rotor flux estimator. The estimator performs

calculations on the basis of measured stator currents and rotor speed, in the rotor flux oriented reference frame, so that stator voltage equilibrium equations can be omitted from further consideration. Application of the rotor flux oriented control constraints on the rotor voltage equilibrium equations of the model given with (3.2-29), (3.2-30), (3.2-33) - (3.2-35) ($\omega_a = \omega_r,\ \psi_{dr} = \psi_r,\ \psi_{qr} = 0,\ d\psi_{qr}/dt = 0$) results in the first pair of the estimator equations:

$$\frac{d\psi_r^e}{dt} + \left(\frac{R_r}{L_r^e}\right)\psi_r^e = \left(1 - \frac{L_{\sigma r}}{L_r^e}\right)R_r i_{ds}^e$$
$$\omega_{sl}^e \psi_r^e = \left(1 - \frac{L_{\sigma r}}{L_r^e}\right)R_r i_{qs}^e \qquad (8.5\text{-}2)$$

Superscript e denotes the estimated quantities in rotor flux oriented reference frame. Inspection of equation (8.5-2) shows that the equations are identical in form to those used in standard estimator with neglected main flux saturation. The only difference is that the rotor self-inductance is a variable and is the function of the instantaneous saturation level in the machine. The two additional equations that enable main flux saturation to be taken into account follow directly from (3.2-34) - (3.2-35). Application of rotor flux orientation constraints on (3.2-34) - (3.2-35) yields

$$\Psi_d = \psi_r^e + L_{\sigma r} i_{ds}^e \qquad \Psi_q = L_{\sigma r} i_{qs}^e$$
$$\Psi = \sqrt{\left(\Psi_d\right)^2 + \left(\Psi_q\right)^2} \qquad L_r = \frac{\Psi}{i_m} = f(\Psi) \qquad (8.5\text{-}3)$$

The torque estimate (which is not needed here for control purposes) is obtained from (8.5-1) as:

$$T_e^e = \left(\frac{3}{2}\right)P\left(1 - \frac{L_{\sigma r}}{L_r^e}\right)\psi_r^e i_{qs}^e \qquad (8.5\text{-}4)$$

Equations (8.5-3) indicate that successful implementation of the estimator requires knowledge of the functional dependence of the rotor self-inductance on a physically

non-existing flux, defined in (3.2-34). However, the structure of the estimator can be simplified if rotor self-inductance is given as function of this flux squared. The saturation adaptive estimator, described with (8.5-2) - (8.5-4), is illustrated in Figure 8.5.1, where all the constant parameters are denoted with an asterisk.

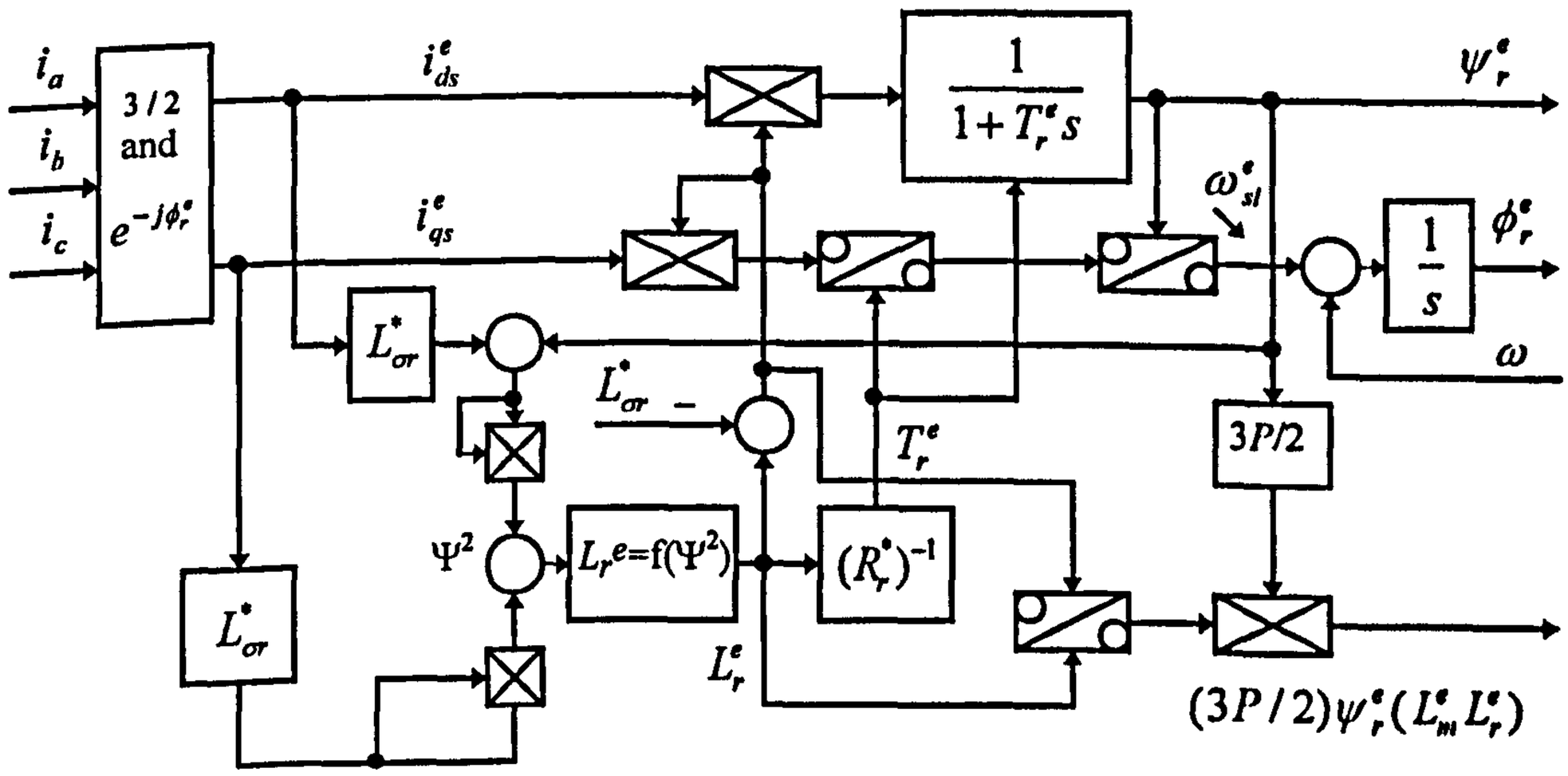

Figure 8.5.1 Configuration of the saturation adaptive rotor flux estimator

The required function $L_r = f(\Psi^2)$ is easily obtained from the magnetising curve of the machine because $\Psi = L_r i_m$. Calculation of the term $(3P/2)\psi_r^e(L_m^e / L_r^e)$, required in q-axis control path of Figure 8.3.5, is included in Figure 8.5.1.

8.6 Simulation of the system

8.6.1 Load at a.c. side

Control of the induction generator system supplying a.c. load is tested at first, by simulation. A small 0.75 kW induction machine, whose parameters (including magnetising curve approximation) are given in Appendix, is used. The induction generator is represented with a model with stator current and rotor flux d-q axis components as state-space variables and main flux saturation is taken into account. The model of the machine is formed in the reference frame rotating at constant speed of $2\pi 50$ rad/s. The generator is assumed to run initially at constant speed of 1 p.u. (i.e.,

$2\pi 50$ rad/s electrical). Self-excitation is started at $t = 0$ s, by connecting the compensator to induction generator terminals under no-load conditions. Capacitor at inverter's d.c. side is selected as $C = 125$ μF and it is assumed that the capacitor is pre-charged to a voltage of $v_{DC}(t = 0) = 350$ V. At time instant $t = 1$ s pure resistive load of 300 Ω per phase is applied in a step-wise manner (approximately one half of the rated load under sinusoidal conditions). Rotor flux reference is constant and equal to rated throughout. Subsequent speed and load profile correspond to the one shown in Figure 7.7.1. Figure 8.6.1 shows variation of capacitor d.c. voltage, stator phase voltage and stator phase current during the described sequence of operating conditions, as well as comparison of actual (i.e., from the generator model) and estimated (i.e., from the estimator) values of rotor flux, electromagnetic torque and magnetising inductance. Figure 8.6.2 gives d-q axis currents within the generator's model and within the rotor flux estimator [Liao and Levi (1998b)].

When self-excitation is initiated, capacitor d.c. voltage initially experiences large reduction with respect to the pre-charged voltage value, Figure 8.6.1a. However, it quickly recovers and process of excitation is completed within few hundreds of milliseconds. Application of the load, as well as speed variation, cause transients in d.c. voltage that die out rapidly and d.c. voltage becomes equal in steady-state to the reference value. Comparison of actual and estimated rotor flux, Figure 8.6.1d, shows that rotor flux build-up is very fast and that estimator at all times correctly predicts the value of the rotor flux. This is enabled by correct prediction of the saturation level in the machine (actual and estimated magnetising inductance values in Figure 8.6.1e coincide). As rotor flux is correctly estimated and controlled, torque change in response to both load application and speed variation is almost instantaneous, Figure 8.6.1f. Figures 8.6.1 thus verify capability of the control system to maintain constant rotor flux operation under all operating conditions.

Generator and estimator stator d-q axis current components, shown in Figure 8.6.2, illustrate the fact that they apply to two different systems of reference axes. While estimator stator d-q axis current components are essentially constant d.c. in any steady-state (apart from high-frequency ripple), generator stator d-q axis current components

are a.c. as generator model is formed in the reference frame that rotates at constant speed of $2\pi 50$ rad/s.

A similar study is performed once more, this time with operation in the field-weakening region. The machine at first operates under no-load conditions, self-excitation is again initiated at $t = 0$ s at speed of 1 p.u., and load of 300 Ω per phase is applied at $t = 0.5$ s. Speed change from 1 p.u. to 1.2 p.u. is initiated at $t = 0.9$ s in a linear manner during the 100 ms time interval. Rotor flux reference is reduced inversely proportionally to the speed. Figure 8.6.3 shows variation of capacitor d.c. voltage, stator phase voltage, generator current, as well as comparison of actual and estimated values of rotor flux, magnetising inductance and torque [Liao and Levi (1998b)]. Once more, saturation adaptive estimator correctly tracks magnetising inductance in the machine, so that actual and estimated rotor flux are in good agreement. This is reflected in waveforms of actual and estimated torque, that basically coincide. Although peak stator phase voltage increases due to an increase in the d.c. voltage, Figures 8.6.3a and 8.6.3b, stator phase voltage fundamental component remains essentially constant, as it should be in the field weakening region. Thus the fundamental output power delivered to the load is the same in Figure 8.6.3 for operation at both 1 p.u. speed and 1.2 p.u. speed. The increase in the torque value in the field weakening, Figure 8.6.3f, instead of a decrease that normally takes place for constant power operation, is explained by the fact that the load is purely resistive. Harmonic load losses in the field weakening increase with respect to operation at 1 p.u. speed, because of the increase in the d.c. voltage. The net result is that the torque goes up rather than going down.

8.6.2 Load at d.c. side

The rotor flux oriented control scheme for an induction generator supplying d.c. load is simulated next. Reference d.c. voltage is set to 500 V and capacitor rating is 250 μF. Battery voltage is here taken as 350 V in order to reduce duration of the self-excitation. Speed of rotation is taken as an independent input. The generator is assumed to run initially at constant speed of 1 p.u. (i.e., $2\pi 50$ rad/s electrical). Self-excitation under no-

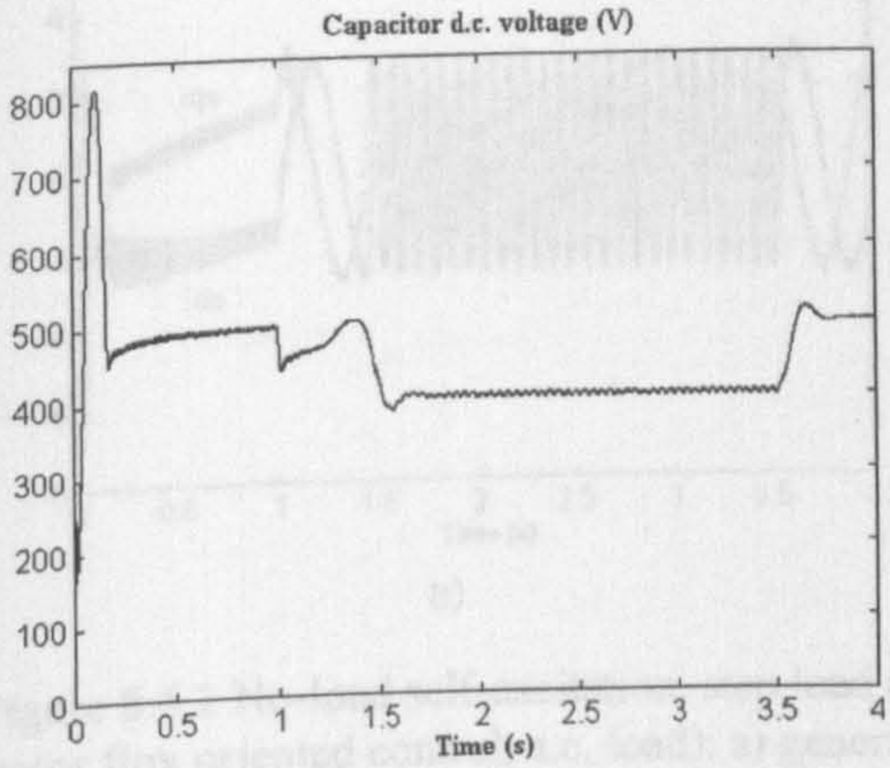

a)

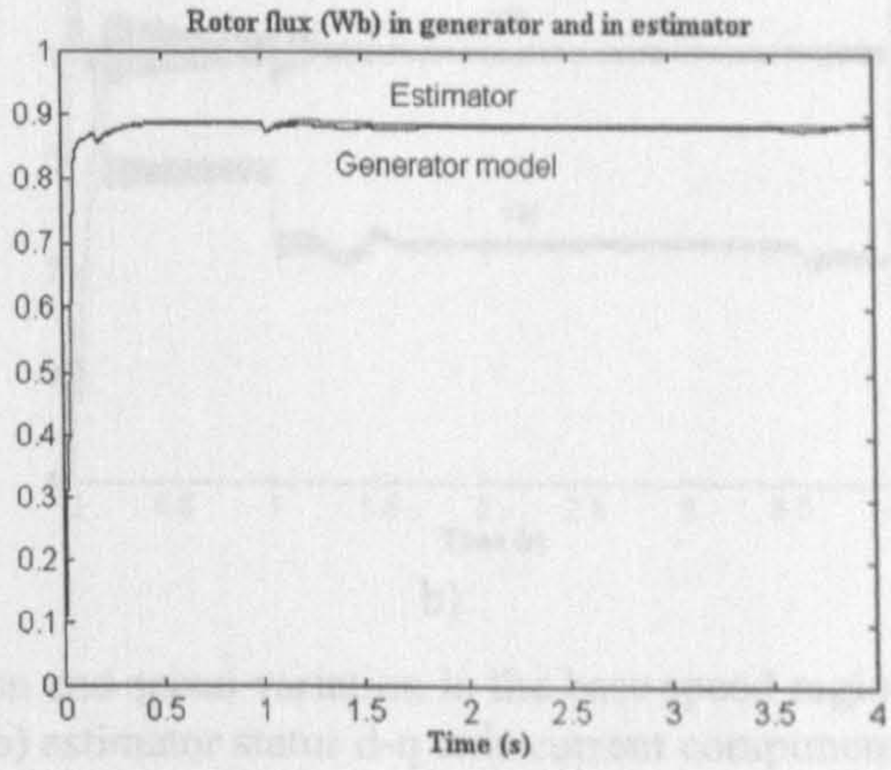

d)

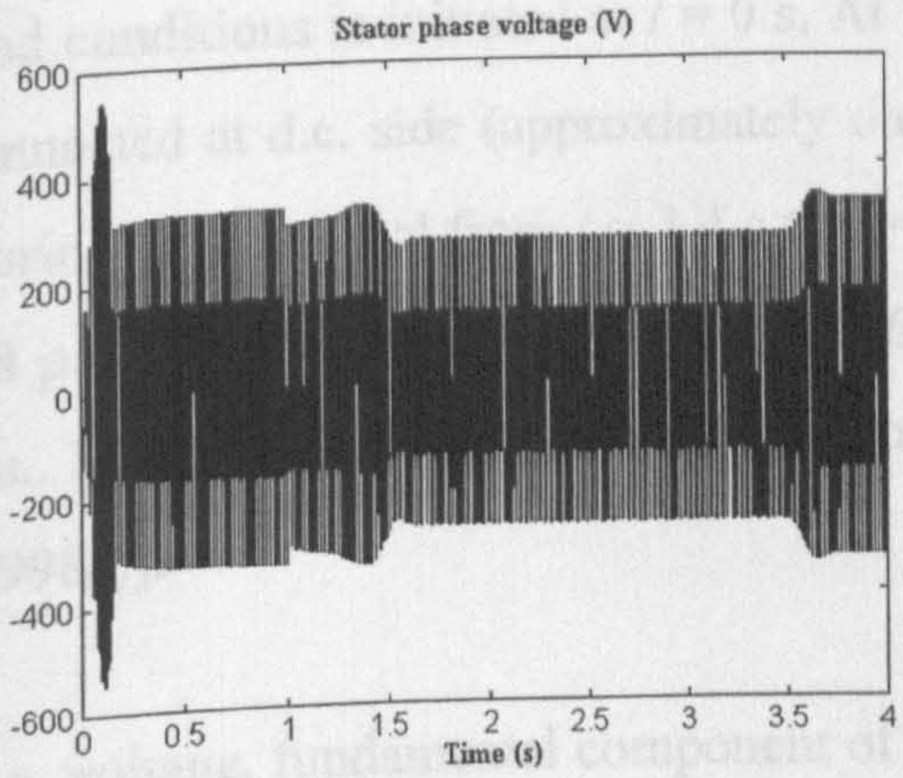

b)

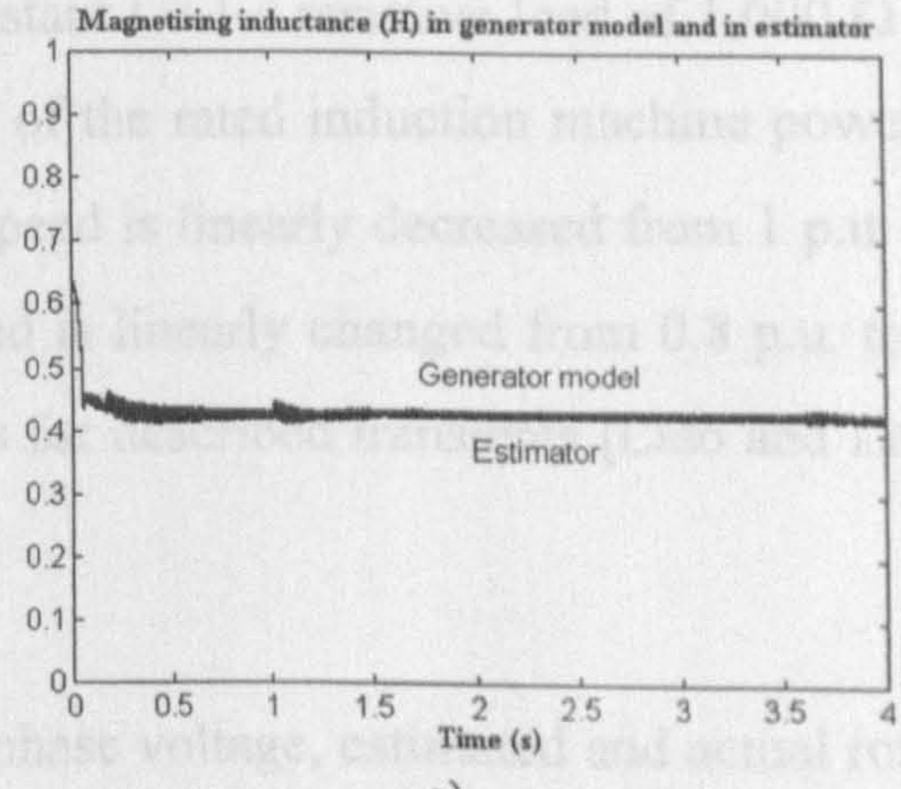

e)

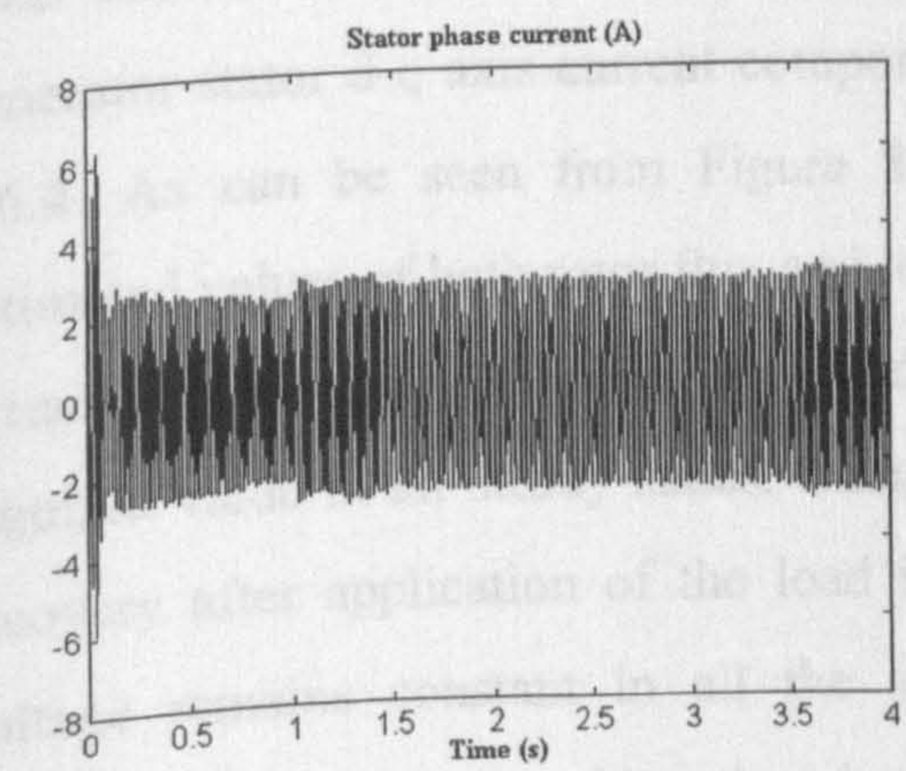

c)

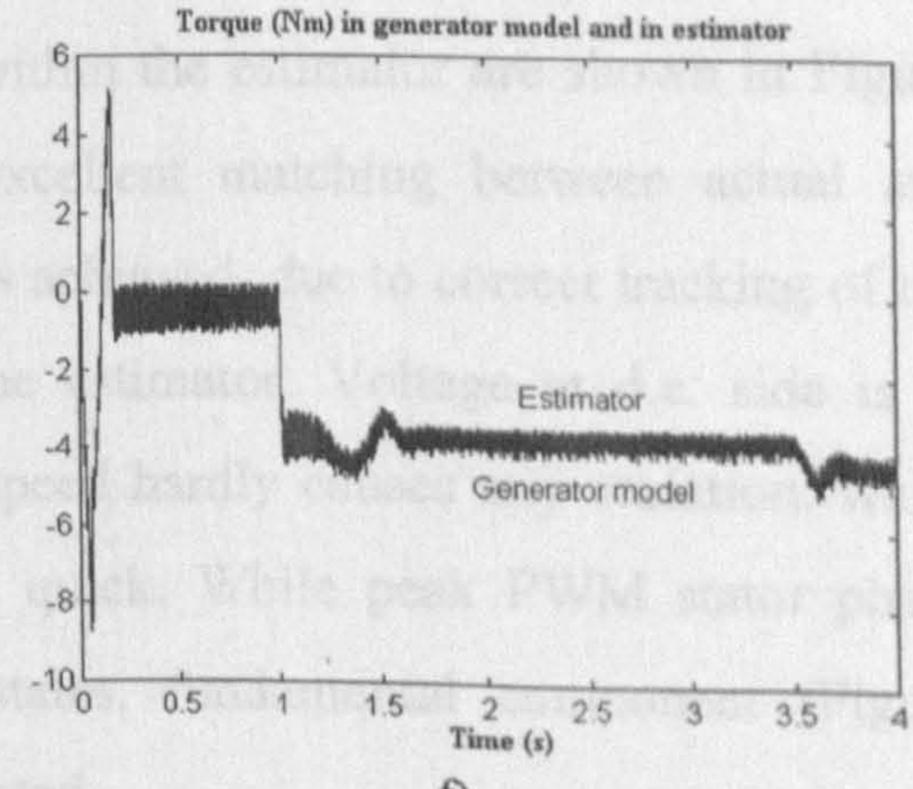

f)

Figure 8.6.1 No-load self-excitation, step load application and speed variation in the base speed region (rotor flux oriented control, a.c. load): a) variation of capacitor d.c. voltage, b) stator phase voltage, c) stator phase current, d) variation of rotor flux, e) magnetising inductance and f) electromagnetic torque within the generator and in the rotor flux estimator

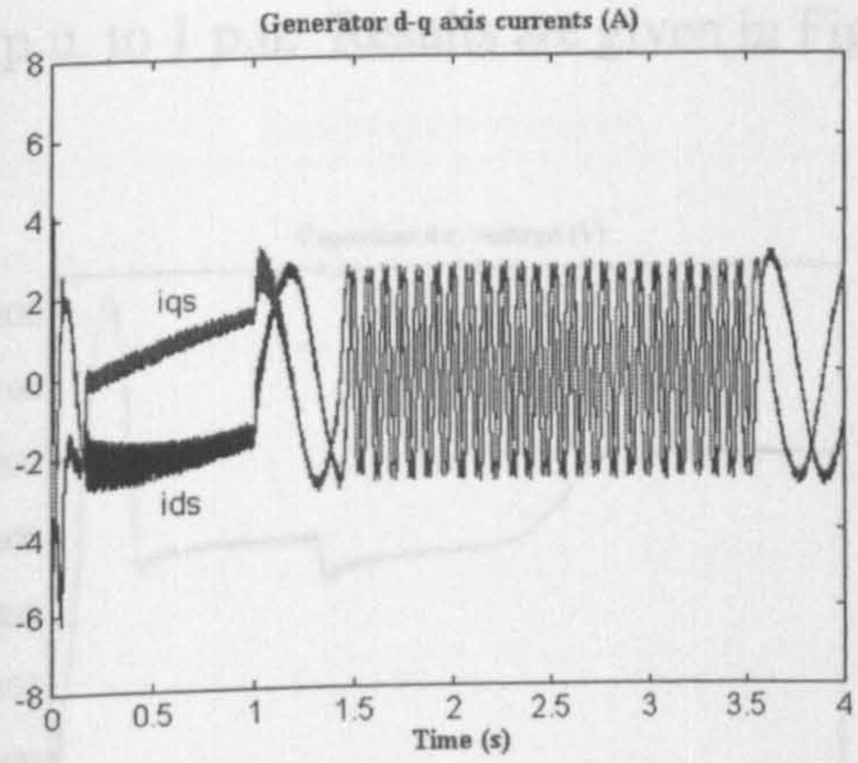

a)

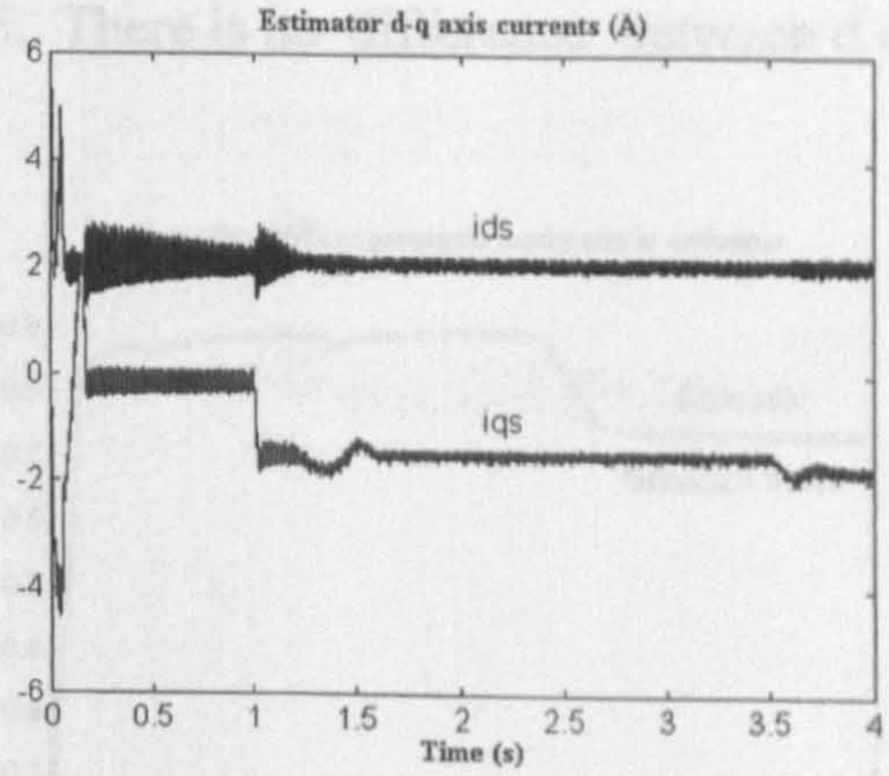

b)

Figure 8.6.2 No-load self-excitation, step load application and speed variation in the base speed region (rotor flux oriented control, a.c. load): a) generator and b) estimator stator d-q axis current components

load conditions is initiated at $t = 0$ s. At time instant $t = 1$ s resistive load of 1,000 Ω is connected at d.c. side (approximately one third of the rated induction machine power). During time interval from $t = 1.4$ s to $t = 1.5$ s speed is linearly decreased from 1 p.u. to 0.8 p.u.; finally, from $t = 3.5$ s to $t = 3.6$ s speed is linearly changed from 0.8 p.u. to 1 p.u.. Figure 8.6.4 summarises simulation results for described transients [Liao and Levi (1998a)].

D.c. voltage, fundamental component of stator phase voltage, estimated and actual rotor flux, estimated and actual torque, estimated and actual magnetising inductance, and generator stator d-q axis current components within the estimator are shown in Figure 8.6.4. As can be seen from Figure 8.6.4, excellent matching between actual and estimated values of both rotor flux and torque is achieved, due to correct tracking of the actual magnetising inductance provided by the estimator. Voltage at d.c. side is at required value in all steady-states, change in speed hardly causes any variation, while recovery after application of the load is very quick. While peak PWM stator phase voltage remains constant in all the steady-states, fundamental component (Figure 8.6.4b) reduces when speed is reduced, as expected.

Simulation is repeated once more, with the same sequence of events. The only difference is that now during time intervals from $t = 1.4$ s to $t = 1.5$ s and from $t = 3.5$ s to $t = 3.6$ s speed at first linearly increases from 1 p.u. to 1.2 p.u. and then returns from

1.2 p.u. to 1 p.u. Results are given in Figure 8.6.5. There is no difference between d.c.

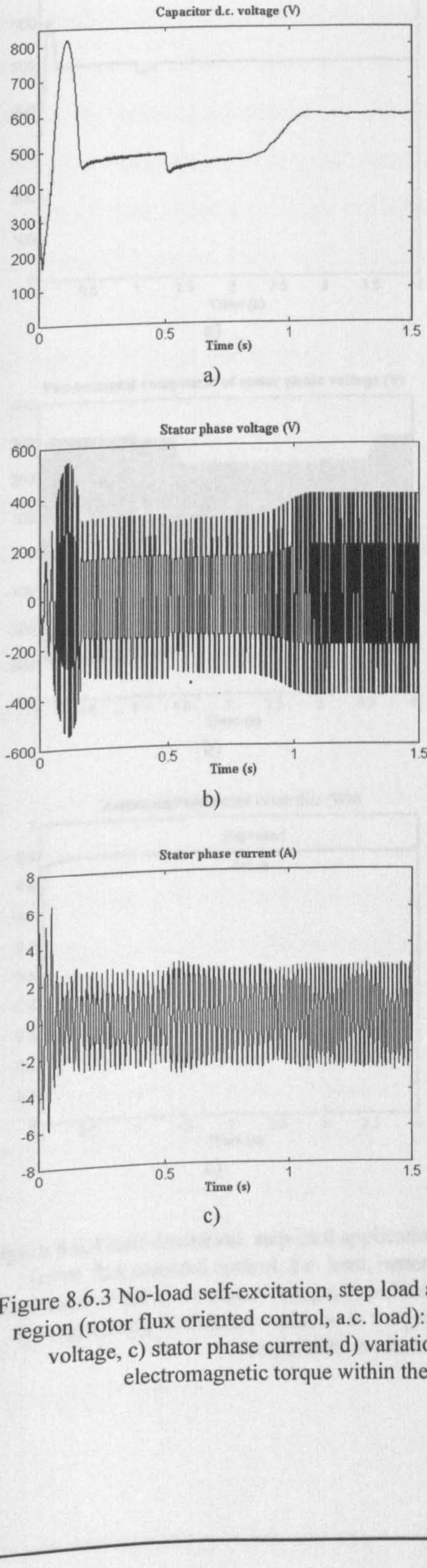

Figure 8.6.3 No-load self-excitation, step load application and speed variation in the field-weakening region (rotor flux oriented control, a.c. load): a) variation of capacitor d.c. voltage, b) stator phase voltage, c) stator phase current, d) variation of rotor flux, e) magnetising inductance and f) electromagnetic torque within the generator and in the rotor flux estimator

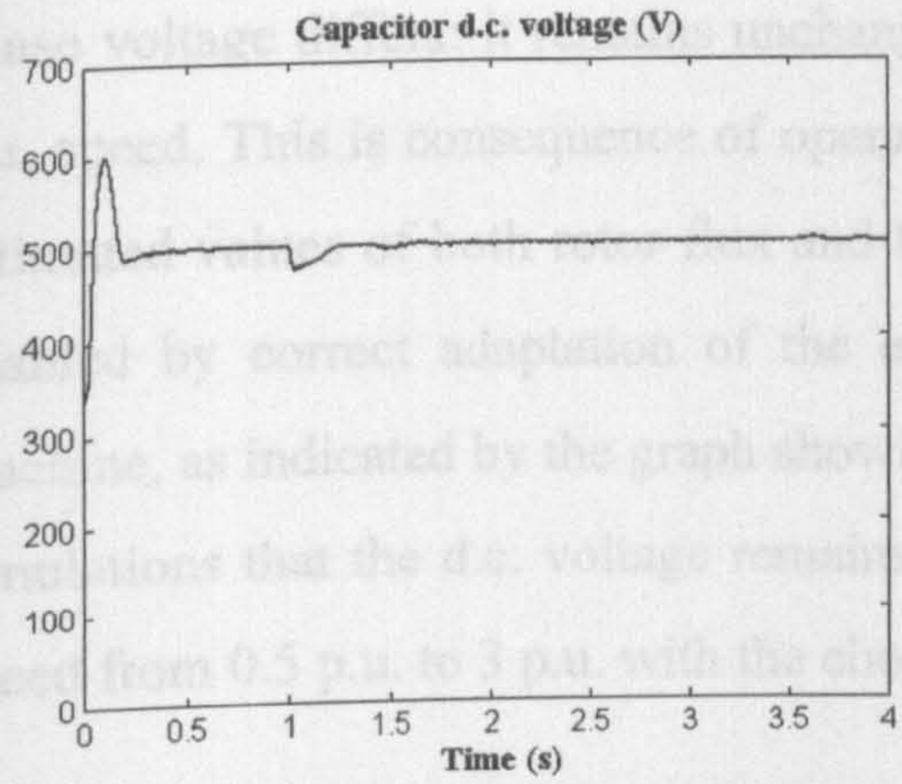

a)

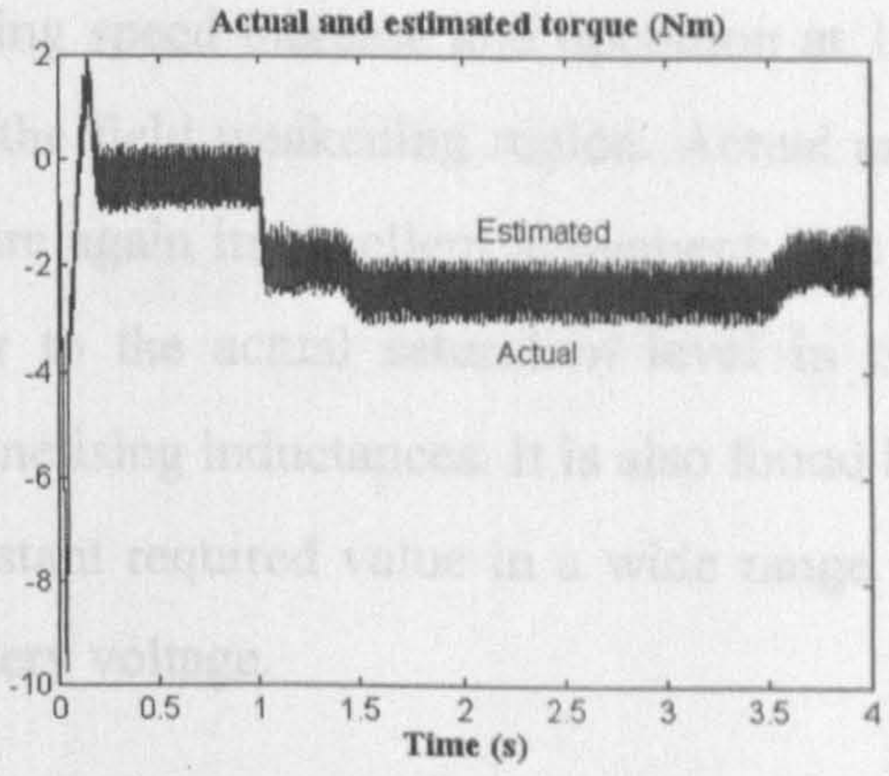

d)

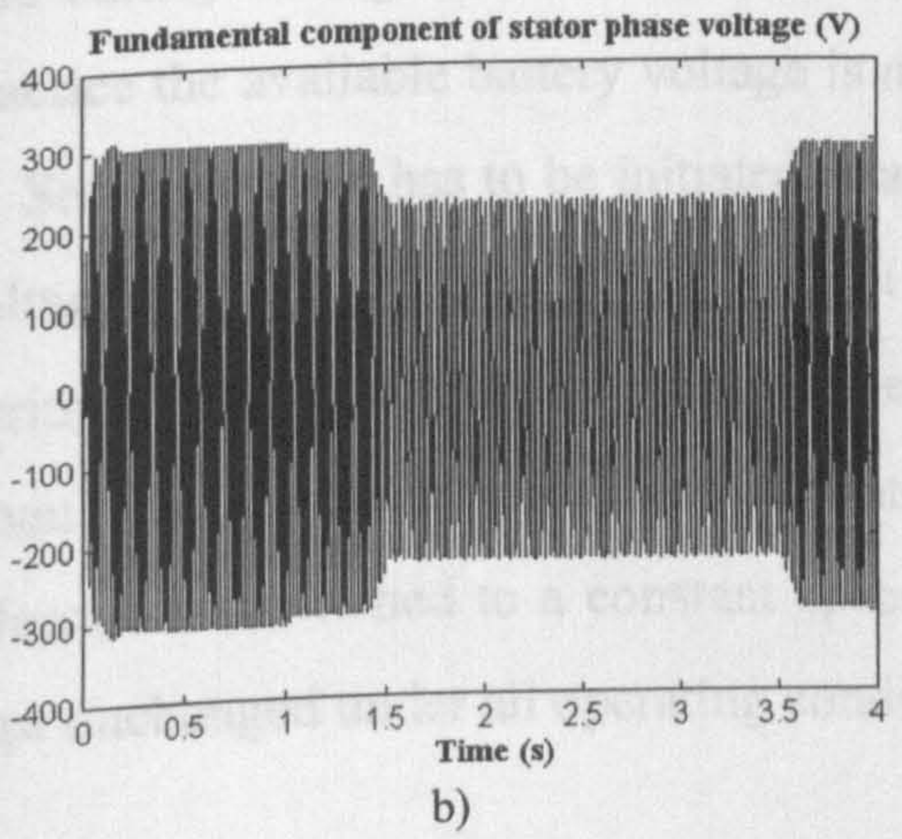

b)

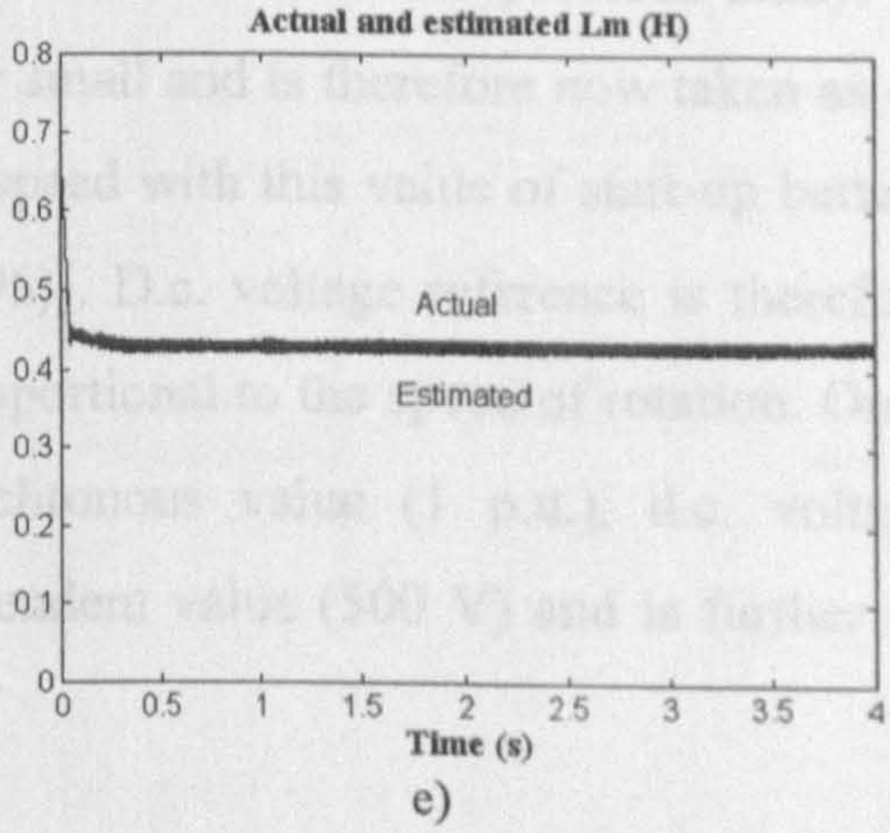

e)

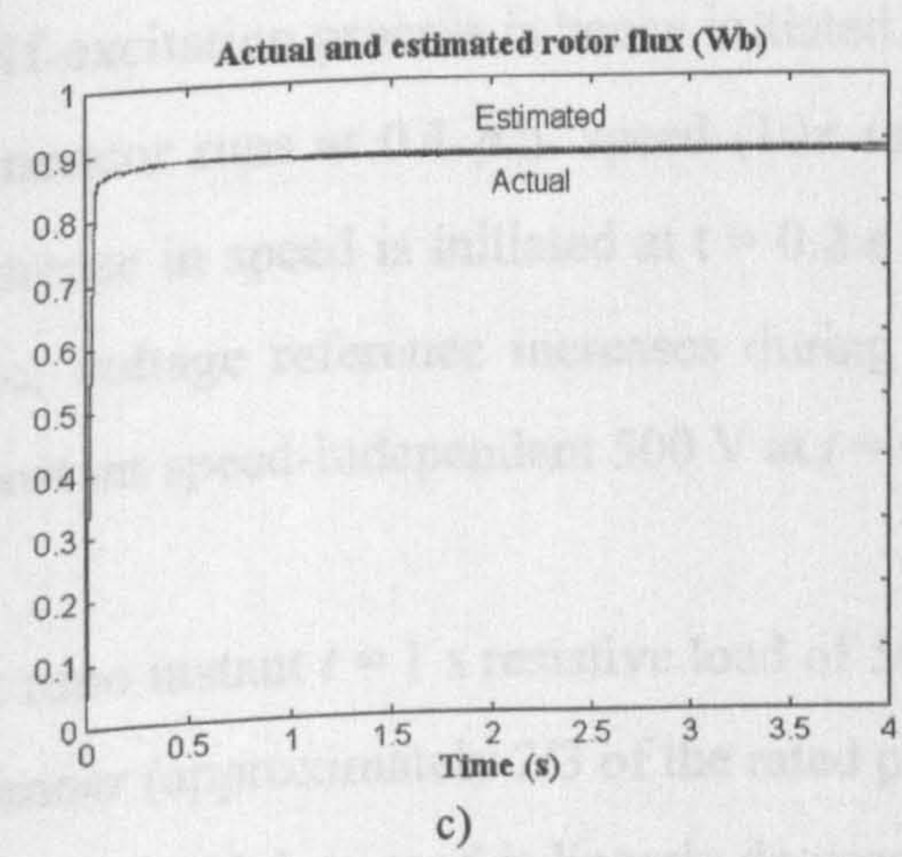

c)

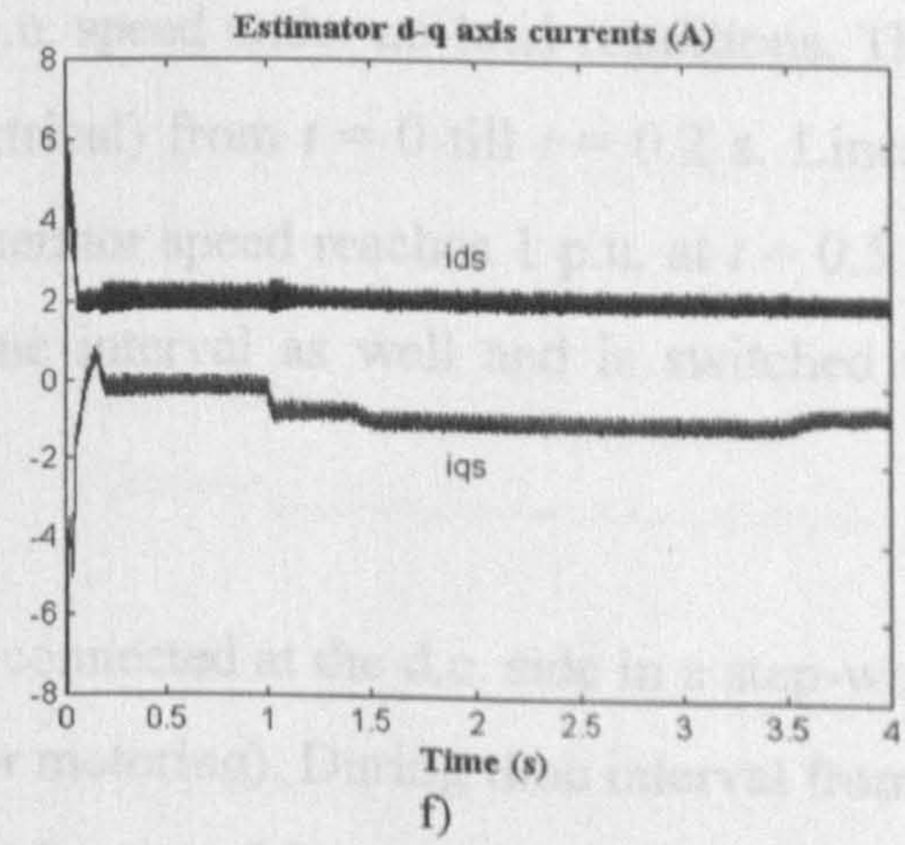

f)

Figure 8.6.4 Self-excitation, step load application and variable speed operation in the base speed region (rotor flux oriented control, d.c. load, battery voltage = 350 V): a) d.c. voltage, b) fundamental component of the stator phase voltage, c) estimated and actual rotor flux, d) estimated and actual torque, e) magnetising inductance variation in the generator and in the estimator, f) stator current d-q axis components in rotor flux oriented reference frame

voltages in Figures 8.6.4 and 8.6.5. However, fundamental component of the stator phase voltage differs: it remains unchanged during speed increase and operation at 1.2 p.u. speed. This is consequence of operation in the field weakening region. Actual and estimated values of both rotor flux and torque are again in excellent agreement; this is enabled by correct adaptation of the estimator to the actual saturation level in the machine, as indicated by the graph showing magnetising inductances. It is also found by simulations that the d.c. voltage remains at constant required value in a wide range of speed from 0.5 p.u. to 3 p.u. with the chosen battery voltage.

The battery voltage for start-up of the generator was 350 V in the previous study. In practice the available battery voltage is normally small and is therefore now taken as 48 V. Self-excitation has to be initiated at a lower speed with this value of start-up battery voltage [Silva and Lyra (1993), Lyra et al (1995)]. D.c. voltage reference is therefore during initial self-excitation taken as linearly proportional to the speed of rotation. Once when the generator speed reaches rated synchronous value (1 p.u.), d.c. voltage reference is switched to a constant speed-independent value (500 V) and is further on kept unchanged under all operating conditions.

Self-excitation process is hence initiated at 0.1 p.u. speed under no-load conditions. The generator runs at 0.1 p.u. speed (10π rad/s electrical) from $t = 0$ till $t = 0.2$ s. Linear increase in speed is initiated at t = 0.2 s and generator speed reaches 1 p.u. at $t = 0.5$ s. D.c. voltage reference increases during this time interval as well and is switched to constant speed-independent 500 V at $t = 0.5$ s.

At time instant $t = 1$ s resistive load of 500 Ω is connected at the d.c. side in a step-wise manner (approximately 2/3 of the rated power for motoring). During time interval from $t = 2$ s to t = 2.1 s speed is linearly decreased from 1 p.u. to 0.8 p.u. and is kept at 0.8 p.u. until $t = 2.9$ s. From $t = 2.9$ s to $t = 3.0$ s speed is linearly changed from 0.8 p.u. to 1.0 p.u.. Finally, load is altered from 500 Ω to 750 Ω at $t = 3.5$ s. The speed and load profile are shown in Figure 8.6.6. Figure 8.6.7 summarises simulation results for the described sequence of transients.

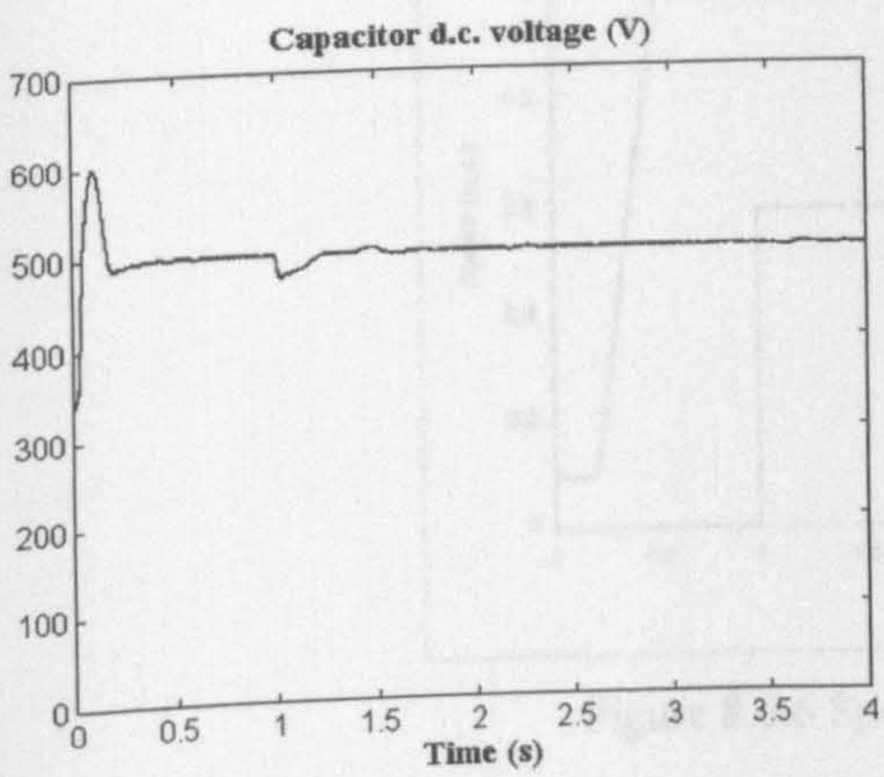

a)

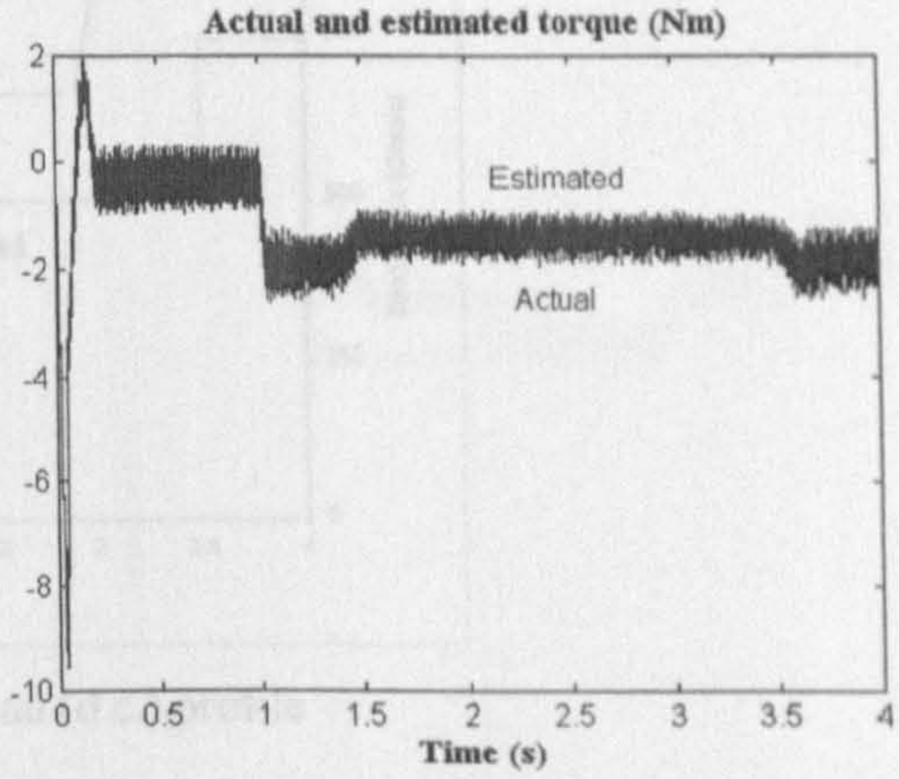

d)

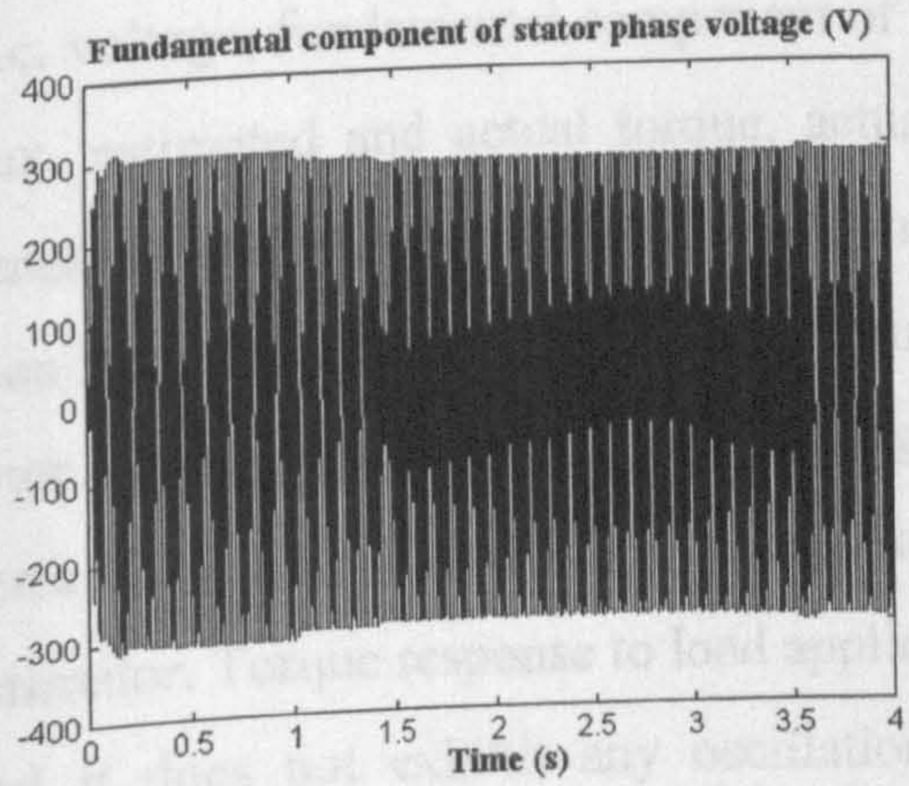

b)

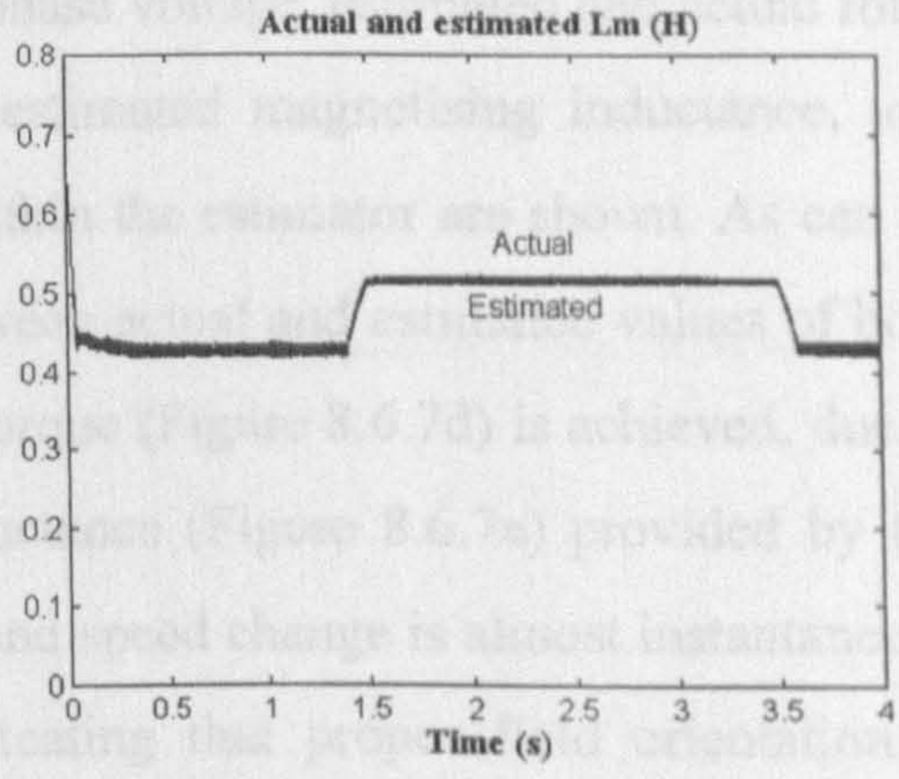

e)

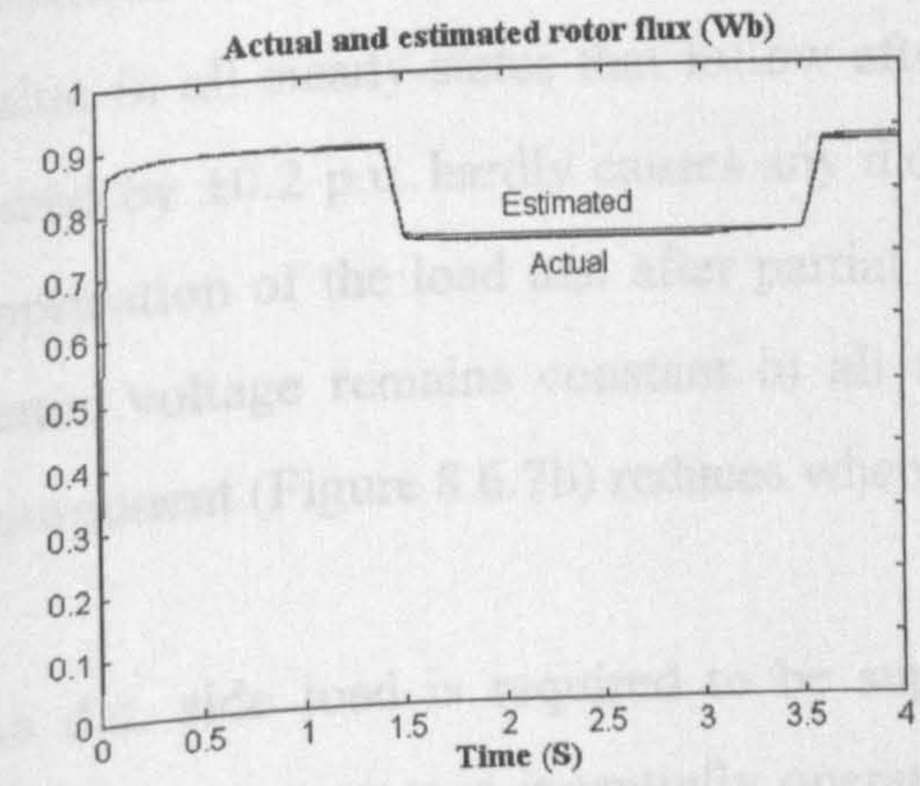

c)

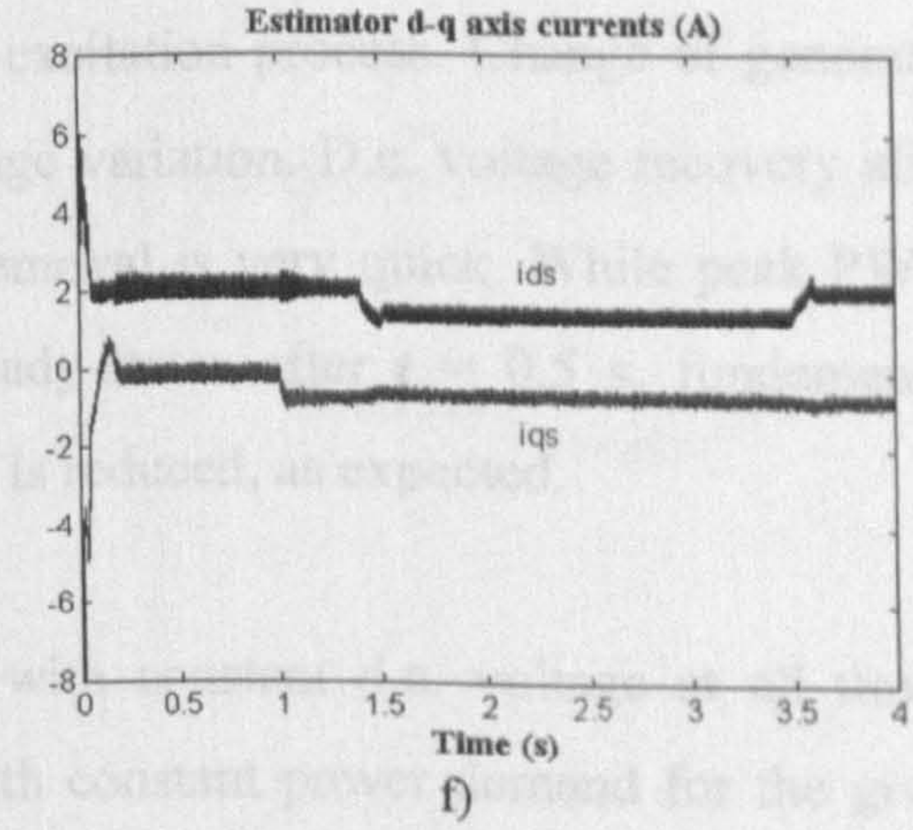

f)

Figure 8.6.5 Self-excitation, step load application and variable speed operation in field weakening region (rotor flux oriented control, d.c. load, battery voltage = 350 V), traces as in Figure 8.6.4

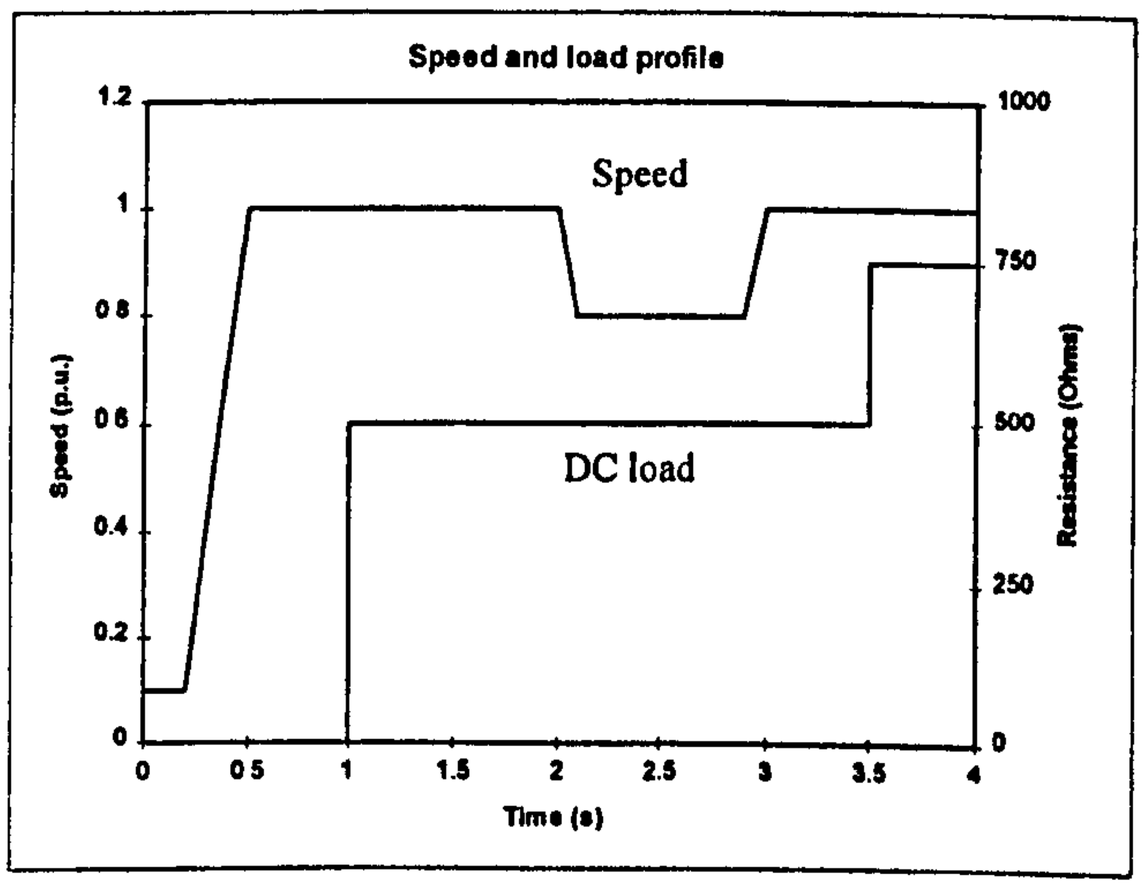

Figure 8.6.6 Speed and load (d.c.) profile

D.c. voltage, fundamental component of stator phase voltage, estimated and actual rotor flux, estimated and actual torque, actual and estimated magnetising inductance, and generator stator d-q axis current components within the estimator are shown. As can be seen from Figure 8.6.7, excellent matching between actual and estimated values of both rotor flux (Figure 8.6.7c) and electromagnetic torque (Figure 8.6.7d) is achieved, due to correct tracking of the actual magnetising inductance (Figure 8.6.7e) provided by the estimator. Torque response to load application and speed change is almost instantaneous and it does not exhibit any oscillations, indicating that proper field orientation is maintained under all operating conditions. Voltage at the d.c. side is at required 500 V value in all steady-states that follow after self-excitation process. Change of generator speed by ±0.2 p.u. hardly causes any d.c. voltage variation. D.c. voltage recovery after application of the load and after partial load removal is very quick. While peak PWM stator voltage remains constant in all the steady-states after t = 0.5 s, fundamental component (Figure 8.6.7b) reduces when speed is reduced, as expected.

As d.c. side load is required to be supplied with constant d.c. voltage at all times, induction generator is essentially operating with constant power demand for the given load resistance, regardless of the speed of operation. From the point of view of generator's utilisation, it appears to be optimal to supply such a load by operating the machine in the field-weakening region (constant power region). Simulation is therefore repeated once more, with the same sequence of events. The only difference is that now

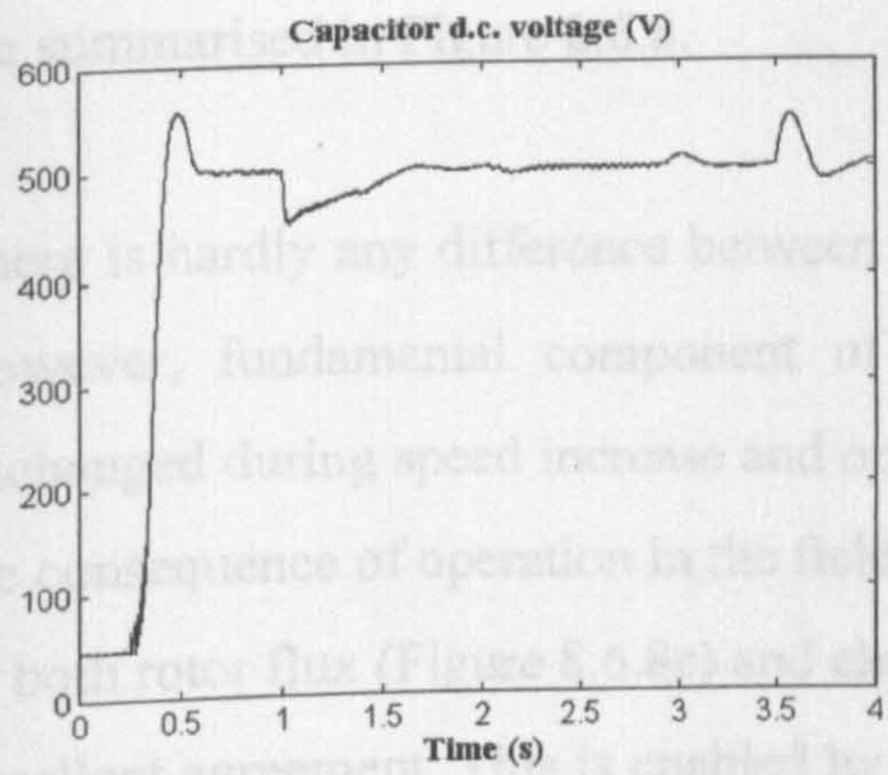

a)

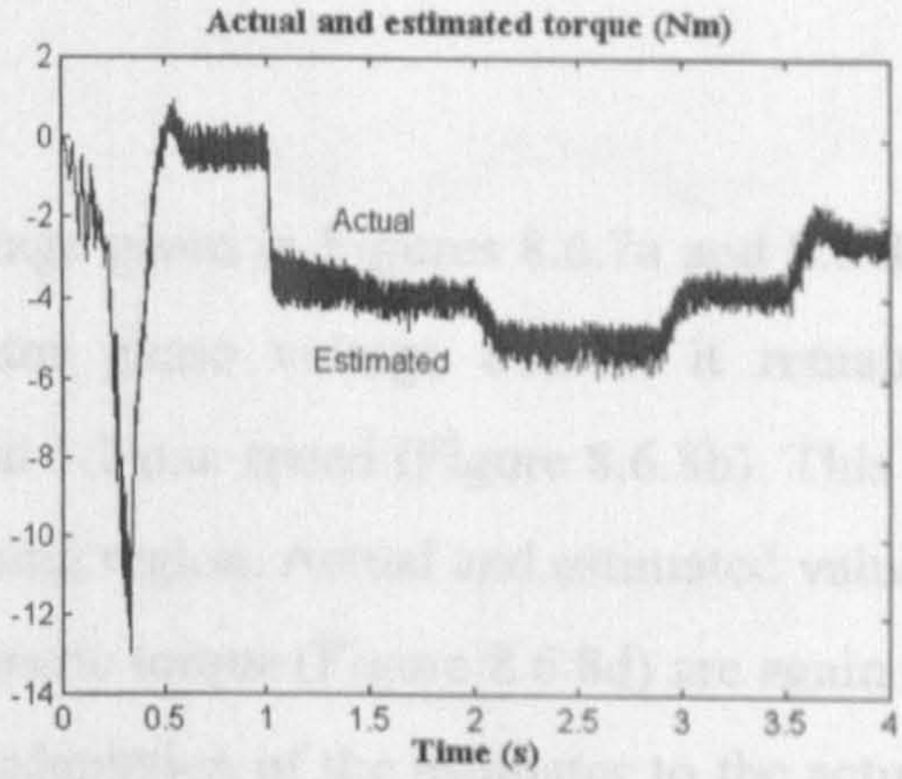

d)

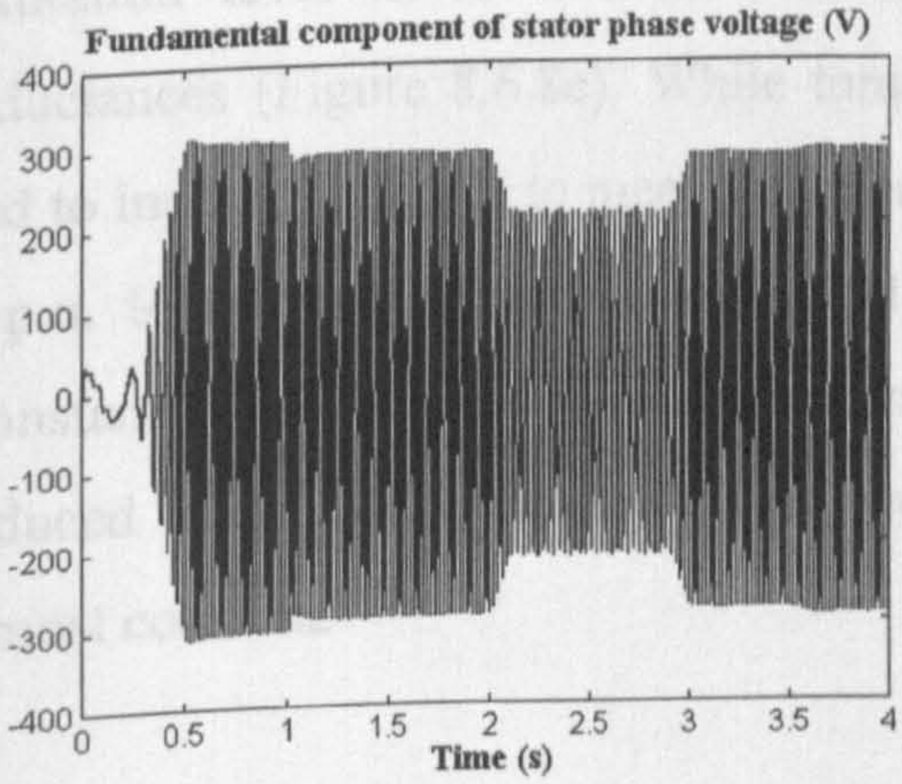

b)

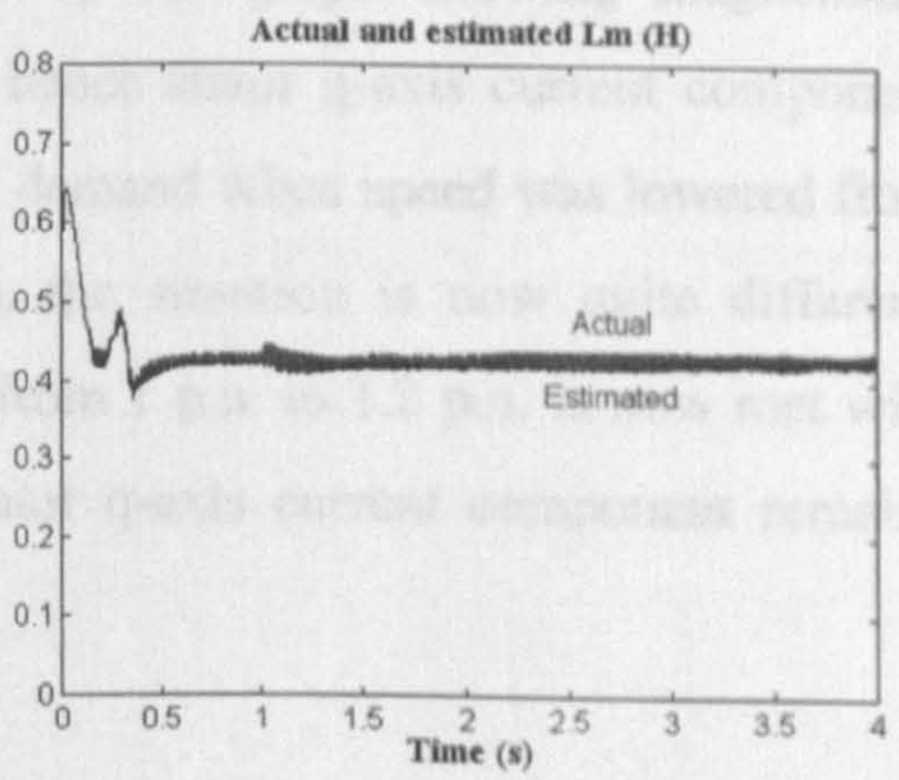

e)

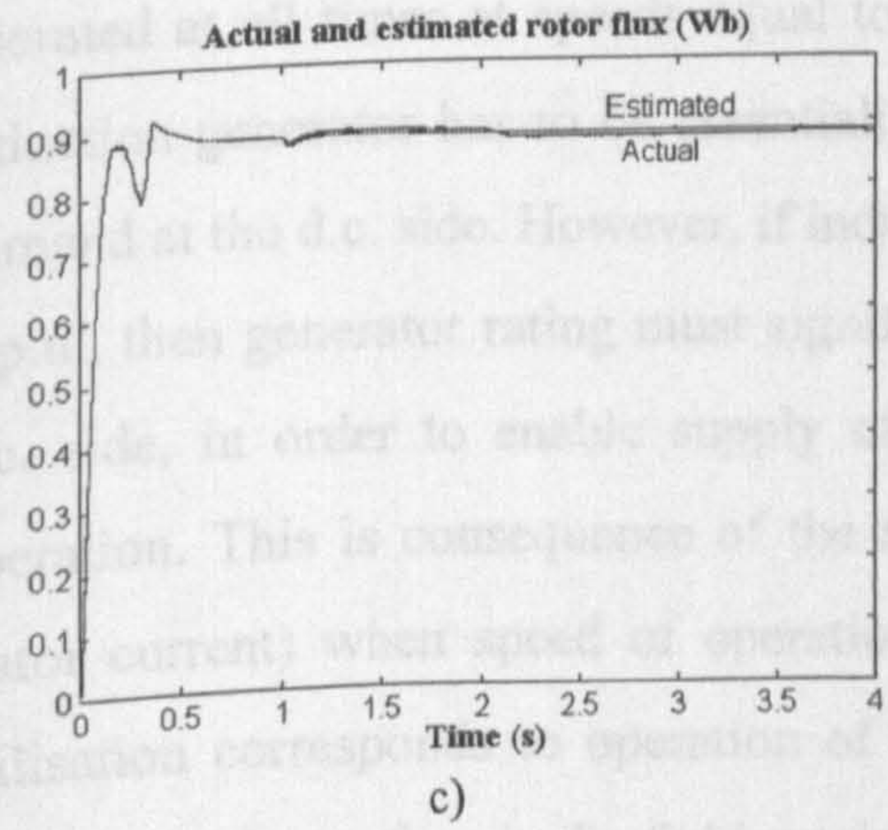

c)

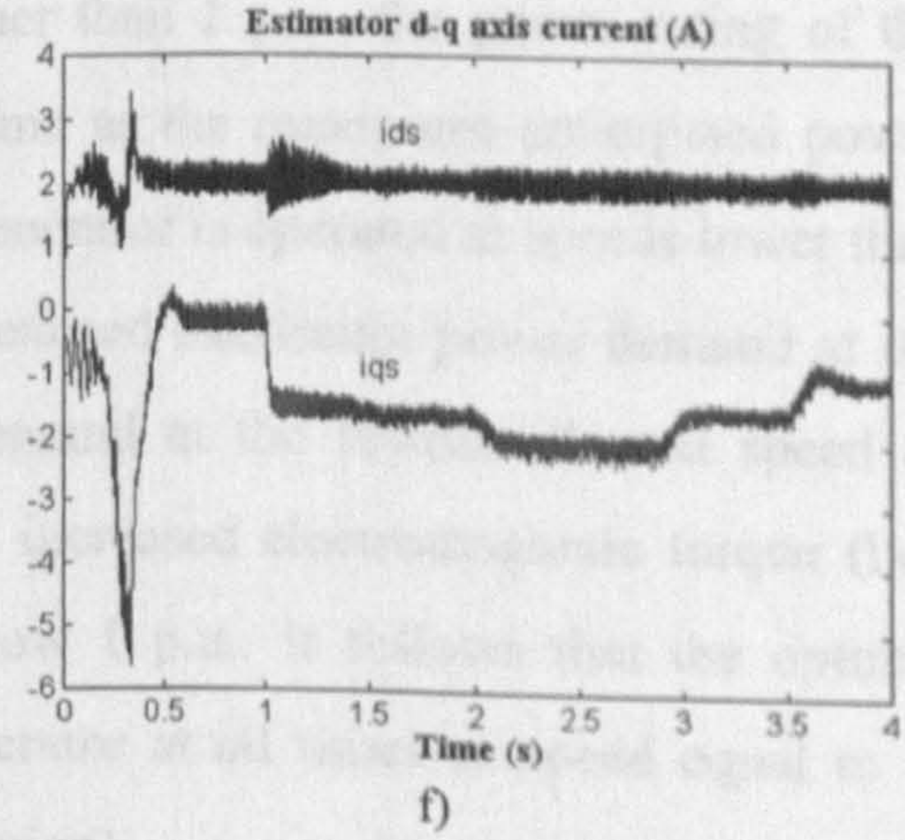

f)

Figure 8.6.7 Self-excitation, step load application and variable speed operation in the base speed region (rotor flux oriented control, d.c. load, battery voltage = 48 V): a) d.c. voltage, b) fundamental component of the stator phase voltage, c) estimated and actual rotor flux, d) estimated and actual torque, e) magnetising inductance variation in the generator and in the estimator, f) stator current d-q axis components in rotor flux oriented reference frame

during time intervals from $t = 2$ s to $t = 2.1$ s and from $t = 2.9$ to $t = 3$ s speed at first linearly increases from 1 p.u. to 1.2 p.u. and then returns from 1.2 p.u. to 1 p.u.. Results are summarised in Figure 8.6.8.

There is hardly any difference between d.c. voltage given in Figures 8.6.7a and 8.6.8a. However, fundamental component of the stator phase voltage differs: it remains unchanged during speed increase and operation at 1.2 p.u. speed (Figure 8.6.8b). This is the consequence of operation in the field-weakening region. Actual and estimated values of both rotor flux (Figure 8.6.8c) and electromagnetic torque (Figure 8.6.8d) are again in excellent agreement. This is enabled by correct adaptation of the estimator to the actual saturation level in the machine, as indicated by the graph showing magnetising inductances (Figure 8.6.8e). While torque and hence stator q-axis current component had to increase in order to meet the same power demand when speed was lowered from 1 p.u. to 0.8 p.u. (Figures 8.6.7d and 8.6.7f), the situation is now quite different. Constant power demand during speed increase from 1 p.u. to 1.2 p.u. is now met with reduced torque value (Figure 8.6.8d) while stator q-axis current component remains almost constant.

Figures 8.6.7 and 8.6.8 lead to the following conclusion. If induction generator is operated at all times at speeds equal to or higher than 1 p.u., the power rating of the induction generator has to be essentially the same as the maximum anticipated power demand at the d.c. side. However, if induction generator is operated at speeds lower than 1 p.u., then generator rating must significantly exceed maximum power demand at the d.c. side, in order to enable supply of this demand at the lowest allowed speed of operation. This is consequence of the need for increased electromagnetic torque (i.e., stator current) when speed of operation is below 1 p.u.. It follows that the optimal utilisation corresponds to operation of the generator at all times at speed equal to or higher than 1 p.u. (i.e., in the field-weakening region).

The need for utilisation of a saturation adaptive rotor flux estimator when the generator is operated in the field-weakening region is verified by performing once more simulation identical to the one whose results are given in Figure 8.6.8. However, instead

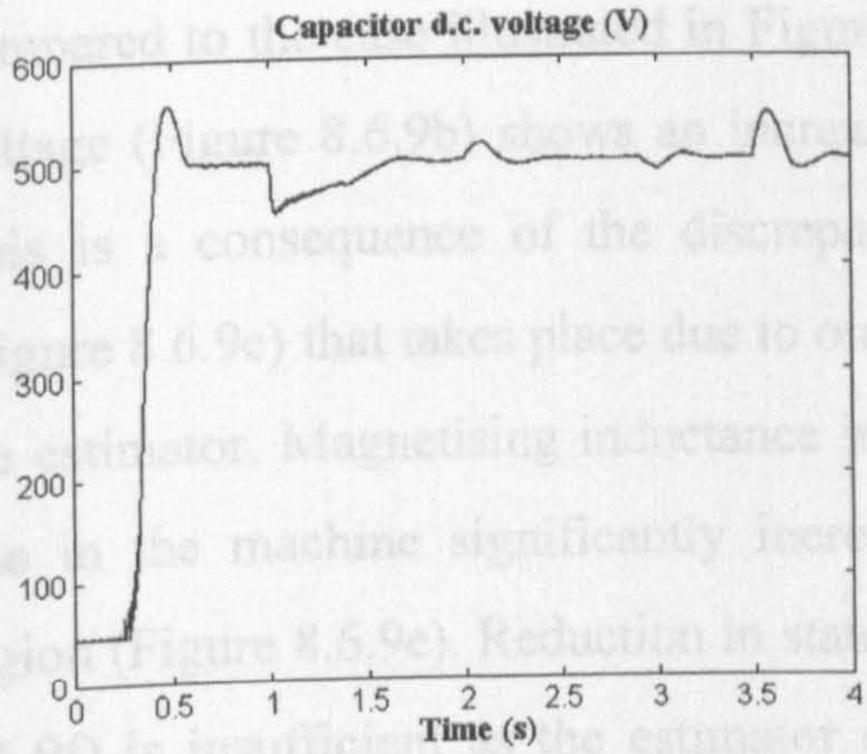

a)

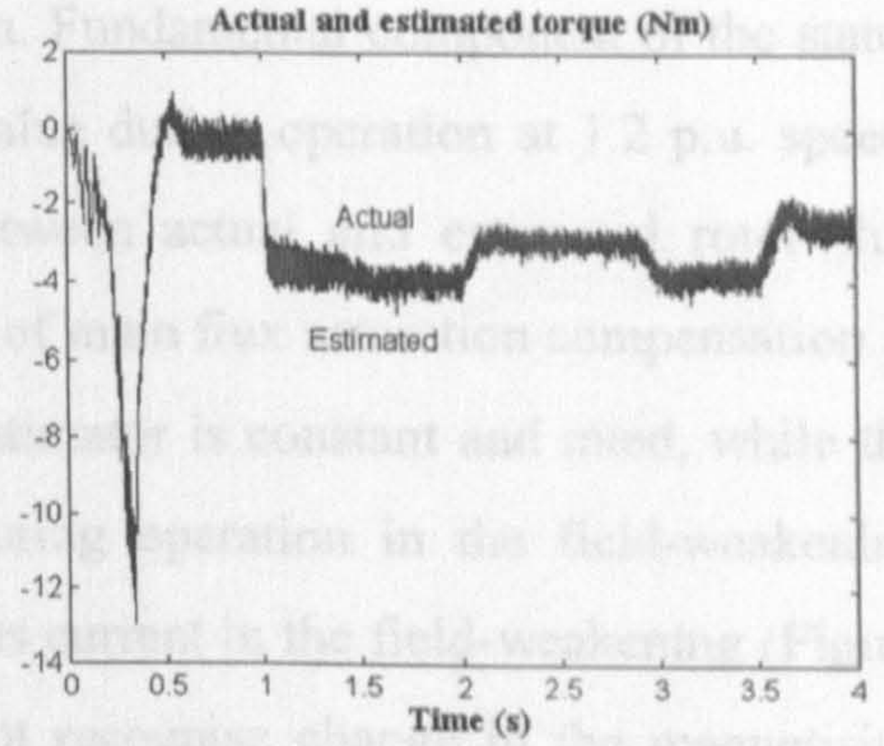

d)

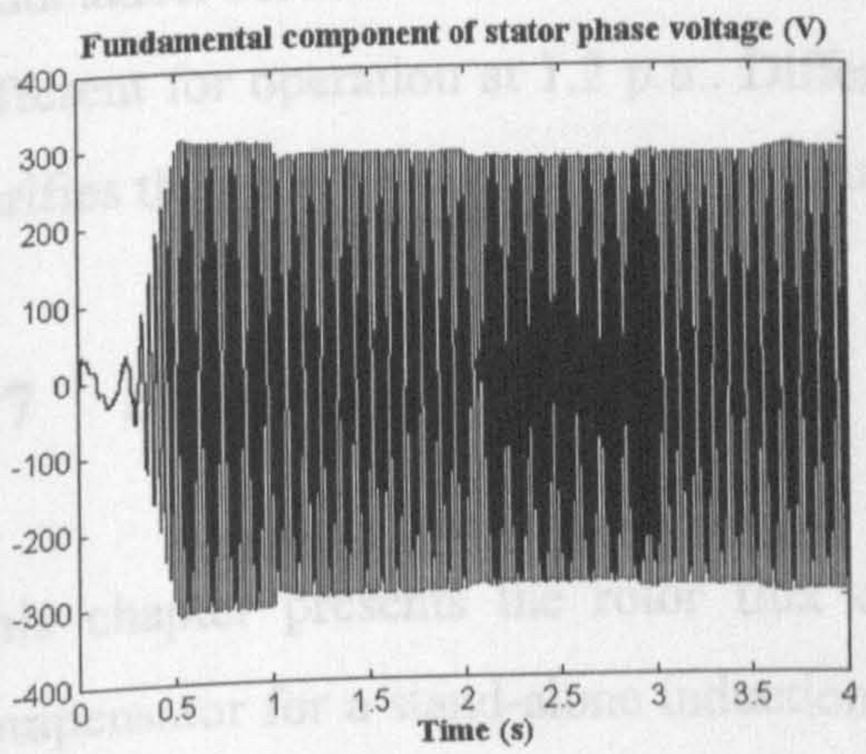

b)

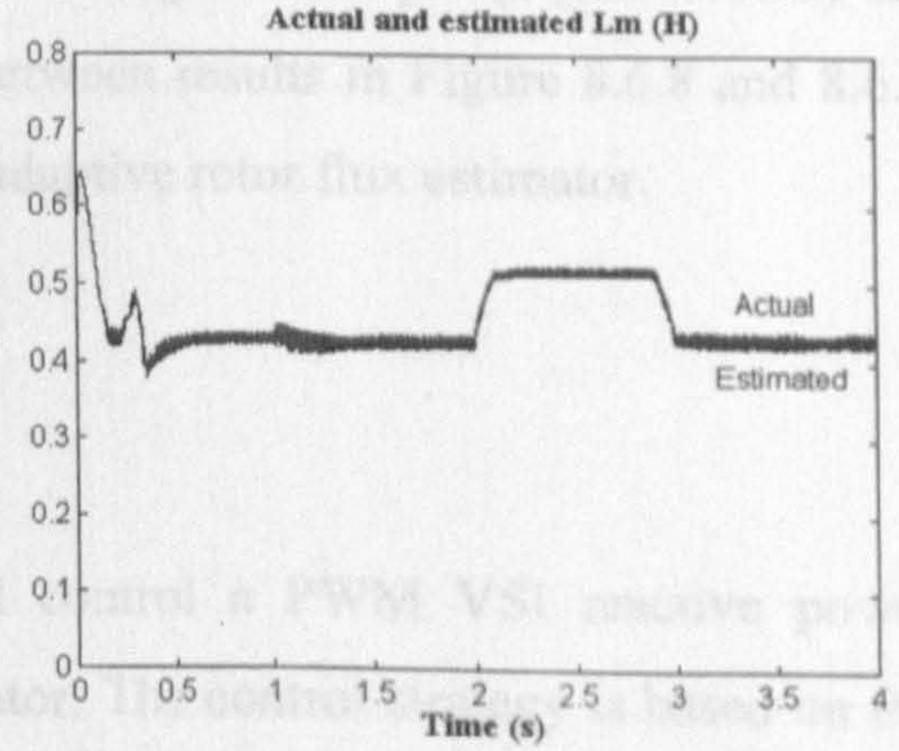

e)

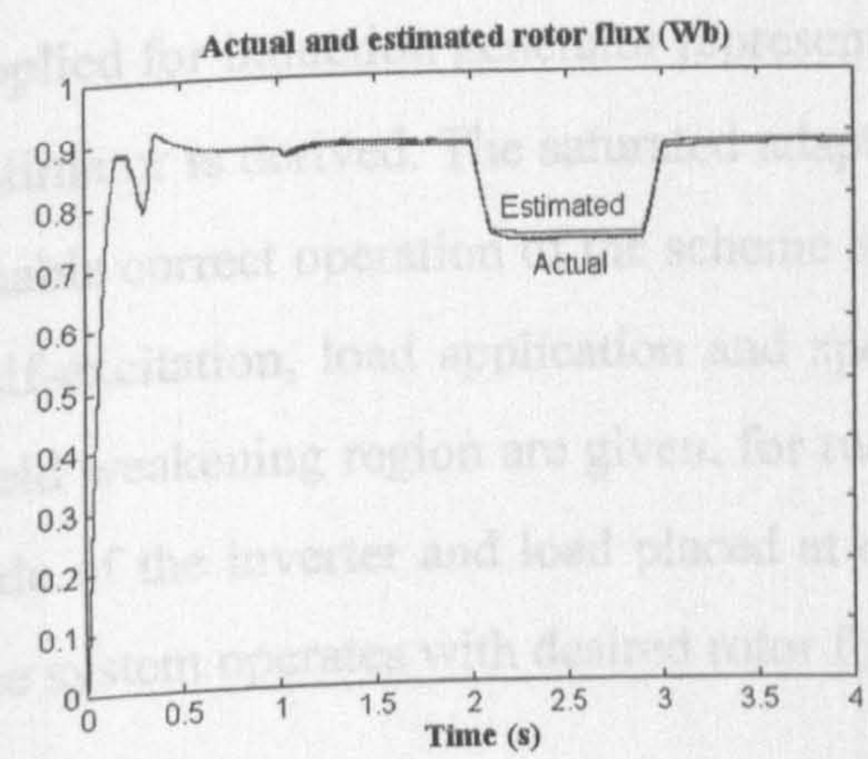

c)

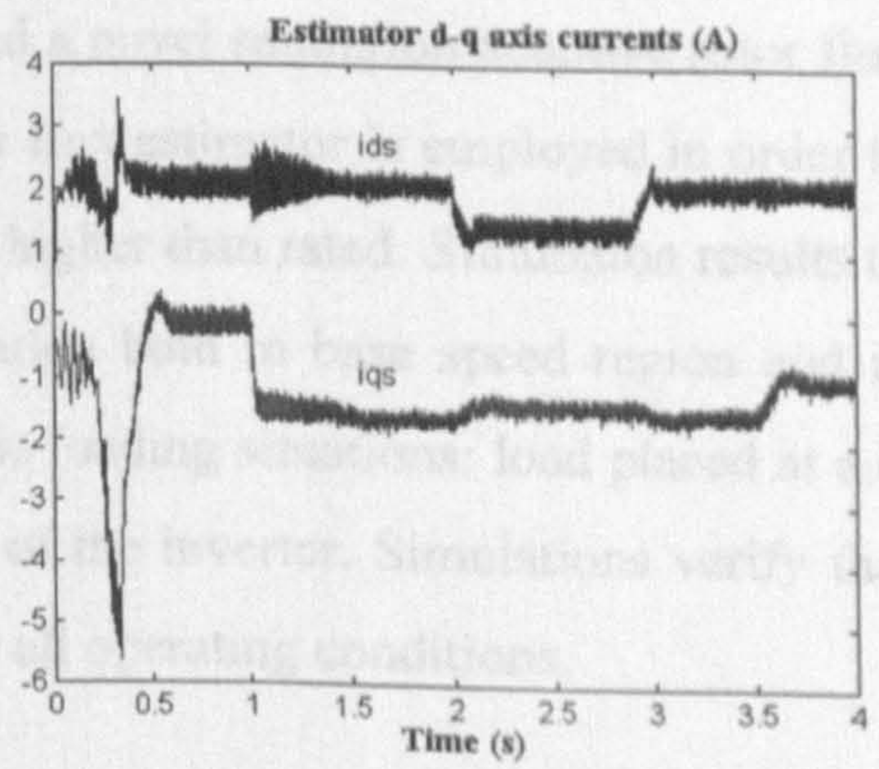

f)

Figure 8.6.8 Self-excitation, step load application and variable speed operation in field weakening region (rotor flux oriented control, d.c. load, battery voltage = 48 V), traces as in Figure 8.6.7

of the rotor flux estimator of Figure 8.5.1, the corresponding constant parameter one is used (Figure 8.4.1), with magnetising inductance set to constant rated value. Simulation results for this case are given in Figure 8.6.9.

D.c. voltage (Figure 8.6.9a) is now significantly more disturbed during speed variation, compared to the case illustrated in Figure 8.6.8a. Fundamental component of the stator voltage (Figure 8.6.9b) shows an increase in value during operation at 1.2 p.u. speed. This is a consequence of the discrepancy between actual and estimated rotor flux (Figure 8.6.9c) that takes place due to omission of main flux saturation compensation in the estimator. Magnetising inductance in the estimator is constant and rated, while the one in the machine significantly increases during operation in the field-weakening region (Figure 8.6.9e). Reduction in stator d-axis current in the field-weakening (Figure 8.6.9f) is insufficient as the estimator does not recognise change in the magnetising inductance. Actual and estimated values of electromagnetic torque (Figure 8.6.9d) are different for operation at 1.2 p.u.. Difference between results in Figure 8.6.8 and 8.6.9 verifies the need for application of a saturation adaptive rotor flux estimator.

8.7 Summary

This chapter presents the rotor flux oriented control a PWM VSI reactive power compensator for a stand-alone induction generator. The control strategy is based on the direct field orientation approach. An appropriate saturated induction machine model is applied for induction generator representation and a novel saturation adaptive rotor flux estimator is derived. The saturated adaptive rotor flux estimator is employed in order to enable correct operation of the scheme at speeds higher than rated. Simulation results of self-excitation, load application and speed variation both in base speed region and in field weakening region are given, for two specific loading situations: load placed at a.c. side of the inverter and load placed at d.c. side of the inverter. Simulations verify that the system operates with desired rotor flux under all operating conditions.

Operation of a variable speed, rotor flux oriented induction generator as a source of constant d.c. voltage is analysed in considerable depth. It is shown that the proposed control scheme is capable of maintaining required d.c. voltage during speed variation in both base speed and field-weakening regions and that d.c. voltage recovery after step load application and load reduction is very fast. Estimated and actual values of the both rotor flux and torque are found to be in excellent agreement for all operating conditions.

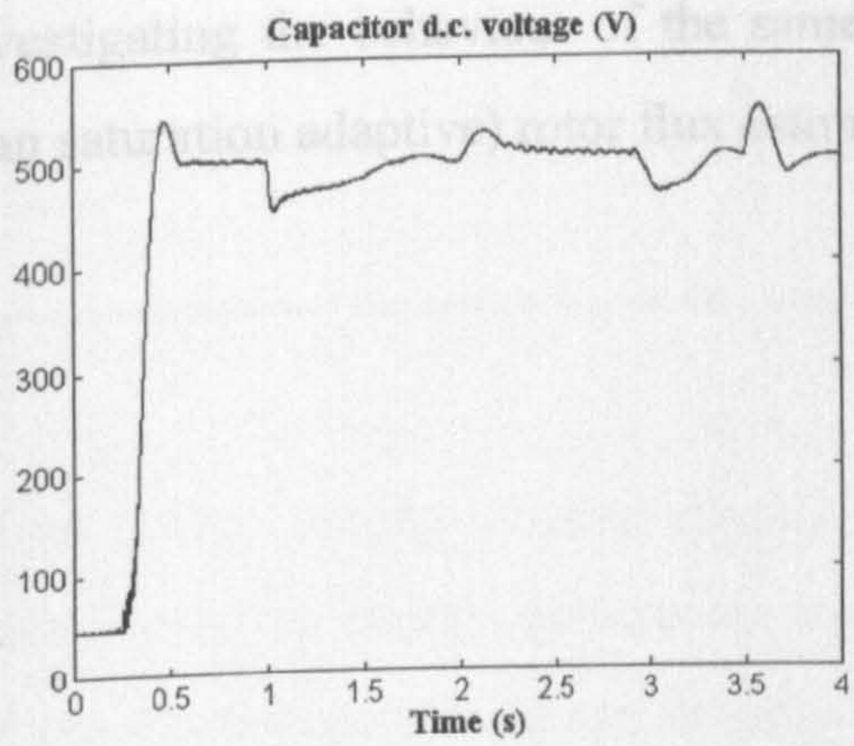

a)

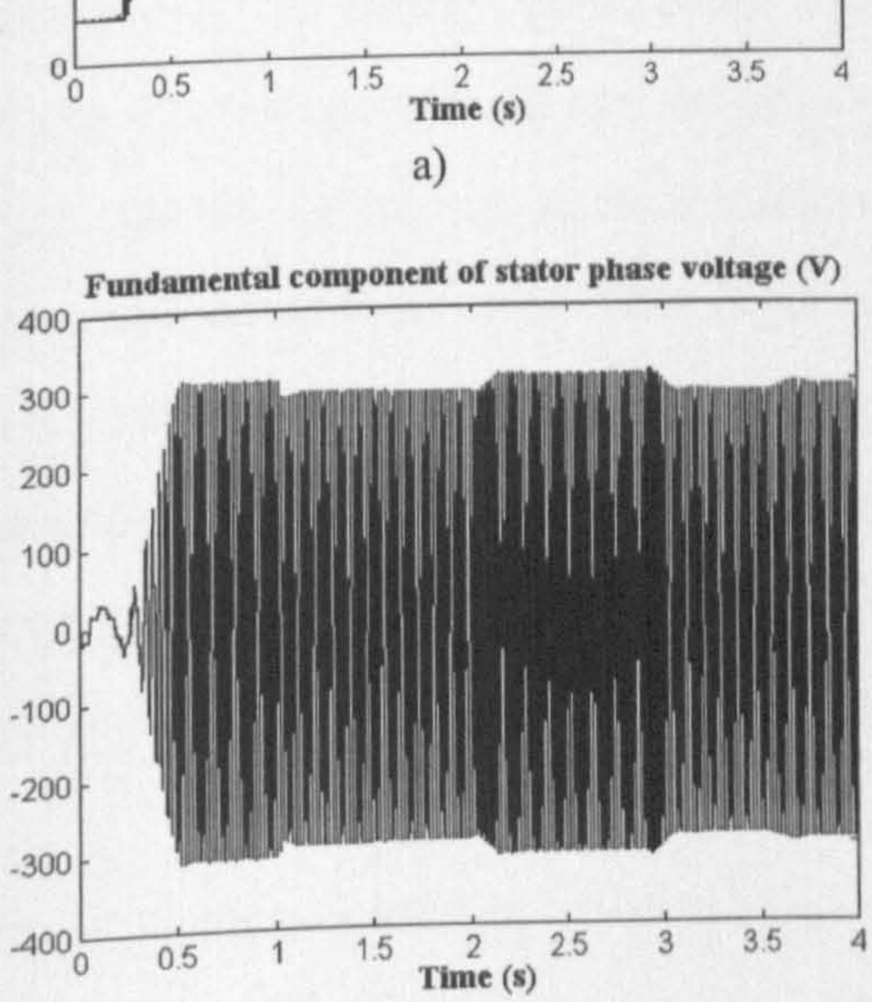

b)

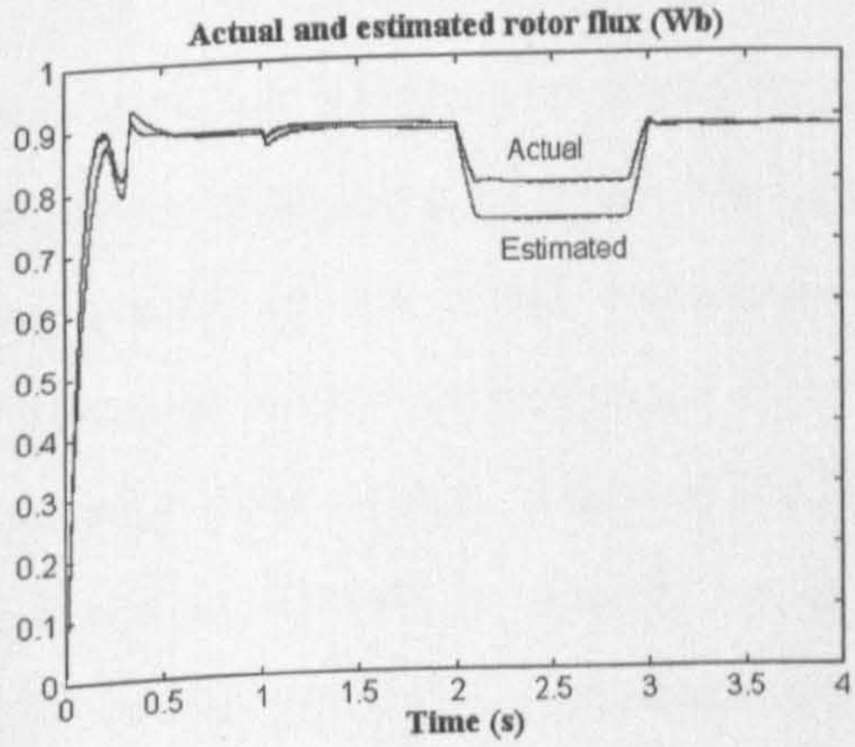

c)

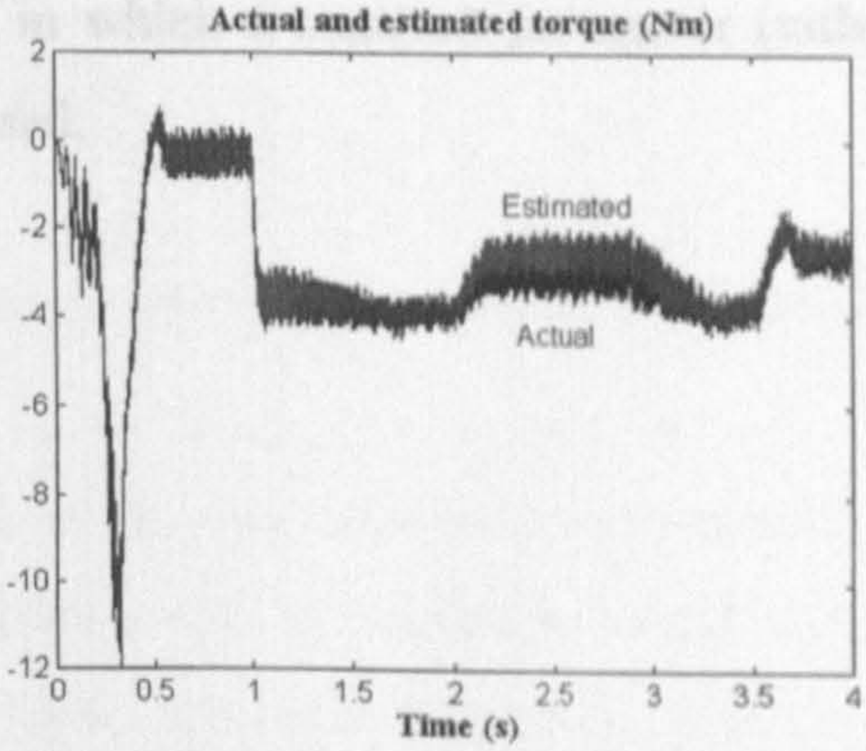

d)

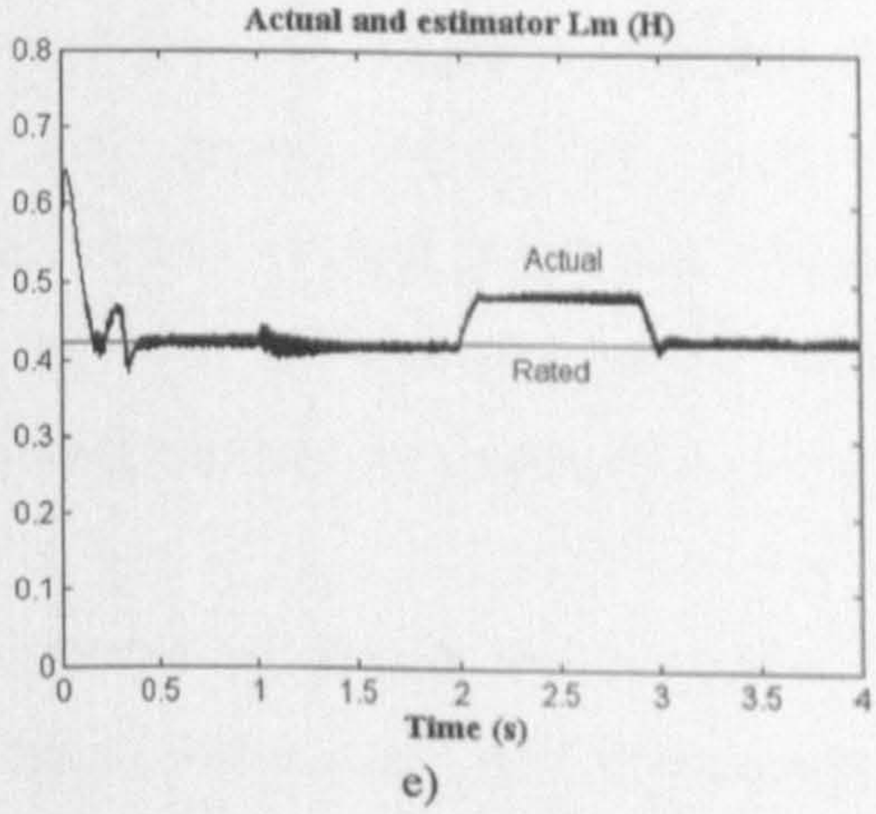

e)

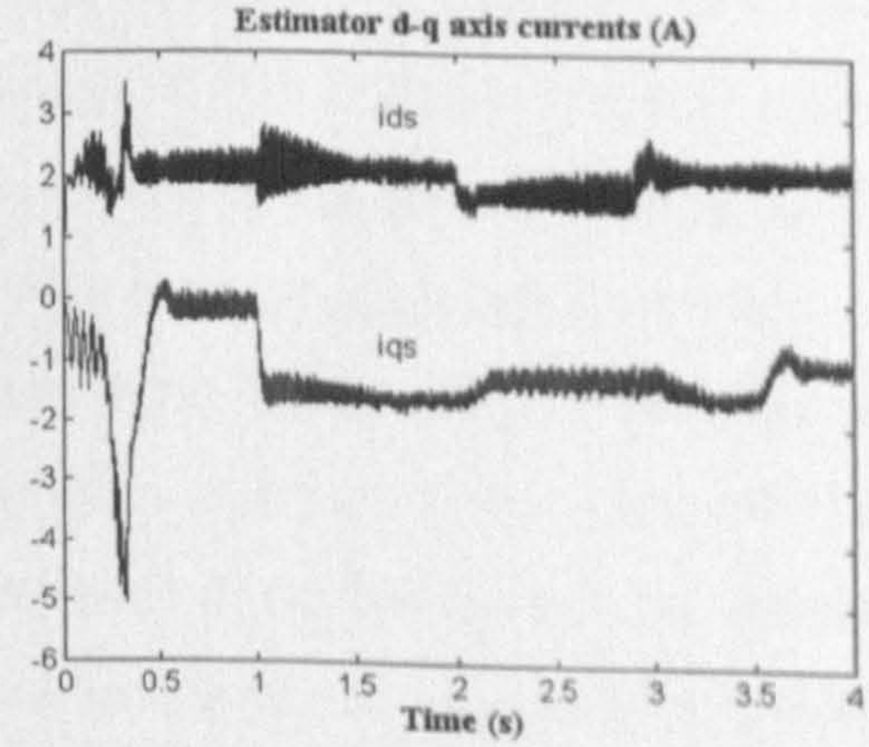

f)

Figure 8.6.9 Self-excitation, step load application and variable speed operation in field weakening region with constant parameter rotor flux estimator (rotor flux oriented control, d.c. load, battery voltage = 48 V), traces as in Figure 8.6.7

The need for application of a saturated adaptive rotor flux estimator is verified by investigating the behaviour of the same system in which a constant parameter (rather than saturation adaptive) rotor flux estimator is used.

Chapter 9

CONCLUSION

Wind power, among other renewable energy sources, can contribute substantially to overall electric energy generation without polluting the environment. Wind turbine driven electric generators can be used as utility grid connected machines or as stand-alone plants supplying an autonomous power system. An induction generator has numerous advantages over other types of generators, due to its simple construction, low cost, self-protection capacity, and minimal maintenance requirement. Induction generators are low cost, reliable option for alternative energy generation systems. Research into application of variable speed induction generators in wind energy generation systems is relative new, especially with regard to autonomous power system.

The first applications of wind turbine driven induction generators were in embedded generation, with direct electrical connection of the generator stator electric terminals to the grid. The inherent shortcoming of induction machines, the need for an external reactive power source, was therefore easily overcome. The necessary reactive power was taken from the grid, while the generator delivered active power to the grid. The consequence of the direct connection is however that the generator operation was restricted to a very narrow range of rotor speeds. Wind energy capture was therefore inherently poor. Much better utilisation of the wind energy can be obtained if the generator is allowed to operate under variable speed conditions. Such an operation however requires that the generator terminals are interfaced with the grid by means of two cascaded power electronic converters, with an intermediate d.c. link. Reactive power remains to be supplied by the grid and active power remains to be delivered to the grid. Introduction of the set of power electronic converters enables this exchange to take place under variable speed conditions.

If a wind turbine driven induction generator is to be used as a sole active power source for an autonomous power system, the problem of reactive power provision for generator operation becomes of utmost importance. Desire to operate the system under variable speed conditions further complicates the problem of reactive power compensation. A review of configurations of available reactive power compensators is provided in Chapter 2. The two types of reactive power compensators, covered in detail in the thesis, are a fixed capacitor bank and a voltage source inverter.

Establishment of stator terminal voltage in a running generator is known under the name of self-excitation process. The voltage build-up will follow the connection of the reactive power compensator to the stator terminals. If a capacitor bank is used as the reactive power compensator, the pattern of the voltage build-up is entirely dependent on the non-linear nature of the machine's magnetising curve. Any model aimed at application in induction generator self-excitation studies must therefore fully account for the main flux saturation. With this in mind, and as transient rather than steady-state analysis is the goal of the study at all times, three dynamic models of a single cage induction machine that fully account for main flux saturation are reviewed in Chapter 3. The models mutually differ with respect to the selected set of state-space variables. Additionally, a current state-space model of a saturated double-cage (deep-bar) induction machine is given as well. This is justified by the fact that many of the off-the-shelf induction machines in the higher power region are of such a construction. If one wants to use an available machine for wind electricity generation rather than to design a new one, there is a great likelihood that the machine will be with deep-bar or double-cage rotor. As dynamic model of a double-cage (deep-bar) induction machine consists of seven differential equations, a reduced order representation, in which two rotor cages are equivalented with a single cage, is developed. A double-cage induction machine is thus represented with a single-cage induction machine model, whose first set of parameters is obtained from the standard no-load and lock-rotor tests on the machine by using the equivalent circuit of a single-cage induction machine, and the second set of parameters is obtained by equivalenting the parallel connection of the two branches in the equivalent circuit of a double-cage induction machine with a single-cage branch.

Different models of saturated induction machines are used for simulation purposes and control system development in subsequent chapters of the thesis.

Dynamics of self-excitation process of an induction generator, using fixed capacitor bank, have been investigated both experimentally and by detailed simulation for a single-cage and a double-cage induction machine. Results regarding no-load self-excitation and subsequent loading are presented for both single-cage and double-cage induction generator. Load voltage variation compensation, using an additional series capacitor bank apart from the parallel capacitor bank, is investigated for single-cage induction generator. The impact of a reduced order double-cage induction machine modelling on simulation results is studied for no-load self-excitation and loading transients. It is found that such simulations yield satisfactory results if the rotor parameters are obtained from standard tests on the machine.

Detailed experimental study of the induction generator self-excitation process with star and delta connected fixed capacitor bank, under variable speed conditions, had been conducted and the results have been presented. Situations that result in voltage collapse and complete demagnetisation are reported. Evaluation of load voltage variation compensation with combined parallel and series capacitor banks has also been done by experiments. The emphasis in experimental work was at all times placed on dynamics during variable speed operation. This is an operating mode that has not been dealt with in detail in the past, as dynamics are usually discussed under the assumption that the operating speed is constant. Some of the frequently quoted conclusions in the literature have been found not to be universally valid, while some others have been confirmed by the experimental investigation. On the basis of results of the experimental study it was concluded that the scheme with fixed capacitor bank is not suitable for variable speed operation of stand-alone induction generator, as the reactive power is not controlled.

In order to overcome the problem of appropriate reactive power provision in variable speed operation and under varying load conditions a more complex reactive power compensator is needed. The one selected for further investigation is the compensator of the voltage source inverter type. Static reactive power compensator of voltage source

inverter type, controlled using PWM, has been at first investigated in detail by simulation, assuming passive R-L load at the a.c. side instead of the induction generator. An original implementation of the PWM voltage source inverter model is developed in MATLAB/SIMULINK environment.

Different ways of controlling the PWM voltage source inverter, when used as the reactive power compensator for the induction generator, are investigated next. The first control method is the open-loop one, in which the compensator is controlled using scalar technique. Performance of the induction generator with scalar method control of a PWM VSI based reactive power compensator, with emphasis placed on variable speed operation, has been analysed by simulation. The inverter output frequency is scalar controlled, sinusoidal PWM is used and V / f_s = constant control law is applied. Self-excitation under no-load conditions, transients after step load application and dynamics associated with speed change are simulated. As a consequence of open-loop control, this scheme exhibits extremely high sensitivity to stator frequency variation and load application. Therefore, speed measurement and closed-loop slip frequency are required in practice.

As the reactive power compensator should provide self-excitation and constant flux operation of the generator during both transient and steady-state operation, both capacitor bank and scalar controlled PWM VSI cannot be used. Appropriate control strategies for an induction generator with reactive power compensator of current-controlled voltage source type, based on vector control theory, are developed with a goal of achieving constant flux operation of the generator under varying speed and load conditions. Two novel control strategies, namely, direct stator flux oriented control and direct rotor flux oriented control, have been developed and verified by simulation. Vector control strategies, applied to the control of PWM VSI, have resulted in independent control of active and reactive power flow in the system. In stator flux oriented control scheme, the reactive power necessary for excitation is controlled by the stator flux control loop while the active power is controlled by the d.c. voltage control loop. Hysteresis current control technique is applied to the control of the PWM VSI reactive power compensator with current control executed in stationary reference frame.

Stator flux is estimated using measured generator stator voltages and stator currents. Self-excitation under no-load conditions and step application of an a.c. load are simulated for variable speed operation in both base speed region and field-weakening region. It is shown that almost constant stator flux value during transients is achieved.

In rotor flux oriented control scheme, rotor flux and d.c. voltage are closed-loop controlled. The decoupled control of stator d-q axis currents enables decoupled control of active and reactive power. Estimation of rotor flux is performed using measured stator current and rotor speed. Hysteresis current control is employed for the control of the PWM VSI compensator. Application of vector control techniques naturally lends itself to the operation of induction generator in field-weakening region with variable rotor flux reference. Constant parameter rotor flux estimator enables satisfactory operation of the system only in the base speed region. In order to fully account for main flux saturation for operation in field-weakening region, a novel saturated adaptive rotor flux estimator is developed. The estimator is based on measurement of stator currents and rotor speed and its structure is derived from one of the full saturated machine models of Chapter 3. Its complexity is judged to be moderate and it can be easily implemented using latest DSP technology. Dynamics of self-excitation process, step load application, load variation and variable speed operation are simulated, for two specific loading situations, load placed at a.c. side of the inverter and load placed at the d.c. side of the inverter. Simulations verify that the system with a saturation adaptive rotor flux estimator operates with desired rotor flux under all operating conditions.

The control scheme developed for the d.c. load is believed to be particularly interesting. It has been shown that it is possible to provide constant d.c. voltage operation for such a load under widely varying speed and loading conditions. Transients in d.c. voltage quickly die off and the desired d.c. voltage level is maintained in both base speed and field weakening region. Due to the nature of the load, it is suggested that the optimal generator utilisation results in this case if the generator is operated in the field weakening region only.

It is concluded that the vector control schemes provide superior performance when compared to scalar control scheme, although vector control schemes require higher d.c. link capacitor values and higher initial voltage than the scalar control scheme. Rotor flux oriented control scheme exhibits the most favourable behaviour. The vector-controlled variable speed induction generators can be used to supply either an autonomous a.c. power system or an autonomous d.c. power system.

The research carried out in this project has resulted in four international conference publications and one international journal publication, as listed in the Appendix B. All the research objectives listed in Chapter 1 are satisfactorily met. Recommendations for further work are summarised as follows.

Alternative control strategies, such as sensorless vector control and direct torque control, may be investigated. In sensorless vector controlled drives speed sensors are not required, thus reducing hardware complexity and the overall cost. The direct torque controlled drives, where the electromagnetic torque and stator flux are estimated, can provide very fast torque response. Applications of sensorless or direct torque control techniques to wind energy generation systems have not been reported yet.

The induction machine models used here account for main flux saturation only. Investigation into the effect of inclusion of iron loss in the models may be another direction for further research.

Different current control techniques, such as for example fuzzy logic and neural network based current controllers, can be researched in the further work. The application of a fuzzy logic controller may also be investigated for maximising power utilisation and enhancing performance of a wind generation system.

The study in the thesis is focused on the stand-alone applications of induction generators, aimed at supplying either a.c. or d.c. loads. The proposed vector controlled variable speed induction generators can be interfaced with the utility grid by means of a second PWM VSI. In this case, high quality, unity power factor, three-phase 50 Hz

supply can be achieved. Further research may investigate the use of matrix converter that avoids two stage a.c.-d.c.-a.c. power conversions.

Last but not least, it is believed to be worth looking at the applicability of the developed rotor flux oriented control scheme for the induction generator in hybrid electric vehicles. Starter and generator (alternator) in combustion engine vehicles are two separate electric machines, doing two separate functions in motoring and generating mode of operation, respectively. It is one of the research trends in vehicle technology to try to substitute these two machines with a single electric machine, that can be operated as both an electric motor and as an electric generator. Induction machine, due to its low cost and high reliability, is a natural candidate. As rotor flux oriented control can be used for both motoring and generating operation, it is believed that the scheme developed for the induction generator supplying a d.c. load with constant voltage could directly lend itself to control of a unified starter/generator machine in future vehicles.

REFERENCES

Abouzeid,M. (1998), Load effect on the output current generated from the switched reluctance generator, *Proceedings of the IEE 7th International Conference on Power Electronics and Variable Speed Drives PEVD*, London, UK, IEE Conference Publication no. 456, pp.560-567.

Akagi,H., Kanazawa,Y., Nabae,A. (1984), Instantaneous reactive power compensators comprising switching devices without energy storage components, *IEEE Transactions on Industry Applications*, vol.IA-20, no.3, pp.625-630.

Al-Bahrani,A.H., Malik,N.H. (1993), Steady-state analysis of parallel-operated self-excited induction generators, *IEE Proceedings - C*, vol. 140, no. 1, pp. 49-55.

Alexandrovitz,A., Yair,A., Epstein,E. (1984), Analysis of static VAR compensator with optimal energy storage element, *IEEE Transactions on Industrial Electronics*, vol.IE-3, no.1, pp.28-33.

Al Jabri,A.K., Alolah,A.I. (1990), Capacitance requirements for isolated self-excited induction generators, *IEE Proceedings*, vol.137, pt.B, no.3, pp.154-159.

Andrieux,C., Lajoie-Mazenc,M. (1985), Analysis of different current control systems for inverter-fed synchronous machines, *Proceedings of EPE'85*, Brussels, Belgium, pp.2.159-2.165.

Basset,E.D., Potter,F.M. (1935), Capacitor excitation for induction motors, *AIEE Transactions*, vol. 54, pp. 540-545.

Bhadra,S.N., Ratnam,K., Manjunath,A. (1996), Study of voltage build up in a self-excited variable speed induction generator/static inverter system with d.c. side capacitor, *Proceedings of the 1996 IEEE International Conference on Power Electronics, Drives and Energy Systems for Industrial Growth*, New Delhi, India, pp.964-970.

Bim,E., Szajner,J., Burrian,Y. (1989), Voltage compensation of an induction generator with long-shunt connection, *IEEE Transactions on Energy Conversion*, vol.4, no.3, pp.526-530.

Blocklehurst,F.K. (1996), Wind energy resource in the UK, *Proceedings of the 18th British Wind Energy Association Conference*, UK, September, pp.371-376.

Boldea,I., Nasar,S.A. (1992), *Vector control of ac drives*, CRC Press.

Bowes,S.R., Mount,M.J. (1981), Microprocessor control of PWM inverters, *IEE Proceedings*, Pt.B, vol.128, no.6, pp.293-305.

Brod,D.M., Novotny,D.W. (1985), Current control of VSI-PWM inverters, *IEEE Transactions on Industry Applications*, vol.21, no., pp.562-570.

Brown,J.E., Kovacs,K.P., Vas,P. (1983), A method of including the effects of main flux path saturation in the generalised equations of AC machines, *IEEE Transactions on Power Apparatus and Systems*, vol,102, no.1, pp.96-103.

CADDET UK National Team, (1997), Europe's largest wind farm, *CADDET Renewable Energy Newsletter*, March.

Catto,G. (1996), Recent developments in the use of electrical machines in wind turbines, *Proceedings of ICEM*, Spain, pp.353-357.

Chakraborty,C, Bhadra,S.N. (1996), Excitation requirements for stand alone induction generators, *Proceedings of the 1996 IEEE International Conference on Power Electronics, Drives and Energy systems for Industrial Growth*, New Delhi, India, pp.700-706.

Chan,T.F. (1993), Capacitance requirements of self-excited induction generators, *IEEE Transaction on Energy Conversion*, vol.8, no.2, pp.304-311.

Chan,T.F. (1995), Analysis of self-excited induction generators using an iterative method, *IEEE/PES Winter Meeting*, New York, NY, Paper no. 95WM076-0EC.

Chan,T.F. (1996), Self-excited induction generators driven by regulated and unregulated turbines, *IEEE/PES Winter Meeting*, Baltimore, MD, Paper no. 96WM151-1EC.

Colliez,C., Tounzi,A., Piriou,F. (1997), Vector control of an autonomous induction generator connected to a PWM rectifier, *Proceedings of the 7th European Conference on Power Electronics and Applications*, Trondheim, Norway, pp.711-716.

Craig,L.M, Davidson,M. (1995), *Integration of wind turbines onto the electrical network*, Harwell Laboratory Energy Support Unit.

De Doncker,R.W., Novotny,D.W. (1988), The universal field oriented controller, *Conference Record of IEEE IAS Annual Meeting*, Pittsburgh, PA, USA, pp.450-456.

De Doncker,R.W., Profumo,F. (1989), The universal field oriented controller applied to tapped stator windings induction motors, *Conference Record of IEEE Power Electronics Specialists Conference*, Milwaukee, WI, USA, pp.1031-1036.

De Doncker,R.W., Profumo,F., Pastorelli,M. (1990), Self tuning of induction motor servo drives using the universal field oriented controller, *Conference Record of*

IEEE Power Electronics Specialist Conference, PESC, San Antonio, TX, USA, pp.649-655.

Dezza.F.C., Gerlando,A.D., Perini,R. (1995), Performance comparison among different converters fed by self excited wind driven induction generators, *Proceedings of IEE Conference on Electrical Machines and Drives*, Durham, UK, pp.438-443.

Dezza.F.C., Gerlando.A.D., Perini.R. (1997), Modelling and experimental investigation of energy conversion systems employing wind-driven induction generators with electronically controlled self-excitation and power output, *Proceedings of the 7th European Conference on Power Electronics and Application*, Trondheim, Norway, pp.652-658.

Elder,J.M., Boys,J.T., Woodward,J.L. (1983) The Process of self-excitation in induction generators, *IEE Proceedings*, vol.130, pt.B, no.2, pp.103-108.

Elder,J.M., Boys,J.T., Woodward,J.L. (1984), Self-excited induction generator as a small low-cost generator, *IEE Proceedings*, vol.131, pt.C, no.2, pp.33-41.

Erdman,W.L., Hoft,R.G. (1990), Induction machine field orientation along airgap and stator flux, *IEEE Transactions on Energy Conversion*, vol.5, no.1, pp.115-121.

Ermis,M., Ertan,H.B., Demirekler,M., Saribatir,B.M., Uctug,Y., Sezer,M.E., Cadirci,I. (1992), Various induction generator schemes for wind-electricity generation. *Electric Power Systems Research*, vol.23, pp.71-83.

Flinders,F., Senini,S., Oghanna,W. (1993), Mixed electrical & mechanical simulations using dynamic system analysis packages, *Proceedings of the 1993 IEEE/ASME Joint Railroad Conference*, New York, USA, IEEE Press, Cat. no.93CH3266-4, pp.87-93.

Gaio,E., Piovan,R., Malesani,L. (1988), Evalution of current control methods for voltage source inverters, *Proceedings of ICEM'88*, Pisa, Italy, pp.345-350.

Gardner,P. (1996), *Electrical issues associated with variable speed operation of wind turbines*, Harwell Laboratory Energy Support Unit.

Gerlando,A.D., Perini,R., Vistoli,I. (1994), Operation analysis of controlled rectifying bridges fed by wind driven self-excited induction generators, *Symposium on Power Electronics, Electrical Drives, Advanced Electrical Motors*, SPEEDAM'94, Taormina, Italy, pp.459-464.

Gipe,P. (1997), *Overview of worldwide wind generation*, Paul Gipe & Associate.

Grantham,C., Sutano,D., Mismail,B. (1989), Steady-state and transient analysis of self-excited induction generators, *IEE Proceedings*, vol.136, pt.B, no.2, pp.61-68.

Gyugyi,L. (1979), Reactive power generation and control by thyristor circuits, *IEEE Transactions on Industry Applications*, vol.IA-5, no.5, September/October, pp.521-532.

Hallenius,K.E., Vas,P., Brown,J.E. (1991), The analysis of a saturated self-excited asynchronous generator, *IEEE Transactions on Energy Conversion*, vol. 6, no. 2, pp. 336-341.

Halliday,J.A. (1993), Wind energy: an option for the UK?, *IEE Proceedings-A*, vol.140, no.1, pp.53-62.

Hammons,T.J. (1993), Perspectives on the future of power generation and transmission world-wide, *Proceedings of the IEEE*, vol.81, no.3, pp.333-345.

Handley,P.G., Boys,J.T. (1990), Space vector modulation: an engineering review, *Proceedings of IEE Conference on PEVD*, London, UK, pp.87-91.

Handley,P.G., Boys,J.T. (1992), Practical real-time PWM modulators: an assessment, *IEE Proceedings*, Pt.B, vol.139, no.2, pp.96-102.

Harashima,F., Kondo,S., Ohnishi,K., Kajita,M., Susono,M. (1985), Multi-microprocessor-based control system for quick response induction motor drive, *IEEE Transactions on Industry Applications*, vol.21, no.4, pp.602-609.

Hayakawa,I., Shimizu,H., Saitoh,F. (1993), Utility-grid interactive three-phase inverter system incorporating wind turbine-driven induction generator and PWM converter, *Proceedings of the 28th Universities Power Engineering Conference*, Stafford, UK, pp.832-836.

He,Y.K., Lipo,T.A. (1984), Computer simulation of an induction machine with spatially dependent saturation, *IEEE Transactions on Power Apparatus and Systems*, vol.103, no.4, pp.707-714.

Healey,R.C., Walliamson,S., Smith,A.C. (1995), Improved cage rotor models for vector controlled induction machines, *IEEE Transactions on Industry Application*, vol.31, no.4, pp.812-822.

Ho,Y.Y., Sen,P.C. (1988), Decoupling control of induction motor drives, *IEEE Transactions on Industrial Electronics*, vol.35, no.2, pp.253-262.

Holtz,J., Stadtfeld,S. (1985), A PWM inverter drive system with on-line optimised pulse patterns, *Proceedings EPE'85*, Brussels, Belgium, pp.3.21-3.25.

Houghton,D., Oghanna,W. (1993), A generalised dynamic induction motor model, *Proceedings of the International Conference on Electrical Machines in Australia*, ICEMA, Adelaide, Australia, pp.1-7.

Jacobina,C.B., Silva,E.R.C., Lima,A.M.N., Ribeiro,R.L.A. (1996), Induction generator

static systems with a reduced number of components, *Proceedings of IEEE Industrial Application Society Annual Meeting*, San Diego, CA, USA, pp.174-178.

Jain,D.K., Mittal,A.P., Singh,B. (1996), Advanced controlled series compensated self excited induction generator, *Proceedings of the 1996 IEEE International Conference on Power Electronics, Drives and Energy systems for Industrial Growth*, New Delhi, India, pp.707-712.

Jayadev,J. (1995), Harnessing the wind, *IEEE Spectrum*, November, pp.78-83.

John,G., Erdman,W., Hudson,R., Fan,C.,Mahajan,S. (1995), Stator flux estimation from inverter switching states for the field oriented control of induction generators, *Proceedings of IEEE Industrial Application Society Annual Meeting IAS'95*, USA, pp.182-188.

Jones,R., Smith,G.A. (1993), High quality mains power from variable-speed wind turbines, *Proceedings of IEE Conference on Renewable Energy - Clean Power 2001*, London, UK, pp.202-206.

Jones,R., Gilmore,I. (1995), Benefits of sinusoidal rectifiers on variable speed wind turbines - high quality mains power from variable speed wind turbines, *Proceeding of the 17th British Wind Energy Conference*, Warwick, UK, pp.339-358.

Kazmierkowski,M.P. (1994); Review of current regulation techniques for three-phase PWM inverter, *Proceedings of the IEEE International Conference on Industrial Electronics, Control, and Instrumentation IECON'94*, Bologna, Italy, pp.567-575.

Kerkman,R.J. (1985), Steady-state and transient analysis of an induction machine with saturation of magnetising branch, *IEEE Transactions on Industry Applications*, vol.21, no.1, pp.226-234.

Kohlmeier,H., Schroder,D. (1986), GTO pulse inverters with on-line optimised pulse patters for current control, *Proceedings of ICEM'86*, Munchen, Germany, pp.668-671.

Kragset,V., Nilssen,R. (1994), A PWM converter for excitation of induction generators, *Proceedings of Power Electronics and Motion Control Conference PEMC'94*, Warsaw, Poland, pp.297-302.

Krause,P.C., Wasynczuk,O., Sudhoff,S.D. (1995), *Analysis of electric machinery*, IEEE Press.

Krzeminski,Z. (1988), Differential equations of induction motor with nonlinear control synthesis with regard to saturation of main magnetic path, *Rozprawy Elektrotechniczne*, vol.34, no.1, pp.117-131.

Lai,J. (1994), Power electronics system modelling and simulation, *Proceedings of the IEEE 4th Workshop on Computers in Power Electronics*, USA, pp.45-55.

Leonhard,W. (1996), *Control of electrical drives*, Springer-Verlag.

Leplat,P.M., Tounzi,A., Clenet,S., Piriou,F. (1996), Study of an autonomous induction generator connected to a PWM rectifier, *Proceedings of ELECTRIMACS'96*, Saint-Nazaire, France, pp.1089-1094.

Levi,E., Vukosavic,S., Vuckovic,V. (1990), Saturation compensation schemes for vector controlled induction motor drives, *Record of 21st Annual IEEE Power Electronic Specialists Conference*, San Antonio, TX, USA, Cat. no. 90CH2873-8, pp.591-598.

Levi,E., Rauski,D. (1993), Modelling of deep-bar and double-cage self-excited induction generators for wind electricity generation studies, *Electric Power Systems Research*, vol. 27, no. 1, 1993, pp. 73-81.

Levi,E., Vuckovic,V. (1993), Rotor flux computation in saturated field-oriented induction machines, *Electric Machines and Power Systems*, vol.21, pp.741-754.

Levi,E. (1994a), Applications of current state-space model in analyses of saturated induction machines, *Electric Power Systems Research*, vol. 31, no. 3, pp. 203-216.

Levi,E. (1994b), Magnetic saturation in rotor-flux-oriented induction motor drives: operating regimes, consequences and open-loop compensation, *European Transactions on Electrical Power Engineering ETEP*, vol.4, no.4, pp.277-286.

Levi,E. (1995a), A unified approach to main flux saturation modelling in D-Q axis models of induction machines, *IEEE Transactions on Energy Conversion*, vol.10, no.3, pp.455-461.

Levi,E. (1995b), Modelling of saturated induction machines using flux linkages as state-space variables, *Proceedings of International Power Engineering Conference IPEC'95*, Singapore, pp.533-538.

Levi,E. (1996), Main flux saturation modelling in double-cage and deep-bar induction machines, *IEEE PES Winter Meeting*, Baltimore, MD, USA, paper no. 96WM136-2EC.

Levi,E., Krzeminski,Z. (1996), Main flux-saturation modelling in d-q axis models of induction machines using mixed current-flux state-space models, *European Transactions on Electrical Power*, vol.6, no.3, 207-215.

Levi,E., Liao,Y.W., Morgan,R. (1996), Single-cage representation of saturated double-cage induction generators for self-excitation studies, *Proceedings of the 31st*

Universities Power Engineering Conference, Iraklio, Greece, pp.207-210.

Levi,E. (1997), Generalised method of magnetising flux saturation modelling in d-q axis models of double-cage induction machines, *IEE Proc.-Electr. Power Appl.*, vol.144, no.2, pp.101-109.

Liao,Y., Levi,M., Morgan,R. (1996), Simulation of PWM voltage source inverter based reactive power compensators using SIMULINK, *Proceedings of the 29th International Intelligent Motion Conference PCIM'96*, Nuremberg, Germany, pp.519-525.

Liao,Y.W., Levi,E. (1997), A study of self-excitation schemes for an isolated induction generator, *Proceedings of the 32nd Universities Power Engineering Conference*, Manchester, UK, pp.1110-1113.

Liao,Y.W., Levi,E. (1998a), Variable speed induction generator as a source of constant DC voltage, *Proceedings of the 33rd Universities Power Engineering Conference*, Edinburgh, UK, pp.759-762.

Liao,Y.W., Levi,E. (1998b), Modelling and simulation of a stand-alone induction generator with rotor flux oriented control, *Electric Power System Research*, vol.46, pp.141-152.

Lorenz,R.D., Novotny,D.W. (1988), A control system perspective of field oriented control for AC servo drives, *Proceedings of Control Expo 88*, pp.18.1-18.12.

Lyra,R.O.C., Silva,S.R, Cortizo,P.C. (1995), Direct and indirect flux control of an isolated induction generator, *Proceedings of IEEE International Conference on Power Electronics and Drive Systems*, PEDS'95, Singapore, pp.140-145.

Malik,N.H., Haque,S.E. (1986), Steady-state analysis and performance of an isolated self-excited induction generator, *IEEE Transactions on Energy Conversion*, vol. EC-1, no. 3, pp. 134-139.

Malik,N.H., Mazi,A.A. (1987), Capacitance requirements for self-excited induction generators, *IEEE Transactions on Energy Conversion*, vol.2, no.1, pp.62-69.

Malik,N.H., Al-Bahrani,A.H. (1990), Influence of the terminal capacitor on the performance characteristics of a self-excited induction generator, *IEE Proceedings*, vol.137, pt.C, no.2, pp.168-173.

Margato,E., Santana,J. (1996), Induction generator excited by current source inverter used as a d.c. power supply - modelling and behaviour, *Proceedings of IEEE International Symposium on Industrial Electronics ISIE'96*, Warsaw, Poland, pp.814-819.

Marino,P., Mungiguerra,V., Porzio,M., Setola,R., Vasca,F. (1995), A simulation tool for induction motor control, *Proceedings of the 6th European Conference on Power*

Electronics and Applications EPE, Seville, Spain, pp.3.610-3.615.

MathWorks Inc. (1992), *Simulink Users Guide*.

Mathew,R., Oghanna,W. (1993), Simulation of a three level inverter-induction motor system, *Proceedings of the International Conference on Electrical Machines in Australia ICEMA*, Adelaide, Australia, pp.216-223.

Mayer,H.R., Pfaff,G. (1985), Direct control of induction motor currents - design and experimental results, *Proceedings EPE'85*, Brussels, Belgium, pp.3.7-3.12.

McMurray,W. (1984), Modulation of the chopping frequency in DC choppers and PWM inverters having current-hysteresis controllers, *IEEE Transactions on Industry Applications*, vol.20, no.4, pp.763-768.

Melkebeek,J.A.A. (1983a), Magnetising-field saturation and dynamic behaviour of induction machines Part 1: Improved calculation method for induction-machine dynamics, *IEE Proceedings*, vol.130, Pt.B, no.1, pp.1-9.

Melkebeek,J.A.A. (1983b), Magnetising-field saturation and dynamic behaviour of induction machines Part 2: Stability limits of a voltage-fed induction motor and of a self-excited induction generator, *IEE Proceedings*, vol.130, Pt.B, no.1, pp.10-17.

Melkebeek,J.A.A., Novotny,D.W. (1983), Small signal dynamic analysis of regeneration and self-excitation in induction machines, *Electric Machines and Power Systems*, pp.259-280.

Miller,T.J.E. (1982), *Reactive power control in electric power systems*. John Wiley and Sons, New York.

Miranda,M.S., Lyra,R.O.C., Silva,S.R. (1997), Wind-power pumping system using induction machines with pulse width modulation (PWM) excitation, *Proceedings of the 7th European Conference on Power Electronics and Applications*, Trondheim, Norway, pp.637-641.

Mori,S., Matsuno,K., Hasegawa,T., Ohnishi,S., Takeda,M., Seto,M., Murakami,S., Ishiguro,F. (1993), Development of a large static VAR generator using self-commutated inverters for improving power system stability, *IEEE Transactions on Power Systems*, vol.8, no.1, pp.371-377.

Mucko,J.L., Gientkowski,Z. (1994), The voltage source inverter applied as reactive power source in voltage stabilisation circuit for the asynchronous generator, *Proceedings of Power Electronics and Motion Control Conference PEMC'94*, Warsaw, Poland, pp.1206-1209.

Muljadi,E., Carlin,P.W., Osgood,R.M. (1993), Circle diagram approach for self excited induction generators, *Proceedings of North American Power Symposium*, USA,

pp.664-671.

Murphy,J.M.D., Turnbull,F.G. (1988), *Power electronic control of AC motors*, Pergamon Press.

Murthy,S.S., Malik,O.P., Tandon,A.K. (1982), Analysis of self-excited induction generators, *IEE Proceedings*, vol.129, pt.C, no.6, pp.260-265.

Murthy,S.S., Prabhu, C., Tandon,A.K., Vaishya,M.O. (1996), Analysis of series compensated self excited induction generators for autonomous power generation, *Proceedings of the 1996 IEEE International Conference on Power Electronics, Drives and Energy systems for Industrial Growth, New Delhi*, India, pp.678-693.

Nabae,A., Ogasawara.S., Akagi,H. (1986), A novel control scheme for current-controlled PWM inverters, *IEEE Transactions on Industry Applications*, vol.IA-22, no.4, pp.697-701.

Novotny,D.W., Gritter,D.J., Studman,G.H. (1977), Self-excitation in inverter driven induction machines, *IEEE Transaction on Power Apparatus and System*, vol.PAS-96, no.4, pp.1117-1125.

Novotny,D.W., Lipo,T.A. (1996), *Vector control and dynamics of ac drives*, Clarendon Press, Oxford.

Ojo,O. (1995), Dynamics and system bifurcation in autonomous induction generators, *IEEE Transactions on Industry Applications*, vol. 31, no. 4, pp. 918-924.

Ojo,O., Gonoh,B. (1996), A controlled stand-alone single-phase induction generator, *Proceedings of the 1996 IEEE International Conference on Power Electronics, Drives and Energy systems for Industrial Growth*, New Delhi, India, pp.694-699.

Osama,M., Sakkoury,K., Lipo,T. (1993), Transient behaviour comparison of saturated induction machine models, *Proceedings of IMACS-TCI'93*, Montreal, Canada, pp.577-580.

Papadopoulos,M.P., Papathanassiou,S.A., Tentzerakis,S.T. (1996), Modelling of induction machine main flux saturation in the arbitrary reference frame - A case study on wind turbine self-excitation, *Proceedings of ICEM*, Vigo, Spain, pp.51-56.

Pena,R., Clare,J.C., Asher,G.M. (1996), Doubly fed induction generator using back-to-back PWM converters and its application to variable-speed wind-energy generation, *IEE Proceedings-Electr. Power Appl.*, vol.143, no.3, pp.231-241.

Quazene,L., McPherson,G. (1983), Analysis of the isolated induction generator, *IEEE Transaction on Power Apparatus and Systems*, vol.102, no.8, pp.2793-2798.

Rajakaruna,S., Bonert,R. (1993), A technique for the steady-state analysis of a self-excited induction generator with variable speed, *IEEE Transactons on Energy Conversion,* vol. 8, no. 4, pp. 757-761.

Rauski,D., Levi,E. (1992), Modelling and simulation of double-cage induction motor dynamics, *Proceedings of International Aegean Conference on Electrical Machines and Power Electronics*, Kusadasi, Turkey, pp.43-48.

Rowan,T.W., Kerkman,R.J. (1986), A new synchronous current regulator and an analysis of current-regulated PWM inverters, *IEEE Transactions on Industry Applications*, vol.22, no.4, pp.678-690.

Saad-Saoud,Z., Craig,L.M., Jenkins,N. (1995), Static Var compensators for wind energy applications. *Proceedings of the 17th British Wind Energy Association Conference*, UK, pp.347-352.

Sakkoury,K, Novotny,D.W., Khater,F.M.H., Ahmed,F.I. (1993), Transient performance of autonomous self excited induction generator system, *Proceeding of IMACS-TCI'93*, Montreal, Canada, pp.165-170.

Salama,M.H., Holmes,P.G. (1996), Transient and steady-state load performance of a stand-alone self-excited induction generator, *IEE Proceedings-Electr. Power Appl.*, vol.143, no.1, pp.50-58.

Schauder,C.D., Caddy,R. (1982), Current control of voltage-source inverters for fast four-quadrant drive performance, *IEEE Transactions on Industry Applications*, vol.18, no.2, pp.163-171.

Shaltout,A.A. (1995), Solid-state control of a wind-driven self-excited induction generator, *Electric Machines and Power Systems*, pp.571-582.

Shridhar,L., Singh,B., Jha,C.S., (1993), A step towards improvements in the characteristics of self excited induction generator, *IEEE Transactions on Energy Conversion*, vol. 8, no. 1, pp. 40-46.

Shridhar,L., Sighn,B., Jha,C.S. (1995a), Transient performance of the self regulated short shunt self excited induction generator, *IEEE Transactions on Energy Conversion*, vol.10, no.2, pp.261-267.

Shridhar,L., Singh,B., Jha,C.S., Singh,B.P., Murthy,S.S. (1995b), Selection of capacitors for the self regulated short shunt self excited induction generator, *IEEE Transactions on Energy Conversion*, vol.10, no.1, pp. 10-16.

Silva,S.R., Lyra,R.O.C. (1993), PWM converter for self-excitation of induction generators, *Proceedings of the 5th European Conference on Power Electronics and Applications*, Brighton, UK, pp.174-178.

Silva,S.R., Lyra,R.O.C. (1995), Pulse width modulation exciter for flux control of an isolated induction generator, *Proceedings of the 6th European Conference on Power Electronics and Applications*, Sevilla, Spain, vol.3, pp.233-238.

Simoes,M.G., Bose,B.K. (1997), Design and performance evaluation of a fuzzy-logic-based variable-speed wind generation system, *IEEE Transaction on Industry Applications*, vol.33, no.4, pp.956-965.

Singh,B. (1995), Induction generators - a prospective, *Electric Machines and Power Systems*, vol.23, no.2, pp.163-177.

Singh,S.P., Jain,M,P. (1995), A new technique for the analysis of self excited induction generator, *Electric Machines and Power Systems*, vol.23, pp647-656.

Smith,A.C., Healey,R.C., Williamson,S. (1996), A transient induction motor model including saturation and deep bar effect, *IEEE Transactions on Energy Conversion*, vol.11, no.1, pp.8-15.

Smith,L.R., Sriharan,S. (1968), Transients in induction machines with terminal capacitors, *Proceedings of IEE*, vol. 115, no. 4, pp. 519-527.

Spooner,E., Williamson,A.C. (1996), Direct-coupled, permanent-magnet generators for wind turbine applications, *IEE Proceedings - Electr. Power Appl.*, vol.143, no.1, pp.1-8.

Spooner,E., Williamson,A.C., Catto,G. (1996), Modular design of permannet-magnet generators for wind turbines, *IEE Proceedings - Electr. Power Appl.*, vol.143, no.5, pp.388-395.

Sumi,Y, Harumoto,Y., Hasegawa, T., Yano.M., Ikeda,K., Matsuura,T. (1981), New static VAr control using forced-commutated inverters, *IEEE Transactions on Power Apparatus and Systems*, vol.PAS-100, no.9, pp.4216-4224.

Sutanto,D., Grantham,C. (1993), The application of induction generators for remote-hydro systems in developing countries, *IFAC 12th Triennial World Congress*, Sydney, Australia, pp.677-680, 1993.

Teissier,M., Jammal,A., Grellet,G., Blanchard,P. (1992), Self-excitation of a saturated non loaded and loaded asynchronous generator, *Proceedings of International Conference on Electrical Machines ICEM'92*, Manchester, UK, pp.1062-1066.

Teodorescu,R., Osu,E., Parra,H.Z., Bresnahan,K. (1995), A Simulink approach to power electronics simulation, *Proceedings of the 6th European Power Conference on Power Electronics and Application*, Seville, Spain, pp.3.954-3.958.

Thorsen,O.V., Dalva,M. (1992), Improved model for simulation of deep bar induction motors. Application to direct start up by open and closed wye-delta transition,

Proceedings of IEEE Industry Application Society Annual Meeting IAS, Houston, TX, USA, pp.115-122.

Trzynadlowski, A.M. (1994), *Field orientation principle in control of induction motors*, Kluwer.

Uctug,Y., Demirekler,D. (1988); Modellling, analysis and control of a wind turbine driven self-excited induction generator, *IEE Proceedings*, vol.135, pt.C, no.4, pp.268-275.

Van Der Broeck,H.W. (1988), Analysis and realisation of a pulsewidth modulator based on voltage space vectors, *IEEE Transactions on Industry Applications*, vol.24, no.1, pp142-149.

Van Wyk,J.D., Marshall,D., Boshoff,S.(1986), Simulation and experimental study of reactively loaded PWM converter as fast source of reactive power, *IEEE Transactions on Industry Application,* vol.IA-22, no.6, pp.1082-1089.

Vas,P. (1990), *Vector control of AC machines*, Oxford University Press.

Vas,P. (1992), *Electric machines and drives. A space-vector theory approach*, Oxford: Clarendon Press.

Vas,P., Li,J. (1992), Effects of saturation in double-cage induction machines, *Proceedings of the International Conference on Electrical Machines*, ICEM, Manchester, UK, pp.662-664.

Vas,P., Li,J. (1993), Digital simulation of saturated double-cage induction machines, *Proceedings of IMACS-TCI'93*, Montreal, Canada, 1993, pp. 591-596.

Vas,P., Levi,E., Oros,D., Jevremovic,R. (1997), Capacitor braking of double-cage induction motors, *Electric Power Systems Research*, vol.40, no.3, pp.161-166.

Wade,S., Dunnigan,M.W., Williams,B.W. (1994), Simulation of induction machine vector control and parameter identification, *Proceedings of IEE Power Electronics and Variable Speed Drives Conference*, London, IEE Conference Pub. no.399, pp.42-47.

Wade,S., Dunnigan,M.W., Willaims,B.W. (1997), Modelling and simulation of induction machine vector control with rotor resistance identification, *IEEE Transactions on Power Electronics*, vol.12, no.3, pp.495-505.

Wagner,C.F. (1939), Self-excitation of induction motors, *AIEE Transactions*, vol. 58, pp. 47-51.

Walker,L.H. (1986), Forced commutated reactive-power compensator, *IEEE Transactions on Industry Applications*, vol.IA-22, no.6, pp.1091-1104.

Wang,L., Lee,C. (1997a), A novel analysis on the performance of an isolated self-excited induction generator, *IEEE Transactions on Energy Conversion*, vol.12, no.2, pp.109-115.

Wang,L., Lee,C. (1997b), Dynamic analysis of parallel operated self-excited induction generators feeding an induction motor load, *IEEE PES WM*, New York, NY, Paper No. PE-337-EC-0-12-1997.

Wang,L., Su,J.Y. (1997), Dynamic performances of an isolated self-excited induction generator under various loading conditions, *IEEE PES WM*, New York, NY, Paper No. PE-230-EC-1-09-1997.

White,T.J., Hinton,J.C. (1994), Improved dynamic performance of the 3-phase induction motor using equivalent circuit parameter correction, *Proceedings of IEE Control Conference*, UK, pp.1210-1214.

White,T.J., Hinton,J.C. (1995), Compensation for the skin effect in vector-controlled induction motor drives, *Proceedings of IEE Electric Machines and Drives Conference*, Durham, UK, pp.301-305.

Williamson,S., Healey,R.C. (1996), Space vector representation of advanced motor models for vector controlled induction motors, *IEE Proc.-Electr. Power Appl.*, vol.143, no.1, pp.69-77.

Xu,X., De Doncker,R.D., Novotny,D.W. (1988a), Stator flux orientation control of induction motor drive, *Conference Record of IEEE Power Electronics Specialists Conference*, Kyoto, Japan, pp.870-876.

Xu,X., De Doncker,R.D., Novotny,D.W. (1988b), Stator flux orientation control of induction machines in the field-weakening region, *Conference Record of IEEE IAS Annual Meeting*, Pittsburgh, PA, USA, pp.437-443.

Zhang,L., Watthanasarn,C., Shepherd,W. (1997), Application of a matrix converter for the power control of a variable-speed wind turbine driven doubly-fed induction generator, *Proceedings of the IEEE International Conference on Industrial Electronics, Control, and Instrumentation IECON'97*, New Orleans, Louisiana, USA, pp.906-911.

Zuckerberger,A., Weinsstock,D., Alexandrovitz,A. (1994), Simulation of three-phase and single-phase matrix converters, *Proceedings of the Power Electronics and Motion Control Conference PEMC'94*, Warsaw, Poland, pp.464-467.

Zuckerberger,A., Weinsstock,D., Alexandrovitz,A. (1996), Simulation of three-phase loaded matrix converter, *IEE Proceedings-Electr. Power Appl.*, vol.143, no.4, pp.294-300.

Zuckerberger,A., Weinsstock,D., Alexandrovitz,A. (1997), Single-phase matrix converter, *IEE Proceedings-Electr. Power Appl.*, vol.144, no.4, pp.235-247.

APPENDIX A: MACHINE PARAMETERS

SINGLE-CAGE INDUCTION MACHINE DATA

Machine used in simulations:

$P_n = 0.75$ kW $V_n = 380$ V $I_n = 2.1$ A $n_n = 1390$ rpm

$f = 50$ Hz p.f. $= 0.72$

Star connected stator winding

$R_s = 10\ \Omega$ $R_r = 6.3\ \Omega$ $L_{\sigma s} = 43$ mH $L_{\sigma r} = 40$ mH

Magnetising curve approximation and dynamic inductance approximation (in terms of rms values):

$$\psi_m = 0.86427 \cdot 0.59976^{I_m} \cdot I_m^{1.1211}$$

$$L = 0.86427 \cdot 0.59976^{I_m} \cdot (1.121 \cdot I_m^{0.1211} - 0.511226 \cdot I_m^{1.1211})$$

Machine used in experiments:

$P_n = 1.2$ kW $V_n = 415$ V $I_n = 2.8$ A $n_n = 1320$ rpm

$f = 50$ Hz

Star connected stator winding

$R_s = 7.65\ \Omega$ $R_r = 10.4\ \Omega$ $X_{\sigma s} = X_{\sigma r} = 10.6\ \Omega$ $X_m = 200\ \Omega$

DOUBLE-CAGE INDUCTION MACIIINE DATA

$P_n = 7.5$ kW $V_n = 380$ V $I_n = 14.7$ A $n_n = 2905$ rpm

$f = 50$ Hz p.f. $= 0.9$

Delta connected stator winding

$R_s = 1.97\ \Omega$ $R_{r1} = 2.82\ \Omega$ $R_{r2} = 1.36\ \Omega$ $R_c = 0.649\ \Omega$ $L_{\sigma s} = 10.23$ mH

$L_{\sigma r1} = 0$ mH $L_{\sigma r2} = 8$ mH $L_{mr} = 2.79$ mH $L_{mm} = 0.44977$ H

Magnetising curve approximation and dynamic inductance approximation (in terms of rms values):

$$\Psi_m = \begin{cases} 0.598\, I_m & I_m < 1.25\ \text{A} \\ \left(q + g/I_m + h/I_m^2\right)^{-1} & I_m > 1.25\ \text{A} \end{cases}$$

$$L = \begin{cases} 0.598 & I_m < 1.25\ \text{A} \\ \Psi_m^2\left(g/I_m^2 + 2h/I_m^3\right) & I_m > 1.25\ \text{A} \end{cases}$$

$q = 0.67905$ $g = 0.067911$ $h = 0.94346$

Speed approximation:

$$\omega = \begin{cases} 346.1 - 28.085t & 0 \le t \le 1.1\ \text{s} \\ 315.206 & t > 1.1\ \text{s} \end{cases}$$

Single-cage representation (first set of parameters)

$R_r = 1.7\ \Omega,$ $L_{\sigma r} = 5.97$ mH

Single-cage representation (second set of parameters)

$R_r = 2.073\ \Omega,$ $L_{\sigma r} = 5.46$ mH

APPENDIX B: PUBLISHED PAPERS

LIST OF PUBLICATIONS

Journal paper:

1. Y.Liao, E.Levi; Modelling and Simulation of a Stand-alone Induction Generator with Rotor Flux Oriented Control, *Electric Power Systems Research*, 1998, vol.46, no.2, pp.141-152.

Conference papers:

2. Y.Liao, E.Levi, R.Morgan; Simulation of PWM Voltage Source Inverter Based Reactive Power Compensators using SIMULINK, *Proceedings of 29th International Intelligent Motion Conference PCIM'96*, Nuremberg, Germany, 1996, pp. 519-525.

3. E.Levi, Y.Liao, R.Morgan; Single-cage Representation of Saturated Double-cage Induction Generators for Self-excitation Studies, *Proceedings of the 31st Universities Power Engineering Conference*, Iraklio, Greece, 1996, pp. 207-210.

4. Y.Liao, E.Levi; A Study of Self-excitation Schemes for an Isolated Induction Generator, *Proceedings of 32nd Universities Power Engineering Conference*, Manchester, UK, 1997, pp.1110-1113.

5. Y.Liao, E.Levi; Variable Speed Induction Generator as a Source of Constant DC Voltage, *Proceedings of 33rd Universities Power Engineering Conference*, Edinburgh, UK, pp.759-762.

PAPERS ACCEPTED FOR PUBLICATION

Journal paper:

1. E.Levi, Y.Liao; An Experimental Investigation of Self-Excitation in Capacitor Excited Induction Generators, Paper Accepted for Publication in *Electric Power Systems Research Journal.*

Conference paper:

2. E.Levi, Y.Liao; Rotor Flux Oriented Induction Machine as a DC Power Generator, Paper Accepted for Publication in the Proceedings of the *8th European Conference on Power Electronics and Applications EPE'99*, Lausanne, Switzerland, September, 1999.